A Robotic Multiaxis Additive Manufacturing System for Nonplanar and Dynamic Orientation Printing

Nicholas Richard Fry

The University of Leeds

School of Mechanical Engineering

Submitted in accordance with the requirements for the degree of

Doctor of Philosophy

March, 2018

Intellectual Property Statement

The candidate confirms that the work submitted is their own, except where work which has formed part of jointly authored publications has been included. The contribution of the candidate and the other authors to this work has been explicitly indicated below. The candidate confirms that appropriate credit has been given within the thesis where reference has been made to the work of others.

The work in Chapter 2 of the thesis has appeared in partial form in two book chapters as follows:
"Integrated Manufacturing: The Future of Fabricating Mechatronic Devices."
In: Hehenberger P., Bradley D. (eds) Mechatronic Futures. Springer, Cham, (2016)
Authors: N. Fry, R. Richardson, J. H. Boyle.
I was responsible for the literature research and writing of the chapter.
The contribution of the other authors was guidance, proof reading and editing.

"Integrated manufacturing of bespoke mechatronic systems" In: Y. Bar-Cohen (ed) Advances in Manufacturing and Processing of Materials and Structures. CRC Press, (in press)
Authors: J. Smith, N. Fry, R. Richardson and J. H. Boyle
I was responsible for some literature research, guidance, proof reading and editing. The contribution of the other authors was: J. Smith wrote the majority of the chapter. R. Richardson and J. Boyle also provided some literature research, guidance, proof reading and editing.

This copy has been supplied on the understanding that it is copyright material and that no quotation from the thesis may be published without proper acknowledgement.

The right of Nicholas Richard Fry to be identified as Author of this work has been asserted by him in accordance with the Copyright, Designs and Patents Act 1988.
© 2018 The University of Leeds and Nicholas Richard Fry.

Acknowledgements

I would first like to express my gratitude to my supervisors - Professor Robert Richardson and Dr Jordan Boyle - for all of their advice, support and encouragement throughout the course of my PhD. Together you make a supervision team that would make many jealous, and for that I am grateful. Rob, you have the ability to have big visions about the future and then translate that into the research required to get there. Thank you for your experience and for allowing me to pursue the project with the right mix of freedom and guidance to make it my own.

Jordan, you are always happy to help and have the ability to break down complex problems into approachable parts. Whether by always being willing to chat or by getting your hands dirty in the lab, your support has been invaluable. Never stop saying things how they are!

I would also like to express my thanks to my friends, both at the university and outside. To those from my office and the Robotics Lab - A PhD can be a lonely pursuit so I am grateful that we could celebrate the highs, and commiserate lows together. I am especially thankful for the Godparents of both of my children. Without your love, friendship, and support to me, and my family, we would not have come out of the end of this process with as much sanity in tact as we do.

Thank you also to my family, especially my parents. Without your love, encouragement and example I would have never achieved so much.

Lastly, and most importantly, I owe my deepest gratitude to my wife. In the course of my work she has twice put to shame man-made 3D printers by 'Additively Manufacturing' the most wonderful children. It is only with you by my side, with your selfless love and constant support, that has enabled me to get this far.

Abstract

In the future an automatic robot fabrication system is envisioned, that would enable a non-specialist user to parametrically design, and autonomously manufacture a bespoke robot, without the need for manual intervention or assembly. Additive Manufacturing (AM) is an attractive method for this as it is digitally driven and tooling free, which increases the speed and flexibility of production, while reducing costs for low volumes. Another unique capability of AM is the ability to embed components within the structure of a robot, while it is being manufactured. However, the state of the art embedding methods involve a series of manual steps. Additive manufacturing also has some inherent limitations which arise from building up parts from many discrete, planar layers. These include; anisotropic mechanical properties; curves approximated by discontinuous steps; and overhangs requiring support.

Addressing these issues, while also enabling functional mechatronic components to be embedded, requires a new approach to Additive Manufacturing. This work introduces a novel 12-axis Additive Robot Manufacturing System (ARMS). This is shown to successfully 3D print high quality parts, comparable to other Fused Filament Fabrication (FFF) systems, using industrial robot arms. Using the multiaxis (i.e. > 3 axes) capabilities, it is demonstrated that the orientation of a print with respect to gravity has no effect upon its surface quality, but the relative orientation of the geometry to the layers has a significant influence. Using this relationship, components are printed using a dynamically varying build orientation, enabling unsupported, 90° overhangs with a constant, tuneable roughness to be produced. ARMS is then used to print nonplanar layers with greater curvature than has previously been demonstrated. Conformal layers are shown to improve the strength of curved parts by 57%. The capabilities are combined to manufacture the first mechatronic system with an integrated actuator that required no manual assembly, intervention, or post processing during or following the AM process. It is concluded that the multiaxis AM system successfully improves upon conventional planar deposition by overcoming key drawbacks to FFF, and could be a key enabler to a new AM process for the manufacture of integrated mechatronic and robotic devices.

Contents

List of Figures

List of Tables

LIST OF TABLES

Abbreviations

AM	Additive Manufacturing	ANOVA	Analysis of Variance
ASTM	American Society for Testing and Materials International	CAD	Computer Aided Design
CLFDM	Curved Layer Fused Deposition Modelling	CLFFF	Curved Layer Fused Filament Fabrication
CNC	Computer Numerically Controlled	DDM	Direct Digital Manufacturing
DED	Directed Energy Deposition	DLP	Digital Light Processing
DOF	Degrees Of Freedom	DW	Direct Write
FDM	Fused Deposition Modelling	FFF	Fused Filament Fabrication
GA	Genetic Algorithm	GUI	Graphical User Interface
IO	Input/Output	MAAM	Multiaxis Additive Manufacturing
MMAM	Multimaterial Additive Manufacturing	MAE	Mean Absolute Errors
NC	Numerical Control	PCB	Printed Circuit Board
PID	Proportional Integral Derivative controller	PLA	Poly(lactic acid)
PVA	Poly(vinyl alcohol)	RP	Rapid Prototyping
SDM	Shape Deposition Modelling or Manufacturing	SLA	Stereolithography
SLS	Selective Laser Sintering	SMA	Shape Memory Alloy
SMP	Shape Memory Polymer	STL	Stereolithography file
UV	Ultraviolet light		

Chapter 1

Introduction

1.1 Background

Additive Manufacturing (AM) has matured into a tool which is now commonly used in the design and manufacture of robots, but a Grand Challenge still remains; to print a robot which 'walks' off the print bed [1, 2]. This goal brings together a range of research topics and demonstrates the practical advantages of extending AM to produce more than just passive mechanical structures.

Robotic systems have the potential to bring advantages to many areas, but a generic robotic platform that can assist in almost any task is too complex, large and expensive to become commonplace. Small, customized robots that could quickly be designed and built for a specific task are more appropriate for many scenarios. However, tooling based processes and complex assembly cause this to currently be an uneconomical approach, especially when considering rapid or inexpensive deployment in real world scenarios. Solving the challenge to print fully integrated robots would enable these customised robots to be produced using the design complexity and flat cost structure that AM allows.

Mechatronic devices are usually built from discrete components including electronic,

actuator, sensor and computation modules. These are integrated together by affixing them inside a mechanical structure using bolts and other fastenings. The use of fastenings can limit robustness and, as the device gets smaller, the space taken up by these fastenings becomes increasingly significant. Assembly of these complex devices is also a big challenge; once a product has been designed, it must undergo a rigorous 'design for assembly' process to make it suitable for manufacturing. This often introduces delays, large costs, and greatly limits the designer. For example: the shape of a mechanical case must be simple enough that it can be released from a mould; circuit boards (both rigid and flexible) can only be populated when held flat, and must incorporate off-the-shelf sensors in specific packages.

AM builds parts in such a way that the internal geometry can be accessed. This opens up exciting possibilities, as parts can be fabricated that are impossible with conventional machining or moulding. Moving mechanisms can be printed in one piece, material properties can be varied throughout the object, and material can be arranged internally to optimise weight or centre of mass position. This stimulates the possibility of building robots and mechatronic devices in a new way. Rather than designing a case and using fastenings to install the components, they could be inserted into the body of the robot, as it is being 3D printed. This would yield a solid part, with no seams or fastenings to break, or come loose. These 'non-assembly' devices could be fully functional, straight off the build plate. By integrating the fabrication and assembly processes, production times may also decrease.

Some envision that AM will be used to manufacture complete mechatronic devices, including all the sub-components, from a small selection of fundamental materials. This would allow manufacturers to just keep an inventory of a few materials and be able to produce an almost unlimited range of items. This would be a significant advance in the field, as it involves replacing many highly specialised manufacturing processes, which go into producing items such as semiconductors or motors, with one generic process. However, currently it is a very distant goal. To build all of the components by combining a small number of materials, the deposition would have to be on a molecular level, which brings significant challenges. Not least of these is the need for a parallel deposition process to make working at this scale practical. By embedding existing mechatronic components into an established AM method, the advantages of integrating these components can be realised in the near term.

Components have previously been inserted into 3D printed parts during the build process, but the procedure is highly manual and has not been significantly developed since it was first published over a decade ago [3, 4]. To improve this embedding process this research looks to utilise a new idea in additive manufacturing, the use of multiaxis mechanisms (i.e. systems with > 3 axes). Systems have previously been developed that, at a fundamental level, show they have the capability to bring advantages to AM such as reducing the support material required, improving some surface finishes or increasing the strength of parts. These motivated the development of a new system that could improve upon the quality of the prints, and be flexible enough to enable research into proposed advantages of such a system. The ability to dexterously manoeuvre and orient both the extruder and build plate in 3D space overcomes inherent limitations in the conventional, planar AM approach, allowing conformal printing of both non-planar and non-horizontal layers. If a multiaxis system is to be used for the embedding of components then these fundamental abilities must first be investigated before utilising these results to produce a robot with embedded components.

1.2 Aim and Objectives

The aim of this work was to develop a multiaxis additive manufacturing (MAAM) system capable of printing curved and non-parallel layers, and to evaluate the advantages of such a system for producing fully-integrated, assembly-free robots.

In order to fulfil this aim the objectives below were defined:

- Review existing literature to develop understanding of; Direct Digital Manufacturing and the fundamentals of AM, how AM has been applied to the field of robotics, and the state of the art in nonplanar deposition and multiaxis AM strategies and systems.
- Critique existing MAAM and draw conclusions to inform the approach and design of a research focused system.
- Complete the design and development of a MAAM system which is high quality and flexible enough for long term research into this area. This includes building the mechanical, electrical and software subsystems.
- Investigate the possibility of changing the direction of the vector along which

layers as stacked during 3D printing and assess how this impacts the properties of the part.

- Explore the printing of curved layers and determine if they have an impact upon the mechanical properties of printed parts.
- Integrate these capabilities to produce a demonstrator system that highlights the advantages of MAAM, including the ability to embed pre-existing components.

1.3 Statement of Contributions

The specific, technical contributions of this work to the AM community can be summarised as;

- The implementation of a novel multiaxis AM system with 12 Degrees of Freedom (DOF) which shows that serial robotic arms can be used successfully for small scale AM.
- An analysis of the relationship between the overhang angle of a surface and the slicing angle, and how this affects the surface roughness when using Fused Filament Fabrication (FFF).
- The novel demonstration of FFF printing at any orientation (with respect to gravity) without adverse surface effects, and the use of dynamic changes in orientation to enable the unsupported printing of extreme overhangs.
- Adding further evidence to the small body of work which shows that nonplanar layers can improve the strength of 3D printed objects.
- Demonstrating that MAAM makes it possible to embed functional mechatronic components into 3D printed parts without the need for manual assembly, shape converters or post processing.

1.4 Thesis Organization

The practical work in this thesis comprises of two major bodies of work. The first, detailed in Chapter 3, is the design and development of the robotic Additive manufacturing system. The second, detailed in Chapters 4-6, is the testing and validation of

this system for use with novel multiaxis printing methods. This was achieved through experimental work and analysis of the results.

1.4.1 Chapter 2 - Literature Review

The relevant literature is reviewed to better understand how AM has been applied to robotics and to understand the state of the art in multiaxis AM.

1.4.2 Chapter 3 - Additive Robot Manufacturing System

The multiaxis AM system is introduced and the design and development of the mechanical, electrical and software components are presented in detail. The results of its use for conventional 3D printing are shown.

1.4.3 Chapter 4 - Dynamic Build Orientation Changes during AM

The system's ability to print in unconventional and variable orientations, which are a prerequisite for many of the proposed advantages of MAAM, is investigated.

1.4.4 Chapter 5 - Multiaxis Nonplanar Layers for Increased Strength

The system's ability to print nonplanar, conformal layers is demonstrated, achieving significantly greater layer curvature than previous systems. The mechanical properties of these parts is investigated and compared to parts produced with standard layers.

1.4.5 Chapter 6 - MAAM Mechatronic Demonstrator

Preliminary work on embedding components is undertaken through the fabrication of a final demonstrator which combines the MAAM advantages that have been explored in the previous chapters.

1.4.6 Chapter 7 - Summary, Conclusions and Further Work

The major contributions of this work are discussed and summarised. The conclusions that can be made from this work are drawn out and the possible future direction of this research is considered.

1.4.7 Appendices

Further details of experiments are provided here along with key information about the system.

Chapter 2

Literature Review

2.1 Introduction

This chapter provides an overview of relevant literature on the research of the Additive Manufacturing (AM) of mechatronic and robotic devices. It begins with an overview of AM, before discussing how it has impacted the manufacture of major components in robotics. Recent advances in Multiaxis AM and how this could benefit the goal of integrated mechatronics manufacturing are then reviewed. The goal of this chapter is to show the need for a multiaxis additive manufacturing system, and address the form this may take based upon the state of the art in this area.

2.2 Direct Digital Manufacturing

Traditionally manufacturing was either manual, making it slow and labour intensive, or automated by predetermined robot operations, making it inflexible and costly to set up - requiring large product numbers to justify the expenditure. Computer control and digital design are helping to change the economic patterns that have defined manufacturing since the industrial revolution.

2.2.1 Automation

The design of a production line revolves around the need to make it as efficient as possible. Adjacent manufacturing operations should be located as physically close as possible and the movement of human workers and parts carefully choreographed to minimise wasted actions and time. While the philosophy behind assembly lines has not changed since they were introduced, the technology that powers them has, and it brings along its own set of advantages and challenges.

Through the application of sensors and actuators factories are becoming increasingly more automated. Where once a human worker loaded parts into a machine, a robot arm can now be coupled with a computer vision system that identifies a specific part and places it in the jig itself. This can increase the speed and efficiency of the process and is often safer, removing the need for a human to work closely with dangerous machinery.

For low volume manufacturing (for example $< 10,000$ units), Computer Numerically Controlled (CNC) machines are arguably having an even greater effect. The first CNC machines were traditional machine tools, such as milling machines and lathes, which were controlled by a computer. They have now expanded to include laser cutters, 5-axis milling machines, and even 3D printers. CNC gives huge advantages as machines can take a digital version of a part and turn it into a very high precision physical model. This disrupts the highly manual process that was traditionally used for small production runs, reducing the time and cost to produce parts while increasing the quality and precision.

2.2.2 Additive Manufacturing

Additive Manufacturing (AM) is a disruptive technology that was first developed just over 30 years ago, but has burst into the public consciousness in recent years, as consumer desktop 3D printers become cheaper and more readily available. Additive Manufacturing and 3D Printing are often considered interchangeable terms to describe a range of technologies. The American Society for Testing and Materials (ASTM) International defines AM as “A process of joining materials to make parts from 3D model data, usually layer upon layer, as opposed to subtractive manufacturing and formative manufacturing methodologies”[5].

There are different methods of depositing material in AM processes, but in all cases the first step is to digitally slice the computer model into thin layers. The layers are

then physically laid down, one after the other, gradually building up a three dimensional part. Thinner layers give finer detail, but also increase print time as more layers are required. Deposition technologies are split into seven categories by the ISO/ASTM 52900:2015 standard [5]. These are listed with the given definition in Table 2.1 and expanded upon below.

Table 2.1: Additive Manufacturing standard terminology from ISO/ASTM 52900:2015 [5]

Process Category	Definition
Binder Jetting	A liquid bonding agent is selectively deposited to join powder materials.
Directed Energy Deposition (DED)	Focused thermal energy is used to fuse materials by melting as they are being deposited.
Material Extrusion	Material is selectively deposited through a nozzle or orifice.
Material Jetting	Droplets of build material are selectively deposited.
Powder Bed Fusion	Thermal energy selectively fuses regions of a powder bed.
Sheet Lamination	Process in which sheets of material are bonded.
Vat Photopolymerization	Liquid photopolymer in a vat is selectively cured by light-activated polymerization.

Binder Jetting uses a bed of powdered material and an inkjet-style deposition head to selectively deposit liquid to bond the powder. This is typically used to create forms for sand casting metals or to create multicoloured items as the liquid can be coloured inks similar a standard inkjet printer. This usually forms brittle parts which need infusing with epoxy resin or similar to be handled but can be useful for product development.

Directed Energy Deposition involves focusing an energy source, such as a laser or electron beam, on a stream of powder (typically metal) as is it deposited from a nozzle. This causes a localised melt pool fusing the material to the previous layer. This is often combined with a subtractive machining process as the surface can be rough.

Material Extrusion is a large category which covers a range of extrusion based ma-

chines. These feed semi-liquid material out of a moving nozzle, which then sets to form a hard layer. Many different materials have been used, including clay and chocolate, although thermoplastics are by far the most common, especially in consumer grade 3D printers. These are commonly referred to as Fused Deposition Modelling (FDM) printers, although this is a trademark of Stratasys. Various acronyms have been coined, but in this thesis this process will be referred to as Fused Filament Fabrication (FFF). It is one of the most accessible and commonly used AM techniques, due to the 'RepRap' movement [6]. The cost effectiveness stems from the relative simplicity of the technique, and the fact that it uses standard engineering plastics (including nylon, PLA and ABS) which are relatively inexpensive. These plastics have been used extensively in other manufacturing processes and are therefore well characterised. Furthermore, their properties are not compromised by the need for UV-reactive chemistry. As a result, the material properties for FFF parts are more stable than items produced from cured resin. That said, material extrusion results in parts that are not isotropic, and are typically weaker across layers than along them due to imperfect bonding [7]. Finally, material extrusion generally has lower resolution than photopolymer-based approaches. An FFF extruder will be used in this work due to these advantages and the unique way in which a multiaxis system can address these disadvantages.

Material Jetting is analogous to standard inkjet printing, however the liquid material that is selectively deposited solidifies through curing or cooling, to form a layer. This material is often a photoploymer but can be wax or other materials. As several jetting heads can be used at once this method is used extensively for multimaterial AM. Materials can be gradated together allowing full colour printing or combinations of flexible and rigid materials. Importantly this allows support materials to be easily removed as they can be printed in a separate dissolvable or soft material. The Stratasys Polyjet range is a common example of this system.

Powder Bed Fusion binds particles of powder together using a heat source (e.g a laser). The part is constructed inside a vat of powder. To form a layer, an arm first sweeps a thin film of powder across the top of the print bed. The print head then traces out the contours of that layer and solidifies the powder. This method can produce strong parts as materials such as nylon or even metals can be used. When using

polymers, this is the only AM method which requires no dedicated support structures to be built, as the powder is able to support the layers built above it. Care must be taken to allow access for the surplus powder to be removed however.

Sheet Lamination is a process in which each layer is formed by cutting the shape from a thin sheet of paper, plastic or even metal. These sheets are bonded together using an adhesive or ultrasonic welding. The paper based approach produces parts with poor mechanical properties, but can be combined with inkjet printing to give full colour models.

Vat Photopolymerization is a term which refers to solidification of a liquid resin using a light source. Lasers, UV lights, digital projectors and even LCD screens can be used. Stereolithography (SLA) was the first form of AM to be developed, and is widely used in industry due to its high resolution. An SLA machine includes a vat of resin which the build plate moves through. A thin layer of resin either flows, or is wiped across the surface, a laser traces out the layer, curing the resin and the build platform moves by one layer thickness before the process is repeated. Digital Light Processing (DLP) speeds up this process by curing a whole layer at once by using a projector to cure a wide area. Very fine features and layer heights are possible with this system and a range of materials have been developed including flexible and ceramic resins.

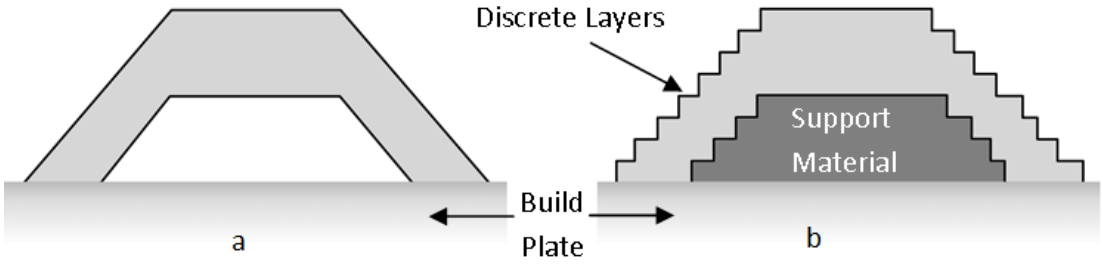

Figure 2.1: Effect of building objects from discrete layers; a) Subtractive machining yields a smooth surface. b) AM part has a stepped surface and requires support material under the overhang.

The layer by layer construction technique that is common to all these processes enables a new freedom in design as very complex shapes, even parts that cannot be manufactured using traditional techniques, can often be realised using 3D printing (e.g. nested spheres). However there are some limitations to the geometry of the parts that can be manufactured. The use of layers can cause a 'stair step' effect on curved surfaces (Fig. 2.1) as the shape must be digitised into discrete layers. Furthermore, each layer must be supported by a layer underneath, so steeply overhanging sections often need dedicated support structures building underneath. Supports are either printed in the same material as the part and designed to be cut, 'snapped' or machined off, or a different material is used that can be washed, peeled or dissolved away.

Although the impact of AM technology is sometimes exaggerated, it has undeniably had a dramatic effect on the way products are manufactured and will continue to do so. Since the Industrial Revolution, Economies of Scale have defined the structure of the manufacturing industry [8]. When a greater number of products are produced, cost per unit decreases. Unfortunately this requires a large initial investment for manufacturing to become cost effective and therefore leads to large scale, centralised, mass manufacturing. Due to the fact that AM requires no tooling or setup, the price per unit levels off very quickly, and is often modelled as a flat line when compared with traditional manufacturing cost structures [9]. As Fig. 2.2 shows, this makes AM a very cost effective option for low volume manufacturing. Currently traditional methods are more cost effective for large quantities, but the breakeven point will improve as 3D printers become more capable, cheaper and faster. This model, however, is limited as it does not take into account other significant costs, such as the design work which goes into creating a part to be manufactured. In the context of this thesis, the design of a complex, integrated device is a significant aspect of the manufacturing process. This is offset slightly by the fact AM has more flexible design rules than conventional manufacturing. There has also been some work in the automatic design of robots [10, 11], which would minimise this cost.

AM will also significantly impact the Economies of Scope. This term refers to the fact that if one set of equipment, processes or materials can be used to make different products then the unit cost falls as the investment is split between more items [8]. 3D printers are extremely versatile in the geometries they can produce and there is little time or cost penalty incurred when swapping between parts. They can even produce

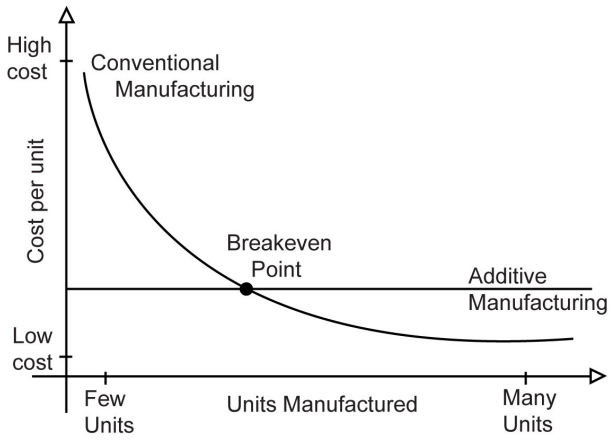

Figure 2.2: A comparison of traditional and additive manufacturing cost models.

different objects side by side on the build plate.

The abilities of 3D printers are so different from traditional manufacturing that they allow new approaches to production that are not practical or possible with current manufacturing methods. For example, the layer based process allows very complex geometries that could not be machined or cast due to object geometry limiting the access for tools or mould removal. Internal features can also be created, without the need to split the part into many pieces. This in turn leads to parts that can be lighter, require less assembly and have complex geometries, all while reducing material waste and lead times.

Additive Manufacturing was originally used exclusively as a Rapid Prototyping (RP) technology, as it allowed product designers to produce a physical model of their design within hours rather than days or weeks. Now, however, AM is expanding into Direct Digital Manufacturing (DDM). This is where AM technology is used to manufacture high quality, final production parts, rather than just protoypes. While the majority of 3D printers available are still aimed at RP, we are currently on the cusp of this exciting shift, where AM is being used to shorten supply chains, produce optimised parts and manufacture custom components. In fact, it is estimated that about 20% of 3D printed parts are already for end use. Within 5 years it is predicted that this will be the majority; producing industrial tooling, individual components or full final

products [12].

Currently in robotics, AM is used primarily to fabricate passive structural components that form part of an overall assembly. In this context, the design freedom and speed of fabrication afforded by AM are significantly limited by the need for subsequent manual assembly. What we and others envision is a future AM system capable fabricating an entire complex robot through a single process, such that it "walks fully formed and functional" out of the build chamber [2]. One day, this Grand Challenge might be achieved by a system that prints individual atoms, creating batteries, electronics and actuators from scratch. Such a system would give unlimited design freedom, but for now remains firmly in the realm of science fiction. However, by combining more feasible approaches and processes currently under development, it may be possible to achieve the same goal within the next decade. For this to be possible, many technologies and principles that are currently in the early stages of development will need to be refined and integrated.

The steps involved in fabricating a fully-functional robot can be broken down into three main categories: building of the physical structure; incorporation of electronics; and incorporation of actuated mechanisms. Most of the technologies required to perform these functions are under development, although they are far from mature [13, 14]. Currently these systems are laborious, requiring multiple processes and often relying on human intervention, but they demonstrate feasibility. The rest of this chapter will review the state of the art in these areas.

2.2.3 Materials

Extending 3D printing processes to work with multiple materials opens up a huge range of possibilities for the technology, and while it is available for some AM methods, it is not yet a mainstream manufacturing technique [15].

Additional materials further extends and adds to the advantages of AM. By eliminating separate processing steps for multimaterial items it gives greater design freedom, helps with size reduction, can improve functionality and make the fabrication more efficient, especially by eliminating assembly [15].

Additionally the mechanical and aesthetic properties can be adjusted. This can increase functionality as compliance could be included in different sections, or different colours or surface finishes could make AM more appropriate for final production runs

as opposed to prototypes [16]. Materials with special properties, such as electrical conductivity, can be incorporated (see 2.3.2), bringing an all-in-one process to fabricate functional mechatronic devices much closer.

2.2.3.1 Metal AM

There is great industrial interest in metal AM due to it's applications in high-value areas such as aerospace and automotive sectors. The use of a strong, functional material means that these processes are not limited to prototyping. NASA, for example, is using a DED process to build rocket engine nozzles with internal cooling channels [17]. This is a design that would not be possible in one part using conventional methods. There are a wide range of AM methods which can process metals, but they fall into two main categories; direct and indirect [18]. Direct methods fully melt metal powders during AM to form the part, whereas indirect processes use a binder to hold the metal powder and this is solidified during using the AM process. Post-processing is then required to remove this binding material and to melt the metal particles together. These are briefly summarised in Table 2.2. Due to the high temperatures involved in melting or sintering metals these processes are not readily compatible with the goal of embedding mechatronic components and therefore are not considered further in this thesis. One metal AM process has been used to embed functional components however; Ultrasonic Consolidation [19]. This is a type of Laminated Object Manufacturing which builds up an object from thin foil layers. These are bonded using ultrasonic welding and are CNC machined to create the required shape. During ultrasonic bonding a plastic flow is induced which allows fibres to be embedded at 25% of the metals melting temperature [20]. This has recently allowed the integration of electronic circuitry within metal parts [21].

Table 2.2: Additive Manufacturing of Metals [18]

Indirect	Direct
Selective Laser Sintering	Selective Laser Melting
Stereolithography	Laser Metal Deposition
Fused Deposition Modelling	Electron Beam Melting
Laminated Object Manufacturing	
3 Dimensional Printing	

2.2.3.2 Multimaterial AM

Considerable research effort is focused upon making many of the different AM processes work with multiple materials. Vaezi *et al.* [15] give a good overview of this progress. Multimaterial Additive Manufacturing (MMAM) can give the designer the ability to change the material properties of an object selectively. This can allow stiffness, damping or other characteristics to be tuned without incorporating extra components. Biomimicry can also be utilised as AM can allow rigid and flexible structures to be tightly integrated together in a similar way to tissue and bone structures [14, 22]. Figure 2.3 shows how a large number of traditional components can be combined by using multimaterials to tune the mechanical properties of a component.

Material jetting currently offers the best resolution and capability, the Stratasys Objet range of 3D printers are the most mature example of this [15, 23]. They can be used to print parts with combinations of flexible, hard, transparent and full colour materials. The printer uses the Polyjet process, somewhat similar to that of an inkjet printer, in which tiny droplets of liquid build material are deposited from holes in the print head. The print head also includes an ultraviolet light that passes over each layer to cure it and solidify the polymer before laying down the next layer. This jetting process allows different materials to be combined in a controlled way to create functional gradients of materials. In a processes such as material extrusion each material is deposited individually with a clear interface between the sections. In contrast, Polyjet allows gradual material transitions that remove the weakness caused by a sudden change in materials. The material properties can even be precisely adjusted at different points throughout a model. In robotics, flexible joints actuated by shape memory alloy wire have been created with this process, showing the potential of integrated non-assembly

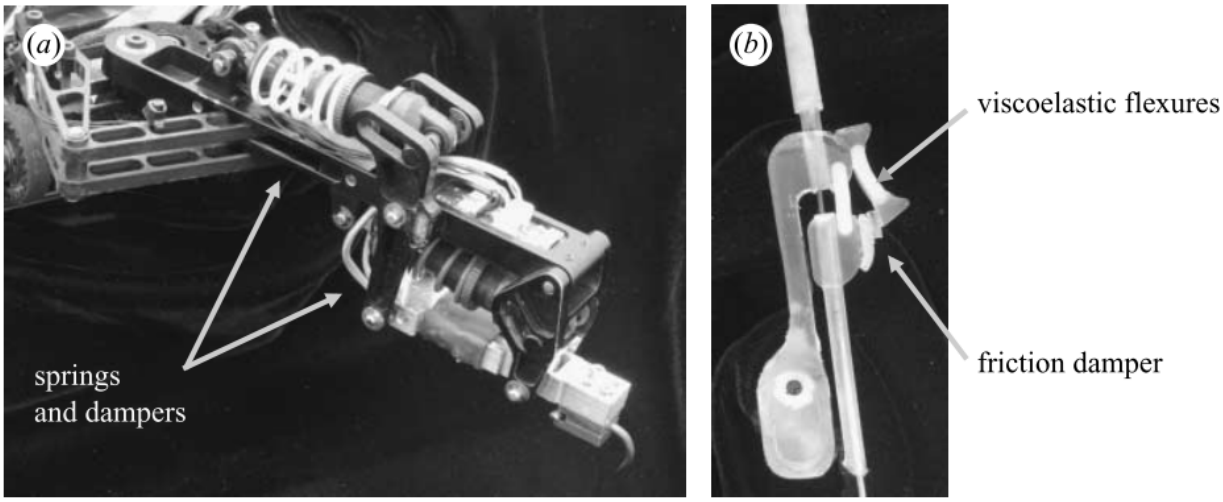

Figure 2.3: Comparison of traditional construction (a) verses integrated multimaterials fabricated using SDM (b) to construct a bioinspired robot leg with passive compliance. From [14]

joints [24].

The Polyjet process, while giving many advantages, also limits the materials that can be used. As the polymers are cured using UV light, each material must be created to work in the printer, giving rise to Stratasys' 'rubber-like' and 'ABS-like' descriptions of its materials. They share similar properties but are not the same as the traditional materials engineers are familiar with using. One of the biggest challenges, and opportunities, for 3D printing is increasing the range of materials that can be reliably used.

Material extrusion offers the next best capabilities for MMAM [15]. Changing the material during a layer is possible, but mixing materials is still not established. Additional extruder heads are often added to FFF printers to support the use of multiple materials in a single print. This is common on FFF machines to enable the production of multi-colour aesthetic models (for example [25]), but materials with different physical properties can also be used [26, 27]. Examples of commercially available FFF filaments include conductive, flexible, carbon fibre filled and metal filled.

Malone and Lipson [28] created the Fab@Home project, in which they designed a multi-material extrusion 3D printer that is open source and low cost. This attempt

to democratise AM has given some excellent results, with the system producing active devices such as electromagnets and electromechanical relays (see 2.3.2). The deposition system is simply a pair of actuated syringes so the results are inexact, but a wide range of materials such as silicone or even chocolate have been printed. For complex, multimaterial objects, process planning is a difficult step as not only are these experimental systems limited, so tools and materials must be changed manually, but also MMAM gives new ways of making parts, so no set way of working has been established. This will continue to be challenging as different technical processes will affect the design and planning stage.

A project carried out at MIT has developed a small 3D printer called MultiFab, which is capable of using up to 10 different materials within a single print, using material jetting [29]. Machine vision is incorporated into this system allowing for material to be printed onto (but not around) existing components. One example given involved creating a handle for a razor blade, though it is worth nothing that this required printing material onto one side of the blade and then manually repositioning the blade to print the other side.

Multi-material stereolithography (MMSLA) has revealed excellent results; due to its high resolution and low layer height micro fabrication is possible [30]. Multicolor examples are the most common although fluorescent hyrdogels have also been used [31]. MMSLA is a complex and slow process however as the object is built submersed within a vat of liquid resin from which it is created [32, 33]. To change the build material the object has to either be removed, cleaned and inserted into a vat of different resin, or the same vat has to be emptied, cleaned and refilled. Therefore, while it is possible to change the material within a layer, or for every layer, it is impractical. In all other AM processes each full layer is completed before proceeding to the next, but in this case large sections could be built in one material before changing it and printing adjacent sections [31]. Unfortunately this created additional problems which must be considered in the process planning. For example this could leave un-built layers of the first material under the second, or the partially built layers could obstruct the laser beam preventing the new material from curing. This is especially crucial when MMSLA is combined with the addition of components or conductive traces. This will be address below in 2.3.2.

2.2.3.3 Digital Materials

In the future 3D printers may no longer simply reshape feedstock material [12]. If machines could deposit and manipulate individual atoms or molecules then they could be fed base elements, combining them to produce any material or object. This is currently just a distant dream, there are a number of challenges to solve, not least the fact that placing individual atoms would be very time consuming. A parallel process is required [34].

In work that could be considered an intermediate step towards this manner of AM, researchers have developed the idea of a Digital Material. Pioneered primarily by two groups, led by Neil Gershenfeld and Hod Lipson respectively, digital materials are comprised of a small selection of basic building blocks which can then be combined to form complex, functional shapes. Using an idea originally borrowed from Computer Aided Design, an object is described by many tiny blocks called voxels (volumetric pixels) [35]. In physical form a voxel can be considered to be like a LEGO block [36]. Voxels can be assembled together to make a larger structure, the bonds can be reversible and they can offer a much larger material set than any current AM system. One key property is that LEGO blocks allow precise structures to be built by children with imprecise motions. By using shapes which interlock and self-align, digital materials can be "error-reducing, error-tolerating and error-detecting" [36]. The same paper also suggests that digital materials bring low cost, simplicity and speed to free form fabrication (i.e. AM) but while this may be true at the meter and centimetre scales, but these advantages do not scale down well. As soon as the individual blocks are scaled down enough to produce relatively high resolution objects the numbers required become huge. For example, if using 20 micrometer voxels to build a $10cm^2$ box one would need 100 billion parts, requiring a printer that can place 1 million blocks in the correct position every second to build the object in one day [34].

Ultralight weight composite structures have been made [37] using digital materials, showing how the density, and other mechanical properties, can be altered by changing the underlying geometry of the voxel [38, 39]. In addition to the advantages given by the geometry of each voxel, the material could be changed on a voxel by voxel level, and standard materials can be used, as they are combined using assembly, rather than curing or melting as in other AM. By combining both conductive and insulating materials, passive electronic devices such as capacitors and inductors have been constructed [40].

By adding resistive materials, any passive electronic component could in theory be constructed, but MacCurdy *et al.* [41] extends this idea further by creating a library of functional blocks. Block types include; battery; short; LED; microcontroller; actuator; flexible joint. By assembling these basic elements, complex electromechanical structures were built, such as a 5-channel infrared remote control, or an inchworm robot. An automated pick and place system was used but it could only manipulate one voxel at once, leading to slow build times. The blocks used are of the centimetre scale and therefore only give very crude, low resolution objects, but the authors state that blocks of 25 cubic micrometers are feasible.

Digital materials offer an interesting method of fabricating functional devices, but they inherently rely upon mass-manufacturing miniature voxels which are then assembled. While combining functional blocks may be appropriate for prototyping, especially due to the reversible bonds, it seems unlikely to become a main manufacturing technique. Unless one is using a very small set of basic voxel types (i.e. conductor, insulator and resistor), the process simply requires existing items, such as LEDs or motors, to be re-manufactured in a specific package such that it can be incorporated into an object being manufactured.

2.3 Integrated Robot Fabrication

AM has matured into a tool which is now commonly used in the design and manufacture of robots, however currently it is used primarily to fabricate passive structural components that form part of an overall assembly. The need for subsequent manual assembly limits the design freedom and speed of fabrication afforded by AM. The author and others envision a future AM system capable fabricating an entire complex robot through a single process, such that it "walks" - fully formed and functional - out of the build chamber [1, 2].

The steps involved in fabricating a fully-functional robot can be broken down into three main categories: building of the physical structure; incorporation of electronics; and incorporation of actuated mechanisms. The layer by layer construction of AM gives the unique opportunity to access the enclosed internal geometry of a part. This gives rise to the possibility of embedding components (motors, sensors, electronics) within object structures - to become an inherent part of the structure. This section will review the current state of the art across these three categories. Following this,

the potential of these technologies to be merged into a systems capable of producing the first generation of single-process robots will be explored.

2.3.1 Joints and Mechanisms

The use of Additive manufacturing gives unique opportunities for creating *in situ* features. As the method gives access to the internal structures of the object being created, it allows voids to be created and interlocking sections to be formed, without the need to consider design for assembly. AM does however have design rules of its own, and while they are not yet so well formalised as other manufacturing methods, careful consideration of the AM method in use is required for successful joints.

2.3.1.1 Mechanical Joints

The first design issue when constructing joints with AM is that the quality heavily depends upon the resolution of the AM machine [42]. The gap between two parts must be as small as possible, without the parts fusing together. It has been suggested that an advantage of *in situ* manufacturing is that the gaps between parts can be controlled directly, rather than being the consequence of two separately manufactured parts [43]. This is not born out in practice however; the resolution and repeatability of the majority of AM system cannot compete with traditional machining. Typically working tolerances must be determined experimentally by the user [3, 42, 44, 45]. Chen and Zhezheng [42] found that the difficulty in the removal of the support structure built between the parts was what limited the minimum clearance, rather than he absolute resolution of the printer. Therefore, they set out to redesign traditional joints to minimise play, while still leaving access to clean out support materials. They used a polyjet 3D printer for their work, which uses a wax-like support material which needs to be washed out with a pressurised water jet. The minimum clearance for a straight pin joint was found to be 0.2mm, but by changing the cylindrical pin to a barrel shape, this gap could be halved. The barrel shape crucially gives access for the water to wash out the supports, and incidentally also improves the stress distribution within the joint. In addition to this they discuss how to apply other features such as chamfers and thin protrusions to optimise other joints for AM. Using this approach they produced a crank slider mechanism that did not require assembly post manufacture.

Lipson *et al.* [44] sought to replicate a collection of classic models using Fused

Filament Fabrication with dissolvable support. They detail a large range of design considerations that goes beyond simply the clearance and support structures. For example some mechanisms rely upon the weight, elasticity or other material property for a component to function, therefore items such as springs, threads and weights required redesigning. Unfortunately, a systematic method is not presented. One noteworthy contribution however is to show how if one prints a shaft, with an axial load, horizontally it will be skewed once the support material is removed due to the relatively large clearances, leading to poor performance and binding. By redesign the shaft to be printed at an angle they overcome this (see Fig. 2.4). Once the supports are removed the initial angle has the effect of giving good tight tolerances and positioning the shaft in the correct place.

Both Selective Laser Sintering (SLS) and top-down Stereolithography (SLA) lend themselves well to the creation of *in situ* joints as the object is built within a vat of the build material (resin or powder respectively) [3, 46]. Being submerged in the build material causes small gaps to be supported purely by this material, rather than requiring solid structures to be built, the excess material is then washed out of the joints after assembly. Mavroidis *et al.* [3] state that there are no support structure considerations for SLS, which is true in terms of building the parts, but care must be taken so that access is still be possible to clean the material out of close joints. This can limit design freedom [45]. While conventional joints have to be redesigned to ensure they function well when manufactured *in situ*, the design freedom offered by AM has enabled the redesign of ball joints to limit the rotations [3, 47]. Researchers used a digital model of the joint, along with the constraints required, and created a program to automate the design [45, 48]. As AM is a direct digital process these files could then be directly printed.

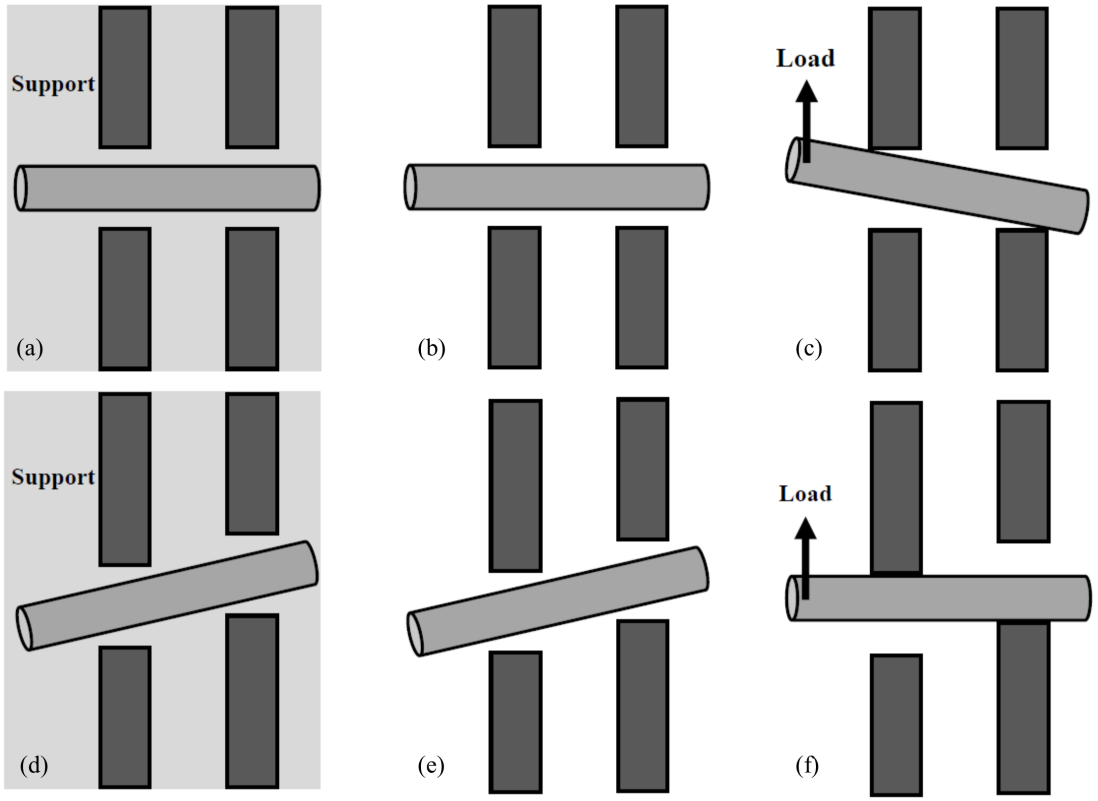

Figure 2.4: Misalignment caused by large gap requirements:(a) A shaft printed with gaps filled with support material, (b) once support is removed, (c) it will misalign when loaded. (d) Shaft misalignment is pre-compensated for so that (e) when the support material is removed (f) the load will pull it into alignment with close tolerances. More complex compensations need to be carried out for more elaborate mechanisms. Adapted from [44]

2.3.1.2 Compliant Joints

The capacity to use multiple materials within one printed object (as discussed in Section 2.2.3.2) allows the use of seamless flexible joints. Researchers 3D printed rigid bodies with sections of rubber-like material to act as joints using the polyjet process [24]. These were then actuated by embedded Shape Memory Alloys. One problem, which is also identified by others who use polyjet technology [24, 49, 50], is that the software does not allow selective support structures. Therefore gaps which are designed for components to be inserted into are filled with support material. In this case the gelatinous nature of the material helped with holding the SMAs in the wire channels.

The researchers found that as the SMAs contracted, the flexible hinge tended to exhibit out of plane bulging, i.e. it compressed, rather than forcing the joint to bend. The longevity of such a joint is also not addressed, but the material is sensitive to UV light so can degrade overtime.

Shape memory polymer (SMP) has also been used to create flexible joints with variable compliance. To do this researchers first needed to create the filament required for use in a FFF 3D printer [51]. This material was then used to develop a robotic gripper based upon a human finger [52]. Stiff bone-mimicking sections are printed using ABS with the joints printed at the same time out of SMP. As the SMP imparts a small force a soft pneumatic actuator provides the gripping motion, and the SMP is used to control stiffness. Compliance is helpful when performing gripping actions as it allows the finger to conform to the shape of the object it is grasping. This can be achieved by heating the SMP, then once the object has been picked up the SMP is cooled, leaving the fingers much stiffer. This provides a more secure grasp, allowing rapid motions of the gripper and higher external forces to be applied, for example in assembly work. The SMP was heated via radiation from an open oven in close proximity which is very inefficient and limits the speed that the gripper can react. A planned development is to embed heaters and wires inside the finger to make a fully incorporated gripper.

Traditional mechanical joints and spring-damper systems can be simplified and combined into one part by utilising MMAM. Consider a humanoid robotic hand, for example. Researchers built two versions, the first of which used traditional assembly and included 60 parts (40 of which were fastenings) in each finger [53]. For the second version each finger was a single part manufactured using a hybrid AM method called Shape Deposition Manufacturing (SDM). SDM is a layer based manufacturing method which involves a cycle of depositing material followed by precision shaping using subtractive methods [54] (Fig. 2.5). This approach allows different materials to be incorporated in a part, and even for components to be embedded inside the structure. It is a complex multi-step process, however, which often is not fully automated. Sensors were integrated into each finger, creating a reliable interface while protecting the sensitive electronics [53]. The joints and finger pads are made of a compliant material, while the link sections are a stiff polymer. This compliance greatly increases the robustness of the gripper; in fact the researchers have released a video of it being repeatedly hit with a baseball bat, with no resulting damage [55]. Researchers also selected the SDM process

for creating bio-inspired robots such as a cockroach [13] and a gecko [14]. While SMD is not a true AM process, they showed that by utilising a flexible material and manufacturing mechanisms as one part, extraneous components can be removed, potential weak spots eliminated, and the overall robustness improved. The inherent compliance in the insect inspired leg enabled the final cockroach robot to navigate rough ground effectively, using an open loop controller.

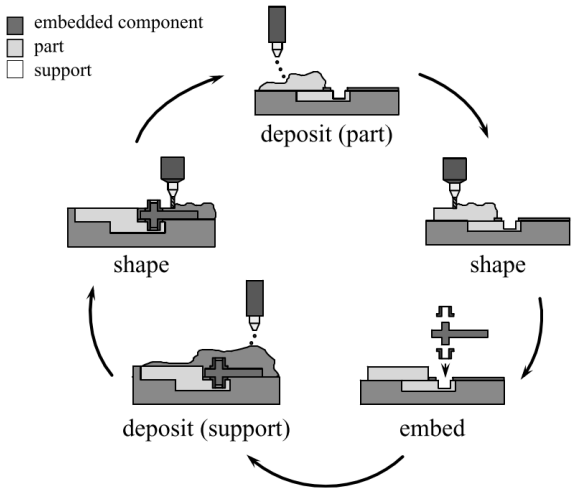

Figure 2.5: Shape Deposition Manufacturing involves both additive and subtractive processes to construct a part. From [14].

2.3.2 Electronics

The ability to print electronics and conductive traces using AM brings rapid prototyping capabilities [56], and would enable functional mechatronic devices to be directly manufactured in one process. Both flexible and rigid circuit boards have to be populated flat, then assembled into the device, AM would remove this constraint and allow novel designs. Wires could be replaced with printed conductive tracks, removing the difficulty of routing wires through complex and tight spaces and reducing the size and weight of the resulting device. In the future many electrical components may be printed from their basic materials, allowing a huge catalogue of parts to be used without the need for each to be kept in stock. Despite this, merely printing conductive connections and inserting pre-made electronic components would still open up a huge range

of possibilities. For the foreseeable future, at least, this will be the preferred method of incorporating electronics into an AM part as the mass manufacturing processes for electronic components are so well optimised [15].

Multimaterial printing has enabled Malone *et al.* [26] to produce a range of electromechanical devices by using combining materials and processes during a build. They used an open source Fab@Home system which uses a syringe to deposit a wide range of liquid, gel or paste materials and a molten-extrusion head to deposit thermoplastics and solder [28]. This enabled the creation of flexible circuit boards, strain sensors, electromagnets [57], electromechanical relays, electroactive polymer relays and even batteries in different shapes [58]. While creating functional electromechanical parts is a huge step for additive manufacturing, the Fab@Home system is low-cost, low-resolution and labour intensive, as processes must be carefully planned and the various materials are manually supplied to the machine. These components were functional, but cannot match the performance of their traditionally manufactured counterparts. For example ionomeric polymer-metal composite (IPMC) actuators were 3D printed in an attempt to make low voltage soft actuators but their performance was one to two orders of magnitude inferior to IPMCs made conventionally [59].

Nano Dimension use a Material Jetting process to enable RP of traditional flat multilayer boards [60]. While this is useful for product development, their printer is not designed to enable innovatively shaped circuit boards which take advantage of the complex geometry enabled by AM.

2.3.2.1 Conductive Tracks

The main options for printing conductive connections can be broadly categorised as: depositing conductive inks; extruding solder; extruding conductive thermoplastic filament or embedding wires. These have been summarised in table 2.3.

Commercial aerosol jet printers are available and have been demonstrated to produce a number of electronics components, including a circuit on the wing of a UAV model constructed via 3D printing [61]. The process uses a mist generator to atomise conductive ink, then aerodynamically focusses it, using a sheath gas, to create a fine flow. Feature sizes less than 15µm are possible and the approach shows great promise for high resolution circuits.

Conductive ink can also be deposited using a pneumatic or volumetric ink dispenser

[62], known as Direct Write (DW) technology. Voxel8 [63] have created an experimental platform which they commercialised as a short run of high end consumer 3D printers that combines FFF and pneumatic ink dispensing to create the first true embedded, 3D, electronics printer. The mechanical system is not particularly impressive here. Rather it is the material and control advances that are key. First, the ink they have created is an order of magnitude more conductive than others and, importantly, cures at room temperature. Second, through a partnership with Autodesk they are offering a CAD program that enables circuit traces to be designed in 3D and for the printer to pause at the correct time to allow components to be inserted. Methods for process planning are still required, while design rules and best practice for laying out circuits in three dimensional space will need to be explored.

At a consumer level, FFF printers are the most common so there is great interest in conductive materials for this process. Researchers have used low melting point alloys, in the form of solder, as filament for FFF printers, which allows circuits to be printed [58, 64, 65]. This is cheap, readily available and can be used in unmodified FFF printers. However it is difficult to control the feeding and cooling rates to give good results [66]. There is much excitement around new conductive filaments that can be used in FFF printers. The filaments are made by mixing a thermoplastic, such as PLA with a conductive material. Graphene and nano-composite materials have been shown to provide the best results but the resistance is still relatively very high. If short traces and low currents are used then functional devices and circuits can be successfully created using this method. An Arduino light sensor shield and single part flashlights have been printed [67]. The fact that this conductive material can be deposited with the same process as the main build material simplifies the task of embedding the tracks within the part and many printers will require no custom hardware. However these conductive materials are far from ideal and the resolution of FFF does not approach that of Aerosol jet or standard PCBs, limiting their application.

Using conductive ink, silicone [68], or thermoplastics all have the inherent issue that a conductive material is suspended within another substance that must be in a semi-liquid state to be deposited and then dried out. Embedding wires is an alternative method of incorporating conductive paths into the AM build process and is appealing due the potential of low cost, low resistance, multicore or shielded wires [69–73]. Wire is difficult to embed, however, as it does not directly adhere to the object and needs to

be in tension to manipulate. Wire has been successfully embedded into a thermoplastic part by heating the surrounding material to soften it and pushing the wire just below the surface [70, 73]. A competing approach has been developed which extrudes the wire (or other fibre e.g. carbon) at the same time as the molten thermoplastic substrate [74]. This method is designed to allow embedding throughout a print with one simple and quick machine. There are difficulties in connecting different lengths of wire, especially across layers and connecting to components is often a separate process such as laser welding or soldering [74, 75]. This has been overcome by integrating a paste extruder into the printer that deposits conductive polymer onto wire joints - this does add some minor resistance to the circuit, 110 and 250 mΩ for interlayer and intralayer joints, respectively [69, 76].

Table 2.3: Comparison of the main methods that have been explored for AM conductive tracks

Technology	Advantages	Disadvantages
Conductive ink. Ink is deposited using a syringe [77], precision pump [68], Aerosol jet [61], inkjet [78, 79] or sprayed using an airbrush [80]. Resistance typically $1 \times 10^{-3}\Omega$-cm [26], Voxel8 $5 \times 10^{-5}\Omega$-cm [63]	Simple to deposit ink with correct equipment. Very fine traces are possible with Aerosol jetting. PLA based masks used to increase resolution with airbrush technique. Direct Write commercialised by Voxel8 [63].	Curing (using heat, chemical or UV) is required to reduce resistance to usable levels [79, 81, 82]. Adding time, complexity and limiting materials [82]. Channels may be required. FFF layers can be porous making liquid hard to embed [72].
Solder Extrusion. Low melting point alloys are heated and extruded in a similar way to FFF printing using thermoplastics, or using Direct Write [64]. Resistance typically $1 \times 10^{-5}\Omega$-cm [26]	Can use standard hardware. Inexpensive and readily available, channel in the substrate not required but helps consistency. Has been fully embedded successfully [65]	Control of feed rate and cooling is difficult often giving non-uniform results.
Conductive thermoplastic filament. A mixture of a conductive material and a thermoplastic in filament form that can be used in standard FFF printers. Resistance ranges from 0.6 to 9 Ω-cm [83, 84].	Works in standard FFF printer. Similar to part material so can be embedded easily. Conductive mechanical interfaces such as plugs and sockets can be made.	Relatively expensive. Very high resistance.
Embed Wire. Standard metal wires are embedded in a part [69–71, 85]. Resistance very low e.g. Copper $1.724 \times 10^{-6}\Omega$-cm	Any wire could be used giving low resistance and the potential for multicore or shielded wires. Very low cost material. Works for high current applications [86].	Requires the substrate to be melted by heating the wire or by ultrasound, limiting it to thermoplastic based processes.

2.3.3 Embedding

The previous sections have shown that there is some good progress in direct additive manufacturing of a wide range of components which are required for robots and other mechatronic devices. They all, however, fall short of the capabilities of a component (e.g. motor, battery or bearing) which is manufactured using the current mass manu-

facturing process for each. Therefore it is logical to attempt to take advantage of both manufacturing methods by embedding common, yet complex, components into a device as it is being built using AM.

This has been demonstrated previously when discussing conductors (Section 2.3.2.1), the method which was the most electrically functional is to embed wires. Larger components than this however interfere with the usual build process for AM and therefore additional process planning and modification is required [46, 87]. The simplest method to embed a component into an AM part is to leave a cavity in the design, then pause the printer and insert the component, before continuing the print. However this simplistic method only works in specific circumstances. 3D printers are designed to work with flat horizontal layers, so the top of the part being built must always be flat to avoid collisions with the print head or recoating wiper arm, seen in Fig. 2.6 (a). Therefore a component cannot be inserted into a cavity until the build level is taller than the component. However, if the upper geometry of the part is convex, then the cavity is enclosed by the time the build level is tall enough to shield the component (Fig. 2.6 (b)).

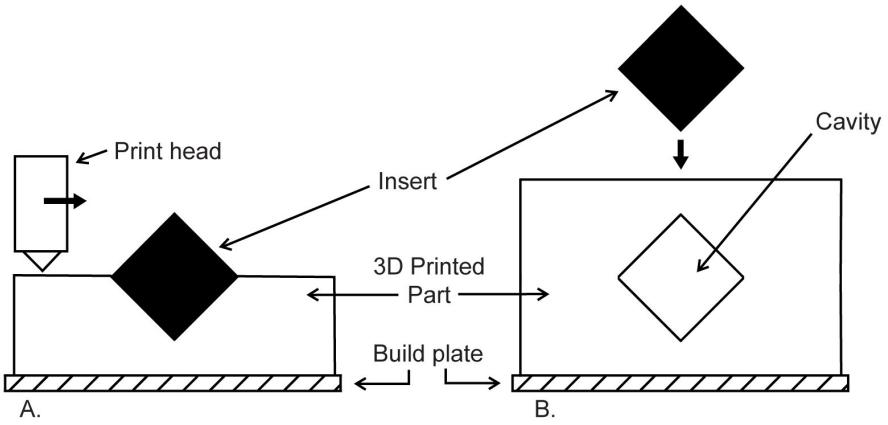

Figure 2.6: Issues with inserting complex components (a) Print head collides with protruding insert.(b) Insert cannot be embedded until the build is as tall as the insert, but by that point the cavity could be enclosed when parts have convex tops.

The AM process used significantly impacts embedding components. SLS builds objects in a heated vat of powder, so to embed an object one has to print a place holder for it, which is then removed when the print is paused, leaving a void for the insert.

This has been demonstrated manually [88, 89], but due to the high temperatures and difficulty of working in powder it has seen little further work. Another factor which may have influenced this is that between each layer a mechanical wiper arm sweeps powder across the top of the build. If the insert was at all proud of the surface it would cause damage to an expensive machine. Components with holes or cavities offer additional challenges as they must first be sealed to stop material ingress. This is especially significant for SLA and SDM where components must be immersed in liquid resin [4, 46]. There are however a number of examples using these processes. Early work showed how a range of components, such as gears and nuts could be embedded, these were combined with *in situ* joints to build a moving model of the stereolithography machine that printed the parts [4] and a robotic buggy [46]. Electrical components and silver ink tracks have been fully embedded in an SLA block [31, 90]. As the components which were covered are rectangular, no special consideration was required for embedding them, but the surface did have to be manually cleaned before the silver ink was deposited and vias were filled manually. While SDM is a hybrid process, the additive nature of adding material sequentially allows components to be embedded. It has been used extensively, although less recently, to enable multimaterial robotics with embedded components. Examples include; a robotic hand with embedded strain sensors [53, 91, 92]; a bioinspired cockroach robot [13, 14, 93–95]; a gecko robot with flexible joints and embedded tactile sensors [96, 97]; an underwater vehicle [98]; a trike with an embedded tube and pin [99]; embedded flexible sections [100] and non-assembly sliding mechanisms [101]. The ability to embed sensors gives greater robustness and ensures that the sensor is fully attached to the surface so can give more reliable results. Embedding has also allowed fully waterproof designs [102].

Based upon the devices reported in literature, embedding functional components is currently the most effective method for creating integrated mechatronic devices which require no post fabrication assembly. It is also the method with allows the widest range of materials to be used in a design. Metal AM is starting to be used in production, yet there are no multimaterial systems that include metal. By embedding metallic components the mechanical properties of a part could be changed, for example by increasing the stiffness, or changing the centre of mass [103].

2.3.3.1 Shape Converters

Much of the literature which involves embedding components skirts around the constraints imposed by building using horizontal layers, such as being unable to let the component protrude above the build level. Components with convenient geometry, such as surface mount electronic components in rectangular packages are often embedded due to this. When a cavity is left for an insert, vertical side walls are required so that the component can physically slide into the void, and so that a protruding section does not block the material deposition - which comes from above.

To overcome these issues Shape Converters have been developed (Fig. 2.7) [4, 104]. These are additional parts that fit around the component, converting its geometry to have vertical sides and a horizontal top, allowing the part to be inserted without protruding. While shape converters are functional, they add additional process planning and assembly steps to the fabrication process. The Shape Converter must be designed (it could have a complex shape) and manufactured, before being manually attached to the component, and lastly inserted into the main build. The assembly and insertion process could likely be automated, but this has not been shown in literature.

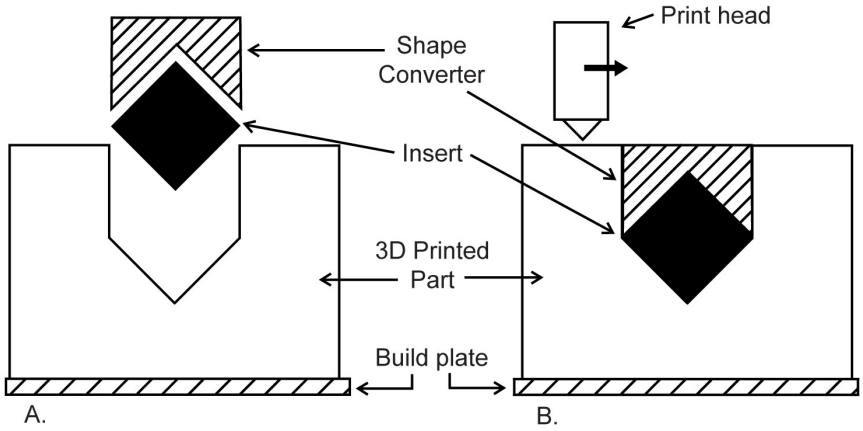

Figure 2.7: A Shape Converter is assembled with the component to be inserted, converting the geometry to vertical sides and horizontal top, avoiding collisions.

2.3.3.2 Multiaxis embedding

It is clear that the limited range of motion of the print head is often what complicates and limits embedding functional components. Conventional 3D printers are 3-axis machines yet their deposition tool paths are 2.5D. That is to say, while the print head can translate in all three dimensions, deposition only happens in two dimensions, in the x-y plane. The print head[1]then moves in the Z axis, before then next two dimensional motion is performed to deposit the next layer.

If the tool head possessed more degrees of freedom (DOF) then it is feasible that it could follow the contours of a component and print over and around it. This concept has been the subject of some research which shows that the concept is sound, but the studies or machines have been limited in scope or capability. This idea of 3D printing using more than 3 DOF will be termed 'Multiaxis' AM (MAAM). A few examples of this being used in practice for embedding are given below and the concept is explored further in the next section (2.4).

Lee et. al. [103] created a hybrid system combining both machining and FFF on a 5-axis machine. Figure 2.8 clearly shows how the additional rotational axes allow the nozzle to print around a component, which would require a shape converter if it was to be printed around or embedded using a 3-axis machine.

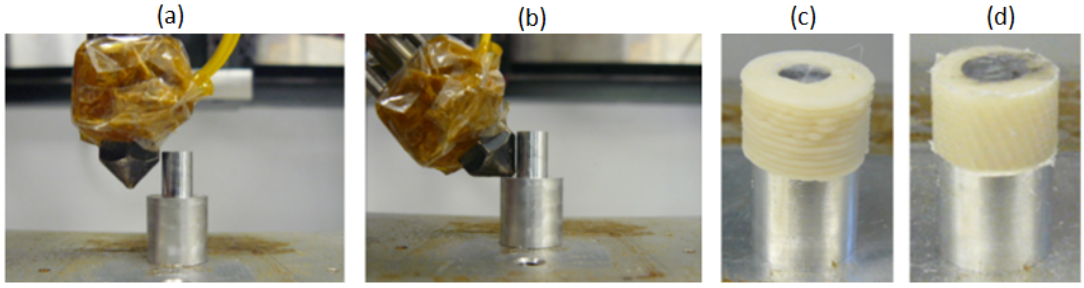

Figure 2.8: (a) 3-axis machine cannot reach but (b) a 5-axis machine can. Aluminium embedded before (c) and after (d) machining. From [103].

Also utilizing FFF, but using a 6-axis Stewart mechanism, printing single lines onto shallow curves and slanted surfaces has been demonstrated [105]. This work shows

[1]A range of machine geometries are possible but the deposition effect is the same. The print head could be stationary and the build platform can move in 3 axes, or vice versa, or more commonly, some combination of the two

that a 6-axis printer could give great advantages but the hardware and mechanism used limits this printer so that the experimental results show a marginal increase in capability over a 3-axis machine using full 3D deposition. Figure 2.9 shows this system. Keeping all six linear actuators within their travel range and the frame and platform joints within theirs are the major constraints upon the freedom of motion of the platform. The paper illustrates how the workspace is smaller when there is a 10° tilt around the X axis and states that the maximum tilt is ±30°. This is the limit at which three axis mechanisms begin to struggle due to nozzle geometry [106] so there is no real improvement.

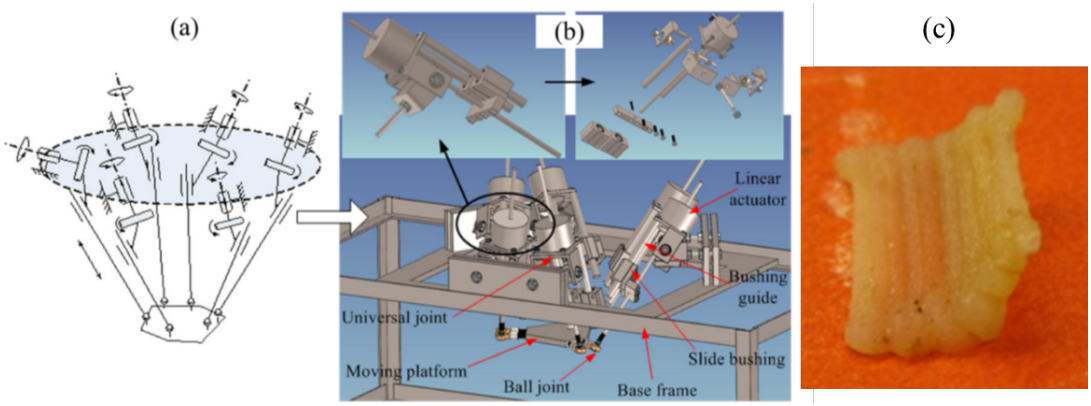

Figure 2.9: (a) Schematic mechanism of a Stewart mechanism and (b) the CAD design on their system showing the rods, universaljoints and ball joints which limit workspace. (c) A sample printed with the system shows how angled layers can be printed but this sample could be printed using an unmodified FFF printer. From [105].

The third example of multiaxis embedding uses an AM method called CNC accumulation. This is a layerless variation of Vat Photopolymerization. A UV LED is manoeuvred inside a vat of resin using a 5-axis system. This allows the resin to be cured at any point within the vat, rather than just at the top or bottom as in conventional SLA or DLP. This enabled the researchers to print upon existing items; they repaired a broken tooth from a gear and added text to the outside of a teapot. It was only possible to print onto the complex surfaces due to the 5-axis deposition [107–109].

2.4 Multiaxis Additive Manufacturing

While embedding components is an excellent application of Multiaxis AM (MAAM), researchers have been pursuing it for the benefits it can bring to fabricating standard mechanical parts. AM has three significant disadvantages; the stepped effect from discreet layers, the anisotropic strength characteristics due to the joins between the layers and the need to use support material on overhangs or orphaned sections (Fig. 2.10). These issues, and the way MAAM can combat them is illustrated in Fig. 2.11. The use of support material increases the complexity of a print as additional post-processing steps are required and the part must be designed in such a way that the material can be removed. The use of high temperature, or high strength part materials like metal or ceramics can make these supports complex to remove [110].

The stair step effect on AM parts is most obvious on curved surfaces. The main method that is in use for improving the surface quality - apart from post processing - is to reduce the layer thickness [111], but this leads to more layers being required and longer build times. Curved layers have been suggested as a method to improve both the stepped effect and the strength of certain parts [112]. When using FFF the bonds between layers are weaker than tracks across a layer [7, 113], so by printing layers which conform to the surface geometry of a part the position and angle of these weaknesses can be changed, increasing the strength in a specific direction [106](Fig. 2.11). The weaker bond between layers could also mean that there would be a higher resistance along a conductive trace printed in layers, as opposed to being continuous using curved layers [114, 115]. This has not been verified in literature using conductive polymers however.

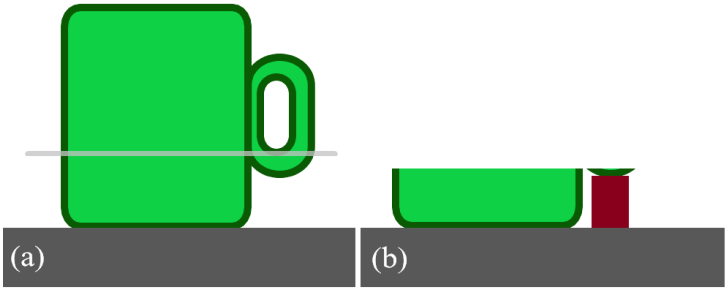

Figure 2.10: If a section of a part attaches to the main body higher up, then it begins printing as a 'orphaned part'. In this case (a) the handle of the mug connects to the mug at the layer shown by the grey line. (b) It will require a support structure to begin printing and stay secured to the build plate until it joins up.

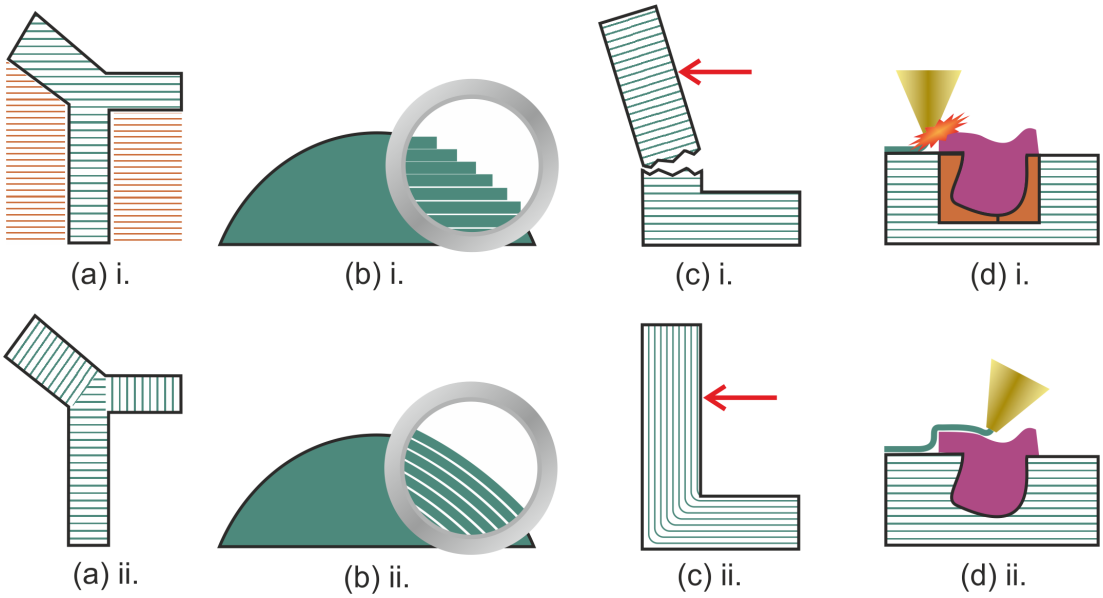

Figure 2.11: Conventional planar layers impose these disadvantages upon AM (a,i) Anisotropic mechanical properties due to weaknesses between layers, (b,i) Surfaces approximated by discrete steps, (c,i) Overhanging surfaces require support structures and (d,i) Embedding components is limited in complexity and scope. Whereas Multiaxis Additive Manufacturing could deposit non-planar and non-horizontal layers, overcoming these limitations. (a,ii) Layers can be optimised to improve strength, (b,ii) Using either curved layers, or by changing the build axis orientation, surface roughness can be reduced. (c,ii) Dynamic build orientations allow unsupported overhangs, (d,ii) Existing objects can be printed onto and around without manual steps.

2.4.1 3-Axis Nonplanar Layers

While theoretical algorithms for curved layer slicing was developed earlier, the first implementation using FFF was by Singamneni and Huang [112, 116]. They used 3-axis systems to print very shallow curved arches and compared these with the same shape printed with horizontal, planar layers. The curved layer arches exhibited significantly higher maximum loads (40% [112] or 52% [116] higher, using ABS) when subjected to a three point bending test. This curved layer slicing algorithm has been extended to work alongside conventional adaptive slicing [117, 118]. Adaptive slicing is where the layer thickness is varied depending upon the curvature of the outer surface of the part. Thick layers can be used on more upright sections and thin layers can be used for shallow angles where steps are more apparent. The authors found that using one thicker curved layer, rather than several thin ones made bridges fail under a slightly higher load. This is expected due to the weaker interlayer bonds, but shows a possible of advantage of curved layers in that it allows the use of thicker layers without compromising upon the surface roughness of a part.

The effect on the surface quality, or roughness, has received less quantitative work. One of the earliest examples is code posted on a hobbyist website [119]. This script post processes code which has been sliced using 'vase mode'. This mode is a feature common across a number of standard 3D printing software which prints an object with one continuous outer wall. The code applies a sine wave to all the Z values, using the layer number to vary the amplitude. This gives the effect of of having standard flat layers to start, which get increasingly wavy. This leaves a smooth top surface, where usually the non-continuous layers would have left a stepped, rough surface. Figure 2.12 (A) shows one example. This has been expanded to a whole surface [106] rather than a thin wall, but the algorithm is not generalised to arbitrary shapes. The finish of a two directional curved surface shows promising improvement however (Fig. 2.12 B & C). While there are still steps present on the surface, due to it being built up of a raster tool path, these have a fixed resolution of 400µm- or the nozzle diameter - while the steps on a part printed with planar horizontal layers are a function of the incline angle [106].

The curvature of all of these examples has been limited to shallow curves, Allen and Trask [106] state their system is limited to printing up to 40° due to the shape of the nozzle, but as the flat tip of the nozzle plays a significant role in flattening the

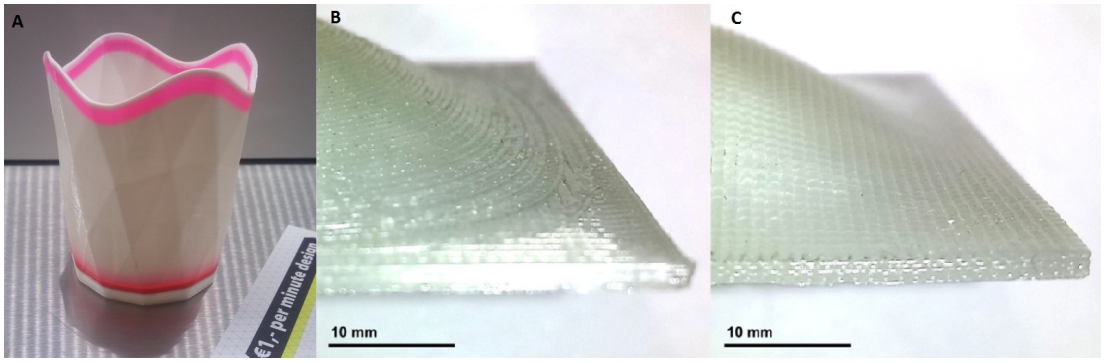

Figure 2.12: Curved layers printed using 3-axis FFF machines; (A) A vase with a sinusoidal top surface generated by editing the Z values of standard gcode [119]. (B) Manufactured using conventional planar layers, (C) has the surface layers printed using Curved Layer FFF (CLFFF), showing an improved surface (B and C adapted from [106]).

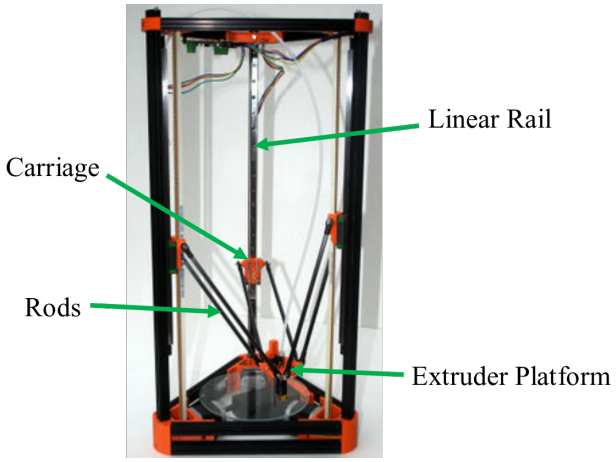

Figure 2.13: A typical delta style 3D printer. The three vertical linear rails also form the frame of the printer. Carriages move linearly along the rails and are connected to the central platform with rods. Changing the height of the carriages moves the extruder platform in the XY & Z axes. From [120].

tracks of plastic, effective deposition is only possible up to 30° inclines. The edges of the nozzle tip interfere with the plastic when it is not normal to the surface. The design of standard Cartesian machines also limits the curvature of a part [116] due to a large time penalty, as the Z axis has a considerably lower movement speed than the X and Y axes. This is why in later research a delta style 3D printer is used [106, 121]. These

machines use a type of parallel mechanism which has three vertical linear rails. Rods attach to each of these and suspend the extruder between them, a typical example can be seen in Fig. 2.13. Unlike Cartesian 3D printers, which use different motion systems for the XY and Z movements, this can move the extruder rapidly in all three axes. This makes printing using full 3D deposition quicker but does not enabling a wider range of angles. Visual comparisons with a range of shallow curved surfaces show an improved surface finish, but this is not quantified in any way [121].

2.4.2 3-Axis 3-Dimensional Deposition

By moving away from the 2.5 deposition strategy, one is no longer limited to layer based printing. If plastic which is extruded in the FFF process is cooled rapidly, self-supporting strands can be produced.

Students from the Institute for Advanced Architecture of Catalonia experimented with FFF printing in quite an artistic and conceptual manor, in a project named Pet Flakes [122]. In their builds each line of plastic is carefully controlled as they aim to show the concept of a new building technique. Long strands of plastic, rather than thin layers, are extruded in 3D space to form spirals and domes, seen in Figure 2.14 (a). Initially the hot end of an extruder was moved manually, but the movement speed and feed rate of the plastic must be more carefully controlled. The use of a 3-axis milling machine mechanism enabled more repeatable results. These revealed that the nozzle deformed the geometry of the strands when it extruded vertically. The use of computer vision to detect deformation and then adjust the subsequent connection points is mentioned but no technical details are given. This work makes good progress in non-layer based AM, but there is little numerical detail. For example simulation results are only shown pictorially and information such as the optimal temperature, feed rate and print speed are missing.

A more practical use for 3D extrusion has been developed by Mueller *et al.* in the project WirePrint [123]. They have developed a method to print wireframe previews of parts to speed up the design process. They argue that these low fidelity models can be used to check ergonomics and other properties before additional time and cost is invested in a full resolution print. A 10-fold decrease in print times compared to layer based printing is demonstrated, allowing designers time for more iterations. Additionally sections of conventional layer wise printing can be included allowing details to be checked,

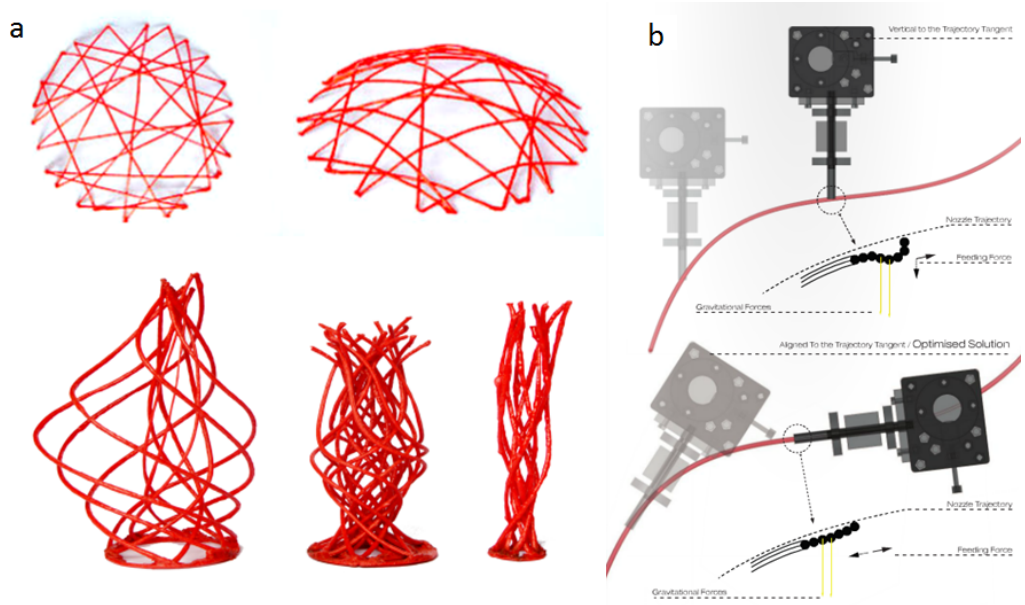

Figure 2.14: Architectural concepts formed by extruding plastic in three dimensions using a 5 & 6 axis mechanisms. (b) Graphical depiction of one benefit of non-vertical nozzle orientation. From [122]).

seen in Fig. 2.15 (b). The wire frame pattern is generated by slicing a 3D object into horizontal slices, the contours of these are then extracted and a zigzag pattern fills the gaps between the slices. The main challenge identified in printing wireframes is stopping the print head colliding with the previously printed material. They must ensure that this does not make some of the volume inaccessible before it has been printed on. The width of the print head sets the minimum spacing between vertical edges, and the angle of the nozzle limits the steepness of downward slopes, so some geometries cannot be printed. An overhang of 90° and 6.5cm in length has been shown. This is achieved by pausing the print head to keep the strand under tension until it is fully solidified. This technique is also used at the top of the vertical strokes to stop warping. Air jets are added to speed up cooling, which can be turning off when the filament needs to stick to another section. This printing technique gives more repeatable results than the architectural work described above but the use of only 3-axes does add geometrical constraints to avoid collisions.

Kanada [124] contends that parts have a 'natural direction' for printing but this often is not the vertical one this is currently used. A theoretical method is presented

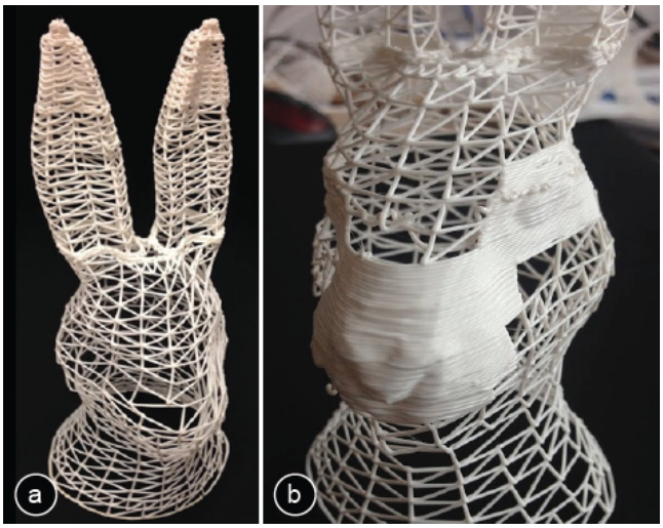

Figure 2.15: WirePrint (a) The basic shape of a design can quickly be printed and checked by carefully controlling cooling while making 3D depositions. (b) Additional details can be printed using conventional planar layers. From [123]

which involves sectioning the model, so that it is printed in an order which doesn't block access to other sections of the model. These sections are then 'hashed' into strings, which are then printed. This theoretically creates a part which has many strings of filament going along the desired direction of the part. The ideas are all very conceptual, there is little thought about how this could practically be achieved and there are several unsubstantiated claims with no reference to any related literature. A chain of rings is printed however, using a 3-axis delta printer and a simplified version of this slicing method, shown in Fig. 2.16. The rings are all oriented at slight angles from horizontal, so that they link with each other. The layers for each ring are oriented along these same angles, so there is no stair step effect on any of the rings. This concept of using flat layers but adjusting their angle to follow the geometry of the object is sound and potentially very useful (see Section 2.4.8), but the author of this paper fails to explain this well or convince the reader of its advantages. He does however suggest that a needle like nozzle or a 5/6-axis machine would increase the range of geometries that could be printed.

A further example of 3D deposition uses direct writing of silver ink to produce self supporting features [77]. These are micron scale bridges of ink which can be used to

make electrical connections. By depositing high viscosity, ink in an arch, electrical connections can bridge over existing tracks, allowing complex circuits which would normally require a multilayer board.

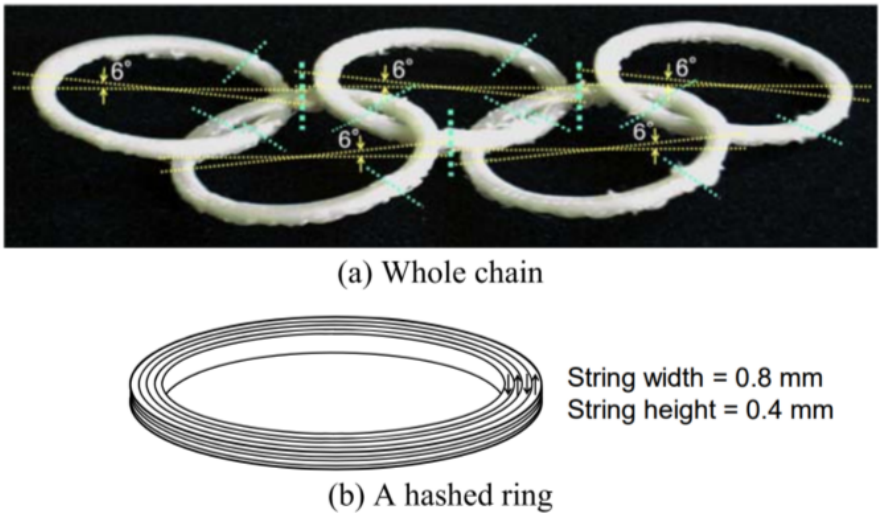

Figure 2.16: (a)Chain of rings printed using layers which are not horizontal removing the stepped effect usually seen on tilted surfaces. (b) Each ring if formed of the same sequence of 'strings' just in different poses. From [124]

2.4.3 Multiaxis freedom

While it is clear that three dimensional deposition can be achieved with a standard 3-axis 3D printer mechanism, extending the manoeuvrability of the nozzle can give more design freedom, as mentioned in Section 2.4.2.

An example which illustrates this well is how a 3Doodler [125] has been used. This is a hand held 3D printing pen which extrudes plastic in the same way as a FFF printer - shown in Fig. 2.17 (a). Users can therefore print plastic in any direction. One user, DeRosa [126], used it to print a hexacopter by printing around the components, shown in Figure 2.17 (b). He explains; *"I am the computer, and not only is my extruder free to move on all axes, but so is the object being printed. I can pick it up and work on any angle at anytime"*.

If one could combine this freedom, with the precision and repeatability of computer aided extrusion it would create a very capable 3D printer.

Others have realised the limitation that a 3-axis system imposes. The Pet Flakes project [122] (introduced in Section 2.4.2) decided that the nozzle should follow the tangent of the curve being printed (Figure 2.14 (b)). This stopped the nozzle contacting any extruded parts, helped the plastic strand to cool evenly and stopped the pressure from the nozzle deforming the strand downwards. To enable this two motors were added to the original 3-axis stage, rotating the nozzle around X and Y, but later a KUKA 6-axis robot arm was used as synchronised movement between the axes was simpler. When printing curved layers using a 3-axis machine the curve angle is limited to around 30° (depending upon the specific system) as the flat end of the nozzle interferes with the layers once it is no longer normal to the surface [106]. Therefore, to extend curved layers to a larger range of geometries and applications, 5 or 6-axis mechanisms are suggested [106]. To embed wires into the curved surface of a FFF part a 4-axis stage was used [71]. By synchronising the movements of a rotatory stage and a 3-axis Cartesian stage, the ultrasonic horn, which embeds the wire, could be kept perpendicular to the surface. They suggest that the platform could be extended to enable the 5th axis, and possibly incorporate a range of subtractive and additive technologies.

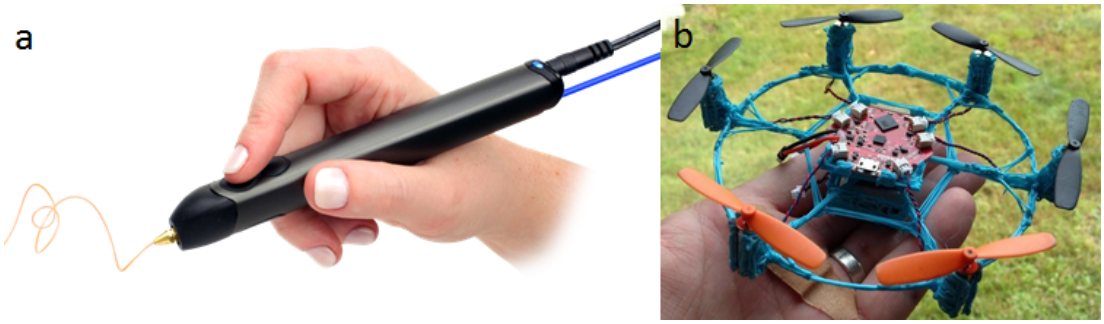

Figure 2.17: (a) 3Doodler 2.0 3D printing pen [125] which was used to make a (b) hexacopter created with embedded motors, benefiting from the increased dexterity of manually manipulating both the extruder and substrate [126]

Multiaxis AM has been realised for the process category of Directed Energy Deposition (DED) for a number of years [127–129]. Much of the early work in slicing algorithms and process planning for MAAM is for these systems (e.g. [130–133]). It is commonly used for repairing existing components [134] but this process is typically used for metals meaning that the high temperatures involved make it unsuitable for use when embedding mechatronic components. When printing a curved overhang with

angles up to 45° the system can reduce the support structures required by roughly 80% [135]. A similar system was used to produce free standing branching, slender structures using continuous deposition, instead of discrete layers [136]. This is significant because these types of structures could result in large amounts of waste material if machined or 3D printed with support structures.

The capabilities of a multiaxis 3D printer are affected by which mechanism is used to give the nozzle 5 or 6 axis of movement. The next three sections will address the main categories which have seen work; Parallel robots, Cartesian stage systems and Serial robot arms. The first is usually used for pick and place operations as fast motions are achievable, the second uses a familiar setup commonly used for 5-axis CNC milling machines. It is compact and accurate, but have small work spaces and are not very flexible. Robot arms on the other hand, have seen less use for machining due to being a lower stiffness mechanism [137], but can have very large workspaces and have been used for a huge range of manufacturing tasks.

2.4.4 Parallel MAAM systems

Song et. al. [105] recognise that 3-axis AM has limitations including the stair-stepping effect and difficulties while building around inserts. Therefore they explore a low cost solution to creating a 6-axis mechanism that could be used for "multidirectional" AM. A Stuart mechanism, comprised of 6 linear actuators, is used to move the print head. The mechanism used has already been introduced in Fig. 2.9. The low cost components caused backlash and other errors meaning the tight tolerances for printing thin layers were not possible. Therefore a feedback system was created using a laser and camera to measure the gap between the nozzle and the surface. Using this system they demonstrated a free standing spiral and a slanted surface showing the use of layers which are not horizontal. One advantage which has not been demonstrated in other literature is the possibility of combining standard flat layers, along with non-flat layers to improve the surface finish. This is shown in Fig. 2.18. This work shows several of the advantages of the use of 5-axis mechanism, but they do not explain why a 6-axis mechanism is used. Additionally, even if the examples were not held back by the low cost mechanical system and the need for better process planning software, the parallel mechanism has a very limited range of motion compared to Cartesian and arm systems.

Mitsubishi researchers have used a delta 3D printer with two additional rotation

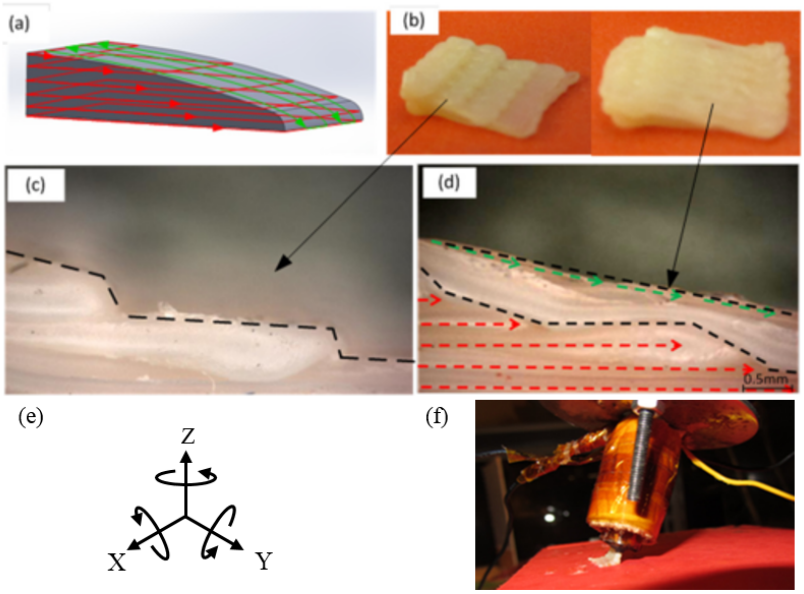

Figure 2.18: Improved surface finish using multidirectional AM: (a) Planned tool paths, (b) the part build using two methods, (c) side view of the steps caused by standard horizontal layers, (d) side view of the surface smoothed by printing confromal layers along the contor of the surface. (e) The 6 DOF along which this mechanism can move allowing (f) the nozzle to tilt away from vertical. From [105].

axes on the base plate to print curved layer domed caps [138]. These can resist pressures 3-5 times higher than domes printed using planar layers. The curved layer domes are approximately 50% of the strength of injection moulded ABS parts.

Another example of a desktop 6 DOF printer has been proposed [139]. Its unusual design is called a Cartesian parallel robot. This is a configuration that has 6 arms that can move along 3 linear Cartesian axis, shown in Fig. 2.19. By change the distance between each pair of arms the extruder can be positioned and oriented in 6 axes. The advantage of this mechanism is that the kinematic model is relatively simple compared to other 6 DOF mechanisms and serial robots. The authors of the paper are in the process of building one of these machines for the purpose of AM. As with the previous example the maximum angle the nozzle can tilt to is low, around 45°, although this may be enough for some applications.

In some innovative work directed at rapid prototyping, Peng *et al.* [140] extend their previous work 'WirePrint', seen previously in Figure 2.15, to provide on-the-fly printing.

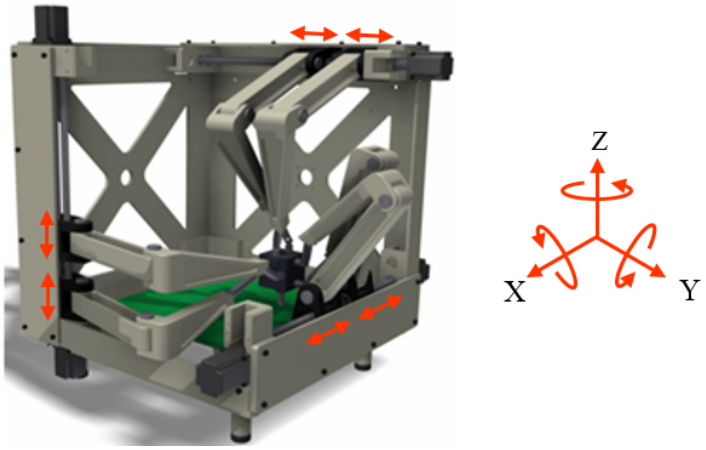

Figure 2.19: Mechanical design of the Cartesian parallel 6 DOF 3D printer named 'Hexapteron'. The Cartesian parallel mechanisms uses pairs of arms which travel along the X, Y & Z axes, enabling 6DOF of motion. However the platform cannot rotate around each axis fully as the hinges and arms would reach their limits before this point. From [139].

In parallel to the user creating a CAD design, the system will print a low fidelity physical model, allowing design choices and dimensions to be verified extremely rapidly. To increase the speed, the extruder was equipped with an extended and widened nozzle. This mean that larger sections could be printed but required two atomizing nozzles to spray water onto the strands of plastic to increase the cooling rate. A heated cutting tool is also incorporated, allowing the designer to remove sections and work iteratively. Two additional rotational axes were added to an off the shelf delta printer, allowing the designer to add to the design on any side. The multiaxis abilities are also demonstrated when printing a curved tube. Rather than just using horizontal layers, which do not represent the shape well when printing low fidelity large cell structures, non-parallel slicing is utilised. The printer rotates the model as it curves so that the current section is always printed upwards. The software is created using a customised plug-in for the CAD software Rhino [141], this is a commonly used software across a range of research groups. The system is referred to as 6 DOF, extrusion being counted as 1 DOF in addition to the 5DOF motion, but this is a misleading description which should be avoided when discussing multiaxis AM. A 6th DOF in the motion system would impart additional functionality and material deposition is a given for any AM system.

2.4.5 Cartesian MAAM systems

A 5-axis hybrid system was introduced when discussing embedding (Section 2.3.3) as it enabled printing around a shaft, something that was only possible by rotating the extruder [103]. The aim of the system was to combine the accuracy of machining with the geometrical freedom that AM brings. The processes works by printing using very thick layers, then machining the part to the correct dimensions. They concede that high quality FFF printers may give smoother results than their hybrid system, but they reduced the print time by 44% and 58% in two test cases. For rapid prototyping applications this is significant. This process just used conventional 3-axis AM and 5-axis machining however. An additional 5-axis AM example was also included which clearly shows another of the main advantages. An overhang is printed without support material. Seen in Figure 2.20, the build platform is rotated so that the section being printed is always vertical. This speeds up printing, reduces cost and removes the post processing step compared to conventional printing with support structures.

An unsupported 90° overhang which incorporated some curved surfaces was also demonstrated by a different group more recently (2017) [142]. By using the motion system from a 7 axis CNC milling machine and adding a narrow FFF extruder they produce a high quality part, and are able to reduce the effect of steps by using the two build orientations. They state the print time was reduced by 75% due to the removal of the support structures. While their system is successful, and will be applicable to their future aims of developing multi-axis trajectory planning algorithms, there is little novelty in this paper compared to other previous work, such as [103].

A similar hybrid system has been created at the Missouri University of Science and Technology [133]. Known as the laser aided manufacturing process (LAMP) it combines a metal deposition tool and a machining tool. This allows the AM parts to be post processed, giving a high quality surface finish but keeping the advantages of AM such a minimal waste material. In addition the system allows 5-axis motion so the parts do not need to be made using standard 2.5D deposition, again removing the need for support structures. This can be seen in practice in Figure 2.21.

Computer Numerically Controlled (CNC) Accumulation been developed in an attempt to make a layer-less AM method [107]. A deposition tool based on fibre optic cable is moved through a tank of resin. In this way UV light can be selectively used to cure parts of the resin. The tool head is controlled by off the shelf CNC software

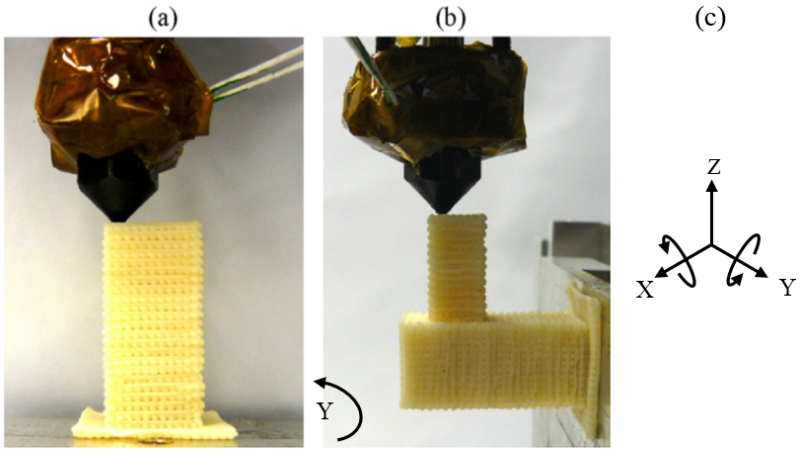

Figure 2.20: Support Free overhang enabled by 5-axis AM. By first printing the (a) vertical section then (b) rotating the build plate around the Y axis, a horizontal overhang can be achieved without requiring any support structure. (c) The extruder on this machine is also able to rotate round the X axis, enabling 5-axis motion. From [103].

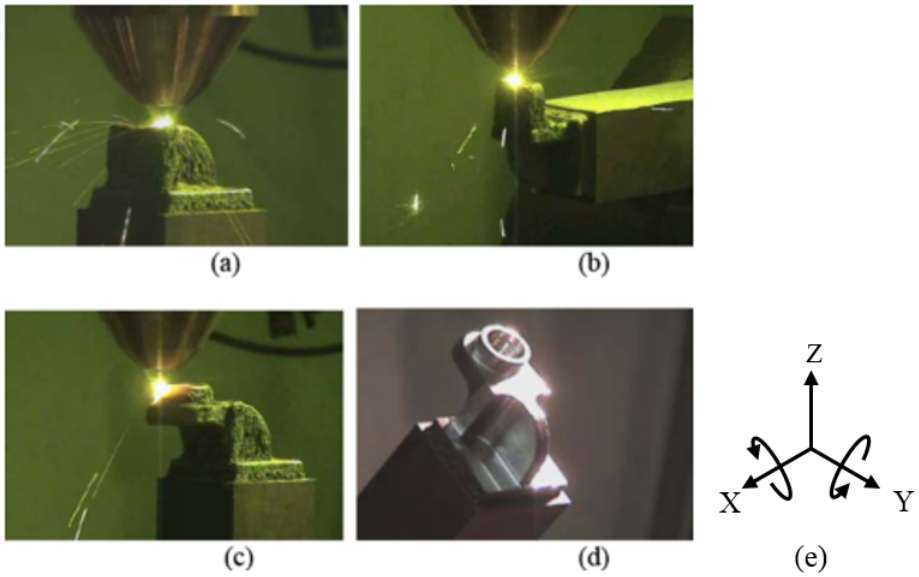

Figure 2.21: (a) Laser Aided Manufacturing Process. (b) & (c) The part can move in 5-axes allowing the overhang to be unsupported. (d) Part post-processed with CNC milling. The hybrid process makes fully dense metal parts for final use. (e) The build plate is able to rotate around the X & Y axes. From [133].

and can move in 5-axes to enable continuous, rather than layer based deposition. This system was then extended to print upon existing parts [108]. The challenge here is to find the exact position of the existing part so that the tool head does not collide with it and prints in the right place. To do this a custom 3D scanner was implemented which uses micro-electro-mechanical systems (MEMS) to adjust the position of a mirror and scan a laser across the surface of the object. A webcam was then used to detect the variations in the reflection of the laser. Using this system a gear with a broken tooth was repaired. This clearly shows the great potential this kind of system has. The researchers added a small head for intricate prints, a larger head to speed up large deposits and a curved head to allow printing on vertical surfaces [109]. CNC machines many sizes of milling tool as standard, but most AM processes use one print head for all operations. The print quality was also compared to SLA printing for an angled rod. Figure 2.22 clearly shows that the lack of layers with CNC accumulation gives excellent results. The print time was also greatly reduced at just 16 seconds, compared to 25 and 60 minutes for SLA with 0.1mm and 0.05mm layer heights respectively. CNC accumulation works well for repairing parts made of the same material and that can be submerged in liquid, but using these resin methods for mechatronic devices would not be practical as the components have to be sealed [4].

Modifying existing 3-axis systems is a common way to experiment with 5-axis 3D printing. A masters student at the University of Oslo has modified an RepRap Ormerod (an open source 3-axis printer) to have two additional rotation axes on the build plate [143]. 3D printing the modifications contributed to some accuracy issues, but once a second iteration was designed the printer was able to produce prints demonstrating two advantages of the system. Firstly curved layers were printed over a hemisphere. Microscope images showed how this smoothed the surface, removing interlayer steps and the print time was also reduced compared to flat layers. The surface was not completely smooth however. This could be due to the resolution of the gcode as curves are actually made up of many short straight lines. The flat surface around the nozzle orifice could also have caused slight facets as it is designed to flatten the plastic. Secondly a 90° overhang was printed by positioning a shaft perpendicular to the nozzle, then continuously rotating it while extruding and lifting the nozzle in the Z axis. This formed a platform which could then be printed on conventionally. Creating gcode which would work with the system was challenging. At first a CNC program (HMSWorks) was utilised to

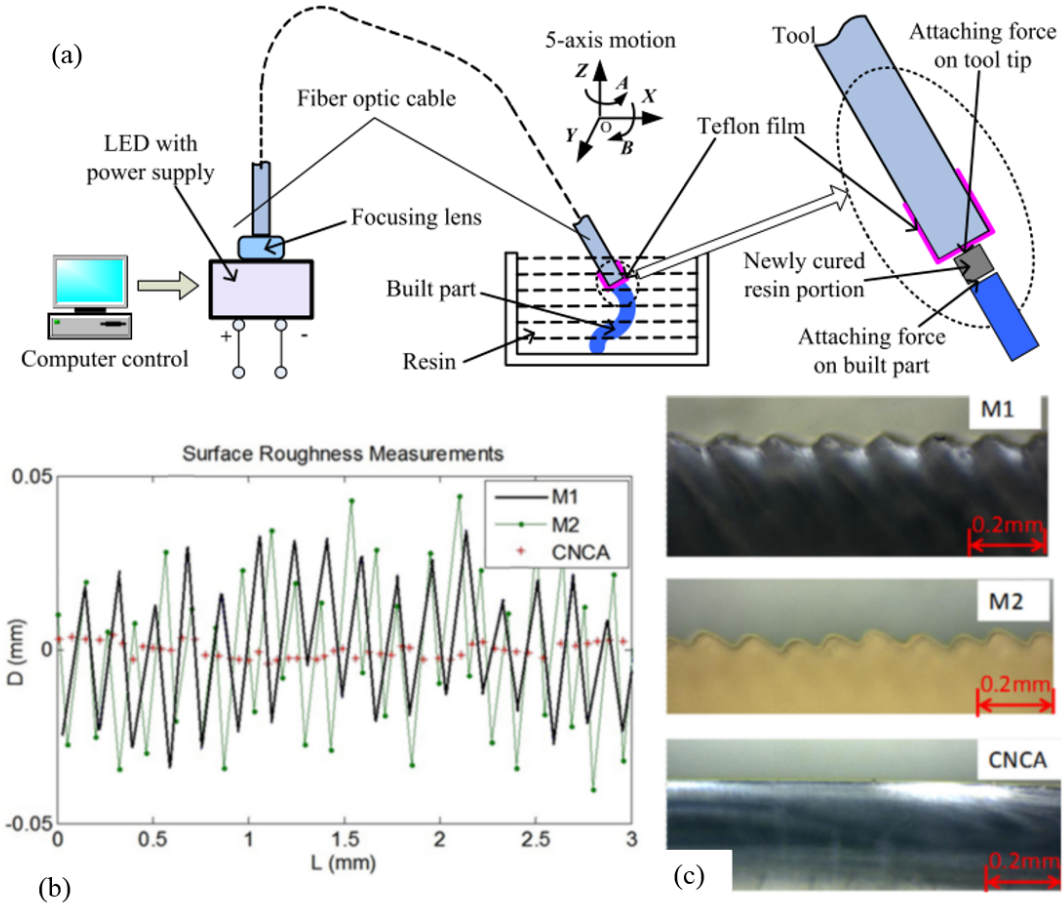

Figure 2.22: (a) Schematic of the CNC accumulation process, showing the 5-axes that the tool can move through, allowing the angle rod to be printed continuously. This yielded surface roughness improvements due to layerless AM. (b) Surface roughness measurements and (c) images of the up-facing surfaces of angled rods printed using SLA and CNCA. From [109].

output 5-axis gcode which was then modified to remove CNC specific commands and include extrusion values. This was limiting, however, as the program is designed for removing material, rather than adding it, so multilayer or support structures are complex to create. Therefore a Java program was created to generate the specific examples. This is possible as only two simple demonstrators were presented, but an extendible method is not considered.

Multiaxis systems can print onto uneven surface and existing objects if sensing and path planning is incorporated into the system. Bausch *et al.* [144] present a system

which is based upon a Prussia i3 system with three additional rotation axes. They use a depth camera to scan the surface of an existing unknown part then superimposes a new object to be printed on top of this surface using Rhino 3D and Grasshopper, which is an algorithmic modelling plug-in. Scanning the surface, then printing is an important step for AM as it enables repair and augmentation of existing objects, which can represent significant cost and material savings. These authors do overstate the novelty of their system though, missing previous work such as [108], discussed above. The conference paper is reporting a system currently in development, so much of it is theoretical and there are a number of issues with the system, such as alignment of the scans is is currently a laborious manual process. These authors refer to to their system as both 6 DOF and 7 DOF - by including the extruder - which does not aid clear discussion. The system is currently limited to using 5 axes at once, the firmware acceleration control imparts jerky motions and the nozzle can collide while printing using rotary motions if the line segments are too long. Although the results aren't shown, they have managed to print the first layer of a new object onto an unknown surface and continue to work on extending this to further layers.

A similar goal is researched using a Makerbot 3D printer and two additional rotation axes added to the base plate [145]. An existing object was scanned and compared to a CAD model with some modification. The software then computed where material needs to be added, and removed, to update the object. A milling head is incorporated onto the extruder carriage allowing subtractive operations. Case studies are shown to illustrate how such a system could help when a print job fails, to update an object due to a new design iteration, to repair or to re-purpose an existing object. The 5-axis mechanism allows modifications to the side of an object, for example adding a handle to a cup. Due to the lack of multiaxis slicing software all operations shown are using 3+2 axis motions, i.e. the object is first rotated, then printed upon using conventional planar layers. This is possible because the milling machine can create a flat surface to start printing upon. This approach works well for the example given in the paper, the modification of a 3D printed object. However as it does not print conformally it can only be used to augment objects which can first be machined, limiting its applications.

Towards the end of 2017, two companies released commercial 5-axis FFF 3D printers. One aimed at the industrial market [146] and another at hobbiests [147]. There is little information on these systems apart from images of a limited number of demon-

strators. Both appear to be focused on the fact support material can be reduced. It is likely that the success of these systems will rely heavily upon the appropriate software being provided to enable the full use of a multiaxis system, but there is little evidence of this being available.

2.4.6 Serial Robot Arm MAAM systems

Robot arms have been used as motion systems for 3D printing for a number of years, but mainly using very large, imprecise arms to do conventional 2.5D deposition for artistic or architectural applications. For example the artist Dirk vander Kooij has recycled plastic from fridges into chairs using a large arm and nozzle [148], and Jasper Menger has created a similar system allowing large scale 3D printing, up to 2000 x 1200 x 1600 mm [149]. These both use large extruders which process plastic pellets, rather than the filament that is usually used for small scale printing. These use a screw to force the plastic through the heated section of the nozzle. Researchers have developed an extruder for large scale robotic depositions with a variable pitch screw which accounts for the effect of the plastic melting along its length, giving greater control [150]. The ability to print at large scales has lead architects to explore using robot arms to print in more unusual materials for use in buildings, including spraying sand and glue [151] or extruding clay [152]. Viridis3D and Palmer Manufacturing are also using robot arms for their large workspaces, but in this case to automate the building of sand moulds and cores for casting [153]. A wide print head full of powder sweeps back and forth across a conveyor belt, alternating between depositing powder and an activating ink.

A feasibility study on the use of industrial robots in AM processes was carried out by ABB, a robot arm manufacturer [154]. They suggest that robot arms are not used as the motion system for small and precise printers as they are not accurate enough. An example of using a robot for DED is given. This process has low accuracy and the deposits are usually post processed, therefore the limited accuracy of the arm is less important than the flexibility it offers. It is suggested that robot arms give larger print areas, and could be set on rails to extend this. Many AM processes are identified as being possible with robots and automation of post processing may be a good use case. The authors note that while robot arms have been used directly for AM, the setups are basic and tighter integration is needed. It is reported that a test cell was set up with an ABB robot arm and an FFF extruder, but unfortunately no results are given.

There is no mention of the possible advantages of utilising 6 DOF.

Others have used robot arms for full 3D deposition, showing novel ways of 3D printing but not actually producing functional objects. In an attempt to mimic silkworms researchers at MIT use a 6-axis robot arm to extrude thread through epoxy adhesive and to spray glue onto twine to replicate different sections of a silkworms cocoon [155]. An external frame with hooks is used to support the print and they suggest that lightweight furniture or building components could be made this way. A similar project used a robotic arm to create a structure by winding carbon fibre around a frame [156]. Once the whole object was cured in a kiln, the internal frame could be disassembled leaving just the composite. They also build similar structures using thermoplastic extrusion, attempting to remove the need for support structures [157, 158]. A large custom extruder was designed which uses plastic pellets instead of filament. High density Polyethylene (HDPE) was chosen due to its high tensile strength to density ratio, which is important if the strands are to support themselves. Various tips were designed for the extruder, including a slot to create flat ribbons and two with multiple holes so several strands are extruded at the same time. Thicker strands were included to retain heat for reconnection and thin strands cool quicker to give support. They also noted how a longer tip gave greater manoeuvrability for extrusion. The same group has also explored other large scale printing approaches including the use of spray-foam polyurethane to build insulated, castable frameworks [158, 159]. A milling head was also added to the end effector of the arm, allowing precision shaping of the foam following its deposition. This set up was also reversed, with extrusion and milling heads being mounted externally and the robot arm now moving the build plate, but only 3-axis shaping and deposition was performed. Additionally a novel mechanism has been explored to give an even larger build envelope. The 'CableBot' and 'SpiderBot' setups use cables to suspend the nozzle [159]. Winches then adjust the length of these cables, moving the head across the print area. Using 'Spiderbot' the idea of swarm printing is to be explored as several of these suspended platforms could be used to print a building scale object. Printing collaboratively stops the use of continuous layers so they suggest deposition of discreet drops should be explored. In another bioinspired architecture project, students at a summer workshop in Shanghai used a robot arm to mimic the structure of spider silk [160]. A custom extruder incorporating 4 nozzles is used. These each extrude ABS in the same way as an FFF printer. The central nozzle

is stationary, while the other three, which are arrayed coaxially around this, rock back and forth in a sine wave motion. Figure 2.23 shows a close up of this. The three external strands reinforce the central structure, allowing the printed structure to support its own weight. Cooling is very important for FFF printing so an air compressor is used to rapidly cool the extruded filament. This project prints strands of plastic and demonstrates how this structure is self supporting if cooled correctly, but there is no suggestion of future applications. Perhaps this could be used to minimise the plastic used in support structures or to print mesh style structures using 6D deposition.

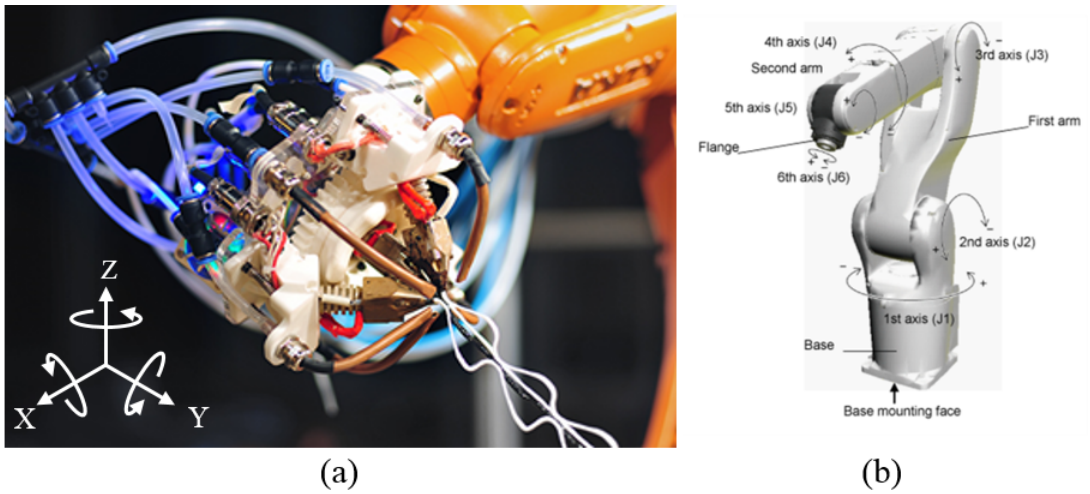

Figure 2.23: (a) Biomimetic print head extrudes self-supporting ABS strands in a geometry similar to spider silk. (b) The print head can move in 6-axes due to the serial robot mechanism. From [160].

A further architectural example uses a robotic arm to print lightweight mesh structures [161], these are very similar in form to WirePrint, which was discussed previously. The stands of plastic are deposited using three dimensional motions, while the structures are still built up with layers. The thickness of these layers was varied to change the overall geometry of the wall, while still having a continuous pattern. A robotic arm was used simply as a convenient actuation system, rather than to provide 6DOF. Unusually, rather than using a large scale industrial robot, a small desktop sized one is used to prove the concept and is then mounted upon a Cartesian stage system to increase it's build volume enough to print architectural scale walls.

Multiaxis printing has also been demonstrated using AM technologies other than

FFF. Architectural students experimented with a novel AM process which they called Suspended Depositions [162]. They used a 6-axis robot arm to inject light curable resin into a tank of gelatinous liquid. The gel acts as support to the resin, allowing full 3D deposition paths. The nozzle is kept vertical throughout the prints however. As the resin is fully supported it does not need to be cured for the rest of the part to be printed, unlike other AM processes. This gave the ability for the design to be changed and resin removed throughout the print, until the end when the whole part is exposed to UV light to cure it. The process is not mature enough for practical uses; the parts produced are incomplete and only roughly represent the designed geometry, but they state that the ability to suspend the resin in space and move the print head freely allows printing on and around existing objects.

Another example of large scale 3D deposition is 'Mataerial', this is an extension of other work by the Institue for Advanced Architecture of Catalonia (IAAC), such as Pet Flakes (Figure 2.14). The process has been dubbed "Anti-gravity Object Modelling" [163]. The details are not available due to a patent application, but the process works by extruding two chemicals at the same time, these then mix and solidify rapidly. Combined with the movement of a 6-axis robot arm, self-supporting strands can be extruded. So far only artistic shapes have been demonstrated but they suggest that the 3D curves could follow the stress line of a part to strengthen it. Strands are also built directly from vertical walls, showing the possibility of printing on more than just flat, horizontal surfaces, seen in Fig. 2.24. Similar results have also been demonstrated using metal [164]. A welder is attached to the end of the robot arm and deposits layers of metal to build up the strands.

More recently (2016-2017) there has been research using robotic arms, but not for architectural work. In the first, the authors identify that shell structures are particularly inefficient to print when using conventional layer based AM as the support structures would take the majority of the time and material to print [165]. In line with many other robotic extrusion systems they develop a pellet based extruder, although this is mounted statically on a frame above the robot. A domed mandrel is affixed to the wrist of the robot arm and this is used as the print surface. They develop software which takes a 2D drawing in a DXF file and maps the Z coordinates to the curve of the dome. As their demonstration piece is a single layer, artistic lamp shade this method is appropriate, but it causes the image to be distorted, especially on steep

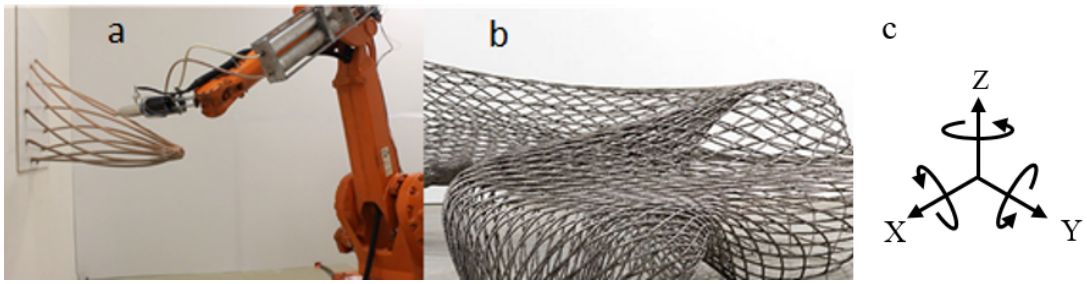

Figure 2.24: Anti-Gravity Object Modelling: (a) Rapidly curing material and 6 axis deposition allows for printing in any direction, from [163]. (b) A metal bench printed using 6-axis deposition, utilising a robot arm equipmed with a welder as the extruder head, from [164]. (c) The extruder can move is 6-axes due to the serial robot mechanism.

curves and cannot be readily extended to more complex shapes, for example concave or composite curves. When printing the mandrel is tilted under the extruder, to keep the surface being deposited on perpendicular to the nozzle. The lampshade prints well, broadly matching the desired shape when visually compared to an SLS model. The inconsistencies can probably be attributed to the pellet extruder as these can be poor at controlling plastic flow rather than the robots' motions, but this analysis is not performed. There is also no comparison of print time or material usage when compared to conventional printing.

Tam *et al.* [166] also print thin shell structures onto a pre-existing support dome, once again for architectural applications. This work however doesn't just use multiaxis AM to allow novel shapes due to 3D deposition, the shell structure is optimised to add material along the principal stress lines using a simulated loading. The design is then printed conformally onto a predefined dome using a 6 axis robotic arm with a FFF extruder mounted as the end effector. The print results are inexact, with uneven surfaces and line widths, but the system does show preliminary results which suggest that curved strands can improve the load bearing capability of a thin shell structure manufactured using FFF.

Another robot arm (Motoman SV3X) with an FFF extruder is presented in [167] but only one preliminary result is shown. A rectangular block is printed with one side using horizontal layers and the other vertical ones to show that the system can print in different planes. The quality is low, in part due to not using an outer perimeter, and the dimensions vary between 3% and 10.25% for the basic block.

In 2015 Arevo Labs released a video of a 6-axis robot arms printing curved layers onto a printed object using FFF [168]. The aim of this was for composite manufacturing, but this initial demonstration focused upon software to simulate and create the tool paths, rather than the hardware to embed fibres. Due to the company being a start-up there is limited information, but the system does appear to be more capable than many of the other examples due to the software integration.

A more developed example of this is termed RobotFDM and it utilises a stationary extruder and a 6-axis robot arm (Universal UR5) to move the build plate [169]. This type of collaborative robot is not very precise and must be moved very slowly to get the best positioning, so the quality of the parts are not high. However this system is used to demonstrate how a model could be split up and printed at different orientations to remove the need for supports. A compression test shows a weak bond between two sections printed at different orientations, with the part having a lower stiffness but similar maximum breaking force to the part made from horizontal layers.

The final robot arm based example is the only one to use SLA, and also the first to go beyond 6 DOF (excluding extrusion) [170]. The workpiece is mounted upon a rotary stage, effectively increasing the build volume of the robot as a large object now only needs to partly overlap with the robots' reach and can be rotated to bring a different side into view. The end effector is a DLP projector which can photopattern down to 10µm. Their first example demonstrates 2D patterning of an image onto a sphere. This a long process as the whole surface is decomposed into triangles, from the STL file, and each section is exposed individually, tiling the image together. For a 19mm diameter ball patterning took approximately 90 minutes, but for a 21cm diameter ball it took 60 hours. For the first, the repositioning time of the robot was the most significant factor to the print time, for the second a lens was used to increase the field of view, but decreased the intensity, creating long cure times for each tile. The bitmap image can be clearly seen, but some errors in the motion system have left lines between a number of the triangular sections where they did not line up fully. Millimetre scale SLA prints are also demonstrated. A clear window is added to the end effector, this is positioned at the desired layer thickness away from the substrate and resin is manually added at this interface for each layer. This allows an arch to be printed with slightly angled layers, but it is still built up using many small, by slightly curved, steps, rather than the layers being conformal to the geometry as previously seen. The benefit at this scale

is unclear. A hanging, unsupported, layer was produced by adding UV absorbing dye to the photopolymer to limit the depth of the cure. As the resin is added manually for each layer, rather than using a vat, the material could potentially be changed at any point in the print, although this possible advantages was not mentioned in the paper.

Robotic arms have been used successfully for a number of AM systems, but they are mainly limited to 2.5D deposition, thin shell objects or strand based mesh structures. The majority of examples has been for larger scale structures where imperfections and inconsistencies in the motion or extrusion are not considered detrimental to the outcome.

2.4.7 Hybrid manufacturing

It is worth noting that while AM has some unique advantages, relying on just one process arguably imposes unnecessary limitations when attempting to integrate mechatronic components during manufacturing [171]. Hybrid CNC, laser engraver and FFF 3D printers are available commercially in 3-axis set ups (for example from Zmorph [172]), although these usually apply each operation individually rather than performing multiprocess builds. Extending this to multiaxis systems is clearly beneficial as, for example, 5-axis mills can create much more complex geometry than 3-axis ones. Much of the work that has already been discussed using DED has an integrated milling head as the deposits from this process are quite rough [133, 135]. A 5-axis mill and FFF machine allowed higher quality parts to be created quickly by machining thicker layers smooth rather than printing many thin layers as is the usual method [103]. These two systems both did the additive fabrication first, then machined the result in a two step process. Having both processes in one machine does simplify the process and minimise difficulties associated with lining up a part in another machine, but this represents a marginal improvement. Where this type of system could be of significant value would be the ability to combine multiple processes during the fabrication of a part. For example by combining additive and subtractive methods with in-process monitoring, the tolerances of the part, including any internal geometries, could be checked. Then the whole geometry could be edited on the fly, rather than just machining the outer surface after the build as a post processing step [173]. In work discussed above, both Teirich *et al.* [145] and Peng *et al.* [140] use subtractive methods to remove mistakes and failed sections of prints before adding additional material. In this way a hybrid system could

be self correcting. Other processes such as Direct Write have been incorporated into standard AM processes such as FFF [72] and SLA [90, 174, 175] to enable embedded electronics. In the latter case, the laser in the system can be used to cure both the resin and the silver ink [82]. Much of the challenge in combining processes is to do with switching between the operations as they often required very different environments to work successfully. For example, SLA requires the part surface to be flat and submerged in resin, whereas depositing sliver ink requires a clean surface for it to adhere. Most of the examples of hybrid processes for electronics place the circuits on the exterior of the part because it is difficult to build further layers on top of the tracks due to material adhesion issues. An alternative method to combining all the processes into one machine is to automate the processes of moving a part between separate machines during its fabrication [159, 171, 176]. This introduces difficulties with registering the position of the part but dedicated machines may give higher quality outcomes [176]. Other hybrid manufacturing systems have been developed using a range of processes including laser cladding, wire embedding, ultrasonic vibration, milling, turning and grinding [173] but these will not be reviewed here as extending the developed system to hybrid processes is outside of the scope of this thesis.

2.4.8 Build Orientation Optimisation

Full three dimensional deposition has been demonstrated using several different systems and the advantages have been shown through simple examples. To extend these examples to practical parts and to make these printers as simple to use as conventional 3D printers, improvements to the slicing and tool path planning procedures need to be made. As the hardware now allows the build direction and layer curvature to be changed, a process is needed that generates the best deposition strategy for each section of the part.

In conventional 3D printers the build orientation of the part within the print volume can have significant effect upon the outcome. This is because the layers are always built in one direction (the Z axis) and these layers impart steps upon the surface, isotropic strength and require support under steep angles. For many AM processes (such as FFF and SLA) the part needs to be firmly attached to the build platform. So one of the first research efforts aimed to orient the part to be both stable and use the minimum supports [177]. There are however a number of parameters that the orientation could

be optimised for including; surface finish, build time, cost, mechanical properties or dimensional accuracy [178–180].

Additional degrees of freedom allow the work piece to be rotated and plastic to be added to another side, rather than just the Z direction. As shown previously (Figs. 2.8 and 2.21) a few researchers have used a rotational base plate to print a tower, then turn this on its side and print another section at 90° to this, leaving a unsupported overhang [103, 133, 140]. These were all performed with the nozzle vertical and the build surface horizontal as usual, but an FFF printer has been shown to print when turned on its side [181]. The quality of the print is not analysed so one cannot determine the effect of gravity upon the print beyond concluding that it is not significant enough to cause total failure in this case. When discussing the applications of their 6-DOF mechanism (seen in Fig. 2.19) Seward and Bonev [139] state that 3D printers have been shown to print both upside down and in zero-gravity however they give no references to back this up. The company Made in Space have since installed a 3D printer on the International Space Station and printed many successful parts. Details about the technology used are sparse but the specifications suggest it uses a FFF process. Only parts with overhangs $\leq 45°$ are guaranteed to print well, indicating that support structures are still required in Zero-gravity, although they are not an option currently offered. This is likely due to the waste material and small debris that removing support can produce, which are a significant hazard in a space craft, rather than a technology barrier. This indicates that the overhang limit is in respect to the layer normal, rather than the direction of gravity [139]. Therefore it is suggested that a printer with additional degrees of freedom could print unsupported overhangs if the layers are kept within $\pm 45°$ of the previous layers' normal.

By changing the orientation during the build it can be optimised for small sections and features, rather than choosing one overall orientation which is a compromise. To ensure the correct print order the part must therefore be decomposed into sections and the relationship between these sections recorded [127, 133, 182]. The parent part must be built before the child part or there will be nothing to support it. Collision detection is also very important. The program must ensure that any geometry that is built does not block access for later operations. Also the shape of the print head limits how close it can print next to other features. Once it has been sectioned the geometry has to be represented in such a way that the print direction can be inferred. Medial axis,

or skeleton, based methods find points equidistant from boundary surfaces to create a simplified description of the part [130]. This method is computationally expensive so a centroid axis is suggested instead [110]. This axis is generated by taking many 2D cross sections of the part in the X,Y and Z directions and then finding the centroid. These nodes can then be linked to create the skeleton. This skeleton is used to define the slicing direction, and in this way the slicing direction varies thought the object.

By doing this a steep unsupported overhang has been demonstrated using DED [134]. This process is affected by gravity due to the melt pool of material that is produced at the interface where more material is added. Therefore by tilting the build plate relative to the nozzle, the gaps between the layers can be controlled. The strategy presented for DED is limited to rotationally-symmetric, thin-walled parts. Figure 2.25 shows how horizontal slicing leads to layers which need support and how continuously changing the orientation could stop this.

While build orientation is recognised to have a significant effect upon the outcome of AM parts only basic proof of concept items have been produced using multiaxis AM. It is clear that significant advantages can be realised, not just in terms of reducing support material, but also with respect to surface finish, mechanical properties or dimensional accuracy.

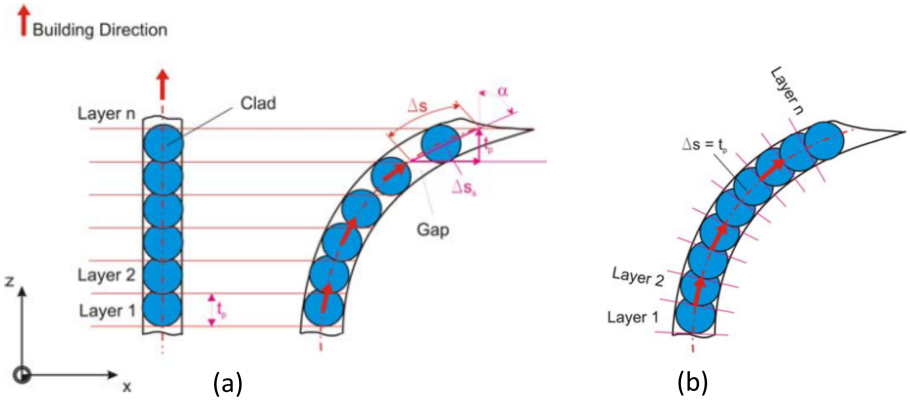

Figure 2.25: (a) Planar horizontal slicing leads to gaps between roads and the requirement for layers to be supported. (b) Both the slicing angle and the layer thickness is adapted to the geometry of the part, leaving no gaps between layers. From [134].

2.4.9 Curved Layer Slicing

While there are practical examples of curved layer 3D printing, the software to generate the curved tool paths is often at a very basic, proof of concept stage as no ready made option is available [183]. For example Llewellyn-Jones *et al.* [121] recently showed very good surface finishes but used an algorithm that required the input to be a thin surface and this is then repeated over a number of layers, rather than truly generating the required paths from a standard CAD model input. Their method is more flexible than previous work as it can work with arbitrary shaped surfaces, while others must use a mathematically defined shape [106].

There are many difficulties in deciding the shape that the layers should take, as while the outer layers should conform to the surface of the part, this may vary greatly or have internal geometries which need conforming to as well [183]. The possibility of aligning the layers along stress lines adds another potential complexity. Chakraborty *et al.* [184] present the idea of "Curved Layer Fused Deposition Modelling" (CLFDM) and develop some guidelines to ensure the adjacent filaments are bonded but an overall scheme is not developed. Their method only works with slightly curved parts so they suggest that if it was extended to complex shapes with abrupt changes to the surface geometry, then multiple sections of curved layers would need to be connected together. In addition the process is relatively simple for thin walled parts but once the layers have to be offset, to increase the thickness, self-intersections can occur.

When slicing, layers which are non-uniform in thickness can be used to remove the stepping effect usually created by discrete layers [110, 132]. In practice, it is difficult to precisely control the deposition of material. For the LAMP system an empirical model was used to predict how the layer height changes depending upon the scanning speed [132]. This information could then be used to plan the path, and speed, of the tool head to adjust the thickness throughout the layer.

Curved layer slicing has also been used to better preserve small surface features, while reducing the number of layers required [183]. The usual alternative using planar layers is to use Adaptive Slicing. This is where the layer thickness is decreased in areas that have fine details, to help reduce the effect of the steps. This can be effective but can also dramatically increases the built time. In this case critical points, which corresponded to important features, were defined on the surface and a genetic algorithm (GA) was used to fit a surface to these points. This allowed the number of layers

required to be reduced by 21% compared to flat adaptive layers, but it is unclear how well this method can be extended to more complex shapes or more common engineering components with internal features, rather than just a curved mountain-like shape. GAs can take considerable time to converge so the number of critical points may be limited, also the results are not physically verified. Chakraborty *et al.* [184] offset points along the normal to the surface by the slice thickness, Singamneni *et al.* [112] also offset along the normal using point cloud data for the top surface. These create an offset surface based upon a number of points and is not ideal as it can be computationally intensive and not accurately represent the surface [117]. In Huang and Singamneni's [117, 185] work the facets are offset, based upon the triangular representation of the surface in either an STL or AMF CAD file. Adaptive slicing was also combined with curved layers in an attempt to keep the advantages of each. That is retaining fine details and smoothing curved surfaces respectively. Three lightly curved arches were printed using adaptived curved layers and then tested using 3-point bending. The results suggest that thicker curved layers give better mechanical properties. The combination of flat and curved layers also aids the construction of internal geometries as these can be built using planar layers with a curved shell to give a smooth geometry [185].

Many of these theoretical examples just focused upon creating the curved slice (e.g. [183]) but to print these the infill pattern also needs consideration. This could be optimised for speed or to minimise voids. The process planning algorithm can use geometric criteria to choose the best pattern, even combining different ones in the same layer [133].

While various methods for slicing and process planning have been proposed there are still limitations and the algorithms have not been tested on a wide range of parts. On the whole they address shallow curves and surfaces without right angles, or in some cases, holes. These are obviously common features which will be required but often require complex exceptions to general offsetting algorithms as sharp changes can cause artefacts such as intersections or distorted surfaces. In addition the majority of the work is for a hybrid system where the part is finished with machining (e.g. [133, 135]), so in some cases optimising the layers to improve the surface finish has not been considered. It was also the aim to make fully dense metal parts and this is often not the case in other forms of 3D printing. The other special case that has been addressed is the curved printing of thin shells (e.g [134, 165, 166]). This is important as these shapes

are particularity inefficient to print with planar layers, but it can also be the simplest case in terms of tool path planning as one does not need to consider how offsetting of surfaces can cause errors. Interestingly two different deposition strategies have been demonstrated, show in Figure 2.26. Both Brooks *et al.* [165] and Tam *et al.* [166] use a domed mandrel as the print surface and then print curves onto this convex surface. Kerschbaumer *et al.* [134] on the other hand prints a wine glass shape without the need for a curved surface to print on. This is achieved by keeping the nozzle normal to the curve of the surface and rotating the build plate. This is much more comparable to standard planar deposition as the shape has to be built bottom up and layer by layer, but the deposition is not planar and the deposition orientation alters throughout the print. In this way the internal concave surface of the object faces away from the build plate, rather than the convex outer surface in the first method. The first method has the advantage of allowing more directional deposition of specific strands of material, but requires a custom shaped mandrel. The second method is support free, and can even print curves which go beyond a hemisphere and would trap an internal support structure, but has to impose a set build order to enable this.

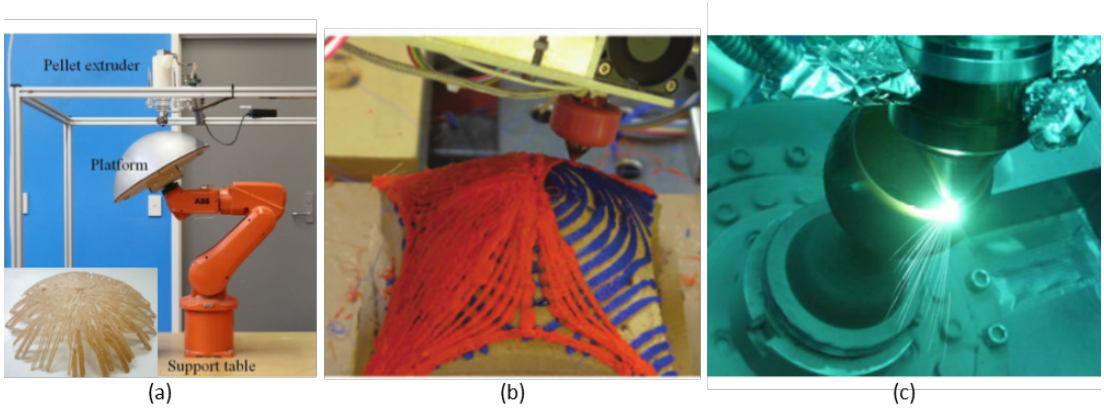

Figure 2.26: Thin shell deposition comparison using Multiaxis AM; (a) Printing discrete strands onto a domed mandrel, inset shows printed structure. Adapted from [165]. (b) The strands can be oriented along stress lines as the mendrel supports the whole internal surface, from [166]. (c) By manipulating the build orientation of the curves the domed structure can be printed without support allowing the lip to curve back in without trapping a supporting mandrel, from [134].

2.5 Discussion and Conclusions from Literature

Manufacturing mechatronic devices, using Additive Manufacturing could bring a range of advantages. The author envisages a manufacturing system which could rapidly produce many centimetre scale robots, which may work together as a swarm, to rapidly respond to a situation, such as search and rescue or disaster response. Robots are usually costly to manufacture, in part because low volume production is more expensive per unit and significant, complex assembly is required. AM has the potential to reduce these costs while also imparting significant advantages. Complex geometry can be created and designs quickly iterated and improved. Throughout this chapter a number of other possible advantages have been revealed through the relevant literature, but many of these either exist in isolation or require more work to become practical.

It is clear that mechatronic devices currently require more manufacturing processes than AM to be fabricated. Joints and mechanisms have been printed *in situ* and are broadly successful if the limitations of the specific process being used are considered. Electronics are receiving substantial attention, especially as traditional PCB manufacturing is inefficient for small quantities, but many of the methods for creating conductive tracks have very high resistance and few components beyond resistors and capacitors have been produced. Multimaterial AM enables complex structures with functionally graded materials and increases the range of applications for AM parts, but the material choices are still limited and are often poor mimics of traditional materials, or process planning considerations limit their use.

A significant alternative to manufacturing components *in situ* is to incorporate pre-existing parts into a mechatronic device as it is being created. This allows the geometrical freedoms of AM to be taken advantage of: Circuits could be embedded in the structure of a device minimising the wasted space or complex internal cavities could house sensors while still being fully sealed. The ability of AM to give access to the internal structure of a part allows objects to no longer be manufactured as split parts so that they can be joined together around other components. For applications where robustness or water-tightness is critical this could be a significant advantage. Embedding components has been attempted successfully, but the only established method is to use shape converters. This requires additional components to be designed and manufactured, which must be conformal to the specific part being inserted. These items are then assembled together and manually inserted while the AM build process is paused.

There is no integration between this and the AM system, it is simply a method to provide a flat surface for subsequent layers to be printed on. Some simple components have been incorporated without the use of shape converters, but these are square packaged electronics components or other items which conveniently can be inserted into a cavity without disturbing the conventional build process.

Multiaxis AM clearly offers additional advantages over and above the usual 2.5D deposition of standard AM machines. One of these is the ability to print conformally over surfaces, and therefore over inserted components, to embed them. While existing work hints at this possibility, embedding has not been thoroughly explored in current literature and the majority of multiaxis system focus on the possibility of improving the surface finish of a part or printing self supporting strands for architectural parts. Lee *et al.* [103] comes the closest when they show that their 5 DOF system can print around an existing shaft due to allowing the nozzle to reach into a step on the shaft.

There are a limited number of MAAM systems, with the majority of the relevant literature having been published during the course of this investigation. Robotic arms have been used as the motion system for AM for a number of years, initially for standard 2.5D deposition at large scales, then for MAAM. However there is no work which verifies their ability to print high quality objects at millimetre scales. The majority of their use has been for architectural scale, strand based constructions or thin shell structures. However it is now possible to get smaller, high precision robotic arms which could potentially provide the precise motion platform required while also offering freedom for experimentation, flexibility and large build area compared to the footprint. Six and seven DOF motion systems have been used to control the direction of the toolhead, but only two address the possibility of utilising shaped toolheads for deposition [109, 157]. In terms of multiaxis FFF, a number of proof-of-concept parts have been printed, often crudely, but there has been no in depth investigation into how gravity affects printing and whether the perceived benefits of changing build orientation play out in a physical system.

FFF is the most appropriate AM process for use when integrating mechatronic components predominately because it does not use a vat of material to print from, can print onto unmodified, unsealed mechatronic components and would gain significant advantages from a multiaxis system due to it's anisotropy and support requirements. The main considerations for each AM category are summarised in Table 2.4.

Table 2.4: Comparison of the AM processes with respect to using for embedding mechatronic components using a multiaxis system.

Process Category	Embedding Considerations	Multiaxis considerations	Material considerations
Binder Jetting	Sealing required. Wiper arm.	Vat of powder limits tool head motion.	Poor mechanical properties
Direct Energy Deposition	Very high temperatures so unsuitable for directly printing onto components.	Hybrid systems have been shown to give good results.	Very good material properties, requires machining.
Material Extrusion	Sealing not required. Outer nozzle angle limits printing next to objects.	FFF shown to print sideways, quality unverified.	Predominately thermoplastics, good mechanical properties, relatively low resolution, anisotropic.
Material Jetting	Conformal printing is only possible on shallow curvatures	Behaviour of the droplets is affected by gravity and the surface they are jetted onto so could become unpredictable.	Materials have to be formulated so they jet then cure on demand, limiting material properties available.
Powder Bed Fusion	Sealing required. Wiper arm. High temperature build chamber.	Not possible without significant changes as the vat of powder limits tool head movement. Gives fewer benefits as no support.	Excellent material properties, powder acts as support allowing inbuilt joints and complex features.
Sheet Lamination	Relies on placing a whole sheet then cutting so cannot build conformally around objects. Has been used to embed components by leaving voids.	Would require complex mechanism for laying sheets at an angle, or over pre-existing surfaces.	Commonly paper or metal so can be functional, requires post processing.
Vat Photopolymerization	Sealing required. Wiper arm. Laser shadowing	Has been shown by moving light source within vat.	Material has to be light reactive limiting material properties available.

Chapter 3

Additive Robot Manufacturing System

3.1 Introduction

In this chapter the design and development of the multiaxis Additive Robot Manufacturing System (ARMS) is presented. First an overview of the system is explained, then the key subsystems; mechanical, electrical, and software are detailed. This includes the additive manufacturing (AM) process to be used, the robotic arms which form the motion system, and the method of their integration. The kinematic model which underpins the control of this complex system is then described. Finally, conventional three axis 3D printing is used to verify the system, before moving on to multiaxis printing in later chapters.

3.1.1 Process Overview

The following sections in this chapter are approximately chronological, but the process for designing and building this system was not actually linear, as subsystems were developed in parallel and intermediate testing and revisions were undertaken for each milestone in the process. Each major section does rely heavily upon the previous ones however, so while aspects could be refined and improved, large changes to the early

work, such as hardware choices, were avoided as the work progressed. The 6 key stages, and the major aspects within them are listed below. Stages 1-5 are detailed within this chapter, stage 6 was completed through the experiments detailed in the following chapters.

1. System Requirements and Design
2. Hardware
   - Robot Arm Cell
   - Material Deposition
3. Software
   - Tool path generation
   - Machine Control
4. Kinematic Model
5. Standard 3D Printing Capabilities Validation
   - Mechanical Properties
   - Aesthetic Results
6. Multiaxis 3D Printing Capabilities
   - Varied Orientations
   - Curved Trajectories
   - Conformal Printing

Each subsection followed the iterative design process of setting requirements, design, implementation and then validation against the requirements. The feedback was also used to review previous modules, for example the results from stage 5 refined how the kinematics from stage 4 were computed. This feedback caused the system to be continuously improved throughout the work.

3.2 System Overview

From reviewing the literature in the previous chapter it is clear that multiaxis additive manufacturing (MAAM) has great potential to allow the printing of curved and

non-horizontal layers, but existing systems are not precise or flexible enough to do more than print low quality proofs of concepts. Section 2.4 revealed that parallel robot mechanisms cannot provide the range of rotational motion required when printing onto complex objects but five axis Cartesian stages and parallel-Cartesian hybrids, have been used successfully to demonstrate basic MAAM. These mechanisms however are not as flexible, in terms of possible applications, as serial robot arms which have been used for a wide array of tasks within the manufacturing industry. The long-term goal for the Additive Robot Manufacturing System (ARMS) presented in this thesis, is to not only allow MAAM but to also be expanded to a hybrid manufacturing system capable of fabricating fully integrated non-assembly robots. Therefore, in the future this platform may eventually include a range of tools including; micro-assembly grippers, subtractive milling bits, AM print heads, direct write dispensers, 3D scanning, and soldering capabilities. When considering the capabilities that may be required in the future for this hybrid system, using multiple robotic arms is the best solution, as it enables complex, yet precise motion of a number of end effectors and has the flexibility to be reconfigured and applied to numerous manufacturing processes. Developing ARMS into a hybrid manufacturing system is outside of the scope of this thesis, instead a single AM process is focused upon.

Prior to the start of this work four robot arms, and a base plate, were purchased by the EPSRC National Facility for Innovative Robotics Systems at the University of Leeds. The commissioning of the robotic work-cell formed the initial part of this work, before MAAM specific components were introduced. The commissioning involved the design and procurement of the safety enclosure, the integration of the safety interlock, and design of the system architecture. Once these essential subsystems were realised, the MAAM specific components were developed, including the material deposition end effector and the kinematic controls.

So that the efficacy of MAAM could be assessed in relation to the established 3-axis AM method, ARMS was first required to 3D print to the same standard as typical desktop 3D printers. Fused Filament Fabrication was chosen as the AM process due to its suitability for printing around existing objects and potential for use in functional devices. This is explained further in Section 3.4.

3.2.1 System Specifications

The system requirements, based upon the literature and the discussion above, are listed below. These informed the decisions which are explained in the remaining sections of this chapter.

- The motion system must enable ≥ 5 degrees of freedom (DOF) for the extruder.
- The build plate must also have ≥ 5 DOF.
- Fused Filament Fabrication must be the AM method.
- The system must be designed to be flexible and extensible to include other end effectors in the future.
- The motion system must use the existing robotic arms within the facility.
- All Health and Safety considerations must be addressed.
- The system should be compatible with existing AM software flows (i.e. accept g-code commands).
- The printing commands must allow for reuse in different positions (i.e. not be in terms of a global fixed reference)
- The print quality must be comparable to existing FFF printers.

Specifications relating to the AM output of the system were determined, based upon the capabilities of other FFF printers [186–188], and are listed in Table 3.1.

Table 3.1: Specifications for ARMS when printing using conventional 2.5D deposition.

Specification	Value
Dimensional Accuracy	±0.5 mm
Minimum Layer Height	0.1 mm
Material	Polylactic acid (PLA)
Material Format	Standard FFF Filament Spools
Build Area	200 x 200 x 200 mm
Print Instruction Format	RS247 Gcode

3.2.2 Layout

The system uses four robot arms arranged on a steel anti-vibration base plate. An image of the whole system can be seen in Fig. 3.1. The base plate is 1.5 x 1.5m and has T-slots across the diagonals, into which the robots are bolted. Along these are a series of dowel holes to allow the robots to be precisely located at a number of positions. The size of the base causes the robot's workspaces to overlap, so they can perform different operations, upon the same object, at the same time.

These arms can move the end effector at a maximum speed of 11,000 mm/s and therefore an enclosure was specified and installed which conforms to ISO 10218-2:2011 "Safety requirements for industrial robots - Part 2: Robot systems and integration". Included in this is a automatic lock on the door which was interfaced with the robot controllers so that it locks automatically when the robot's motors are activated, and it stops the robots being activated if the door is open. Alongside this, a control panel was built which uses outputs from the robot controllers to display the error state of each robot, and whether the door is closed. It incorporates switches to enable automatic motion for each robot and a main emergency stop button which connects to all four robots.

The four robots are used as follows:

(a) Camera Robot - This robot holds a stereoscopic 3D video camera (Panasonic HDC-Z10000EZ) which connects to a 3D TV outside of the enclosure. This is vital for obtaining a close-up view of the print, due to the safety enclosure.

(b) Pick and Place Robot - This robot was not used in this body of work, but in the future it may be equipped with a gripper to allow the insertion of components.

(c) Extruder Robot - This arm has the FFF print head attached to its wrist and performs the majority of the motions required for printing.

(d) Build Plate Robot - This robot holds the base upon which objects are 3D printed.

The printing instructions for an object are described in coordinates which relate to the build plate, rather than a global position, which would require the instructions to be regenerated if the position of the build plate was altered. See Section 3.6 for more details.

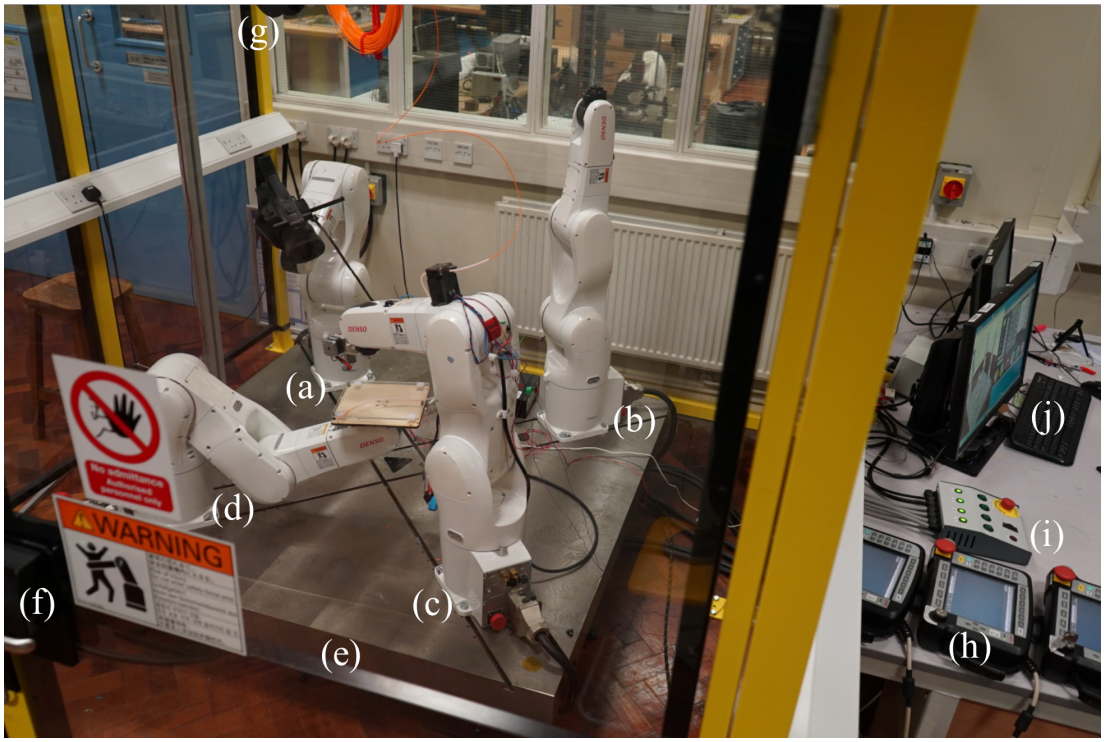

Figure 3.1: Photograph of the Additive Robot Manufacturing System (ARMS). Briefly this is comprised of: (a) Camera Robot, (b) Pick and Place Robot, (c) Extruder Robot, (d) Build Plate Robot, (e) Steel base plate, (f) Safety enclosure with door interlock, (g) Spools of filament suspended overhead, (h) Robot teach pendants, (i) Control Panel, (j) System Computer.

3.2.3 System Architecture

The system is comprised of a number of hardware and software subsystems. A schematic of how they interact is in Fig. 3.2. The central piece of software, which communicates between all the different peripheral devices, is a program that has been developed in LabVIEW. This does the majority of the computing, including parsing gcode, calculating robot positions and performing kinematic simulations. It includes a Graphical User Interface (GUI) and is the main way the user interacts with the system. The input instructions it accepts are in the form of gcode, a numerical control (NC) programming language, the details of which are in Section 3.5.3. To generate gcode a user must first create a 3D model using Computer Aided Design (CAD) software, the output of which is an STL file which is imported into another software package. This slices the model into the layers which will make up the AM part and generates the gcode instructions.

Section 3.5 describes this further. The central program then parses the gcode and performs the kinematic calculations to work out the required instructions for the robot arms and the extruder. These instructions are communicated via network connections to distributed sub-controllers, which each communicates with its own peripheral device.

The microcontroller generates the pulses required to move the stepper motors on the extruder and outputs them to the hardware. It also runs a PID loop to control the nozzle temperature. This reduces the communication overhead as the value can be checked and corrected at a high frequency but the temperature needs to only be communicated back to the PC occasionally, so that it can be displayed upon the GUI.

The robot controller receives instructions to move the robot to a specific pose and then runs the calculations and control logic to ensure that the arm is capable of doing the movement and stops in the correct place. These controllers also have input/output (IO) pins which mean signals can be passed to the control panel and door interlock, completing the required safety circuit.

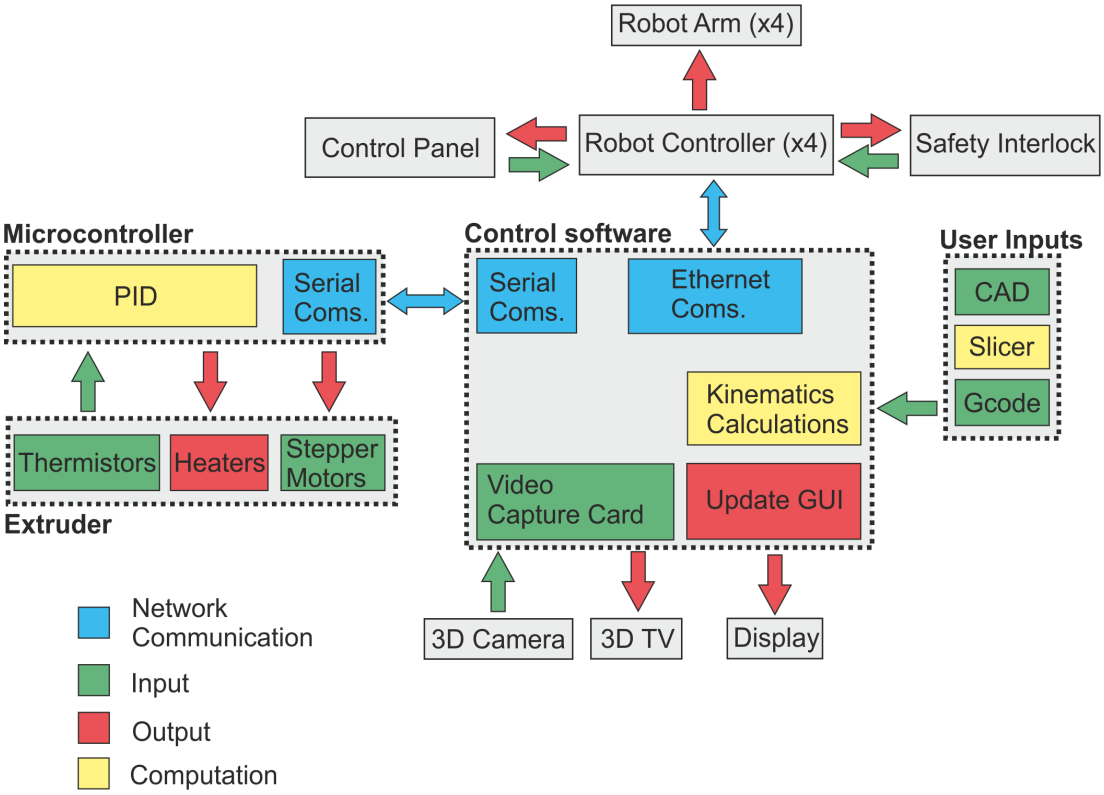

Figure 3.2: A schematic of the system architecture for the ARMS showing the main hardware devices, software components, and the data flow as they communicate.

3.3 Robotic Arms

Previous work which used robot arms for AM was concerned with printing large scale structures, and chose robot arms as they are more compact and flexible than using a large Cartesian gantry to move an extruder over a large area. In fact ABB (a large company which manufactures robotic arms) published a feasibility study into the use of industrial robots[1] in AM. They stated that due to AM machines requiring high accuracy motion, it was unlikely that robot arms would be used. They expected them to be used for larger scale architectural printing or support tasks such as post-processing [154]. The results at the end of this chapter will show that industrial robot arms can be more than capable of this kind of small scale work, and this was made possible by using industrial robots produced by Denso.

[1]Commonly used as a synonym for robotic arms.

In this system there are four Denso VS-068 robot arms, Fig. 3.3 shows one of these and the position of its 6 joints. The key specifications are listed in Table 3.2. These are relatively small for industrial robot arms, with a reach of 710mm, but this provides a much larger workspace than many 3D printers. The precision of the arms is an order of magnitude better than the typical layer thickness and dimensional accuracy found in FFF 3D printing, usually in the range of tenths of millimetres. Unfortunately the manufacturer gives no details about the minimum motion step size or accuracy of the arms, but this is common across industrial robot manufacturers and these parameters will not be considerably different in magnitude from the precision, in practice. The arms are capable of moving their wrist at a maximum speed of 11,000mm/s so will readily achieve the speeds used for FFF, which are typically in the range of 40-100mm/s.

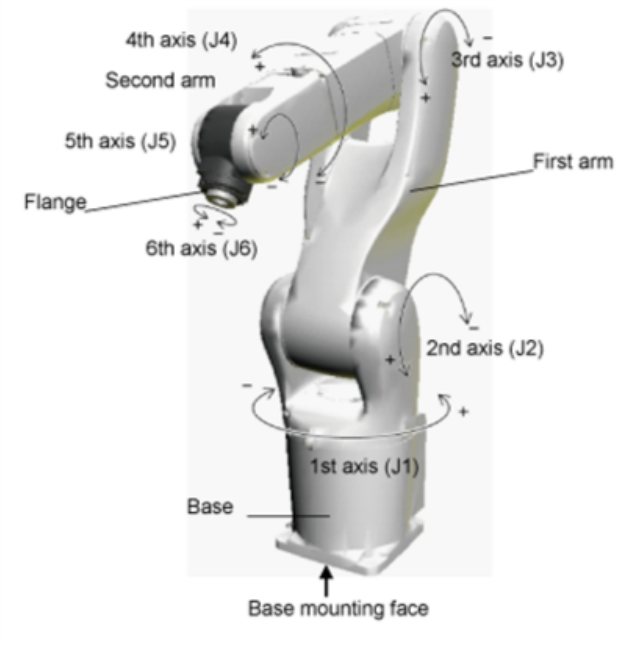

Figure 3.3: Render of a Denso VS-068 robot arm with the joint axes and rotations annotated. From Denso user manual.

Each joint in the robot arm has a limited range of angles (Table 3.3) and it is important to keep any motions within these. To help visualise the robot's range of motion the workspace of each arm was calculated and plotted using Matlab. To do this the transformation matrix for each link was defined and a script looped through

Table 3.2: Specifications for DENSO VS-068 robot arm.

Specification	Value
Number of axes	6
Maximum Reach (for wrist centre)	710 mm
Payload	7 kg
Maximum composite speed	11000 mm/s
Position Repeatability	±0.02 mm
Weight	49 kg

Table 3.3: Joint limits for DENSO VS-068 robot arm.

Joint	Maximum Angle (°)	Minimum Angle (°)
1	170	-170
2	135	-100
3	153	-120
4	270	-270
5	120	-120
6	360	-360

the allowable range of motion for each joint. By multiplying together these matrices, the end position of the wrist can be found. This working envelope was plotted in Fig. 3.4. The workspace is almost spherical, but the arm cannot reach directly behind itself. Notice also that the left hand graph goes below $Z = 0$, which cannot happen in practice or the arm will collide with the base plate.

From a control point of view the robots have their own computer controller (Denso RC8) which does all of the low level control and calculations and is usually used as a stand alone unit in industry. It can be sent higher lever commands, via Ethernet, such as move the joints to specific positions, and the controller will check whether the robot can perform such a motion, then calculate the trajectory and acceleration and run its own control logic to position the arm. This is very useful as these basic requirements do not have to be developed from scratch. By the end of the project, however, this controller was the last 'black box' in the system. That is to say, the only part which had not been developed or was not open enough to allow an unrestricted understanding

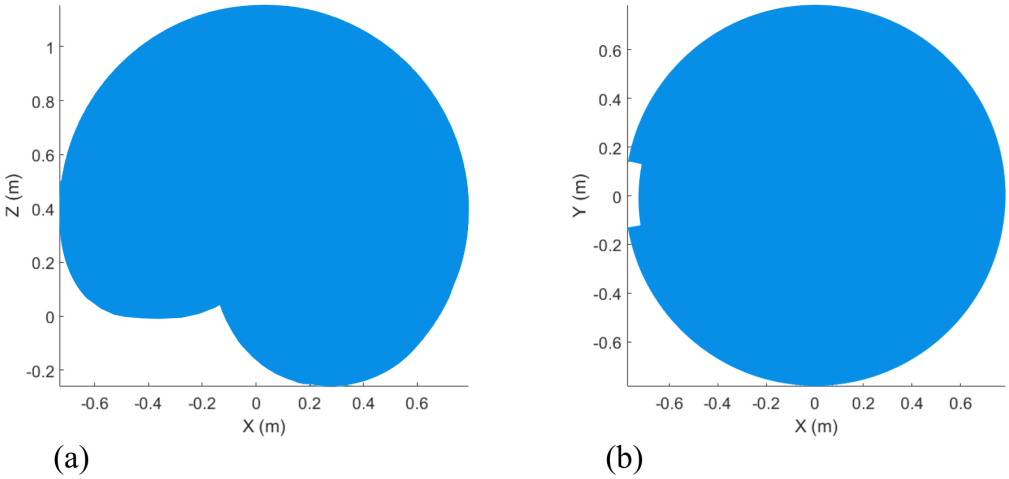

Figure 3.4: The front of the robot is facing right in both plots (a) Cross section of the workspace, through the XZ plane. Note how the end of the arm can go below the floor ($Z = 0$). (b) Top down view of the workspace across the XY plane. There is a section where the arm cannot reach, around Y=0, as the base joint cannot rotate all the way around.

of how it functioned at a more fundamental level. This did limit the flexibility in some cases, as the robots are designed for industrial applications where they are programmed with one motion sequence which it repeats. The software is designed with this in mind. One example is that while the interpolation between commanded points was set to linear, the actual path taken could vary from this (see Chapter 5). There was no way to determine how this would change each time, so a work around was used. Another example is that the speed of the robots must be set as a percentage. There is a function within the robot controller which converts this percentage to an actual speed in mm/s, but this had not been implemented within the LabVIEW library which was used to communicate with the robots. To overcome this issue a program was created on a robot's teach pendant. This is a hand-held controller which connects to the robot controller directly and is usually the main method used to program these types of robots in industrial settings where complex online control is not required. The short script used the conversion function to convert a range of percentages into speeds. By plotting this data it was clear that this is a linear relationship and therefore the inverse can easily be implemented in LabVIEW to convert the required speed into an percentage that the robot controller would understand. This relationship can vary if the robot's

settings are changed however. In the initial set-up it is important to input the weight of the payload into the robot, as this allows it to automatically calculate the speeds and accelerations such that the maximum allowable inertial force is not exceeded.

3.4 Fused Filament Fabrication

FFF has been chosen as the most appropriate AM process for the application of embedding mechatronic components, as discussed in Section 2.5. It is commonly used in desktop style 3D printers due to its relatively low cost components, and because of this, the technology has rapidly matured in recent years. In this case it was chosen due to the fact it can be used to print directly onto existing items with little to no changes to the physical deposition mechanism. The process does not rely upon building in a vat of resin or powder and the narrow nozzle of the deposition head lends itself to dexterous movements, unlike material jetting processes. The use of thermoplastics is also a significant advantage. These are well characterised materials and can be used for functional parts. FFF printers can print a wide range of materials, including PLA, ABS, Nylon, Polycarbonate, Ultem, PETG, PVA and others. Manufactures are now commonly creating blends specifically for FFF, designed to improve the ease of printing while retaining the desirable mechanical properties of the material. Some polymers, such as Ultem, require specialist equipment such as a high temperature extruder or heated enclosure. In this work PLA and PLA based blends are used for the majority of the work as it requires the fewest environmental controls to print successfully. The specific materials that were used throughout this work are listed in Table 3.4. These materials are supplied as a continuous filament wound onto a spool. There are two common filament diameters 1.75mm and 3mm. There is no definitive difference in the outcome when printing either, but users suggest that the thinner diameter allows faster print speeds due to quicker melting times and at standard speeds the filament drive mechanism does not require a reduction gearbox to increase the torque. Each step of the drive wheel also moves a smaller volume of plastic at a time, allowing for higher precision. Therefore 1.75mm filament was chosen for this system.

Table 3.4: FFF materials used on this system.

Material (Acronym)	Brand	Function	Notes
Polylactic acid (PLA)	Faberdashery or E3D	General purpose parts	Standard 3D printing filament with no additives other than colouring.
Polylactic acid (PLA)	Polymaker PolyMax	General purpose and functional parts	Modified PLA with enhanced mechanical properties.
Polylactic acid/Polyhydroxy-alkanoate (PLA/PHA)	colorFabb	General Purpose and Functional Parts	Modified PLA with enhanced mechanical properties, comparable to PolyMax PLA.
Polyvinyl Acetate (PVA)	Dutch Filaments PVA-M	Cold water soluble support structures	Modified to be more thermally stable than regular PVA.
Thermoplastic polyurethane (TPU)	NinjaTek Ninjaflex	Flexible parts	Formulated for FFF but difficult to print due to flexible feedstock.

3.4.1 Extruder Mechanism

There are a number of designs for FFF extruders, but they all operate under the same principal, one section - the Cold End - grips and pushes the feedstock down into the second section - the Hot End. This is where the filament is melted and then forced through a narrow orifice onto the substrate below. Figure 3.5 depicts the extruder

which was used in the majority of this research. A design more suited to multiaxis printing is presented in Chapter 6. The Cold End consists of a sprung idler wheel and a drive gear which attaches to a stepper motor (NEMA 17) to grip and actuate the filament. The specific design used was adapted from a 3D printable open source design [189], to fit the components that had been purchased, and a bracket was lasercut from 5mm plywood to attach this to the robot arm. A gear with sharpened teeth is attached directly to the motor shaft and a lever arm pushes a bearing, pinching the filament against this, allowing the plastic to be gripped. It is crucial that the gear bites into the feedstock as precise amounts of plastic are required for good quality results, so the gear must not slip on the filament. The motor is also often used for retractions. Retractions are used when no extrusion is required, so the drive gear is reversed and the filament is pulled up slightly, reducing the pressure in the Hot End, stopping the flow of material. The configuration used is called Direct Drive because the feed mechanism is mounted directly above the Hot End. The two could be separated with the filament fed through a Bowden tube between. This is common on standard 3D printers as a way of reducing the weight of the carriage that must be moved around to draw each layer, but the tube can introduce additional friction and backlash which can affect the success of retractions.

The Hot End is a commercially available system (E3D Chimera) which has an all metal construction and is designed to create a specific thermal profile along its length. The top section is actively cooled using a fan and finned heatsink and it is separated from the bottom section via a component called the Heat Break. This is a thin walled aluminium tube which is designed to thermally isolate the melt zone from the top of the extruder with an air gap. Below this the heater cartridge is clamped in an aluminium block, alongside a thermistor, with a brass nozzle screwed into the bottom. The heat is contained in a small area to improve the responsiveness of the filament feeding. If large sections of the filament were to heat up enough to deform then the ability to feed and retract the filament precisely would be impaired.

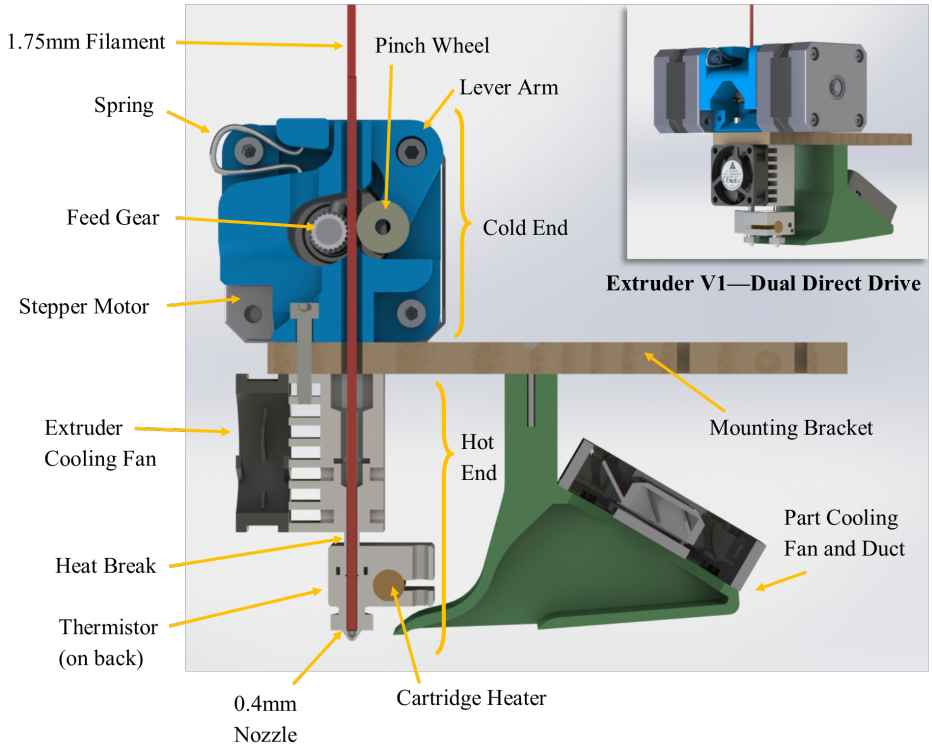

Figure 3.5: Cutaway side view of the direct drive extruder. Inset shows how this arrangement is mirrored to provide two extruders for use with multiple materials.

3.4.2 Extruder Control

The control of the extruder subsystem is handled by a dedicated microcontroller (Arduino Uno). As well as being used as an electrical input/output (IO) interface, it handles low level control of some tasks. Subroutines which generate the pulses required to step the motors and the heater Proportional-Integral-Derivative (PID) control loops run on this board. The control values for the PID were determined using the following manual tuning procedure. The temperature measured by the thermistor was graphed using a data acquisition device (DAQ) so that the response to a step change (i.e. turning on the heater) could be seen. The proportional parameter is set first such that the system has a quick response, but oscillates. The integral term is then adjusted to minimise any steady state error. The derivative parameter is then increased until the response settles quickly. These three parameters must be tuned using trial and error to create a fast response, without excessive overshoot or oscillations.

Distributing the computing reduces the communication overhead between the computer and the Arduino and improves the reliability of the pulse timings. String commands are sent from the computer via a serial port, these are then parsed and used to control the IO pins as required. The program, which runs continuously while the system is on, is described in pseudo code in Appendix A.

3.4.3 Printed Circuit Board

The microcontroller functions as an interface device which has a number of analogue and digital IO connections, these are connected to the components on the extruder. Due to the current limits on the board, the devices cannot be connected directly but must be connected to an external higher voltage power supply and triggered using transistors switched from the IO pins. The stepper motors require driver boards which take the step pulses and direction signal from the microcontroller and actuate the correct armatures in the motor to cause it to turn. To ensure these connections were robust a Printed Circuit Board (PCB) was designed and manufactured. This PCB is designed as a 'shield' - i.e a board which has the correct footprint to slot directly onto the microcontroller headers creating a robust, yet modular system. The circuit diagram and corresponding PCB design were drawn in a PCB CAD software package (Autodesk EAGLE) and are in Fig. 3.6.

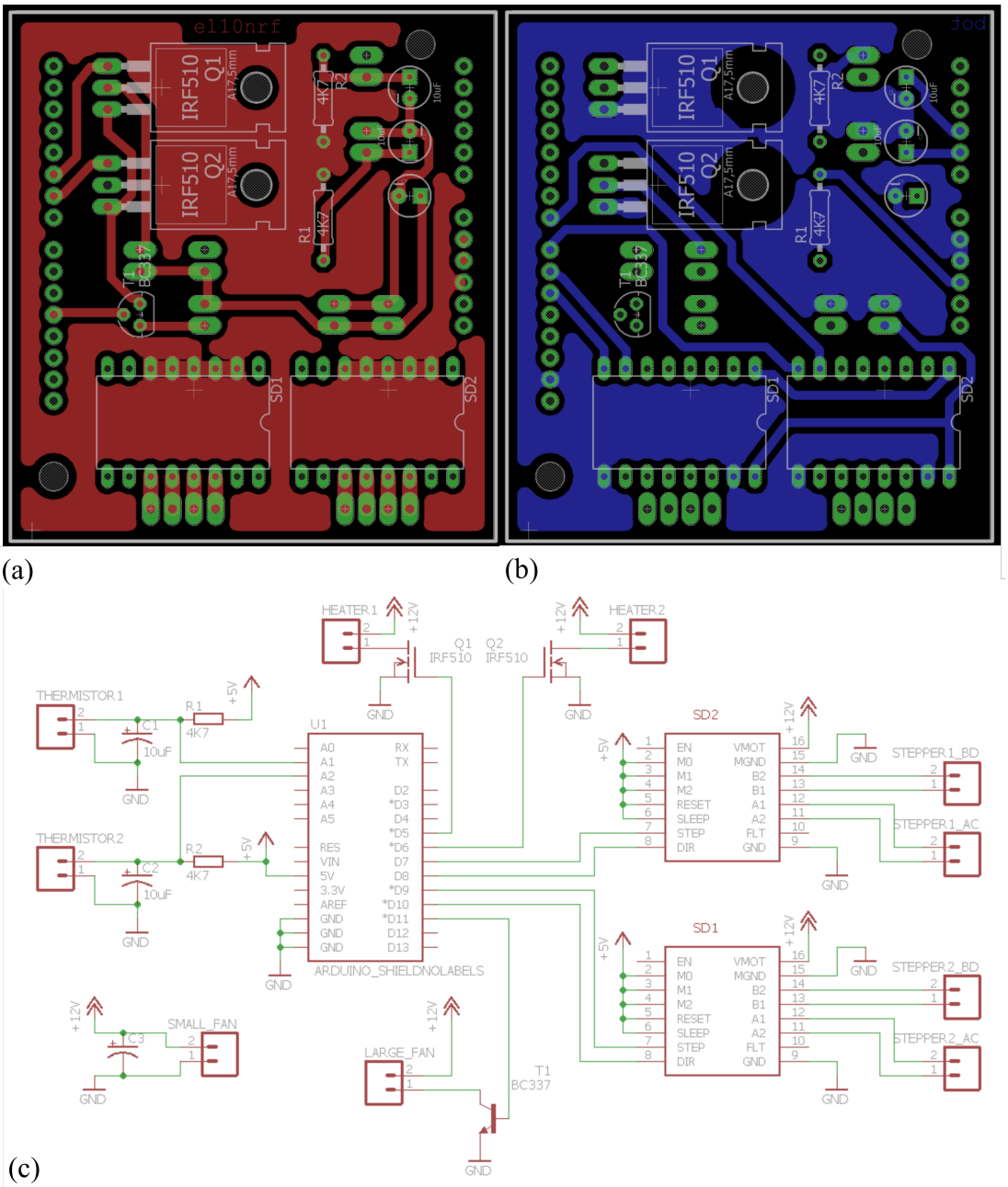

Figure 3.6: PCB track layout - (a) Front and (b) Back. (c) Circuit diagram of the extruder Arduino Uno Shield.

3.5 Software

To prepare an object for AM there are a number of steps to complete, usually in separate software packages. A typical work flow is depicted in Fig. 3.7. First a 3D model of the object is created in a CAD program. This is exported as an STL file and imported into a slicing program. This will decompose the file into many thin layers which will be built on top on each other. The tool paths and instructions are saved in the format of gcode. This is then loaded onto a 3D printer where the firmware interprets these instructions to control the hardware. In this section each of the software packages will be explained in greater detail.

The ARMS was designed so that it is compatible with current software which is used in FFF. Therefore, the programs used for preparing the 3D file for conventional 3D printing will be familiar to people who have used other 3D printers. The main portion of the software that has been developed is analogous to the firmware on a standard 3D printer. This is the program which runs on the printer's hardware and takes the gcode instructions and translates this into electrical signals to move the deposition mechanism. As standard software packages are only designed to work with three axis systems, some gcode was generated using Matlab scripts for specific prints. In the future ARMS would benefit from a slicing software specifically designed to work with, and take advantage of, the additional DOF this system has.

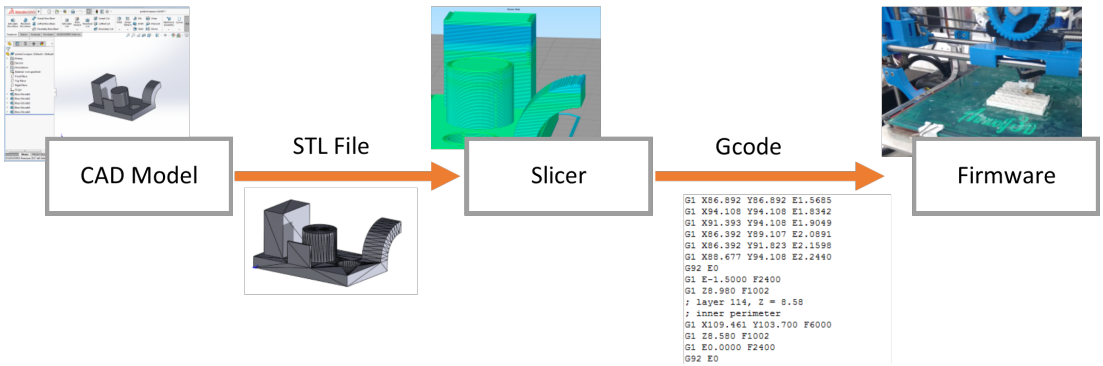

Figure 3.7: Workflow for preparing an object for AM. First a CAD model is created and exported as an STL file to be transferred to a Slicing program which calculates the thin slices and toolpaths required to build up the object. These toolpaths and instructions are saved as text in gcode. This is then loaded into the 3D printer, where the firmware running on its microcontroller interprets the gcode and moves the hardware accordingly.

3.5.1 3D Model

AM is a direct digital process, meaning that the manufacturing instructions are generated directly from a 3D model and by simply updating the model, the manufacturing process is also altered. Therefore, the first step for an 3D printer is to have a computer model of the object that will be fabricated. This can be created using Computer Aided Design (CAD) software, captured from an existing item using a 3D scanner or downloaded from an online repository of design files. The standard format which is used for almost all slicing software is the STL file, which describes an object as a series of triangular facets. This originated alongside the first Stereolithography process and has become the standard, although recently AM specific formats are being introduced to try and overcome some of its disadvantages. These include the fact that decomposing curved features into triangles can reduce the resolution of the part, reducing its precision. Also, no material or texture information is retained in the STL, making it unsuitable for complex multimaterial printing, as an individual STL file is required for each material. Once an STL has been acquired it then must be imported into a program which generates the tool paths for printing.

3.5.2 Slicers

A 'Slicer' is a program which takes in a CAD file and generates the machine instructions to send to the 3D printer. It will split the part into the layers which are inherent to AM and then create the tool paths within each layer so that the nozzle will outline all the features and fill the inside. These paths are turned into gcode, a human-readable set of instructions which contain the coordinates and other parameters for each movement. There are a huge number of settings which can be controlled when slicing a file. The main ones, which will be reported for any experiments, are described in Table 3.5.

An example of how these setting impact the results of 3D printing can be seen in Fig. 3.8. Often these parameters must be altered for different printers, materials and CAD files to get the best outcome.

The are several different programs available for slicing. In this work two were used; 'Slic3r' and 'Simplify3D'.

Slic3r has been developed by the open source community, and of the freely available options it is the one which has had the most development and offers more control over the lower level settings. This was used successfully for the initial development

Table 3.5: The major slicer settings used to generate gcode.

Setting	Description
Layer height	The thickness of each slice which will make up the printed object. Typically 0.1-0.3mm for a 0.4mm diameter nozzle.
Print Speed	Nominal speed to print at. This is modified by a number of other considerations, such as being; reduced on the first layer to improve adhesion; reduced for small layers to improve part cooling; increased for non-printing (travel) moves.
Temperature	Extruder temperature, this is material dependant and must be broadly matched with the print speed to ensure that enough molten plastic can be extruded.
Material	This affects a number of the other settings such as temperature and speed, so preset profiles are used for each variant. The correct diameter of the filament feedstock must be set.
Cooling	The part cooling fan speed can be varied depending upon the layer and feature being printed. Usually for PLA it is off for the first few layers to improve bed adhesion, then on full to improve the surface and stop thin sections curling.
Infill Density	FFF parts are usually semi-hollow, to save time and material. This impacts the mechanical properties so a balanced choice should be made. Typically $\leq 50\%$.
Infill Pattern	Several patterns can be used to fill the internal space. It has some impact upon the print time and mechanical properties.
Perimeters	The number of walls that are printed around the outsides of a layer. Significantly impacts the mechanical properties, but also the print time as perimeters are usually printed at a slower speed as these tracks will be visible once complete, unlike the infill.
Top and Bottom Layers	The number of solid layers with 100% infill to print on the top and bottom of the part. These increase the strength and cover up the gaps in the previous semi-hollow layers.
Software	The slicing program used. In this work either Slic3r or Simplify3D.

of the system, but when attempting to print more complex objects the software was too limited. Slic3r is very slow when slicing large (approx. 30cm high) objects or highly detailed STL files. It also is less flexible, for example the support structures are automatically generated across the whole part and the same settings must be used for the whole object.

Simplify3D was purchased and used for the majority of this work as it enables the user to selectively position support only where required, calculates tool paths very quickly and is able to handle large and complex files.

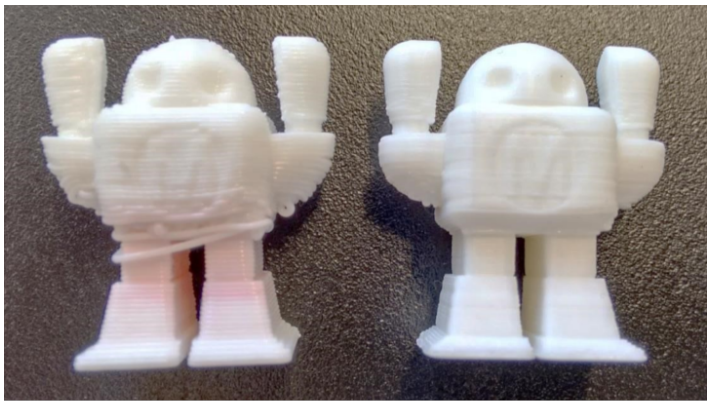

(a) (b)

Figure 3.8: An example of how slicing setting affects the output of a 3D printer. (a) Robot printed without a cooling fan causing the overhung areas around its waist and under its arms to sag. A layer height of 0.4mm was used giving the coarse stepped effect. (The red colouring is due to pen marks made on the filament when spooled so that its movement could be visually checked.) (b)Robot has printed with a cooling fan running and a layer height of 0.2mm giving much better results, but taking longer to print.

3.5.3 Gcode

Gcode is a programming language that is commonly used for computer numerical control (CNC). In AM it is the standard method of describing the machine specific toolpaths, and other instructions, that are generated when an STL is sliced. There are variations, but the majority of open-source firmware is based upon the RS247 standard from the National Institute of Standards and Technology in the U.S.A. [190]. Therefore, commands from this standard are used in this work. Only a small subset of commands

are used in standard FFF printing, as many are for use with milling machines and other CNC systems. The commands and their usage are listed in Table 3.6. The linear movement command has been extended from the standard convention and also includes parameters for setting the rotation of the extruder in relation to each of the axes. An additional command to move the base plate has also been created which has 6 parameters which correspond to the 6 joint angles of the base plate robot. The documentation for these commands is in Appendix A.

Table 3.6: The gcode commands used in this system to describe the machine instructions.

Command	Description
G0 or G1	Linear Movement of Extruder
G28	Home Extruder
G92	Reset Extrusion Length
M104	Set Extruder Temperature
M109	Set Extruder Temperature and wait until it is reached
M106	Fan On
M107	Fan Off
M117	Display Message
T0	Use Extruder 0
T1	Use extruder 1
M333	Move Build Plate Robot

3.5.4 System Control

This section will detail the main program which was developed to communicate across the various hardware modules in the system, perform all the required calculations and interface with the user. This was developed in LabVIEW (National Instruments), although Matlab (Mathworks) functions are called in the background for some computations. The reasons for this are explained in Section 3.6. LabVIEW was chosen as it is capable of communicating with a variety of hardware, it provides the tools to develop a GUI, it can be used to develop programs with complex parallel architecture and a library of functions was already available for interfacing with the Denso robots (from DigiMetrix GmbH).

The overall program architecture is depicted in Fig. 3.9. There are seven main modules, these run in parallel and each have a number of cases. The modules wait until they receive an instruction, either from the user via the GUI or from elsewhere in the program and then execute the case that has been instructed. A list of the cases in each module is shown in Fig. 3.10. Message queues are used to communicate between the different modules. These allow messages and corresponding data to be passed around the program in such a way that the messages will be executed in the order that they are added to the queue and no command is overwritten due to the producer loop operating faster than the consumer loop, as can often happen if using global variables to pass data around a program. These seven loops, and the main functions that each performs, are described below. In addition to the cases listed specifically, each has three basic cases. The *Initialise* state is called when the program first starts. This preforms actions such as connecting to a COM port for serial communication or resetting the GUI. The *Default* case is used to catch any messages that are not recognised and generate an error message. The final standard case is *Exit* which is called if the user presses the stop button or closes the window. This ensures that the program quits elegantly by shutting down any communications and closing any open files so that there are no hanging references.

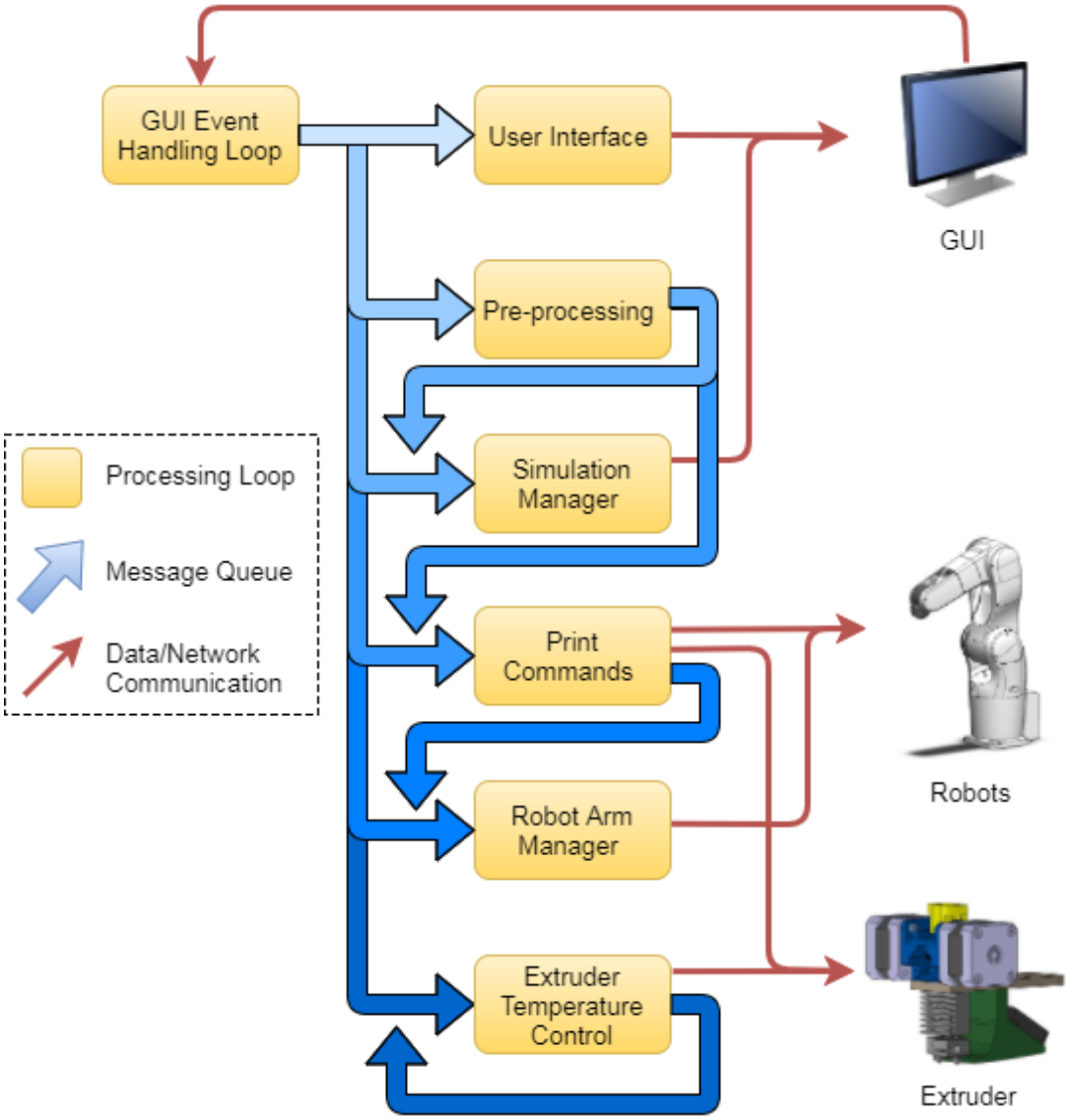

Figure 3.9: Schematic of the control program architecture. There are seven modules which are connected by message queues, the event handling loop raises messages depending upon the users input to the GUI. Other modules also send messages to related parts of the program. The extruder control keeps repeating to get the updated temperature. The robot and extruder are communicated to by their own dedicated modules when the user is manually controlling them, and by the Printing module during automatic motion to reduce delays.

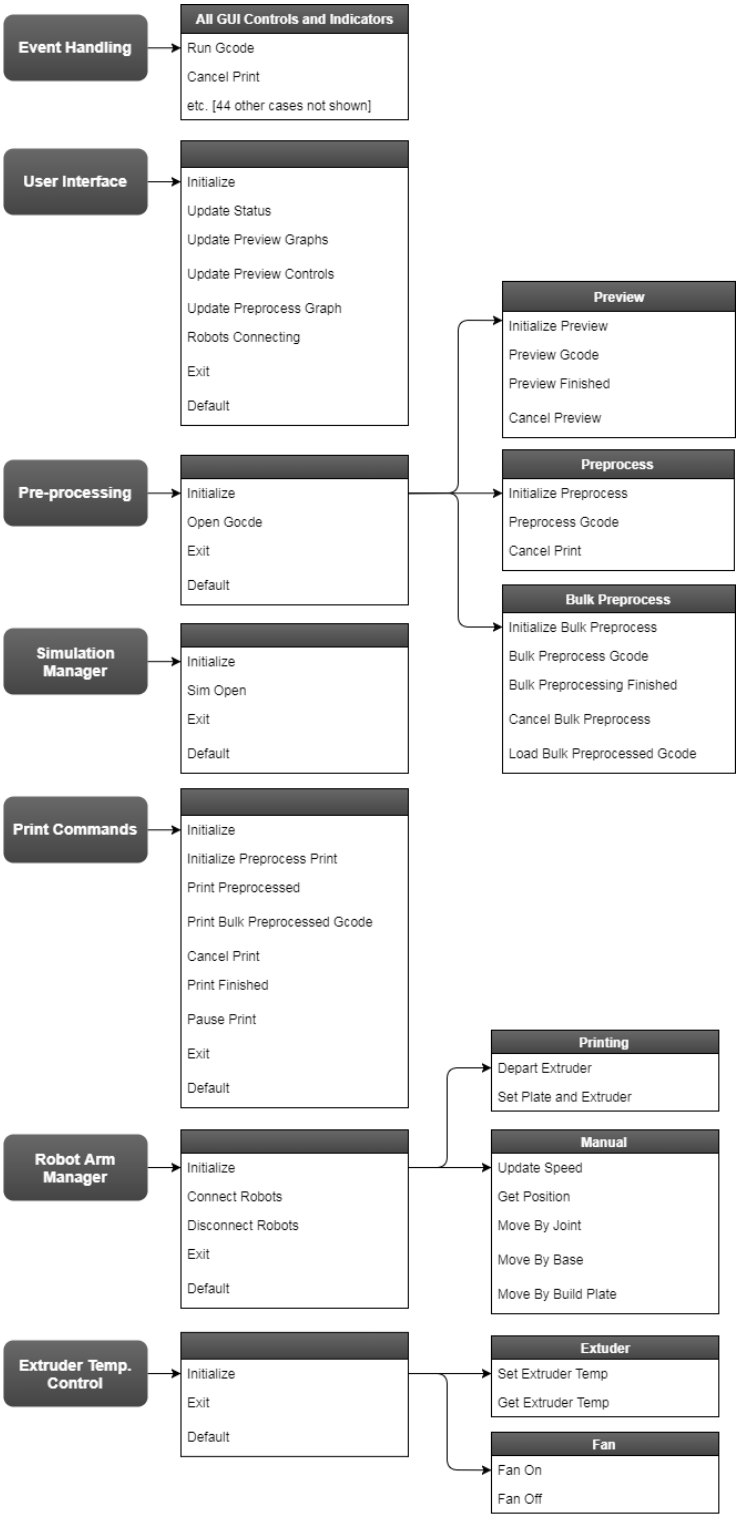

Figure 3.10: List of the messages which each message handing loop will respond to. This allows a distributed, parallel and extendible architecture as each module handles a well defined part of the program and can be independent to the other sections.

3.5.4.1 Event Handling Loop

The top module is an event handling loop, this listens for user generated events, such as mouse clicks on GUI buttons. It then either executes the required code if it is a small function or raises a message to activate a state in one of the other modules. It contains 46 cases which correspond to controls on the GUI.

3.5.4.2 User Interface Loop

This loop is used to update items on the GUI which are not time critical, but could slow the program if executed in another loop. Examples of this include updating the status message bar or the 3D graphs with information about the current line of gcode being printed or processed. Updating the GUI is slow, relative to processing other operations such as calculations. Therefore it makes sense to enqueue these updates, then publish them separately, so the processing loop is not held up. This module is also timed to only run every 150ms as updating the screen any quicker would not be perceived by the user.

3.5.4.3 Pre-Processing Loop

The pre-processing module handles the majority of the computing within this program. In this loop the gcode file is opened, parsed and each line is processed to calculate the required robot positions and other instructions for the hardware. There are three subsets within the cases for this loop (see Fig. 3.10). *Preview* allows the user to load a gcode file and simulate the output before physically using the robots. The gcode coordinates and paths are displayed upon a 3D graph on the GUI and the same kinematics calculations which would be used when printing are performed, but the output is sent to the 3D graphical simulation which shows how the robot will be positioned as each line of gcode is printed. *Preprocess* cases are used during 3D printing. Rather than directly calculate the motions of one line of gcode, move the robots, then calculate the next line, the calculations and printing are decoupled. The gcode is processed and enqueued to a buffer, without waiting for the robot to move in between, and the robot takes instructions from this buffer and moves without waiting for a calculation each time. Figure 3.11 shows this program flow. The details of the preprocessing are then expanded in Figure 3.12.

Depending upon the kinematics solver used, the preprocessing can be slower than the printing, leading to delays. This is explained more in Section 3.6. To overcome this *Bulk Preprocess* is used. This subset of cases allows the user to load a gcode file, run all of the calculations and then save all of the enqueued instructions to an external file. This preprocessed code can then be loaded in at another time and printed directly, without requiring any complex processing. All of the preprocessing is completed on a line by line basis, as the previous position of the robot must be known to calculate the best joint angles to reach the next coordinate.

3.5.4.4 Simulation Manager Loop

This loop is used to initialise and open the 3D Simulation of the kinematics of the system. If this is open, when previewing the gcode the robot arms will also move in the simulation, so that their position can be checked. A collision detection algorithm is also incorporated to help warn the user if the movement will cause an issue. The simulation and collision detection programs are further detailed in Section 3.5.6 and Section 3.5.7 respectively.

3.5.4.5 Print Commands Loop

The Printing module takes the calculated robot position, required speed, temperature, fan speed and extrusion length from the front of the queue and then communicates with the robot controller and microcontroller to physically print that instruction. Each setting is checked against the previous value and if there is no change, an update is not sent to cut down on needless communications which could slow down the system. Figure 3.12 (b) shows a flow chart of this process.

This loop communicates with the robot arm manager before printing to set the robots in their defined initial positions, and after printing to lift the extruder away from the completed part. The program also has the capability to pause and cancel the print. Pausing is very useful as it allows for the robot motors to be turned off and the safety enclosure opened so that the printing results can be inspected in person. It can also be used to change material during the build. To cancel the print a message must be inserted at the front of the queue, so that it is executed before the processed gcode, and all of the other messages are then cleared.

3.5.4.6 Robot Arm Manager Loop

During printing the commands for the robot arm are sent directly from the Printing loop, so that the sending of command is synchronised with extruder. For all other motions and setting changes this loop is used to communicate with the robots. There are cases to connect the robots, update their speed settings and move them using joint angles, build plate coordinates or robot base coordinates. These correspond with commands on the GUI to allow the user to manually control the robots. Before printing, the initialise print case sends a message to this loop so that the extruder robot is moved up out of the way and the position of the base plate robot is set. Once the print is finished or cancelled the extruder is lifted up to allow access to the print on the build plate. If the user chooses, or if the the program is exited, the connection with the robots is terminated though another case.

3.5.4.7 Extruder Temperature Control Loop

This module only has four main cases; Get/Set Extruder Temperature and Cooling Fan On/Off. This is because much of the control is performed on the microcontroller connected to the extruder. For this reason this loop is run at a low priority by adding a small delay between iterations. By default this loop keeps polling the serial port to read the temperature of the extruder, unless another message is added to the queue. This module allows manual control over the temperature, and is used to turn off the heaters if the print finishes, is cancelled or the program is exited.

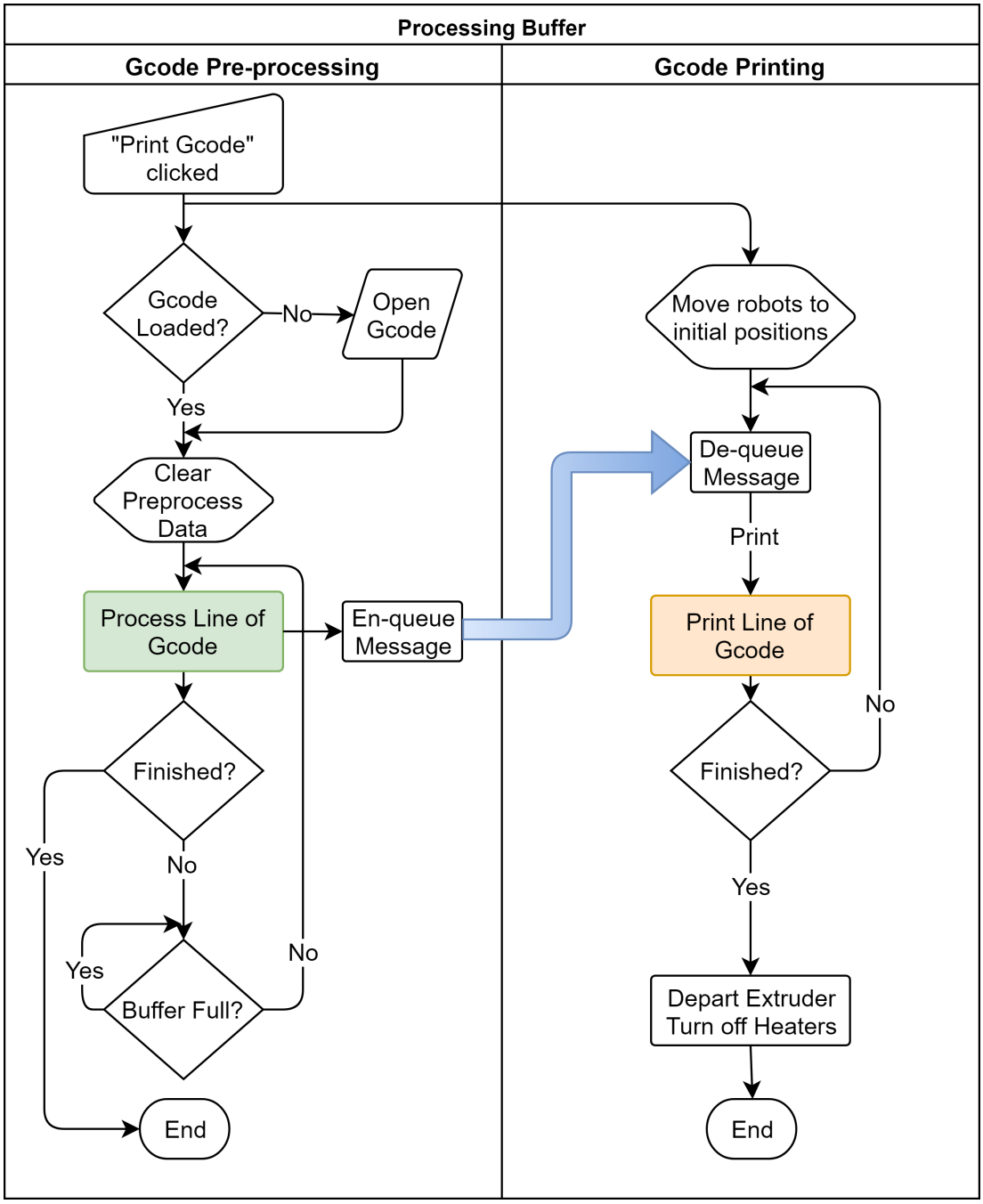

Figure 3.11: Flow chart depicts how the program progresses when 3D printing from a gcode file. The preprocessing and printing modules run in parallel. Each line of gcode is processed and added to the end of a message queue, the printing queue then takes each message from the front of this queue in turn and sends the instructions to the hardware. Details of the 'Process line of gcode' block and the 'Print line of gcode' block are in Fig. 3.12.

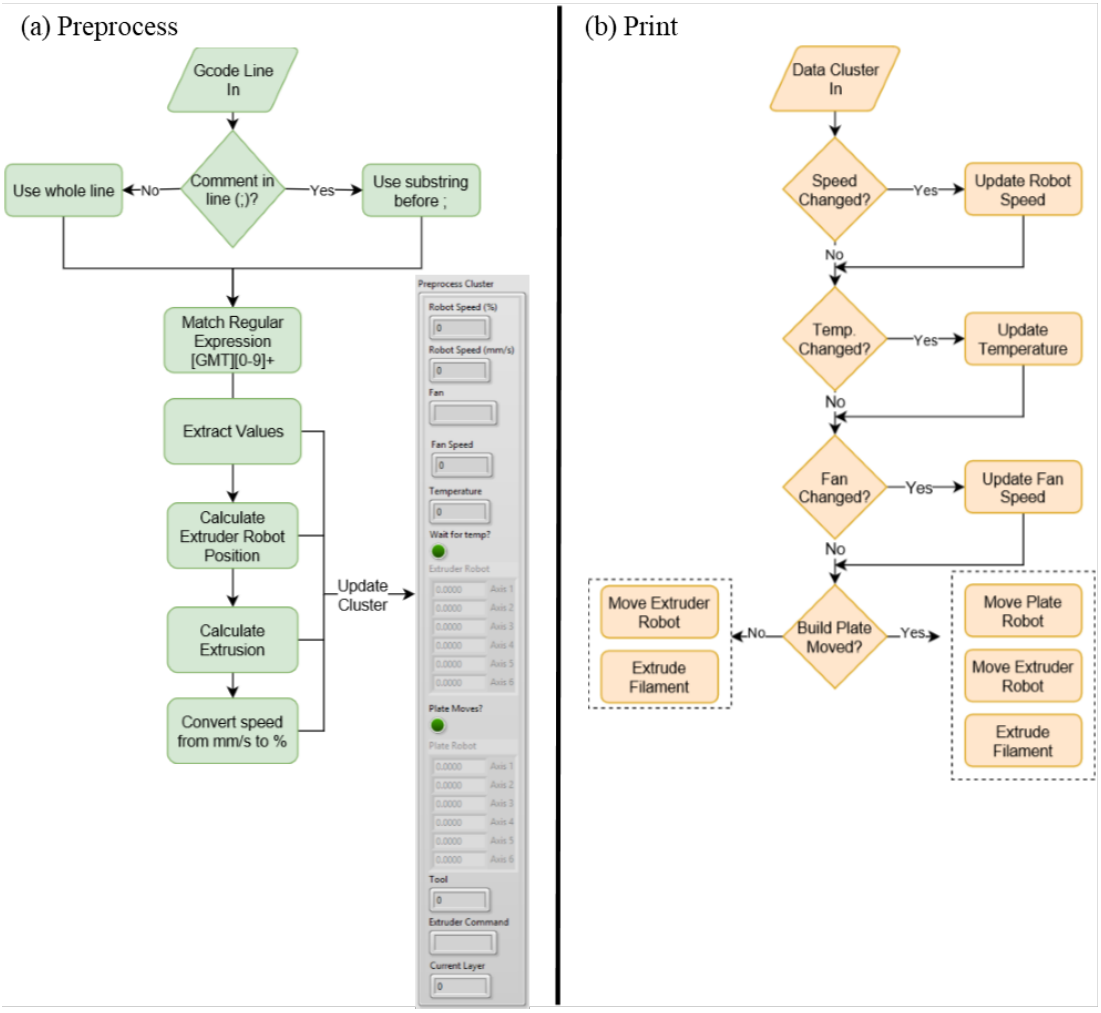

Figure 3.12: (a) Procedure for processing a line of gcode. First the text string is parsed, looking for key codes which correspond to functions in gcode. The values from these are extracted and used to perform the calculations. The results are saved into a cluster of data, which is sent using a message queue to the print loop (shown in Fig. 3.11). A screen capture from LabVIEW shows the graphical representation of this data cluster which lists all of the information which is needed to print each line. (b) Flow chart showing the details of sending instructions to hardware. When 3D printing from a line of gcode, the current state of the system is first checked to minimises unneeded communications. The instructions to move the robot(s) and extrude filament are timed to be sent at the same time, helping to synchronise the two movements.

3.5.5 Graphical User Interface

To make the system intuitive and user friendly, a Graphical User Interface (GUI) is used as the main way for the user to interact with the system. There are five main pages which contain all of the controls and indicators the user needs to interact with ARMS. These are briefly described below in Table 3.7. A screen capture of the *Print* screen is shown in Fig. 3.13. The other screens are similar and can be seen in Appendix A.

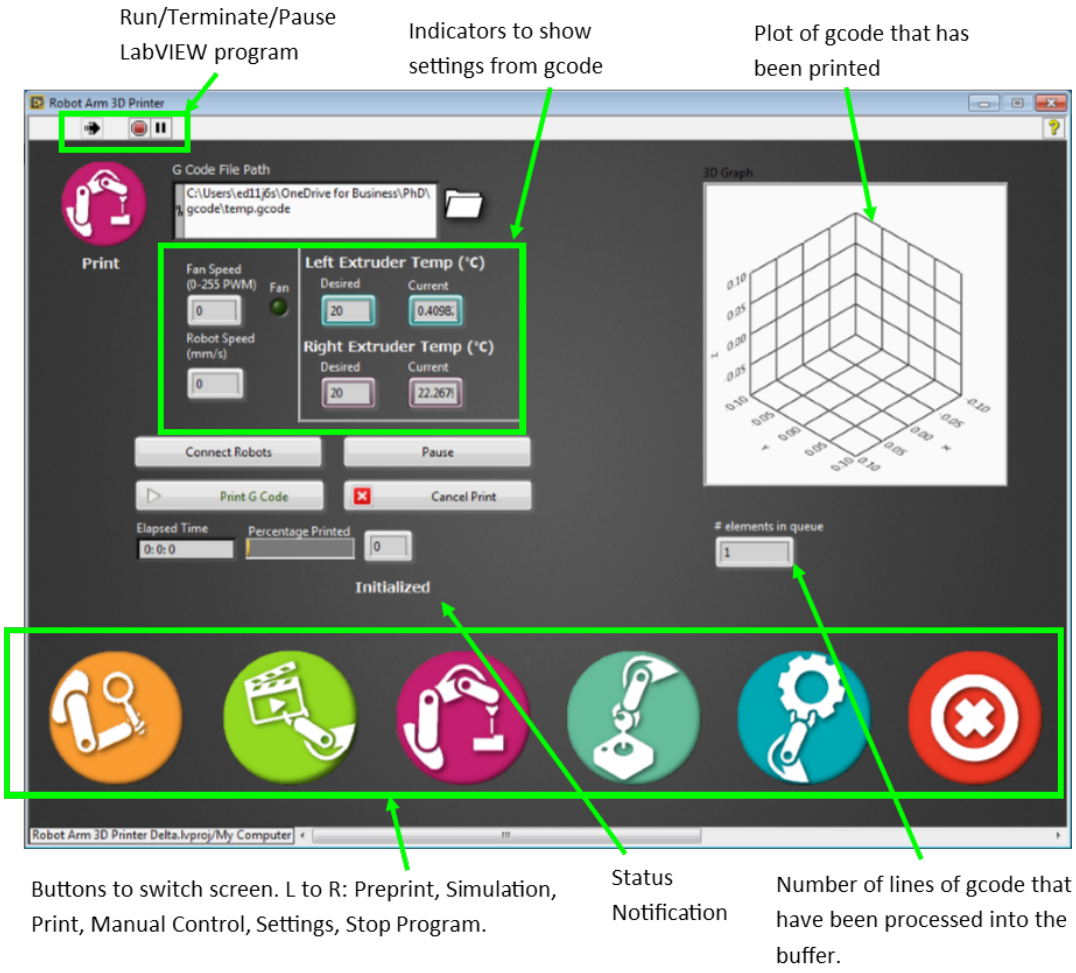

Figure 3.13: Screen capture of the GUI, showing the Print screen. The bottom buttons and the status notification are the same on all screens. The controls and indicators are specific to each screens function.

Table 3.7: Descriptions of the main screens that form the GUI.

Screen	Description
Pre-Print	Used to open a gcode file and either preview it on a 3D graph, and the robot positions in 3D graphical simulation, or to bulk preprocess it for printing later.
Simulation	Here the simulation can be opened and each of the robots controlled manually. A button sets the built plate at the initial position that is used for printing, and another kinematically links the extruder motion to the build plate position. The extruder can then be controller by changing the parameters which would be varied in gcode: The coordinate on the build plate and the rotation around each axis.
Print	This screen contains all the information and controls needed to 3D print using the system. Before starting, the robots must be connected and gcode opened. Indicators show the fan and robot speed, the extruder temperatures, the elapsed time and the percentage printed.
Manual	Controls to move the robots and the extruder can be found on this page. Three buttons swap between methods of moving the extruder and plate robots. These are by joint angles, robot base coordinates and build plate coordinates. The camera robot can be moved by jogging joint angles, and poses can be saved and recalled to quickly move between them. The manual extruder controls let the user extrude or retract filament by preset distances of 0.1, 1 and 10mm. The temperature can also be controlled which is useful for preheating before printing or keeping the extruder hot to change material.
Settings	Some important settings are shown here, including which of the four robots is assigned each job, the COM port the microcontroller is connected to, the size of the build plate and the position in which the plate robot will begin.

3.5.6 Simulation

A kinematic simulation of the four robot arms was also implemented. This is vital for checking the positions of the robot arm before running gcode on the system. Both the simulation and the printing use the same code to calculate the robot's positions, so the user can check how gcode will be interpreted, before testing upon the hardware. As the extruder and build plate robot are often in close proximity, and can move faster than one could react, this is an important step within the printing process when using any non-standard gcode.

The simulation program uses a combination of LabVIEW 3D picture functions and robot simulation functions from the robotics toolkit. As standard, the robot arm simulation was not able to display CAD files, instead the robot was formed from simple cylinders and boxes. To overcome this and improve the utility of the simulation, these functions were modified to use STL files to represent each link in the robot. Figure 3.14 shows a screen capture of the graphical simulation and the GUI used to control it. The user can rotate, zoom and pan around the 3D scene using the mouse to see either the whole scene, or close up details. Each robot can be controlled manually by dragging sliders to adjust each joint angle. The response to gcode input can be visualised either by loading and previewing a whole file, or by inputting values directly into the control on the screen. A toggle button is used to switch between control via build plate coordinates, or joint control, for the extruder robot. When simulating the extruder position on the build plate, a visual representation of the kinematic links is displayed. In Fig. 3.14 the orange link represents the extruder and the grey cylinders correspond in length to the X, Y and Z coordinates that have been entered into the control. In this mode the manual sliders for the extruder robot are disabled, but the other robots can be moved. The kinematic link allows the build plate to be moved and the extruder robot will follow it, so that the extruder remains in the same position relative to the plate.

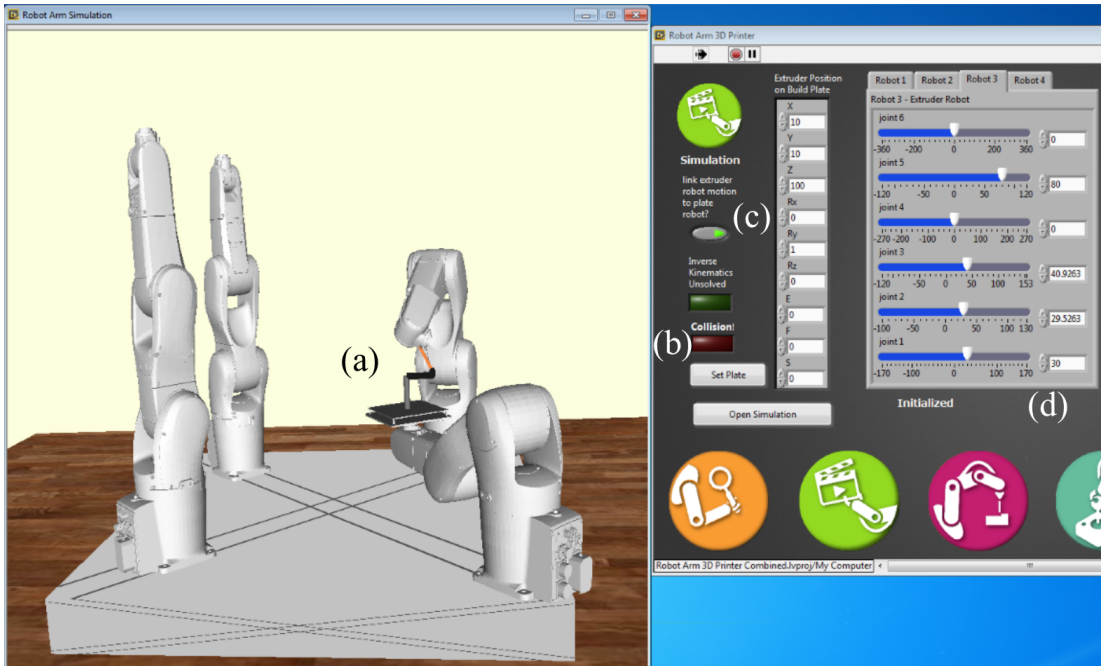

Figure 3.14: (a) 3D graphical simulation of the robot kinematics using CAD models of the robots. Here the extruder robot is positioned in relation to the build plate and the virtual kinematic links are visible as cylinders. (b) Collision detection runs in the background and will light up this indicator if the robots collide. The indicator above displays if the kinematics cannot be solved. This typically happens when the build plate is positioned so that it's work space does not overlap with the extruder robot, so the required coordinate cannot be reached. (c) This set of controls are the values which would be extracted from gcode and can be altered to move the extruder in relation to the build plate. (d) Tabs containing sliders which move the joints for each robot.

3.5.7 Collision Detection

A collision detection algorithm was implemented within the simulation so that the user would be warned of potential collisions when previewing gcode. The Gilbert-Johnson-Keerthi (GJK) algorithm was used for this. GJK is commonly used in computer games as it can run in real-time due to decomposing the complex issue of whether two items overlap, in 3 dimensional space, into relatively quick calculations [191, 192].

The function first does a coarse detection, then a fine one if needed, using progressively smaller bounding boxes around the robots. This is to reduce the number of comparisons that need computing. The first run uses a cube as the bounding box

around a robot arm. If two of these cubes are overlapping then there is potentially a collision. However the arms may only be taking up a fraction of the volume within a cube, by being diagonal across it for example, so a closer check is needed. The second check uses six cylinders to surround each of the links in the robot arm. These approximate the shape much more closely, but not exactly, so the results of this test are useful for flagging potential issues to the user, but may be incorrect if the robots need to work very closely together. The shape could be more exact but this would slow down the calculation considerably, as using a mathematically defined shape allows simplifications to the mathematics. This algorithm is implemented using Matlab script nodes, within the main LabVIEW program. These open a Matlab server in the background and use this to run Matlab codes, then output the results to be used in LabVIEW. As this algorithm contains a lot of equations, logic cases and calls to other functions it was most efficient to develop within the Matlab environment and incorporate in this way.

3.6 Kinematics

The extruder and build plate robots are mathematically linked in one, 12 DOF, kinematic system. This allows the nozzle to be positioned relative to the build plate, no matter which orientation or position the build plate has been set to. To make the system compatible with existing slicing software, and to ensure the same gcode could be used irrespective of the built plate's pose, the system is set up to take gcode which describes the coordinates in relation to the build plate origin.

3.6.1 Robot arm positions

The steel base has T-slots along the diagonals, allowing the position of the robots to be adjusted. There are locating holes at intervals along these, meaning the robots can be placed at known locations. This allows the set-up to be easily adjusted for different purposes. The position of each robot is described in relation to the global coordinate frame, G, located at the bottom right of the base, shown in Fig. 3.15. This allows each robot to be repositioned with only minimal changes required to the mathematical model. Each has its base angled toward the centre. The first robot, R_C, is used to hold a HD 3D camera that allows the user to monitor the printing process closely while still being outside the safety fence area that surrounds the robotic arms. R_G, is not

currently used in this set-up but in the future may have a gripper attached to be used to pick and place components or move a 3D scanner over the assembly. Robot three, R_E, holds the extrusion mechanism and the fourth robot, R_P, holds the build plate.

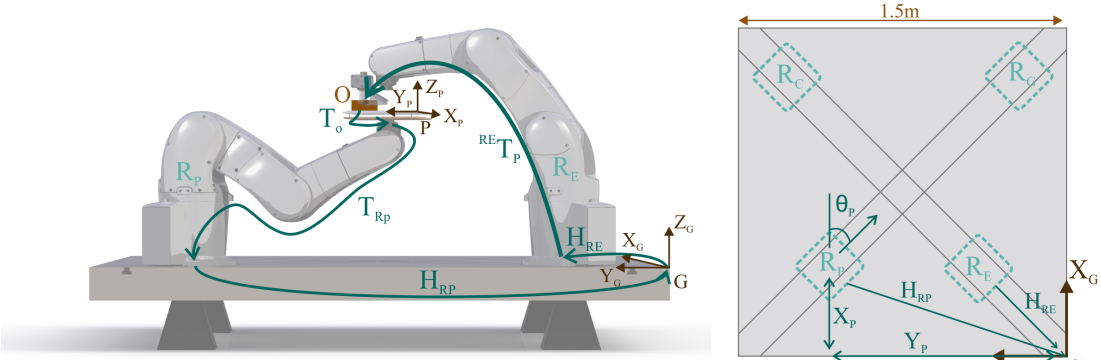

(a) Side View (b) Top View

Figure 3.15: (a) Side view of system showing the Build Plate, R_P, and Extruder, R_E, Robots, the printed object, O, and the build plate origin, P. The global origin, G, is at the bottom right corner. The transformation used in the kinematic model are also denoted. The Camera, R_C, and Gripper, R_G, robots are removed from this view for clarity. (b) Top down view of the system, four robot arms are located in T-slots which cross the diagonals of a steel base plate.

To calculate the position and orientation of both the build plate and the extruder, the poses of the robot bases are first required. The homogeneous transformation matrix for the position of R_P, in relation to G, is composed of a translation and rotation to form Eq. (3.1). Transformations for the other robots are formed similarly.

$$H_{R_p} = \text{Trans}(X_p, Y_p), \text{Rot}(Z, \theta_p) \tag{3.1}$$

3.6.2 Denavit-Hartenburg Parameters

A serial-link manipulator, such as these Denso robotic arms, can be described as a chain of links, each connected by a joint. These joints have a single DOF and can be either revolute (rotational motion) or prismatic (translational motion). The extruder robot, RE, build plate robot, RP, and the printed object, O, are each described using the original Denavit-Hartenburg (D-H) notation which is a method of describing the links using a small set of parameters [193, 194]. For a chain with N joints there will be $N + 1$ links, numbered 1 to N and 0 to N respectively, starting at the base of the

manipulator. Each link and corresponding joint can be described with four parameters, presented in table 3.8.

Table 3.8: Denavit-Hartenberg parameters.

Name	Symbol	Description	
Joint angle	θ_j	Angle between the x_{j-1} and x_j axes, about the z_{j-1} axis	Revolute joint variable
Link offset	d_j	Distance along z_{j-1} axis from frame $j-1$ to the x_j axis	Prismatic joint variable
Link length	a_j	Distance between z_{j-1} and z_j axes along x_j axis	Constant
Link twist	α_j	Angle from z_{j-1} axis to the z_j axis, about the x_j axis	Constant

The procedure used for assigning coordinate frame j is as follows:

1. z_j is aligned with the joint j axis
2. x_j points along normal from z_{j-1} to z_j. For joint axes that intersect, x_j is parallel to $z_{j-1} \times z_j$.
3. The right hand rule is used to place y, completing the frame.

In this system there are three distinct sections which are defined by kinematic links; the extruder robot, the build plate robot and the gcode, or printed object, coordinate.

3.6.2.1 Extruder Robot

This robot has the extruder assembly attached to its wrist. The last coordinate frame is set to correspond with the nozzle where the melted plastic exits. The extruder is set up for dual extrusion but only one nozzle is used for the multiaxis experiments. This nozzle is slightly offset from the centre line of the robot leading to a small angle on the

last link, see Fig. 3.16. The convention for the last, or tool, frame is usually decided to make it more intuitive when a parallel gripper is used. The z axis points away from the centre of the gripper and is referred to as the approach vector and the x axis points along the line of motion for the fingers. In this case however it is more convenient for the z axis to be rotated 180 degrees so that it points back towards the robot. Later, when the motions of the two robots are linked this allows the tool frame of the extruder robot to be aligned with the last frame of the plate robot, positioning the nozzle above the build plate, without needing additional rotations to be applied to the commands.

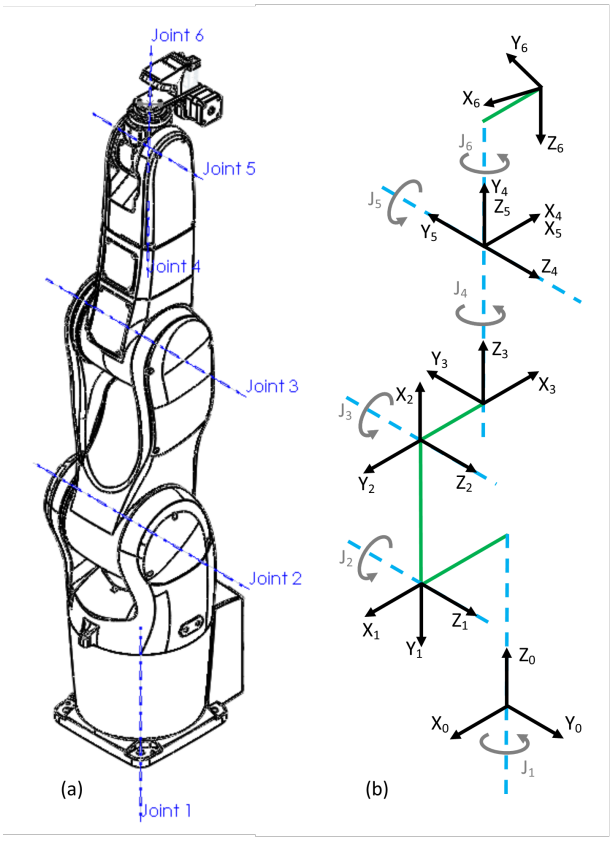

Figure 3.16: Extruder Robot Joint positions (a) and Coordinate Frames (b). Blue dashed lines depict joint axes and green lines common normals.

Table 3.9: Extruder Robot D-H parameters.

Frames	Link	$\alpha(rad)$	a (m)	$\theta(rad)$	d (m)
0-1	1	$-\pi$	0.030	J_1	0.395
1-2	2	0	0.340	$J_2 - \pi$	0
2-3	3	$-\pi$	0.020	$J_3 - \pi$	0
3-4	4	π	0	J_4	0.340
4-5	5	$-\pi$	0	J_5	0
5-6	6	2π	0.075	$J_6 + 0.121$	0.136

3.6.2.2 Build Plate Robot

This robot holds the build plate and has a very similar kinematic chain to the Extruder Robot however the final frame, 6, is not offset from the wrist but is central to the build plate. Rather than setting the plate robot in a static position, the plate can be moved to allow experiments with different orientations or changing position for printing larger parts. The configuration of the robot can be described with the kinematic model of links and joints and can be used to calculate the desired position of the extruder robot. A diagram depicting the robot and the corresponding coordinate frames is in Fig. 3.17 and the D-H parameters are summarised in Table 3.10.

Table 3.10: Plate Robot D-H parameters.

Frames	Link	$\alpha(rad)$	a (m)	$\theta(rad)$	d (m)
0-1	1	$-\pi$	0.030	J_1	0.395
1-2	2	0	0.340	$J_2 - \pi$	0
2-3	3	$-\pi$	0.020	$J_3 - \pi$	0
3-4	4	π	0	J_4	0.340
4-5	5	$-\pi$	0	J_5	0
5-6	6	0	0	J_6	0.08

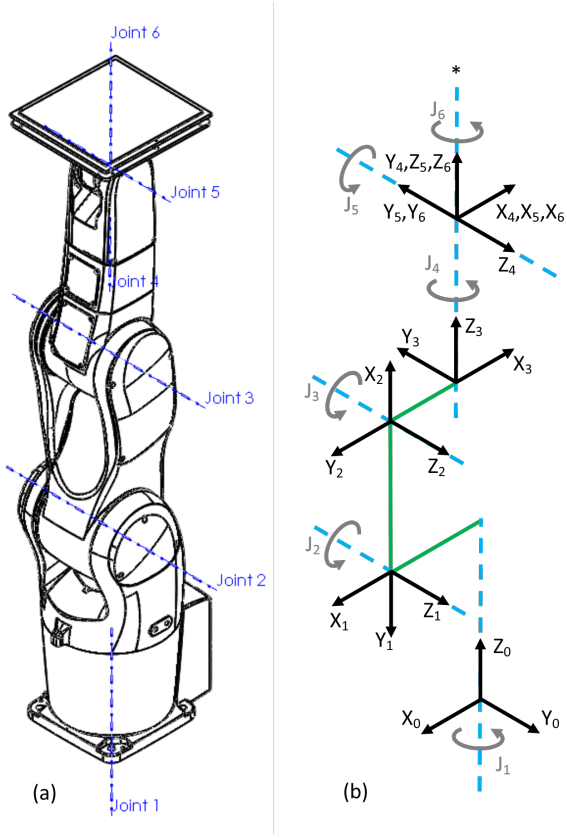

Figure 3.17: Plate Robot Joint positions (a) and Coordinate Frames (b). Blue dashed lines depict joint axes and green lines common normals.

3.6.2.3 Printed Object

The input instructions for this system are in the format of gcode which consists of a list of coordinates and orientations that the nozzle must move to. These coordinates are relative to the build plate origin, as in normal 3D printers this is at a known location. In the kinematic model a chain of links is used to represent this coordinate. This chain is comprised of three prismatic joints, the length of each is a variable which corresponds to the X, Y and Z coordinates, and three rotational joints which corresponds to the desired rotation of the nozzle around each of the three Cartesian axes. Later these phantom links are added to the end of the physical robots' kinematic chain giving a representation of the gcode coordinate in relation to a known physical location such as the base of the robot arm. Figure 3.18 shows the set of coordinate frames that are

used in this model, the * in this and Fig. 3.17 indicates where these two chains are connected. Table 3.11 gives the corresponding D-H parameters.

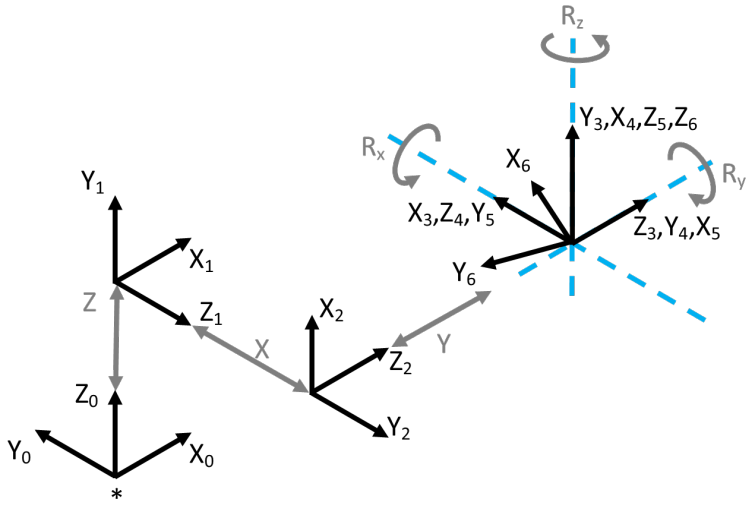

Figure 3.18: Coordinate Frames for the virtual links that represent the printed object. Blue dashed lines depict joint axes and grey arrows the joint motions.

Now that the kinematic links for each section have been defined they can be combined, along with the matrices defining the robot positions. In Fig. 3.15 the loop which these transformations represent is marked by green arrows. They could be combined in the opposite order, so that the nozzle remains stationary and the build plate is moved, but for multiaxis printing it makes more sense to move the smaller end effector and keep the larger surface stationary so that it does not collide or obscure the print area.

Table 3.11: Printed Object D-H parameters.

Frames	Link	$\alpha(rad)$	a (m)	$\theta(rad)$	d (m)
0-1	1	π	0	0	Z
1-2	2	π	0	π	X
2-3	3	0	0	$-\pi$	Y
3-4	4	$-\pi$	0	$R_y + \pi$	0
4-5	5	π	0	$R_x + \pi$	0
5-6	6	0	0	$R_z + 1.44$	0

To calculate the required joint angles for R_E to position the nozzle at the point defined by the gcode input, the pose has to be described in relation to the base of R_E. The first step is to find the configuration of the printed object set of links, O, by using the input gcode, p, in forward kinematics, Eq. (3.2). As the links between each joint are defined by the Denavit-Hartenberg parameters the values from the gcode can be directly entered to find the transformation matrix that defines that link, ${}^{N-1}A_N$. Combining these gives the homogeneous transformation T_O, Eq. (3.3). This describes p in relation to the wrist of RP. $T_{(R_P)}$ is calculated similarly using the current joint angles of the plate robot.

$$\xi_O = K(\mathbf{p}) \tag{3.2}$$

$$\xi_O \equiv T_O = {}^0 A_1 \, {}^1A_2 \ldots {}^{N-1} A_N \tag{3.3}$$

These transformations, along with matrices which describe the robots position on the build plate, are combined to give one transformation matrix which relates $\mathbf{p}$ to the base of R_E.

$${}^{R_E}T_p = H_{R_E}^{-1} H_{R_P} T_{R_P} T_O \tag{3.4}$$

Now that the desired pose of the extruder has be calculated, Inverse Kinematics, K^{-1}, is used to calculate the joint angles, d, required for R_E to achieve that configuration, Eq. (3.5). These values, and other information such as the temperature and amount of plastic to extrude, can then be sent to the hardware to print that track of plastic. The same calculation is then performed again on the next line of gcode.

$$d = K^{-1} \, {}^{R_E}T_P \tag{3.5}$$

3.6.3 Inverse Kinematics Processing

Both the algorithm used to solve the Inverse Kinematics and the program architecture to do these calculations changed during the course of this research as the system requirements evolved and limitations were discovered.

Originally each line of the gcode was taken as an input, the robot joint angles were calculated and the robot was then commanded to move before the next line was processed. This worked to prove the concept and gave acceptable print quality results for standard planar layer prints. The gcode generated by the slicing software does not

use arch or circle commands, and there is no function to instruct the robotic arms to describe arches. To overcome this curved shapes are split into many short straight lines and each end point is written as a single line of gcode. When printing these geometries the short delay while the calculation is completed becomes apparent. These pauses were only a few miliseconds long but can visually be seen in the surface quality of the prints as these changes in velocity are reflected in the width of the plastic tracks. The overall speed of the print was also significantly affected.

To address this the program was changed to allow the calculated commands to be saved, rather than sent to the hardware. This processed data could then be loaded and printed without having to perform the calculations at the same time. This is inefficient as the whole file has to be processed before printing can take place, increasing the overall process time. However, while the total processing and print time was 40% longer than previously, the actual print time was 30% quicker and the surface was also visually much smoother. The times for these and the following print are summarised in Table 3.12. After this test it was clear that pre-calculating the joint angles can improve the process outcome, but needs to be calculated in parallel with the printing to reduce the overall time and make the system more practical. The use of LabVIEW aided this change, as creating parallel loops for different processes to run in is a standard architectural feature. The processing part of the program was separated out from the printing part, which communicates with the hardware. A message queue connects these and works as a buffer, so the calculations can be performed at any time, whether the robot is in motion or not, and are added to the end of the queue. The printing loop then takes data from the front of the queue each time the robot has completed its movement. As this is now a case of passing data to the hardware in a format that it can read, rather than having to first do kinematic calculations, there is no perceptible delay. This program structure is explained in Section 3.5.4. Using the online preprocessing and buffer architecture, the print time is twice as quick as the unbuffered test and the surface has fewer bumps when visually inspected (Table 3.12).

The inverse kinematics solver that was used for these tests, and all the planar layer prints, was the numerical solver built into the Labview robotics module. This is based upon Peter Corke's robotics toolkit for matlab which is widely used in research [193]. This worked well for the planar layer work, but when proceeding to the multiaxis work a limitation of this function caused difficulties. The function ('ikine') calculates the

Table 3.12: Print and processing times for different software architectures when printing the same STL file [195], using identical gcode.

	In-line Calculations	Preprocessed	Buffered
Processing Time	Combined	1:47:47	Combined
Print Time	2:13:52	1:32:22	1:06:03
Total	2:13:52	3:20:09	1:06:03

joint angles which cause the robot end effector to be at the required configuration, without any regard for the physical limitations of the robot's joints (see Section 3.3 for these limits). This causes the function to output angles to the robot which its joints cannot achieve. As the robots have their own controller, it stops them from attempting to do these movements and outputs an error, causing the printing program to quit. For the planar layer work, the robot positions did not differ greatly from the initial configuration, where none of the joints are close to their limits, so it was unlikely that this error would occur. Multiaxis printing, however, required the robot to go through much greater ranges of motion and to positions which could be achieved via multiple joint configurations. This caused errors which could not be easily predicted, as while the pose may be within the robot's capability, the algorithm may choose one of the solutions which was not physically achievable. The outcome of the inverse kinematics can be influenced by changing the initial pose that it is seeded with. By ensuring the gcode is made up of closely spaced points it is more likely that the solver would converge on a pose similar to the previous one, but this approach did not afford enough control as errors could still occur.

An alternative function, 'ikcon', was then used which limits the search space of the minimisation function to the allowable joint angles. This is available as part of Corke's Matlab toolkit, but National Instruments have not created a version of this in LabVIEW. It was therefore accessed using Matlab script nodes, which are blocks within the LabVIEW development environment which open up Matab in the background and allow M scripts to be executed and the results fed back into LabVIEW. While this does add additional dependencies to the main program, it allows access to the resources that are included in Matlab. Ikcon relies upon the Matlab Optimization Toolbox so it would have not been trivial to convert it to a LabVIEW only function.

This function solved the issue of the incorrect angle commands being sent to the

robot arms, but the minimisation function is slower to converge upon a solution. This caused the buffer to be depleted quicker than the calculations can be performed, once again leading to uneven motion and poor prints. Bulk preprocessing was reinstated so that gcode can be processed and saved separately before printing. As this is a research machine this trade-off is acceptable, a large throughput of objects is not required. The calculations could be sped up in the future by the addition of more computational power and the use of the 64-bit version of LabVIEW, which benefits from allowing greater parallelisation of tasks.

The error from this inverse kinematics function was assessed by using it to calculate the required joint angles, as usual, and then feeding the output back into forward kinematics, which gives the pose of the robot using that joint configuration. This can then be directly compared to the required pose from the gcode input. When using the Labview function, 'ikine', the error was less than 1×10^{-6}m. For the Matlab function with joint limits, the first results highlighted a steady state error which was removed by ensuring that both the inverse and forward kinematics are using π to the same precision.

Following this the function still exited before minimising the error to a level that is acceptable in this system. To change this, two tolerances were varied. `TolCon` is the upper bound of any constraint functions used in the minimisation and `TolFun` is the lower bound of the step size for each iteration. Therefore, by making these two values smaller the algorithm will continue to iterate, getting closer to the minimum value of the function. Fig. 3.19 shows three graphs, in the first the tolerance values are set at the default. The second two show a decrease in the error which corresponds with reducing the tolerances. As increased iterations slows down the calculations when printing the tolerances were not reduced further.

(a)

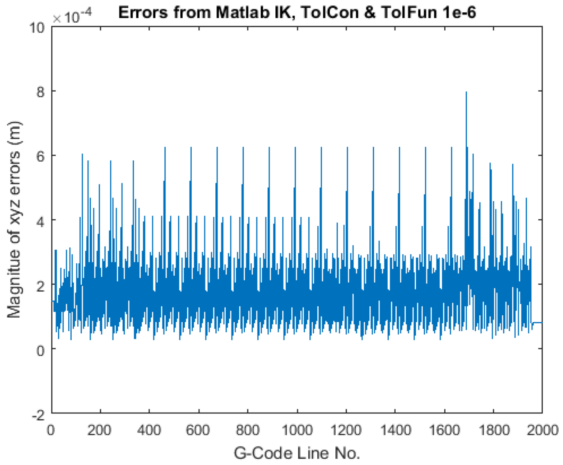

(b)

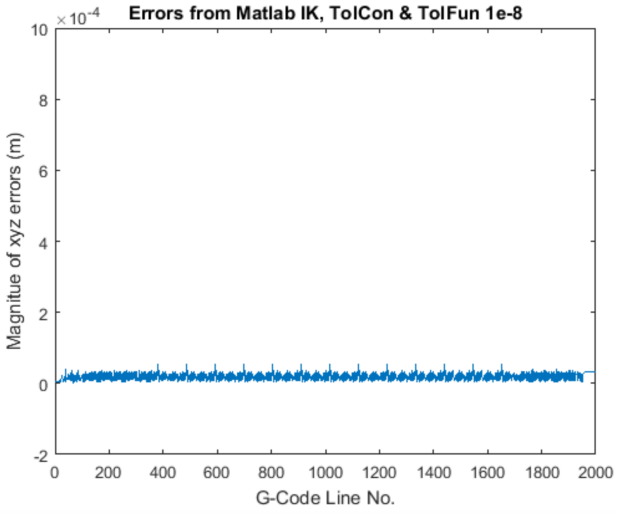

(c)

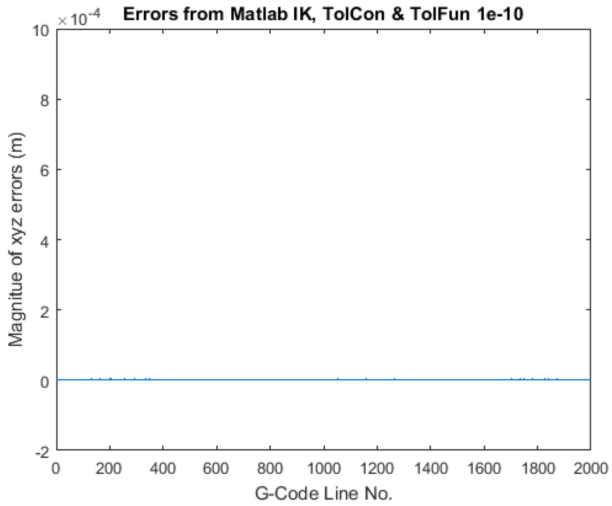

Figure 3.19: Positional errors from inverse kinematics solved using using a bounded minimisation function to return joint angles only within a certain range. Tolerances used as conditions for exiting the minimisation algorithm were set to; (a) default, $1e^{-6}$, causing large errors, (b) $1e^{-8}$, reducing the errors significantly, and (c) $1e^{-10}$, reducing the error to be low enough for precise sub-millimeter movements.

3.7 Experimental Design for System Validation

Following the integration of the various sub-systems described above, the efficacy of ARMS to 3D print conventionally, i.e. using 2.5D deposition, was assessed both qualitatively and quantitatively. To verify that the system is capable of 3D printing items which are of a comparable quality to existing FFF printers, four methods of testing were used: visual inspection, tensile strength, dimensional accuracy and surface roughness. The experiments and parameters used are presented below, before the results are given in Section 3.8.

3.7.1 Visual Inspection

The first experiment involved printing objects which are commonly printed on other 3D printers and assessing the results subjectively. The criteria below was used to fist iteratively tune to printing parameters (a process which is required on any FFF 3D printer) before a selection of items were printed. It was also decide to test a small range of filaments, including a flexible TPU (see Table 3.4), as these filaments are compatible with many standard FFF 3D printers.

To visually check the 3D prints the following criteria was used:

1. Part stuck to the bed, no lifting at the corners.
2. No under-extrusion. No gaps between tracks or bowed top surface, small features printed.
3. No over-extrusion. Tracks flat, no excess material causing ridges or the top surface to bulge.
4. Solid top and bottom surfaces. Shows the correct starting height for the first layer, and there is enough infill and dense layers to close any gaps.
5. Correct retraction settings. No strings of plastic or oozing on travel moves due to too little retraction. No delay in the start of tracks due to too much retraction.
6. No distortion due to overheating. Cooling fan effective for small and thin features.
7. Consistent layers. No excessive marks, spots, lines or other blemishes.

3.7.2 Tensile Strength and Dimensional Accuracy

To compare results between other FFF printers and ARMS, a standard 'dogbone' tensile test sample was used. As there is currently no standard for tensile testing of plastic AM parts, ASTM D638: Standard Test Method for Tensile Properties of Plastics [196] was used with 7mm thick Type I samples. As it is well known that FFF pasts are anisotropic [7, 113, 197], these were printed in two orientations to compare the two behaviours across different printers. Horizontal samples were printed flat upon the bed so that the layers are along the length of the sample, and upright samples were printed standing on end, so the layers are perpendicular to the length of the sample. Figure 3.23 shows these two types of samples after being printed on a common desktop FFF 3D printer (Ultimaker 2+ Extended). The printers used were; E3D Bigbox, Wanhao Duplicator 4S, Ultimaker 2+ Extended and ARMS. Previously it has been shown that the tensile properties of FFF parts are comparable between both low cost 'RepRap' style machines and industial 3D printers, so this range of machines can be considered representative [198]. The settings were kept the same between the different printers, as was the filament make and colour. Details are in Table 3.13. It should be noted however that the Ultimaker uses 2.85mm diameter filament, whereas the others use 1.75mm diameter. This is unlikely to have any significant effect upon the print quality as once the plastic is melted it is forced out of the same sized nozzle so the functional part of the extruder system is the same. Following printing, the width and height of the central section was measured using digital callipers. The ends were then held with parallel grippers and tensile force was applied by pulling these apart at 5mm/s, using an Instron 3369 testing system.

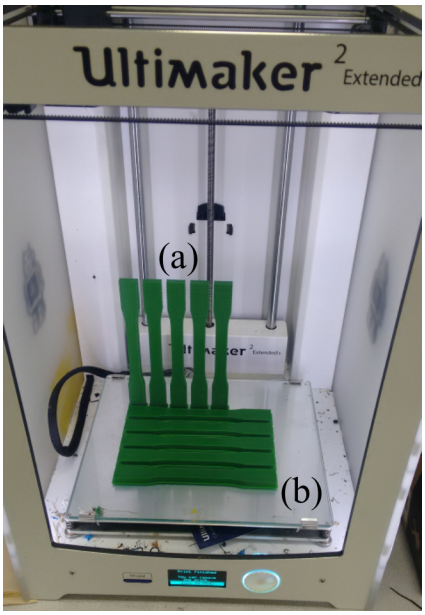

Figure 3.20: Dogbone samples printed on an Ultimaker 2+ Extended, showing the two orientations used; (a) Upright and (b) Horizontal.

Table 3.13: Settings used for printing tensile test samples across a range of FFF printers.

Setting	Value
Layer height	0.2mm
Print Speed	50mm/s
Temperature	205°C
Material	Colorfabb PLA/PHA Leaf Green
Support Material	N/A
Cooling	On
Perimeters	3
Infill Density	50%
Infill Pattern	Rectilinear ±45°
Top and Bottom Layers	5
Software	Simplify3D

3.7.3 Surface Roughness

The surface roughness of a 3D printed sample is one method that can be used to quantify the quality of a part. It will be used in later experiments to assess external effects on the print quality, so here it is compared to a common desktop FFF 3D printer (Ultimaker 2+).

The samples and methods used are detailed in Section 4.2, but briefly; a sample with five flat surfaces which overhang at 30°, 45°, 60°, 70°, and 80° from vertical is printed. Conventional planar layers, a horizontal build plate and vertical extruder orientation are used and the sample is printed three times on both ARMS and on the Ultimaker 2+. Three traces are taken on each surface using contact surface roughness measurements (from a Talysurf 120L) and the resultant roughness's (Ra) are averaged across the three samples for each system.

3.8 3D Printing Results

3.8.1 Visual Inspection

Many of these potential issues with FFF printing can be tuned out by adjusting print settings within the slicer, therefore a trial and error method was used to adjust these. Following this process, various objects were successfully 3D printed using this system. Visual inspection revealed that they contained few, or none, of the defects listed above and therefore compare favourably to items produced on other FFF printers. A selection of popular models from a 3D printing file repository were chosen as examples and these are shown in Fig. 3.21. Objects ranging from 3cm - 26cm tall were printed.

A range of PLA filaments in different colours and from different suppliers were successfully used as well as TPU. This is a flexible filament with a shore hardness of 85A (NinjaFlex from NinjaTek). As the feedstock is only 1.75mm in diameter it is not at all rigid, so printing this plastic is difficult. The extruder must be modified to constrain its path through the drive wheel and it is difficult to retract well, as the elasticity delays the change in pressure in the nozzle when it is reversed by the drive gears higher up. It must also be printed slower than PLA to improve the adhesion between layers. Having performed the required modification and tuned the printing parameters to allow this material to print with minimal strings of plastic due to oozing, or other issues, a large object was produced. This item can be seen in Fig. 3.22 and was chosen as it shows

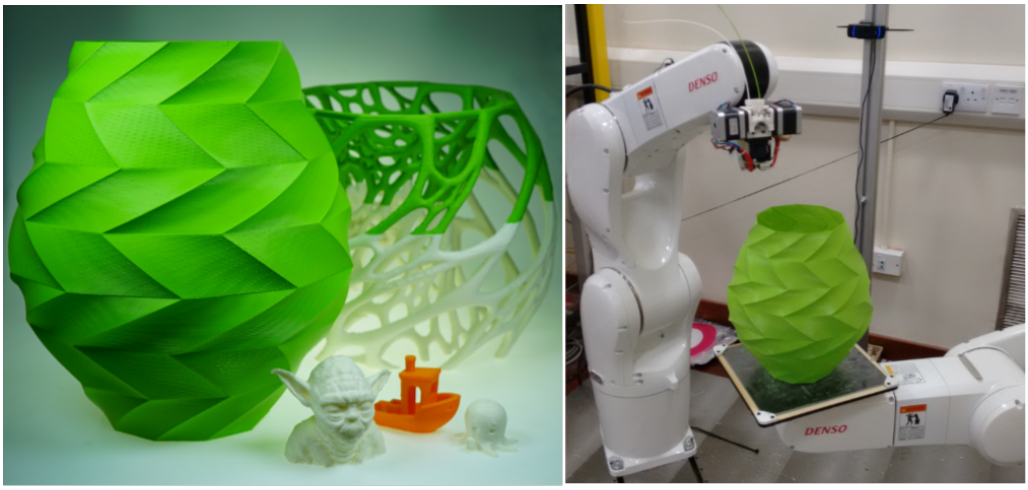

(a) (b)

Figure 3.21: (a) A selection of items 3D printed with conventional planar, horizontal layers, using ARMS. (b) The large green vase is constructed with a single perimeter and is 26cm high and 23cm in diameter. CAD models from [195, 199–202]

some of the advantages of both flexible filament, and AM. It is a model of a (four fingered) human hand which can open its fingers when a button in the wrist is pressed. Internally through the palm there are linkages and hinges which connect to the fingers allowing this actuation. Manufacturing this all in one piece is only possible using AM with the capability to deposit flexible material.

(a) (b) (c)

Figure 3.22: Hand model printed in flexible filament. (a) When uncompressed the fingers are curled over. (b) and (c) A plunger in the wrist is pushed upwards and internal linkages and printed hinges cause the fingers to straighten out. Model from [203].

3.8.2 Tensile Strength and Dimensional Accuracy

The results from the tensile tests can be seen in Fig. 3.23, and Table 3.14 shows the maximum forces, dimensions and tensile strength at break.

From the graph it can be seen that there is variation in the level of force the samples can take, but the data for each type of sample follows similar profiles. As expected horizontal samples stretch plastically before breaking and fail at a higher force than the corresponding upright ones. These fail suddenly, and break cleanly, as the bond between two layers is broken. In general the upright samples break at approximately 80% of the maximum load of the horizontal. The samples from the robot arms clearly require more force to break. The dimensions were also the furthest from the designed width and height (12mm and 7mm), but well within the 0.5mm specified as being acceptable. These results could indicate that the robot system is slightly over extruding, so excess plastic is causing an increase to both the dimensions and the strength. It is also possible that the strength improvement is due to the printing parameters being tuned better in this system. While the main settings were kept the same there are many others which can be varied to make a printer give the optimum output. For example in the firmware there is a setting for the extruder which defines the number of steps the stepper motor has to turn to extrude 1mm of filament. This was tuned through several trials to make it accurate in the robot system, but the other printers were likely to be running with the default number, which can vary for reasons such as the spring tension on the lever arm changing or the feed gear wearing.

From these results it is clear, however, that ARMS can produce parts with as good or better inter layer adhesion as other FFF printers, and it can produce parts within the acceptable tolerances required by the specification.

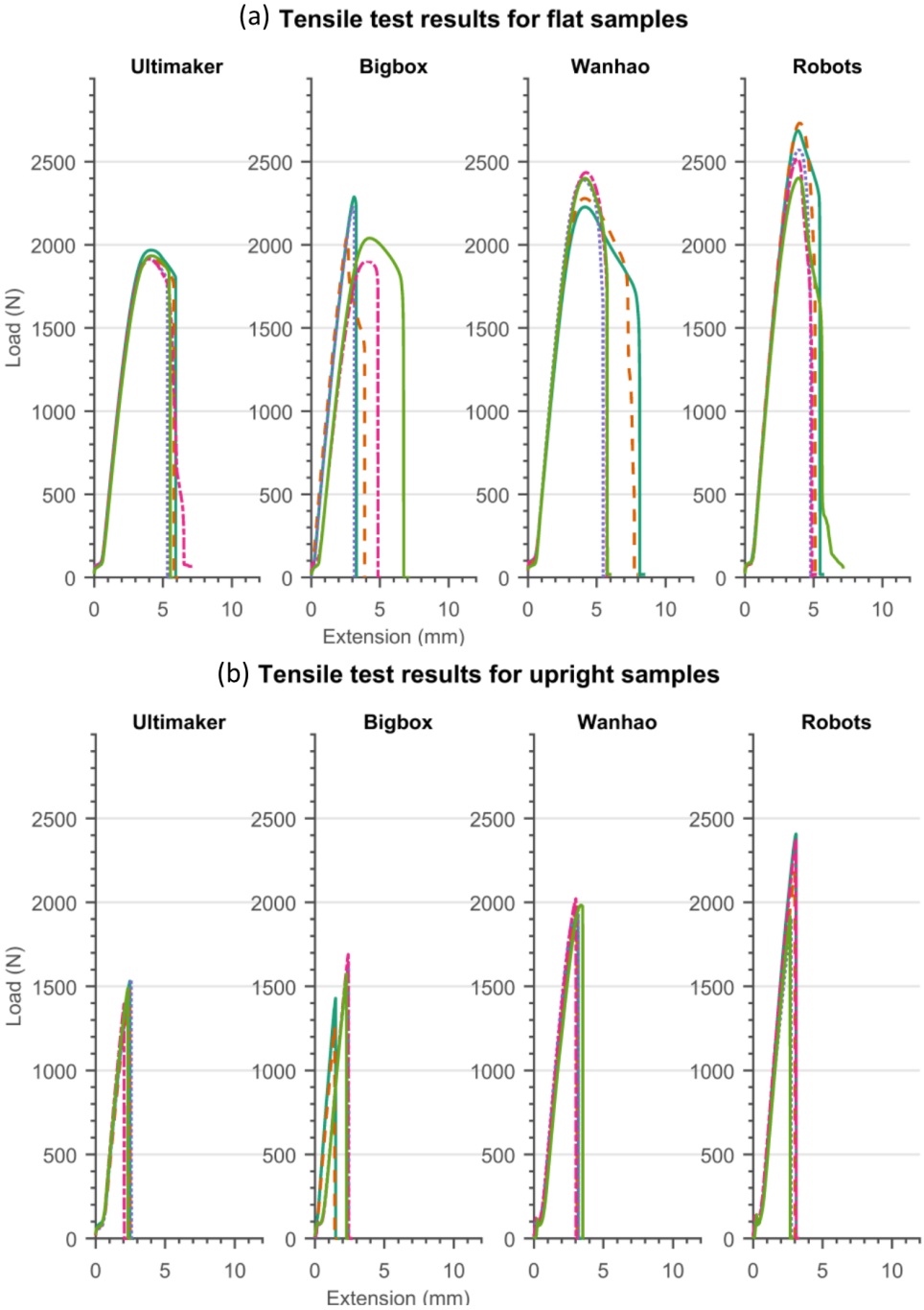

Figure 3.23: Graphs of tensile force against extension for dogbone samples printed in (a) horizontal and (b) upright upright.

Table 3.14: Tensile test results upon samples printed in two orientations on a range of FFF 3D printers.

Printer	Orientation	Mean Max Force (N)	Std. Dev. (N)	Mean Width (mm)	Std Dev. (mm)	Mean Thick-ness (mm)	Std. Dev. (mm)	Mean Tensile Strength (MPa)
Ultimaker	Flat	1929	24.7	12.94	0.14	7.15	0.05	20.8
Bigbox	Flat	2102	155.3	12.90	0.09	7.02	0.06	23.2
Wanhao	Flat	2348	88.6	13.25	0.07	7.09	0.04	25.0
Robots	Flat	2583	132.6	13.38	0.08	7.29	0.10	26.5
Ultimaker	Up	1486	58.2	13.03	0.01	7.06	0.03	16.2
Bigbox	Up	1522	173.2	12.96	0.10	6.98	0.04	16.7
Wanhao	Up	1980	32.8	13.06	0.08	7.12	0.02	21.3
Robots	Up	2155	242.5	13.14	0.03	7.07	0.03	23.2

3.8.3 Surface Roughness

The results from these measurements can be seen in Fig. 3.24.

The parts from the commercial printer have a slightly smoother surfaces on the shallower angles of 30° and 45°, but significantly higher roughness values for the steeper surfaces. It is likely that this is because the commercial system has been tuned to provide very consistent extrusion, improving the initial results, but the part cooling is not as strong causing drooping and deformatin in the strands of plastic for steeper surfaces. Ultimaker slicing software (Cura) does use support material on overhangs above 45° by default, so this result is unsurprising and could be altered by using support material. In practice the surfaces of the 70° and 80° overhangs from either printer would not be acceptable for the majority of applications. The roughness of the 60° section from ARMS may be low enough is some circumstances though. This test shows that the ARMS can produce items of comparable or better surface roughness to other systems and it exhibits the same step in roughness above 45°, but not to the same magnitude.

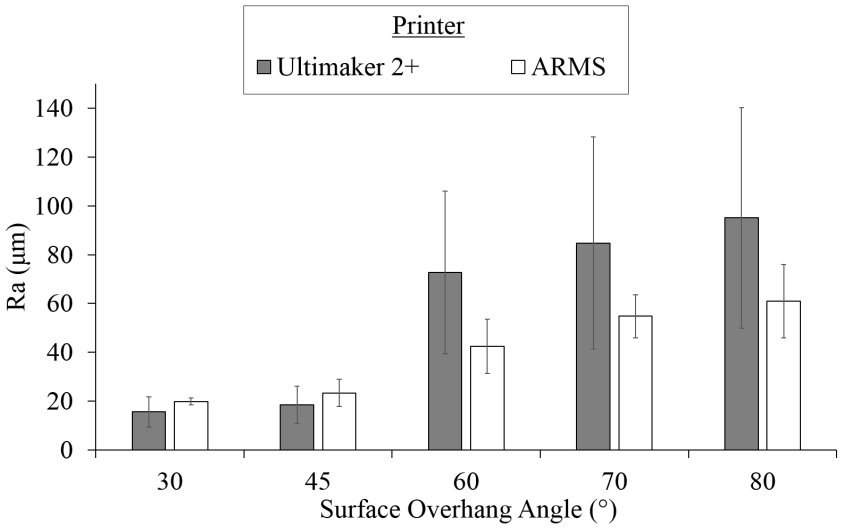

Figure 3.24: Surface roughness (Ra) comparison between a commercial FFF 3D printer and the ARMS for overhanging surfaces. Ra is lower for the Ultimaker on shallow angles of 30° and 45° but much higher for the other surfaces.

3.9 Discussion and Conclusions

In this chapter the Additive Robot Manufacturing System (ARMS) has been presented. It has been designed to provide a high quality, flexible research platform and has required the creation of a bespoke set of software and control to integrate the hardware. Fused Filament Fabrication (FFF) is a useful AM method which lends itself to use in this platform as the open source community around it aids quick adoption and development, but also some of the major disadvantages of it could be address using multiaxis 3D printing. The software subsystems have been explained, these form an important part of the system and were developed to use a parallel architecture which helps streamline processing. As this is a prototype system there are inefficiencies in some of the calculations. For example, increasing the speed of the kinematic calculations would improve the system. The simulation provides a very useful method of checking both the mathematics for bugs and the gcode input before printing. It is only a kinematic representation currently, but the full dynamics, along with the trajectory between positions would be very useful. Unfortunately the one subsystem that was not developed in this work, is the robot controller. This limits the accuracy of the simulation as the calculations and logic the controller uses would have to be replicated

by reverse engineering.

After the system was developed and tuned, the parts produced were of very high quality. Objects of complex shapes, with different features and of various sizes have been printed successfully and with a minimal number of defects which are typical when extruding molten plastic. The system was found to be reliable, with some prints taking over 24 hours. Tensile strength and dimensional accuracy measurements also show that the system is capable of conventional AM to a standard that is at least comparable with other FFF machines.

This is is a novel system as both the build plate and the extruder can be moved in 6 DOF, and it uses serial robot arms to do AM at a micro scale, with sub-millimetre precision. Such results are not yet present in literature and mean that the motion system does not limit the output of the process.

Chapter 4

Dynamic Build Orientation Changes during Additive Manufacturing

4.1 Introduction

In Chapter 3, the Multiaxis Additive Manufacturing (MAAM) system was presented and it has been established that the conventional print results are comparable to other Fused Filament Fabrication (FFF) 3D printers. In this chapter the system will be used to explore the first advantage that a multiaxis system enables over conventional 3 axis 3D printers: The potential for dynamically altering the orientation in which the layers are added to the part, during the manufacturing process.

The majority of Additive Manufacturing processes build objects by adding layers one on top of the other in the vertical direction (i.e. the build axis is along Z). To physically do this, either the build plate moves down by one layer height between each layer, or the print head moves upwards by the same distance before continuing to deposit material. Some Photopolymerization processes flip this mechanism over and lift the build plate up out of the top of a vat of resin while each layer is cured to the underside of the plate by a light source that shines through the resin tank. In either

case the flat, horizontal, layers are stacked vertically. Figure 4.1 demonstrates this; a complex structure is being printed with standard horizontal layers using the robot arm system. In this case the build plate remains stationary and the nozzle height increases vertically as each layer is added to the top of the object. As the print progresses the object has the appearance of 'growing' up from the build plate.

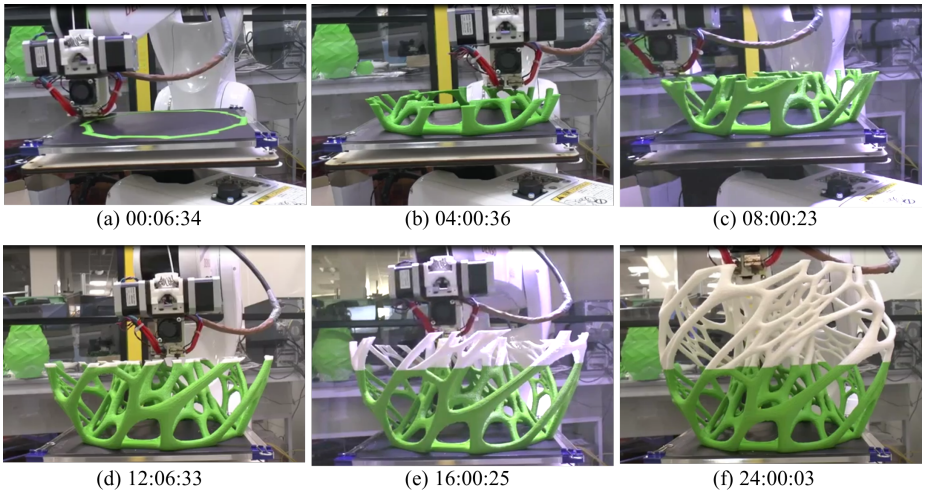

(a) 00:06:34 (b) 04:00:36 (c) 08:00:23

(d) 12:06:33 (e) 16:00:25 (f) 24:00:03

Figure 4.1: Conventional 3D printing of a cellular structure. As the print time progresses the layers are built up vertically to create the object. The build plate remains stationary during the whole print (the camera angle was adjusted between (c) and (d) to keep the extruder in the frame for longer). The nozzle height increases by 0.2mm as each layer is added to the top of the printed object. The print was paused just before (d) and the filament colour manually swapped. The 3D model was downloaded from [199].

The orientation an object is built in has a significant effect upon surface finish, dimensional accuracy, speed, material use, mechanical properties and bed adhesion when using FFF [178–180, 182, 204]. A few examples of features which can be affected by the part's orientation in relation to the build axis are shown in Fig. 4.2. By rotating the part, the angle of overhangs can be changed, potentially removing the need for support. When printing using FFF, a common way that the print can fail is if the base detaches from the build plate. Therefore, it is important to have a large surface area in contact with the plate. Another issue which is depicted in Fig. 4.2 (c) and (d) is that the discrete layers used in FFF mean that features in the build axis (Z) are approximated by steps (typically 100-200 microns). Features in the layer (XY) plane are drawn continuously by the extruder, the motion of which is controlled by stepper

motors. An Ultimaker 2+, for example, has 12.5 micron movement resolution in X and Y. This disparity causes printed parts to be non-uniform in their mechanical properties and must be oriented so the most important features are in the plane which gives the best resolution. The discrete layers cause steps upon curved or angled surfaces. By changing the orientation of a part the impact of these steps can be reduced, but this may introduce other issues, as seen in Fig. 4.2 (f). In the figure all of the examples are viewed from the side and rotated around one axis. For complex 3D shapes, for example if all the sides were curved, the best way to orient the part is often less obvious. A number of computerised methods have been developed to aid in this choice, which determine the best overall orientation based upon a range of factors [178, 179, 182]. In practice this is usually a manual decision made by the machine's operator and the choice is limited to a compromise for the overall build, as what is best for one section may be completely different for another.

The ability to stack the layers in different orientations, for different sections, could remove some of the compromises and limitations that currently exist. An example of this is shown in Fig. 4.3. In this case layers are stacked along multiple axes depending on the features of the object. This would only be feasible with a multiaxis system that can either rotate the build plate or extruder to enable the deposition of these layers. It has not been established, however, whether the outcome of the FFF process is affected by having the extruder in an orientation other than vertical. The prior literature which addresses build orientation does so by rotating the object to be printed within the build volume of the machine. The build plate remains horizontal and the extruder vertical. There are a few examples where a build axis is chosen which is not along the Z axis, but there is only anecdotal evidence that this is effective. A typical FFF printer has been shown to print on its side [181] but there was no analysis of the effects of this. Recently Stratasys have developed their 'infinite build' concept, where the object is printed horizontally but all the details of this are proprietary [205]. An innovative idea, which has recently been commercialised, is to print with layers angled at 45° from the build plate. As Fig. 4.4 (a) shows, angled layers can remove the need for support material. To physically print these layers the machine needs to be reconfigured from the standard Cartesian axes. The extruder is still moved in the XY plane, but this is now at 45° from Z, as depicted in Fig. 4.4 (b). To enable motion in the Z axis, the build plate is replaced with a convayor belt which moves the part along as each layer is added. This

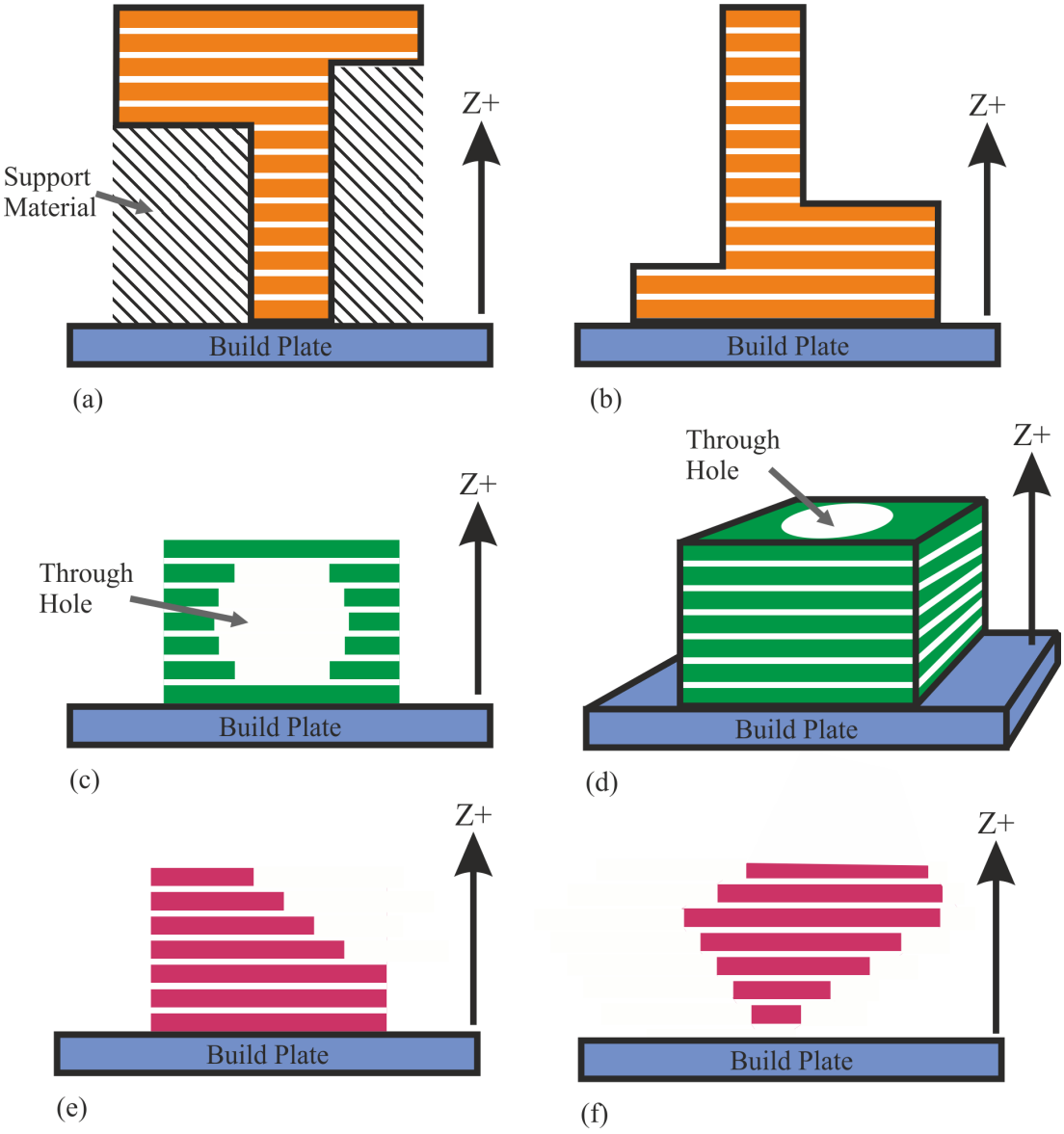

Figure 4.2: The orientation of a part, in relation to the build axis, has a large effect upon the mechanical properties of a part. Some examples are shown in this figure. The layers are stacked in the positive Z direction, as in conventional 3D printing. (a) If the part is oriented in this way the overhangs will require support building underneath them and the surface area in contact with the build plate is small reducing adhesion. By rotating the part (b) these issues can be resolved. Due to the discrete layers curves are approximated with steps. In (c) a hole is oriented horizontally so will not be perfectly circular. The top may sag and need support depending upon the diameter. (d) By orienting the part so the hole is vertical, the edge will be smooth and more accurate. (e) Another example of how the steps affect a surface. (f) When this part is rotated the side which was previously stepped is now flat, but the others would now not be smooth and may require support. For this example there is no optimal solution for all surfaces so an orientation which gives the best average surface finish would have to be used.

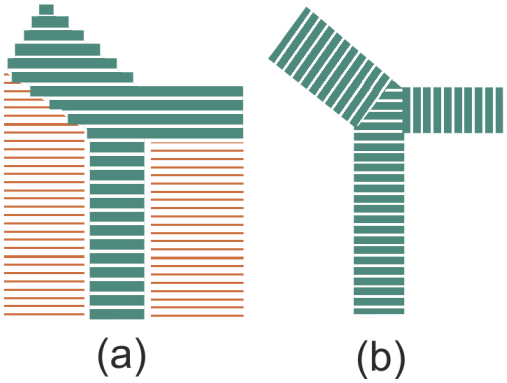

Figure 4.3: (a) In conventional 3D printing the layers can only be stacked in one direction, leading to stair step effects and the need for support structures. (b) If the build orientation could be locally varied then overhangs could be self supporting and the steps between layers hidden more readily.

concept was first developed for powder bed fusion [206] to enable continuous printing, but has now been developed using FFF [207] where the additional benefit of reducing support structures is also realised. Figure 4.4 (c) shows the commercial 'Blackbelt' 3D printer which utilises this concept. While this printer is obviously capable of 3D printing objects, there is no information about how these compare to conventional parts in terms of surface roughness. Visual inspection of marketing media reveals that there may be some unevenness between the layers but it is not known whether this is due to the specific hardware or inherent to the layer orientation. One situation where the nozzle orientation has a significant effect upon the extruded plastic is when printing unsupported individual strands of plastic [122, 123]. By aligning the nozzle so that the feed forces were directed along the extruded strand, drooping could be reduced. A graphical representation of this is in Fig. 4.5. As this approach does not use layers it is unknown to what extent gravity and feeding forces affects the drooping of strands when printing planar layers.

There is little information about using FFF hardware at orientations other than vertical and there is no work which addresses the impact this may have upon the surface roughness of objects. Therefore the first half of this chapter addresses question of how gravity affects the surface roughness of printed parts with an experiment which involves effectively rotating the whole fabrication process. This is to test the assumption that results of the FFF process are not affected when the build plate or nozzle are moved from

their customary horizontal and vertical orientations (with respect to the gravitational frame of reference). Surface roughness is used to assess the impact upon surface quality as it is a commonly used method [178, 188, 208–211] and the other parameters that could be used to quantify the effects may be affected more by other external influences. For example the machines mechanical design may mean that it moves at different speeds when printing at different orientations. Mechanical strength varies due to the interlayer bonding and can therefore be affected by the ambient conditions, which may vary due to the different positions that the arms must be in to print at different orientations. Surface roughness is a function of the layer height, which can therefore be kept constant between the different orientations, but it is also a function of the overlap between the tracks of plastic in each layer [212]. It is at this junction where we might expect rotation with respect to gravity to exert some influence as, if the track does not adhere to the previous layer, it is free to move and droop under its own weight.

The second half of the chapter details an experiment in which the build axis is changed during the printing process, to test the theoretical advantage depicted in Fig. 4.3. For each experiment the motivation, method, results and conclusion are presented, before the main conclusions that can be draw from these two tests are then discussed together.

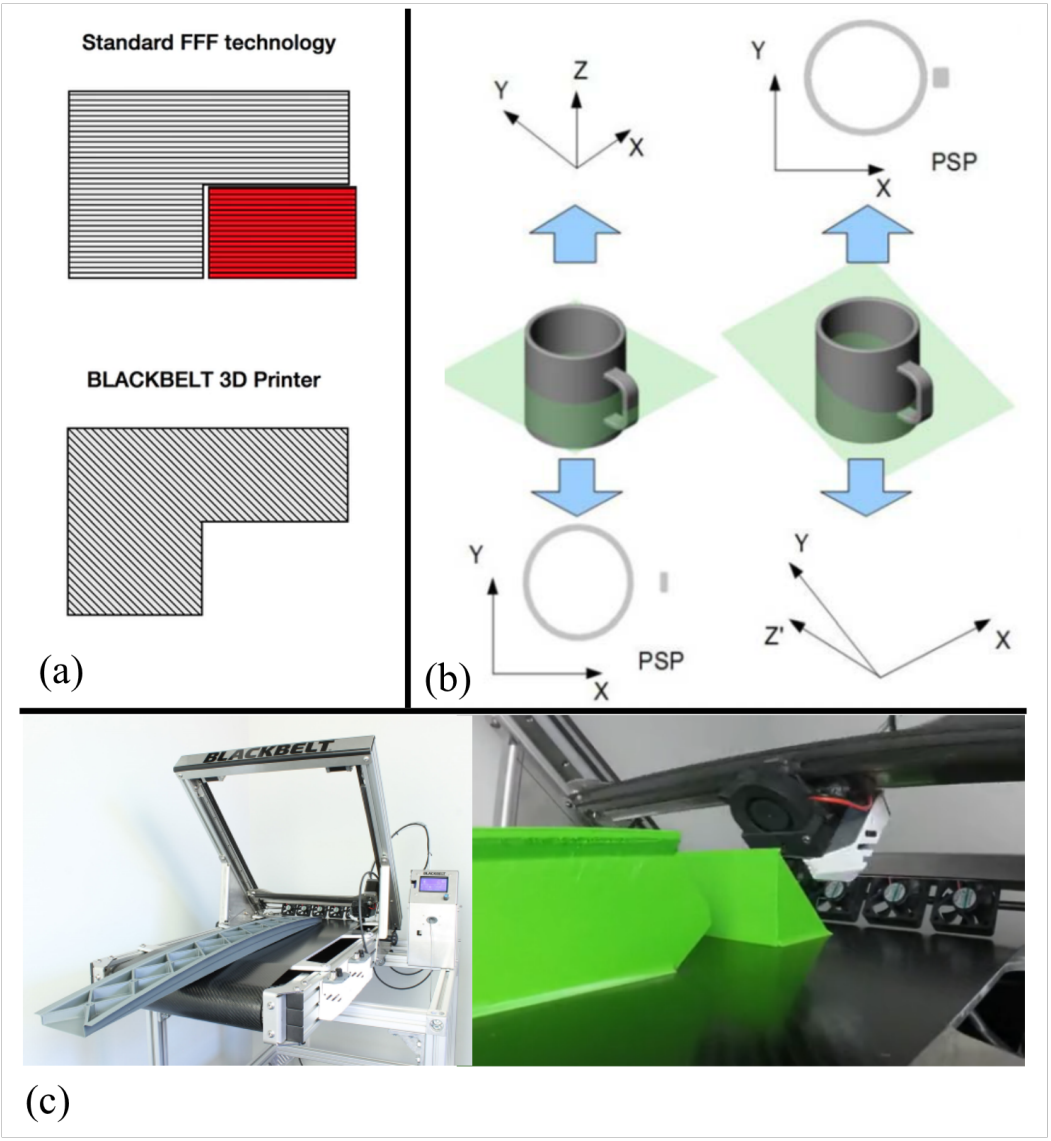

Figure 4.4: (a) By orienting the layers at 45°, overhangs which would usually require support can be printed without. From [207]. (b) In conventional 3D printing (left) the layers are stacked vertically in the Z axis and each slice is taken through the XY plane, this is also true for the angled printer, but the slices are now taken at an angle through the object and the Z' axis is horizontal. From [206]. (c) Photographs of the Blackbelt 3D printer from [207]. The gantry is angled and the build plate is replaced with a conveyor belt. The right hand image shows a box during printing which is being built up with layers angled at 45°. The conveyor belt allows objects to be continuously be produced without the need for any intervention to remove the part, a significant advantage in many industrial or production applications.

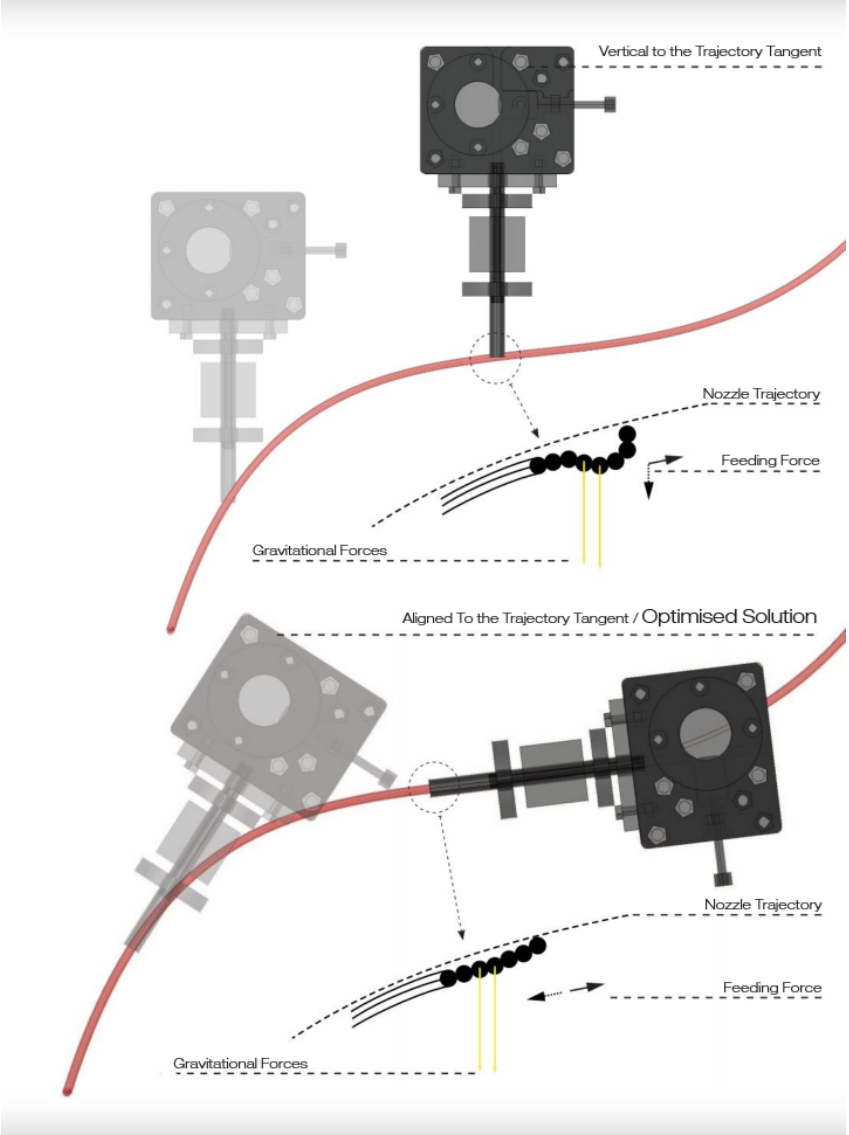

Figure 4.5: The top of this image depicts a strand of plastic being printed with the extruder remaining vertical throughout the trajectory. This causes the strand to droop below the planned path as both the feeding force and the gravitational force act downwards. The bottom section depicts the same strand being printed but this time the extruder is aligned to the tangent of the trajectory. The feeing force is then directed into the plastic that has previously been printed, so the drooping is lessened. From [122].

4.2 Experiment 1: FFF Printer Orientation Effects

Previous work has researched how changing the orientation of the printed object in relation to the build axis has affected the structural properties. The orientation of the printer's mechanisms remained stationary and the object was rotated within the machine's printing volume. This experiment, however, aims to assess the effect of rotating the whole printing process. The object remained in the same pose on the build plate, the layers were always deposited parallel to the plate and the nozzle remained perpendicular to the build plate. This has the effect of removing the usual consequences of changing the part's build orientation, such as no longer having a stable base or requiring support structures. The effect of gravity upon the surface roughness of the part can then be seen when printing with the whole system at a number of different orientations. Once samples have been printed at a variety of orientations, the surface roughness is measured and a statistical test is used to determine if the variation in roughness is significant.

4.2.1 Sample

The sample used for this test is an overhanging curve comprised of five flat sided sections which are angled progressively further from vertical as the height increases. A 3D render of this can be seen in Fig. 4.6. The flat foot is printed upon the build plate and the whole part is printed without supports to allow the effect of gravity to be determined upon surfaces which would usually be supported. It was possible that changing the printer orientation could improve these surfaces, as strands which would usually droop may not if gravitational force could be used to counteract this tendency.

The sample is sliced using standard software and the same gcode file was used for each print as the system is set-up to print directly onto the build plate no matter where it is located. The settings that were used for slicing are summarised in Table 4.1. The sample was printed four times in each orientation

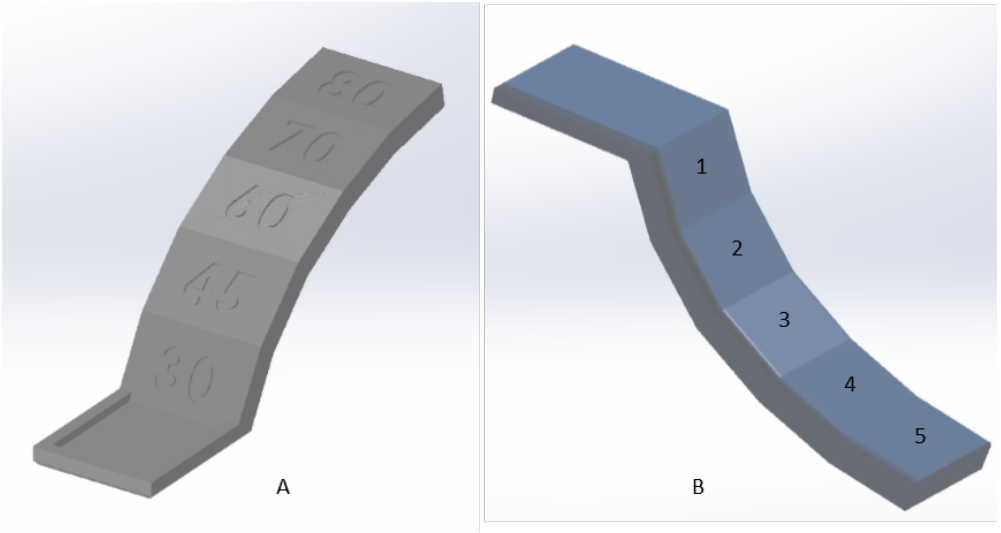

Figure 4.6: A. Render of sample object with angles from vertical marked on each section. B. The five surfaces where surface roughness measurements were taken. STL modified from [213]

Table 4.1: Slicer settings for printer orientation samples.

Setting	Value
Layer height	0.2mm
Print Speed	80mm/s
Temperature	200°C
Part Material	Polymaker PolyMax PLA
Cooling	On
Infill Density	20%
Infill Pattern	honeycomb
Perimeters	3
Top and Bottom Layers	6
Software	Slic3r

4.2.2 3D Printer Orientations

The sample is placed upon the build plate as shown in Fig. 4.7 (a), the layers are built up along the local Z axis and are sliced perpendicular to the build plate. The nozzle is also perpendicular as usual in conventional 3D printing. Throughout the experiment

these relationships remain the same locally, but the orientation of the build plate is altered. Figure 4.7 (b) shows the five orientations in which samples are printed.

Between each orientation, θ was incremented 45° around the global Y axis. As labelled in Fig. 4.7, having the build plate horizontal and the nozzle vertical was designated as 0° and θ was measured from this reference. The last orientation in this experiment sees the robot printing with the build plate horizontal, but upside down and the nozzle extruding vertically upwards. An example of how printing at these orientations is physically achieved with the robot arms can be seen in Fig. 4.8. To ensure the extruder robot could reach all of the required positions to print each sample, each set-up was tested in the kinematic simulation before printing. This remained stationary throughout the print while the extruder robot moved the nozzle to draw each layer. The joint angles for the build plate robot are recorded in Appendix B.

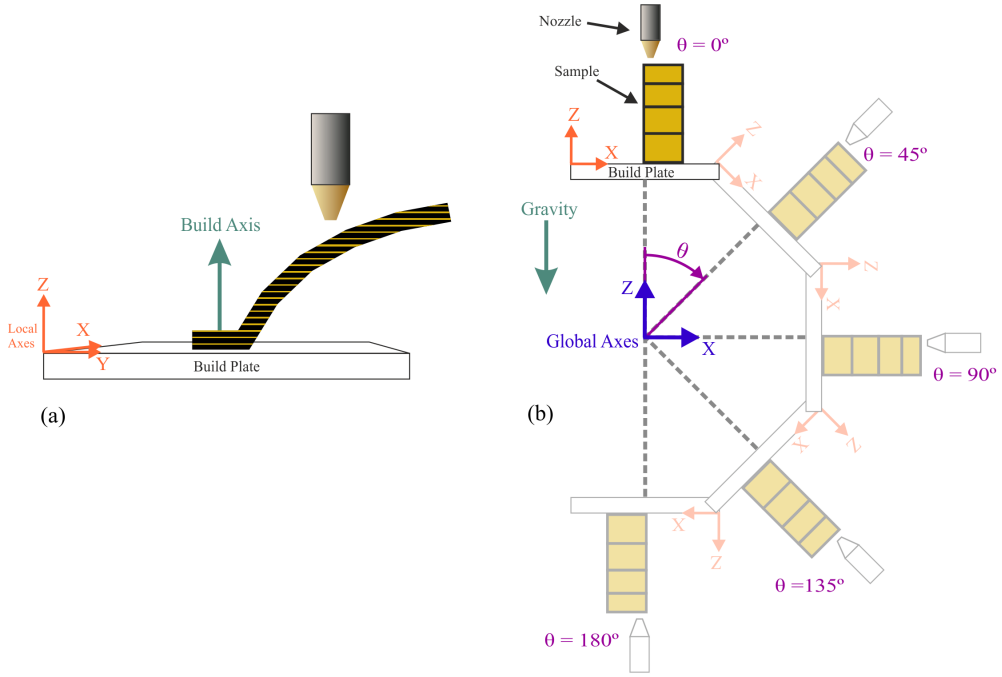

Figure 4.7: (a) Schematic showing how the sample is printed in each orientation, viewed from the ZY plane. In relation to the local coordinate frame, the build plate is horizontal, the nozzle vertical and the sample is sliced conventionally. (b) These stay constant, relative to the local coordinate system on the bed. For each trial in the experiment the printer orientation is changed by rotating the bed θ around the global Y axis. These are the five orientations used in the experiment, when viewed from the ZX plane.

Figure 4.8: Robot Arms printing a sample while the build axis is angled 135° from vertical. Background of scene removed for clarity.

4.2.3 Roughness Measurements

The surface quality was assessed by contact surface roughness measurement on the underside of each overhanging section, numbered 1-5 in Fig. 4.6. This is an often used method of quantifying the quality of an AM surface [178, 188, 208–211]. A Taylor-Hobson Form Talysurf 120L fitted with a 2µm conical stylus was used. The mean value for each surface was calculated using the three passes from all four samples printed at each orientation. The position and direction of the passes, P1, P2 and P3 are shown in Fig. 4.9. Due to the curvature of the sample it must be repositioned to measure two of the five surfaces otherwise the end of the sample would be high enough to interfere with the cantilever arm holding the stylus. The direction of the trace should have no effect upon the result as the stylus is conical and the edges of the layers can be assumed to be parabolic [178, 214].

The measurement parameters were set as 2.5mm cutoff, which was chosen using ISO 4288:1996 [215] and has been used for other AM investigations [188, 209, 210], 100:1 bandwidth and a 10mm evaluation length was used due to the size of each section.

Analysis was performed by fitting data to a least squared line and filtered using a Gaussian filter [216]. The roughness for one path was then expressed by the arithmetic mean, denoted as Ra. The mean Ra for each section is then calculated from the three passes on that surface.

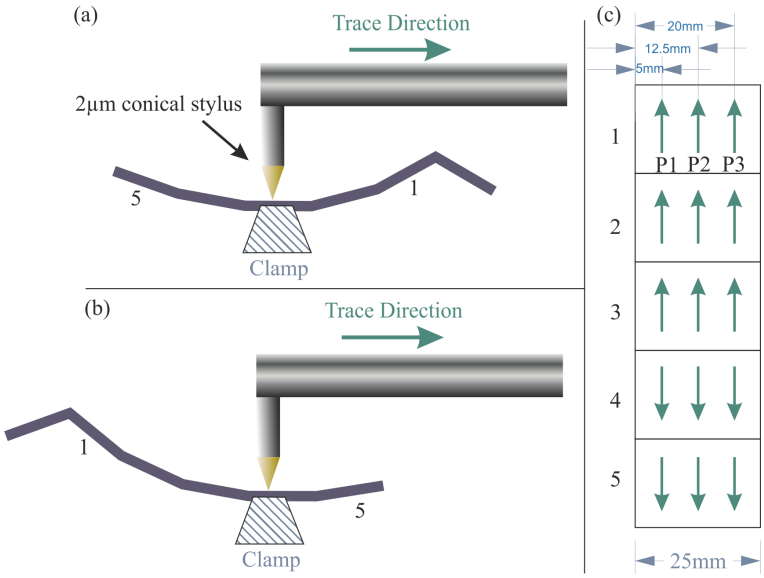

Figure 4.9: All traces were taken perpendicular to the layer lines, (a) surfaces 1-3 are measured in one direction but due to the curvature of the sample (b) the final two surfaces (4,5) are measured in the opposite direction once the part has been repositioned. (c) Flattened view of the trace paths.

4.2.4 Statistical Analysis

To assess the effects and interaction between the two factors a two way analysis of variance (ANOVA) test was performed using IBM SPSS software. This determines whether any interaction between the variables is statistically significant. The independent variables are; Overhang Angle, which was a 5-condition variable (30°, 45°, 60°, 70° and 80°) and Printing Orientation Angle, which also has 5 conditions (0°, 45°, 90°, 135°, 180°). The dependent variable was underside surface roughness (Ra).

The three main effects being tested with the ANOVA test are formalised as the following null hypotheses:

1. There is no significant effect on the mean Ra due to Print Orientation.

2. There is no significant effect on the mean Ra due to Overhang Angle.

3. There is no interaction between Printing Orientation and Overhang Angle.

If the test shows that there is not enough evidence to support these hypotheses then a logical alternative can be accepted. The alternative hypotheses for each case are:

1. The Print Orientation has an effect upon the mean Ra of an overhanging surface.

2. The Overhang Angle has an effect upon the mean Ra of an overhanging surface.

3. There is an interaction between Printing Orientation and Overhang Angle.

The ANOVA test can only report if there is a statistically significant interaction between variables, but it does not give more details about the extent of this interaction. Therefore a post hoc test is performed. The Tukey post hoc test compares each condition in the independant variables against every other condition to determine if there is a significant difference between the values. For example the mean Ra for the 30° overhang will be compare to the mean Ra of the other four overhanging sections. We would expect there to be a significant difference between the results for the 30° and 80° overhangs as visually they are very different, but it is difficult to tell between some of the adjacent sections. This test, like the ANOVA test, will give a probability that the variation in the results is due to chance. If the probability, p, is < 0.05 then it can be concluded that the difference is significant and unlikely to be purely due to the natural variation in the system.

Before performing this experiment it was known that the overhang angle affects the roughness of the surface, but the effect of printing orientation had not been determined. The variety of overhang angles allowed the experiment to not only test if the print orientation has an effect, but also if that effect varied depending upon the overhang angle of a surface. At the more extreme angles it would appear that gravity has a greater effect as the edges of layers droop downwards, so it was important to test this.

4.2.5 Results

Once printed, all the parts were visually inspected. To the naked eye there is no discernible difference to the surfaces of any of the samples. A photograph of one sample from each orientation is in Fig. 4.10.

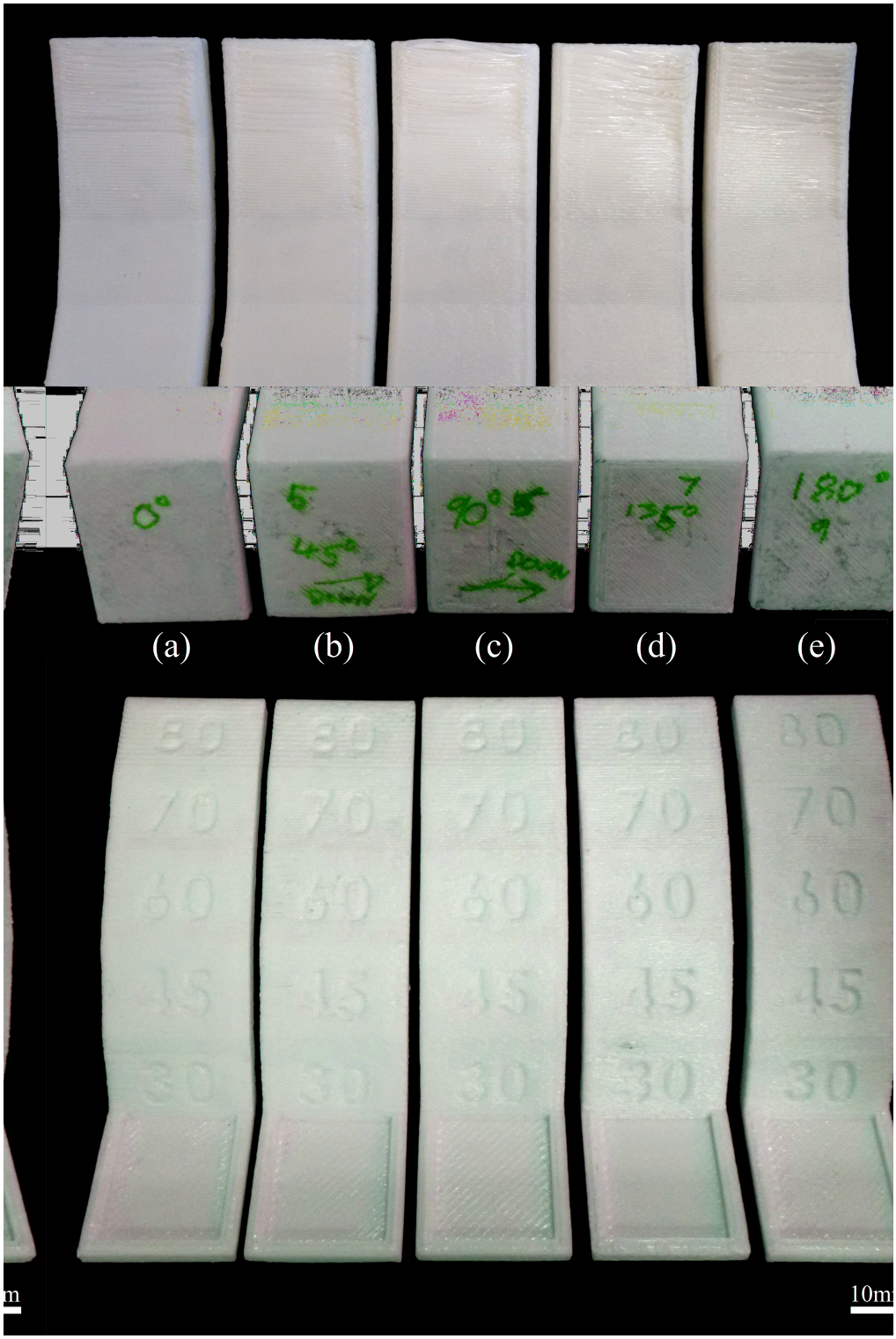

Figure 4.10: Example arch samples that have been printed at (a) 0°, (b) 45°, (c) 90°, (d) 135°, (e) 180° from horizontal. Visually they are indistinguishable from each other. The surface gets rougher as the overhang angle increases. Top and bottom views are from the same samples.

The mean and standard deviation for the Ra results from the contact surface measurements summarised graphically in Fig. 4.11. It can be seen that the roughness increases as the overhang angle increases. The standard deviation is small for 30°, 45° and 60° but increases for 70° and then further for 80° surfaces. A table of these results is available in Appendix B.

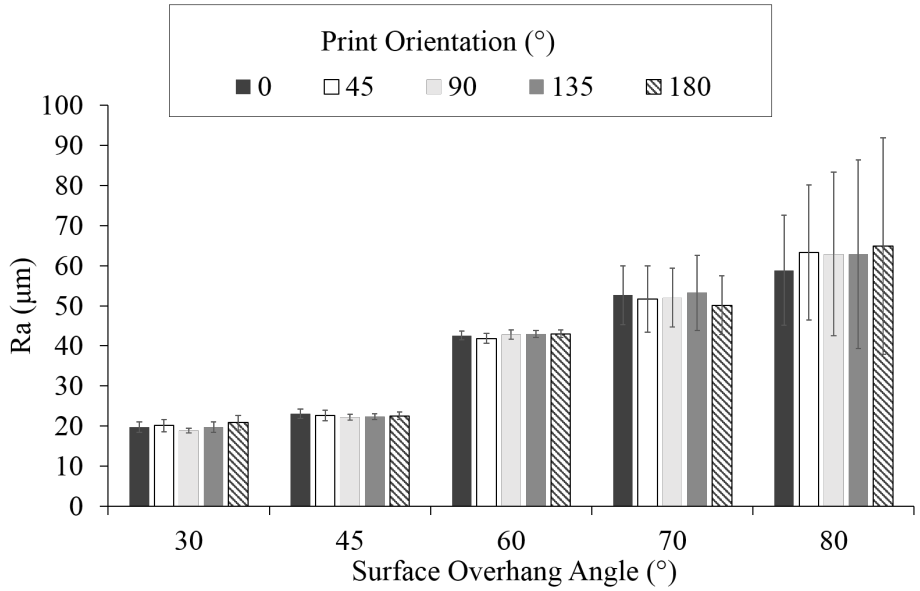

Figure 4.11: Mean Ra values ($n = 12$) for samples printed at each printer orientation. There is a clear increase in the roughness between each of the overhang angles along the x axis. Within these groups, however, there is little variation. The shaded bars correspond to the orientations that samples were printed in. There is no clear trend between the Ra and the different orientations. The error bars do suggest that the variation in Ra increases as the surface overhang angle increases, but the means remain very similar.

In the plot of the mean Ra for each Overhang Angle against the Printing Angle (Fig. 4.12) the roughness for each surface remains similar for each Printing Angle and, as the lines do not cross over, the plot suggests that interaction between the two variables is unlikely. This is confirmed by the results of the ANOVA test (ANOVA table is in Appendix B). There is no significant interaction ($p = 0.99$) between the two main effects, therefore these effects can be interpreted directly. As expected, the null hypothesis for the Overhang angle must be rejected ($p < 0.05$), and the alternative hypothesis accepted: The Overhang Angle has a significant effect upon the underside surface roughness.

Again confirming the visual inspection, the Printing Orientation has no significant effect ($p = 1.00$) upon the roughness.

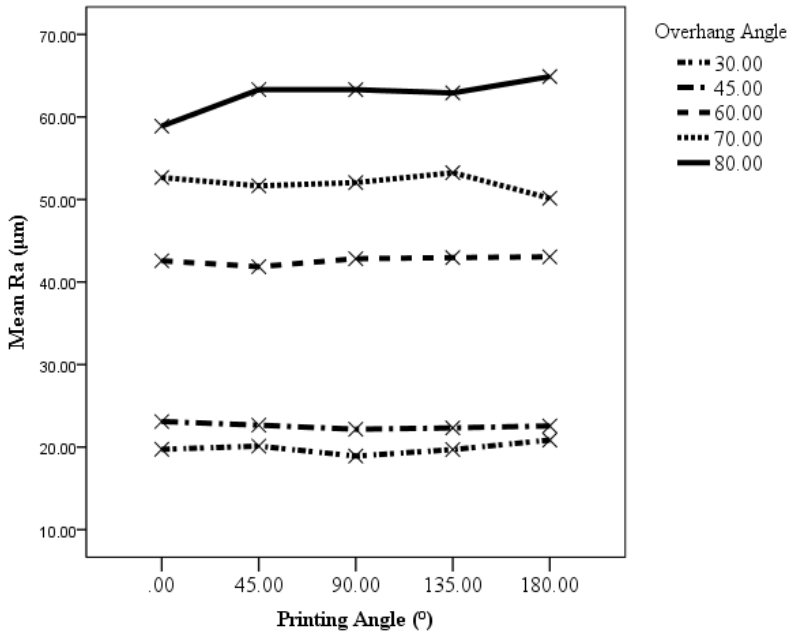

Figure 4.12: This chart displays the same Ra data as above, but grouped differently to help illustrate the lack of any significant trend between the printing orientations, for each of the surface angles.

The Tukey post hoc test results compared each printing oreintation and found that there is no statistically significant difference between any of the printing angles, $p \geq 0.987$ in all cases. A second Tukey test for the different overhang angle shows that there is a statistical difference between the roughness on all overhang angles apart from between 30° and 45°. The full output from this test can be found in Appendix B.

4.2.6 Discussion and Conclusion

The results of this first experiment support that there is no significant difference in the surface roughness value when the print orientation is rotated. This is interesting, as intuitively one may expect the that the printer orientation could alter, or even improve the roughness in specific cases. For example the 80° overhang has strands which droop downwards when printed conventionally with the build plate horizontal. When this plate is rotated 180° it was possible that these strands may not droop so

much, improving the surface. The data shows that this is not the case, in fact the mean roughness for the 80° overhang printed at 180° is higher than the others, although well within the standard deviation so no correlation can be concluded. When forming an 80° overhang, the outer edge of the layers protrude past the previous ones significantly. As this is further than the thickness of one track of plastic, it has nothing to stick to and cools in mid-air. Even when upside down, the pressure forcing the plastic out of the nozzle causes the plastic go above the level of the previous layer, it then cools rapidly due to the active cooling fan, leaving unconnected 'drooping' strands. The extrusion and cooling rates could be tuned to allow unsupported printing, as in [122, 123] but this is not required for the objectives of this work so was not addressed further.

As Ra increases, the standard deviation also increases. The 80° overhangs have considerable variation, this is likely due to the variations in heating and cooling when the unsupported strands are deposited as there is no overall environmental control around the system. The mean Ra measurement cannot be considered as reliable at extreme overhangs, as the standard error of the mean has increased. This indicates that there is a greater uncertainty around how closely the estimated mean reflects the true mean of all possible samples. The 95% confidence intervals for means at each overhang angle are shown in Fig. 4.13. This effect is partly due to the measurement technique. At the larger overhangs there begins to be surface features which the Talysurf probe cannot detect. The surface is extremely rough and the features reach a scale which interfere with the stylus. Figure 4.14 illustrates how the conical shape of the stylus can act to smooth out the surface when there are extremely deep or tall features with high aspect ratios.

The post hoc analysis reveals that the roughness between 30° and 45° is not statistically different. This reflects the common suggestion that overhangs over 45° should have support structures. Below this threshold the surface may look homogeneous but after this stage the edges of the layers start to protrude over the edge of the previous layer by more than half the road width. In reality this limit can be increased by increasing the part cooling. On this system overhangs of 60° look visually acceptable, although the roughness threshold will vary with the application. The ability to print steep overhangs without requiring support is an advantage, both because support requires the use of extra time and material, but also because it can mar the surface it is supporting, increasing the roughness by 1.2 times [217].

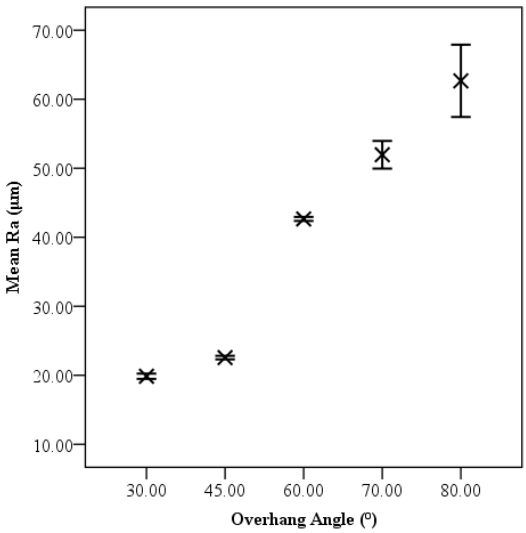

Figure 4.13: Total mean roughness for each overhang angle with 95% Confidence Intervals depicting the range in which the true mean value is expected to lie. As the samples showed more variation at the larger overhangs, this corresponds with a larger range in which we are confident that the true mean lies.

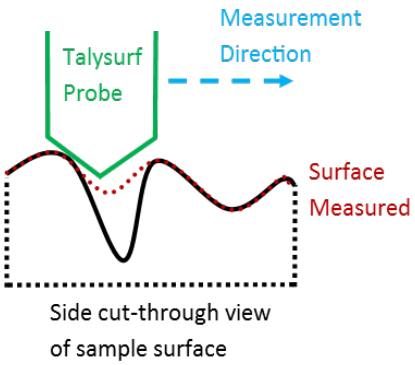

Figure 4.14: Schematic showing how, at large aspect ratios, the measurement probe may not reach the extremes of the surface. This has the effect of filtering extreme values potentially affecting the measurements when testing extremely rough surfaces.

4.3 Experiment 2: Dynamic Build Orientation

In this section, the second experiment dynamically varies the build orientation during printing to deposit layers which are not perpendicular to the build plate. Changing the build orientation over time is a unique capability of a multiaxis system. It could

be used to overcome some of the usual issues with AM, specifically, the requirement to print additional support structures to provide a surface to print upon. Early on in the development of this system a simple 90° overhang was printed without support material as a proof of this concept; Fig. 4.15. At this stage the system could only print conventional 2.5D horizontal layers and the kinematic model had not been extended to allow the nozzle or build plate to deviate from being perpendicular to one another. The print was achieved by printing a rectangular prism, then rotating the base plate by 90°, but not updating this within the kinematic calculations which worked out the extruder position. In this way the nozzle remained vertical and a second tower was then printed on the side of the first, yielding an unsupported overhang. This demonstration was to show that even at an early stage the system was capable of printing parts which cannot be achieved without a multiaxis mechanism. It also served as a comparison to a part that had been published recently, at the time (2014)[103]. Figure 4.15 shows how the system in this thesis is capable of printing much higher quality parts, allowing the assessment of parameters such as surface roughness and for conclusions to be drawn with respect to commercial FFF systems.

Following the development of the full capabilities of the system, the nozzle orientation can be programmatically controlled and varied throughout a print using gcode commands. In this experiment the build orientation is chosen according the the relationship defined above (Section 4.2.6) and then assessed via surface roughness measurements, allowing comparison to the static build orientation used previously.

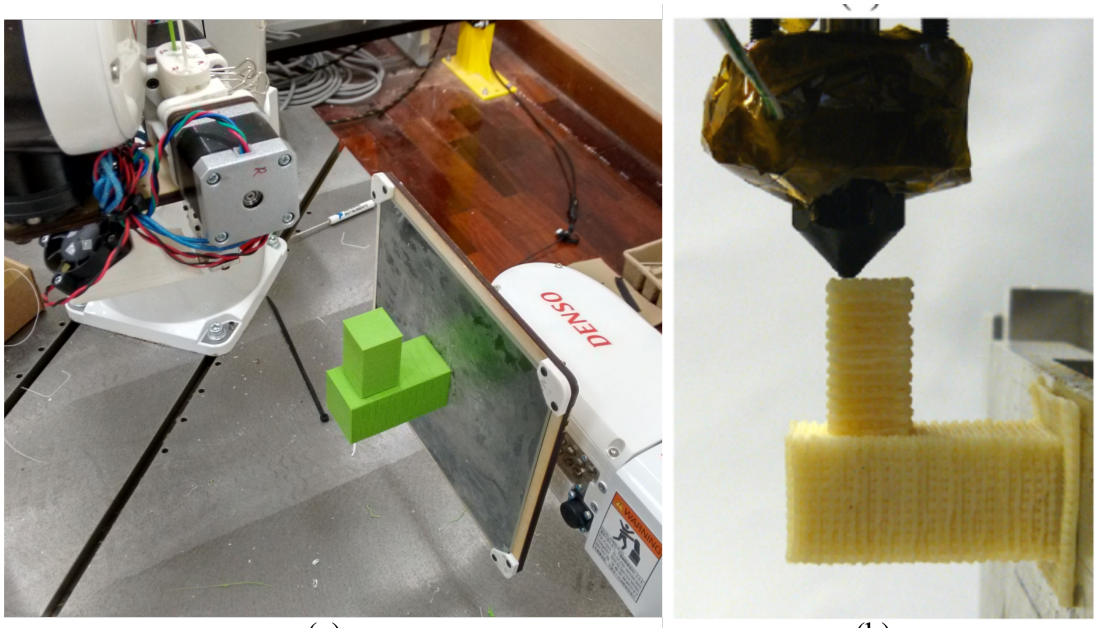

(a) (b)

Figure 4.15: (a) An early proof of concept printed on ARMS, showing a 90° overhang printed without support material by rotating the build plate so that the protruding section could be printed upright. (b) A similar object printed on a 5-axis system by Lee *et al.* [103].

4.3.1 Roughness Model

From the previous experiment a theoretical model of the surface roughness of an overhang can be created. It has been established that the orientation of the nozzle and the build plate does not, by itself, affect the surface roughness. What does affect the surface quality is the overhang angle of the surface (β) compared to the slicing angle, α (see Fig. 4.16 for notation). This is defined as Eq. (4.1). For all printing orientations the surface got progressively worse as the overhang angle tended towards 90°. In conventional 3D printing the part is cut into horizontal layers, or put another way, the slicing angle, α, is 90° (when measured from vertical).

The build axis of a part is defined as the vector along which the planar layers are stacked. Usually α is at right-angles to the build axis B, i.e. Conventionally planar horizontal layers are stacked vertically to produce a 3D printed part. There is, however, the potential for this to be varied with a multiaxis system, but this is not explored in this thesis.

The results match previous models of surface roughness for FFF [212, 218] but when

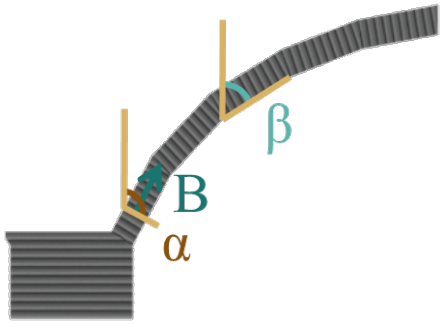

Figure 4.16: Definitions of symbols of orientation terms: Build Orientation (B) is the axis along which layers are stacked, Slicing Angle (α) is the angle with respect to vertical that is used to slice planar layers, Overhang Angle (β) is the angle, with respect to vertical, of the lower surface of a part.

the slices aren't limited to being horizontal this model can be extended and used to guide multiaxis printing. It is clear that Ra reaches it's upper limit as the overhang tends towards the slicing angle, Eq. (4.2). Figure 4.18 helps to depict this limit by having sections of layers highlighted which are printed with no lower layer to support them. As the overhang increases this unsupported section also gets bigger, until the 90° overhang, where the whole underside of the part is unsupported and is therefore unprintable. Conversely, the difference between the layers and the overhang angle is 90° for the base section. At this point the roughness is at its minimum Eq. (4.3). These relationships are shown graphically in Fig. 4.17 where the red curve corresponds to a conventional horizontal slicing angle ($\alpha = 90°$). It is clear from this graph that for an overhang to print at a low roughness, and not require support material, the overhang must remain within approximately ±45° of vertical when $\alpha = 90°$.

A multiaxis system, however, is not limited to depositing only horizontal layers, and therefore the value of α can be varied. The green line in Fig. 4.17 shows how the minimum roughness can correspond with a different overhang angle when non-horizontal layers are used, and potentially more importantly, the maximum overhang angle which can be printed has also been shifted. Figure 4.18 shows how this may correspond to a physical part when slicing the layers at 135° from vertical. The 45° overhang has the minimum roughness, and the 90° section would now be printable without support structures.

The following experiment tests this theory by varying the slicing angle while printing

different overhangs to test whether the roughness can indeed be kept at a minimum through the method of manipulating this relationship.

$$\mathbf{f} : \mathbf{R^2} \rightarrow \mathbf{R}$$

$$\mathbf{f} : (\alpha, \beta) \rightarrow Ra \tag{4.1}$$

$$\lim_{\beta \rightarrow \alpha} f(\alpha, \beta) = Ra_{max} \tag{4.2}$$

$$\lim_{\beta - \alpha \rightarrow |90|} f(\alpha, \beta) = Ra_{min} \tag{4.3}$$

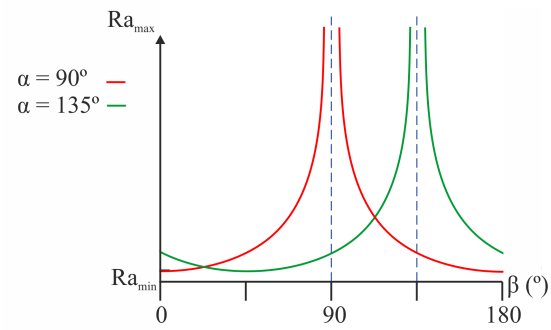

Figure 4.17: Graph of $f(\alpha, \beta)$ illustrating how Ra increases as the difference between α and β decreases, until the overhang becomes unprintable at $\beta = \alpha$. By varying α this critical angle can be varied.

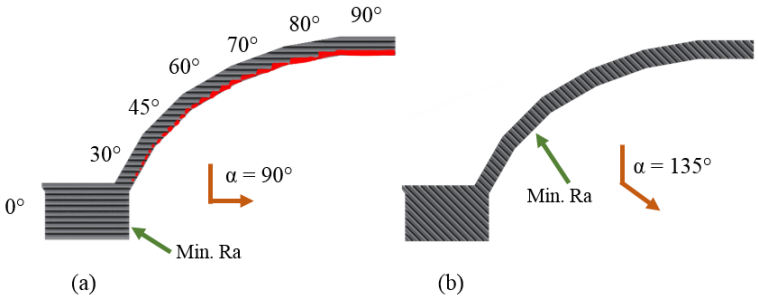

Figure 4.18: Schematic showing the arch samples, which has overhanging sections from 30° to 90°, with (a) layers sliced horizontally. The unsupported sections of each layer are highlighted in red. As the overhang angle increases these sections are larger. (b) Layers sliced at 135°. This layer angle means that the minimum roughness is now on the 45° section and the 90° overhang is not completely unsupported, so could be printed.

4.3.2 Method

In this experiment the same overhanging arch object (Fig. 4.6) is printed, with one slight modification. The foot height is extended so that when the first section (30°) is printed there is sufficient clearance between the extruder and the build plate. Rather than varying the whole printer orientation as in the previous experiment, the build axis, B, was changed dynamically throughout the printing process. The build platform was kept horizontal and the orientation of the nozzle was varied. As the printer orientation has no significant effect, the bed could have been moved while the nozzle is kept upright, but this option was not used as the large size of the platform may limit the orientations it can achieve while in close proximity with the extruder robot. Equation (4.3) was used to set the slicing angle to be normal to the overhang of the geometry. In all cases B is kept normal to α to ensure that the flat end of the nozzle smooths the tracks as usual. The layer orientations are shown in Fig. 4.19. In order to test whether this method will be effective, even on the roughest surfaces, the layer height was changed to 0.3mm in this experiment. This is generally the largest recommended layer height with a 0.4mm diameter nozzle. A set of arches were printed with the same setting on an Ultimaker 2+ to provide a direct comparison between the conventional tools and ARMS.

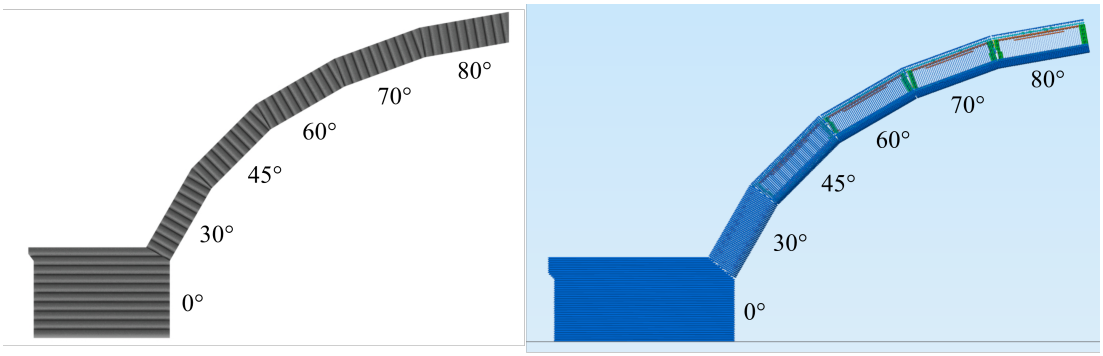

Figure 4.19: Layer orientations for the Dynamic Build Orientation experiment with the overhang/build orientation angle marked, measured from vertical. (a) schematic representation, (b) slicer preview of gcode.

Conventional slicing software has been utilised for the previous experiments, however it is not designed to allow build orientations other than normal to the build plate. Therefore a procedure was designed which allows the creation of gcode with a variable

build orientation, using mainly existing software. This procedure is shown in Fig. 4.20 and explained below.

To create the gcode with a varying build orientation the CAD file was first split into separate sections depending upon the required build orientation. For this overhanging arch sample this meant there were six separate parts; the base which is printed conventionally, and five overhang sections, each printed with the build axis at the same angle as the overhang. To ensure all the sections line up after slicing they were saved with the same origin. However, the direction of the Z axis was changed for each section to align with the build axis.

After this, each section could be loaded into the slicing software individually (Simplify3D). The position is set the same for all parts, and the software loads the file so that the Z axis is vertical. This allows the section to be sliced conventionally and the layers are in the correct orientation, perpendicular to the overhang surface. The slicing settings used are summarised in Table 4.2. These layers need transforming, however, as the layers may be correct in relation to the section geometry, but the section's orientation is not correct. To do this a program was developed, using LabVIEW, which takes in the gcode and can transform and rotate the coordinates, then save them back in the original format. The gcode must be saved so that the X, Y and Z coordinates are printed on every line, even if one has not changed. This allows the program to go through the gcode file line by line and rotate the coordinates. The origin for the part and the angle by which it needs to be rotated are set manually, then the program uses homogeneous matrix transformations to translate the coordinates in that line of gcode to be around the origin, rotates them, then applies the translation in reverse. Once all the gcode has been processed, this has the effect of rotating the whole section of layers around the part's origin.

This process of slicing and rotating is repeated for each of the sections required. The separate gcode files can then be combined using a text editor. Between each section a line of gcode is inserted which commands the nozzle to change orientation to be perpendicular to the layers.

This combined gcode was used to print the part three times and the roughness of the underside surfaces was measured using the same procedure as in Section 4.2.3. The roughness data is analysed using the same procedure as in Section 4.2.4, but in this case there is only one independent variable, the overhang angle, so a one factor ANOVA is

Table 4.2: Slicer settings for dynamic build orientation samples.

Setting	Value
Layer height	0.3mm
Print Speed	30mm/s
Temperature	200°C
Material	Polymaker PolyMax PLA
Cooling	On
Infill Density	20%
Infill Pattern	fast honeycomb
Perimeters	2
Top and Bottom Layers	3
Software	Simplify3D

used. The null hypothesis is that all the mean roughness's are equal across the different overhang angles. The alternative is that there is some difference between the sections.

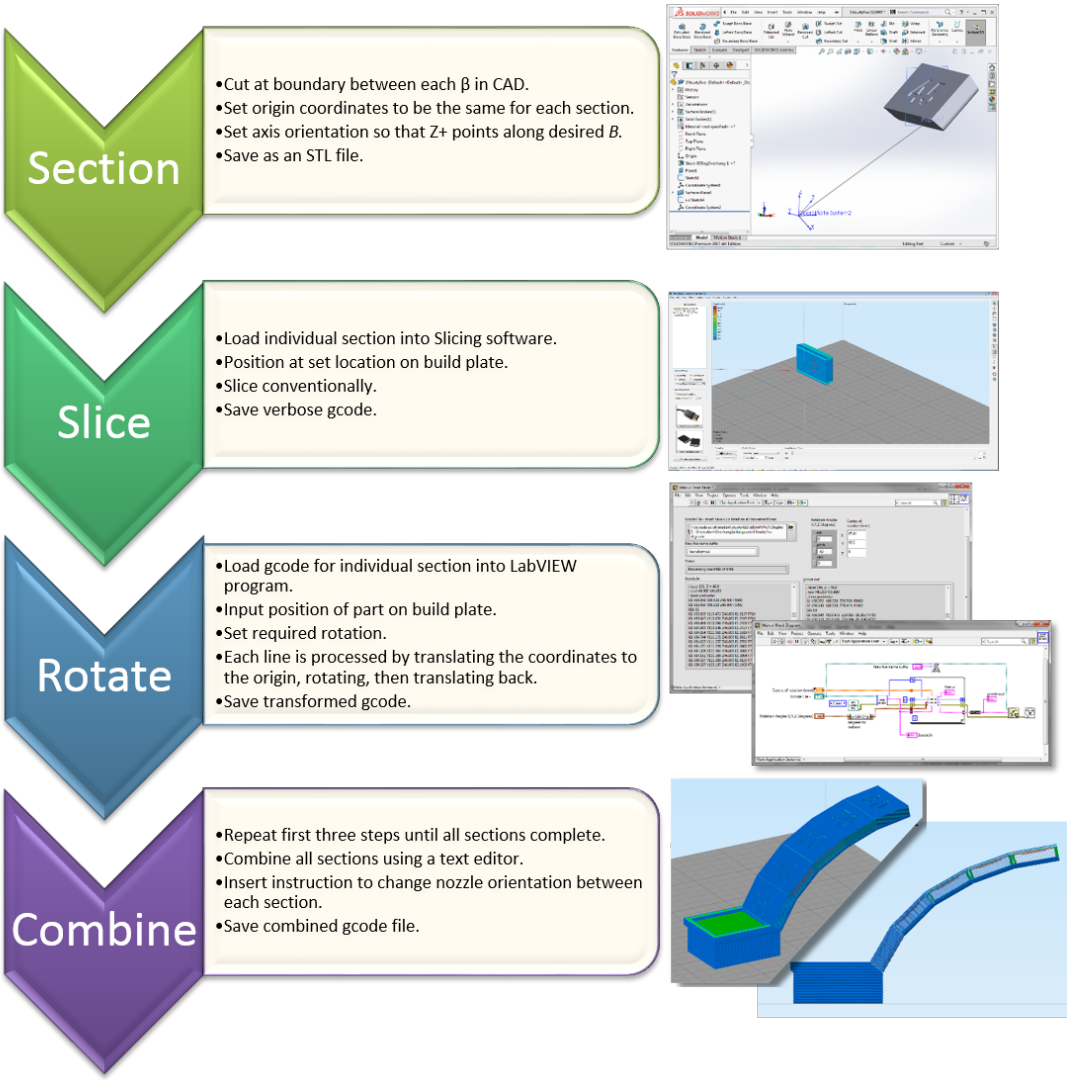

Figure 4.20: Process for creating gcode with a Dynamic Build Orientation

4.3.3 Results

The samples were printed successfully with the nozzle orientation varying along the build. A photograph taken during one of the prints is below, Fig. 4.21. Visual inspection reveals that all the sections look identical. Images taken from the side using a microscope can be seen in Fig. 4.22 and clearly show both the layer orientations and the comparison between a sample printed conventionally. In this figure the photographs were taken from the side of the sample, so the edges of the overhanging layers can be seen in profile. The left set of images shows layers which are all horizontal, so as the

overhang angle increases the edge of these droop further as there is nothing underneath to support them. The right hand set of images shows layers which are always perpendicular to the overhang, due to being printed with the dynamic build orientation. The corner is clean on all of these photographs and no layers bulge or droop.

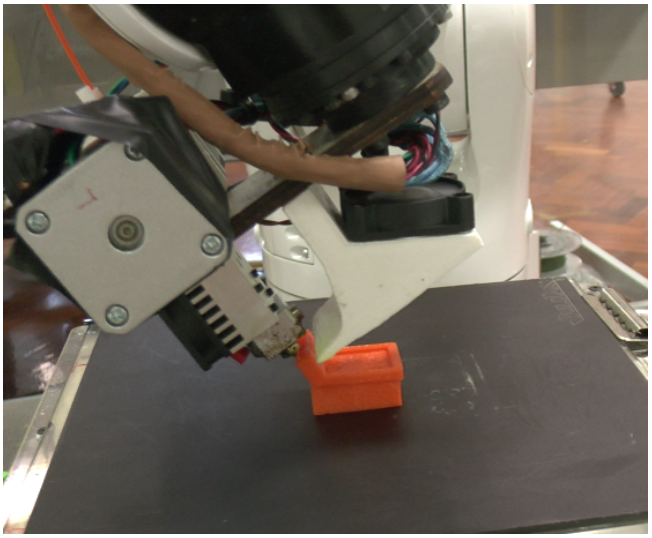

Figure 4.21: Photograph showing 3D printing of the 30° section using a dynamic build orientation. The nozzle has been angled away from vertical so as to remain perpendicular to the layers being printed

The mean and standard deviation for Ra for each overhang angle section are displayed graphically in Fig. 4.23, alongside the results from the previous section to help provide context. The roughness remains the same across the different overhang angles, in contrast to the results when the build axis remains constant.

The higher level analysis of variance suggests a statistically significant difference between the roughness of the different overhanging sections ($F(4, 40) = 2.681, P = 0.045$) when using a significance level of $P = 0.05$. However the post hoc test results reveal that there is no significant difference between any of the pairwise comparisons ($P \geq 0.061$ in all cases). The detailed tables for these tests can be found in Appendix B. The ANOVA significance results imply that the null hypothesis should be rejected. The Tukey test, however, is not in agreement, the results show that there is no significant difference when comparing any of the individual sections. The Tukey follow up test is conservative as it tries to correct for the probability of making a Type I error [1] when

[1] i.e the incorrect rejection of a true null hypothesis, also called a false positive.

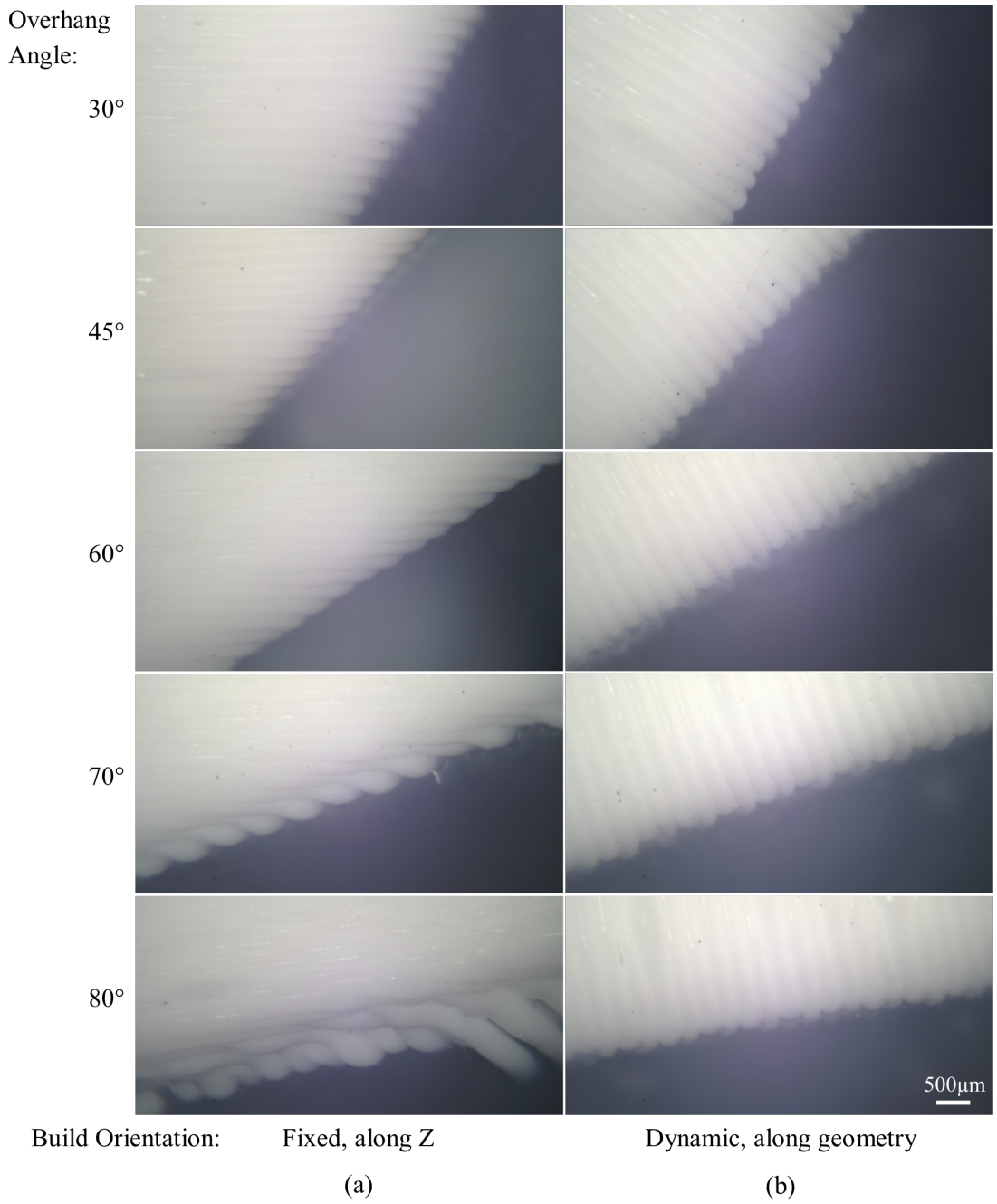

Figure 4.22: Microscope images from the side of overhang arch samples showing (a) how the layers remain horizontal and the edges droop due to less overlap with the previous layer as the overhang angle increases. Conversely (b) shows the layers staying perpendicular to the overhang angle, so all the edges are uniform.

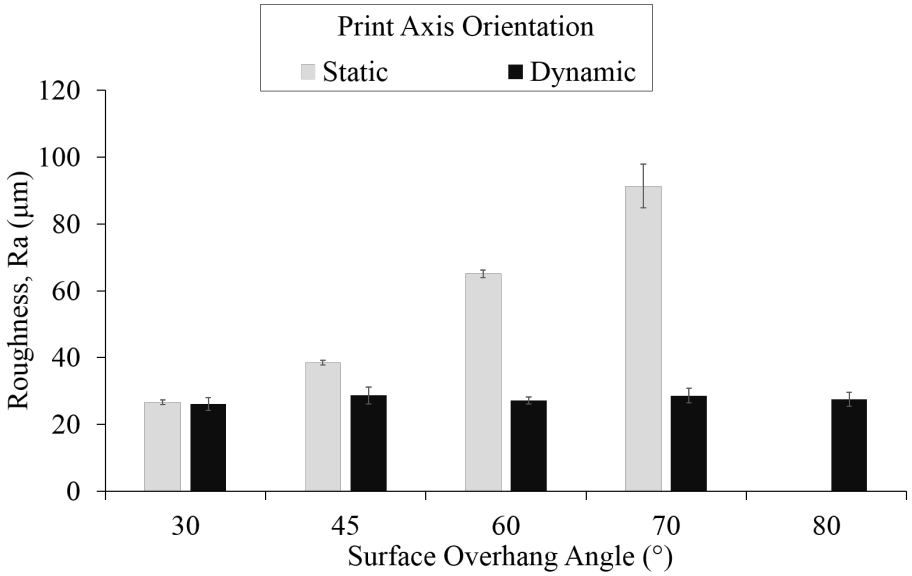

Figure 4.23: Mean and Standard Deviation of Ra values for each surface on the Dynamic Build Orientation (DBO) samples (n = 3). The roughness for the DBO samples does not have an upwards trend, in contrast to samples with a static build orientation which were printed on an standard FFF printer (Ultimaker 2+).

performing multiple comparisons. Considering the post hoc results, and the fact that the P value is only just under the 0.05 threshold, it would appear that in this case rejecting the null hypothesis is likely to be a Type I error. Therefore we can conclude that the evidence does not support there being a significant difference between the Ra for each section The 95% confidence intervals of the mean for each overhang angle are shown in Fig. 4.24, and indicate that there is unlikely to be a significant difference between the five means as the bars overlap for all categories.

Following the successful prints of the samples with 80° overhangs, the part was extended to include a 90° overhanging section, which was printed with the nozzle horizontal. This sample is not included in the roughness measurements, but Fig. 4.25 shows a direct comparison with the same STL file printed conventionally, with all layers built along the vertical Z axis. The underside of the sample which has a static build orientation is clearly much rougher, and the 90° section has large drooping strands of plastic. The layers eventually resolved themselves so that the section did complete but there are few applications where this amount of distortion and required post processing

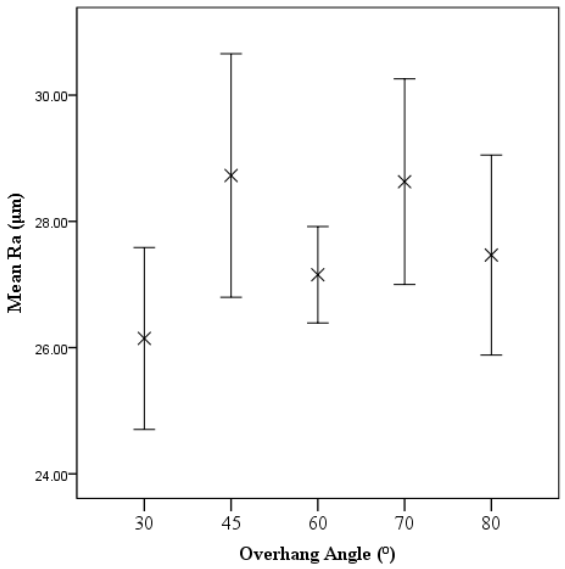

Figure 4.24: Total mean roughness for each overhang angle with 95% Confidence Intervals depicting the range in which the true mean value is expected to lie.

would be acceptable. On the other hand, the part printed with the dynamic build orientation printed every section cleanly, with no rough edges or drooping layers.

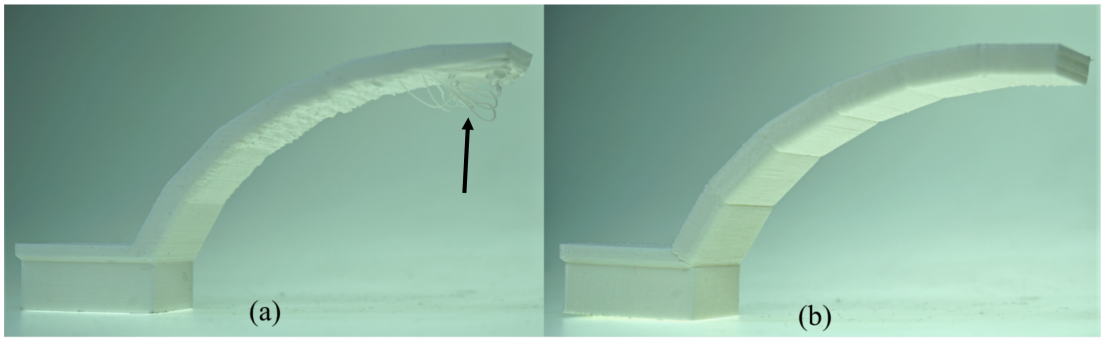

Figure 4.25: The arch has been extended to include a 90° overhang and printed unsupported using: (a) A vertical build orientation, which caused large strands of plastic to hang down from the 90° surface (marked with arrow). (b) A dynamic build orientation which follows the overhang angle. All sections were cleanly printed.

4.3.4 Experiment 2: Discussion

Visually it is clear that changing the build orientation has dramatically improved the surface quality of the overhanging faces. This is especially evident in Fig. 4.25 where the 90° section cannot be printed successfully using a vertical build orientation. To the eye there is no difference between the surface quality of the sections and this is borne out by the measurements in Fig. 4.23. There is some disagreement between the two statistical tests that were performed, however considering the conservative nature of the Tukey test is is reasonable to conclude that the significant difference is a false positive. This disagreement between the statistical tests could be due to the ANOVA test identifying significant differences for combinations of means as well as differences between pairs of means. The other reason this could happen is because the estimates of the population mean are calculated from sample data which is subject to sampling error [219]. Using a large number of samples in the future would help minimise the effect of sampling errors.

This experiment has shown that dynamic build orientations can not only improve the surface roughness of parts, it can allow horizontal overhangs to be printed without support, something that is not achievable without a multiaxis system. The dexterity of this robotic system allows overhangs of arbitrary size and angle to be printed, without needing any support structures.

4.4 Chapter Conclusions

In this chapter it was first established that the printer orientation has no effect upon the surface roughness of overhanging features, and therefore part surface quality in general. This is important as it verifies that novel techniques for 3D printing can be pursued without requiring the nozzle, or build plate, to remain in their traditional orientations. This is a novel contribution which has not been reported before, although others have experimented with multiaxis printers and presented photographs for proof of concept, this is the first quantified experiment to verify that FFF can be used in orientations other than vertical with no adverse effects to the surfaces.

The roughness results from this experiment agree with other models of surface roughness for FFF, but the relationship has been extended to reflect that the critical overhang angles, where Ra reaches either its maximum or minimum, can be altered.

This was achieved by identifying that the ability of FFF to print overhangs breaks down as the overhang angle tends toward the slicing angle.

The ability of the system to change the axis along which the layers are stacked enables layers to be sliced at angles other than 90°. This opens up the possibility of optimised slicing which varies the nozzle orientation to keep Ra within a desired range.

This relationship was then used to inform the use of a dynamic build orientation, that is, varying the axis upon which the layers are stacked. These results verified that the roughness can be kept at a minimum by matching the build orientation with the overhang angle. This allowed overhangs to be printed which would be impossible using existing FFF systems, as even using support structures increases the roughness.

The effects of varying the slicing angle in relation to the build angle have not been investigated beyond being perpendicular, as it is likely that the flat tip of the nozzle would reduce the surface quality if it is not perpendicular, but there is certainly scope for further work in this area. One interesting avenue may be to experiment with round ended nozzles, for example. To extend this work further, new software for multiaxis slicing is required. The object was manually sectioned, but with the right software the build orientation could be continuously varied allowing smooth transitions between angles and continuous printing of arbitrary curvatures and overhangs.

Chapter 5

Multiaxis Nonplanar Layers for Increased Strength

5.1 Introduction and Motivation

The use of nonplanar layers in FFF is desirable for three main reasons. The first is that is can be used to print continuously along the top surface of a non-flat part, thereby removing much of the stepped effect that is created by the use of discrete layers to approximate a curve. This has been some initial research which explored this using 3 axis systems, as discussed in Section 2.4.2. As illustrated by Fig. 5.1, the smoothing effect is most noticeable on shallow curves, therefore the technique is applicable on 3-axis systems, but the low DOF does limit the maximum curvature that can be printed to 30° [106]. This has been attributed to the flat tip of the nozzle needing to be as close to parallel with the layer as possible, so that it flattens and smooths the plastic rather than gouging into it with the corner. It is often suggested that the nozzle must be perpendicular to the deposition [105, 144, 165] due to these effects, but multiaxis FFF research is in its infancy so no study has been reported that quantifies this effect. Some straightforward tests were completed using a 3 axis FFF

printer which practically verified the limitations of 3 axis printers for curved layers. Figure 5.2 shows a comparison, while the details can be found in Appendix C.

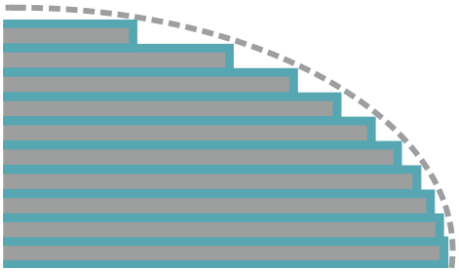

Figure 5.1: Discrete planar layers can only approximate a curve, the difference between the desired curve and the stepped representation increases as the curve gets shallower.

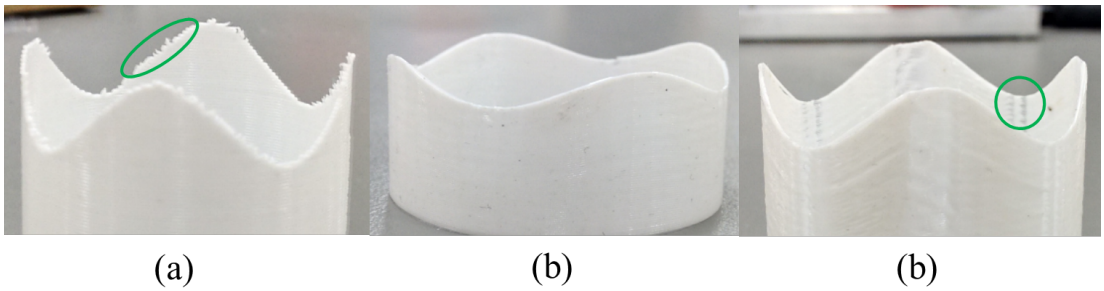

Figure 5.2: (a) Curved top surface approximated using discrete layers showing stepped effect. (b) A smooth curved surface due to sinusoidal layers, but as the curves get steeper (c) the side of nozzle contacts the slope and a discrepancy in the speeds of the Z axis compared to the X & Y causes areas of under extrusion.

The second advantage of nonplanar layers is that it allows printing onto existing complex surfaces. By mapping the contours of the added layers to the existing object a strong bond could be created, opening up the possibilities of augmenting or repairing existing objects [109, 134, 144]. This has commercial applications when applied using DED as the metal substrate bonds to the added section due to the process creating a melt pool on the surface, welding the sections together. With FFF the bonds would heavily depend upon the surface being printed upon. Even if limited to modifying FFF 3D printed items this would still be an advantage when iterating through designs or in cases where items may be customised for the user. A stock item, for example glasses frames, could be edited through the use of multiaxis AM, allowing rapid mass customisation without the associated inefficiency in 3D printing parts which could be

mass produced.

The third advantage is an increase in strength. FFF parts are anisotropic, with weaknesses across the layers [7, 113, 197]. Nonplanar layers could be used to either reduce these weaknesses by reducing the number of layers required to print a section, or by reorienting these weaknesses such that they are less likely to be pulled apart by the forces applied. Previously a shallow arch was printed using curved layers on a 3 axis FFF machine. The curved part was 1.41 times stronger than a conventionally printed part when subjected to a 3 point compression test [112, 116]. Mitsubishi researchers have used a delta 3D printer with two additional rotation axes to print curved layer domes which could resist pressures 3-5 times higher than domes printed using planar layers [138]. These two tests show the potential of this type of system to increase the strength of FFF parts. In this chapter curved arches with steep sides of 45° will be printed using the multiaxis system and then tensile tested to add to this body of work and evaluate whether the improvement in strength can be realised.

5.2 Methods

To assess the impact that changing the layer shape to match part geometry can have, two planar layer and one nonplanar layer sets of arches are printed. The planar layer arches are sliced using conventional software, the nonplanar arch gcode is generated using a Matlab script that was devised for this purpose. This approach enables the rotations required for the extruder to remain normal to the part surface to be calculated. Tensile tests are then performed on all of the samples. A motion tracking experiment is also undertaken to ascertain how rotating the end effector of the robot affects its ability to do linear interpolation between points.

5.2.1 Tool Path Generation

As curved layer slicing software is in its infancy, the gcode of the curved layer samples was generated using a script written in Matlab. A flow chart depicting the process is in Fig. 5.3 and it is described in more detail below.

An arch shape was chosen for the sample as it clearly displays the stepped effect created by horizontal layers, it can be gripped for tensile tests and it has curvature in only one axis. While this technique should be extended to complex curvatures in the

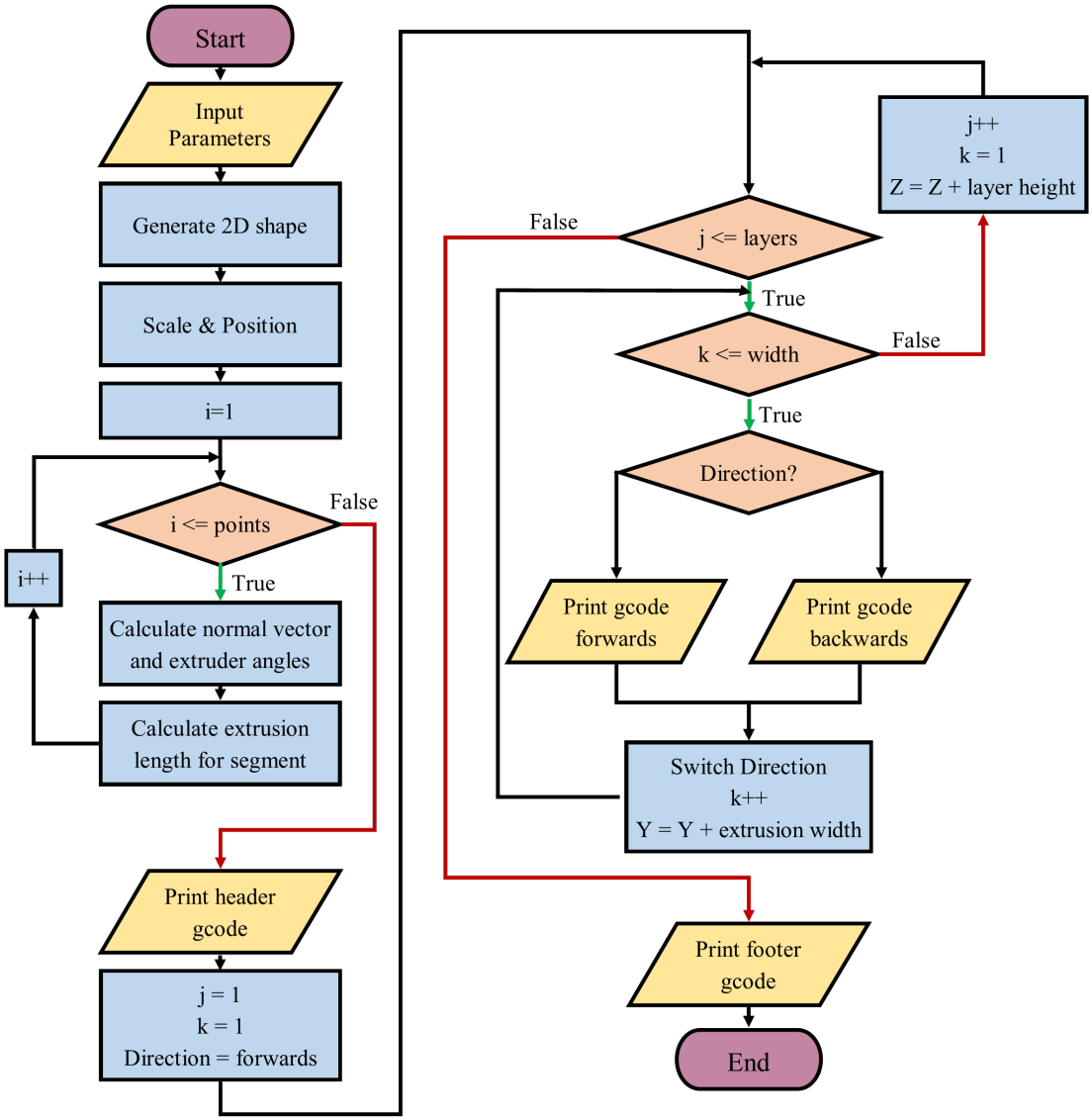

Figure 5.3: Flow chart of program to generate curved layer gcode for nonplanar 3D printing of an arch. See text for explanation.

future, the purpose of this test is to find whether there is a fundamental difference in the maximum tensile force that can be resisted when the layers are conformal. When an arch is printed upon its side the perimeter tracks of plastic are conformal to the outside of the object so this gives the opportunity to compare curved layers to orientation which would give the highest strength when using horizontal layers. The arch was created using the equation $z = cos(x)$. Therefore the sample shape is defined by a small number

of key parameters and allows for the calculation of normals to each section directly. The script calculates the z values for $-\pi \leq x \leq \pi$ using the number of steps determined by the 'resolution' parameter. This varies the number of lines of gcode which describe the shape. The robot performs linear interpolation between each coordinate it moves to, so fewer points mean a more angular shape, as seen in Fig. 5.4 (10 points). A horizontal foot is added to each end of the arch by taking the first and last z values and offsetting the corresponding x coordinate. This shape is the scaled and translated to position it for printing. Following this a for loop iterates along each set of coordinates and calculates the normal vector, Fig. 5.4 (b), and the amount of plastic that should be extruded for each section. This gives the poses to print a single curved strand of plastic in the X-Z plane.

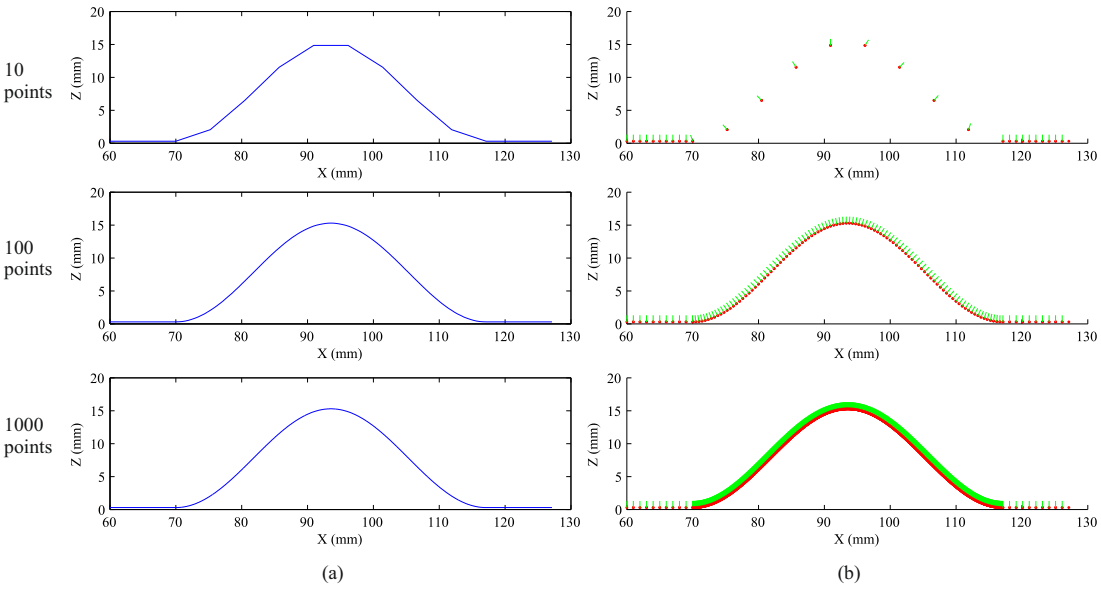

Figure 5.4: Arch shape with various resolutions showing (a) how the shape is approximated and (b) the individual points and their corresponding normal vectors.

To find the vectors that are perpendicular to the surface, the movement vector **v**, from one gcode point (Eq. (5.1)), to the next (Eq. (5.2)), is first calculated by Eq. (5.3). The two normal vectors are then given by Eq. (5.4) or Eq. (5.5). In this case, the normal vector that is needed will always be in the positive Y direction so Eq. (5.5) can be chosen directly. This vector is normalised to give a unit vector and trigonometry used to calculate the required nozzle angle compared to vertical.

$$\mathbf{a} = \begin{pmatrix} x_1 \\ y_1 \end{pmatrix} \tag{5.1}$$

$$\mathbf{b} = \begin{pmatrix} x_2 \\ y_2 \end{pmatrix} \tag{5.2}$$

$$\mathbf{v} = \mathbf{b} - \mathbf{a} = \begin{pmatrix} dx \\ dy \end{pmatrix} \tag{5.3}$$

$$\mathbf{n} = [-dy, dx] \tag{5.4}$$

or

$$\mathbf{n} = [dy, -dx] \tag{5.5}$$

5.2.1.1 Extrusion Volume

To print plastic along the curve that has been generated, the quantity of plastic to be extruded for each movement must be calculated. The equations used are based upon open-source slicing software developed by the RepRap community [220–222]. When plastic is extruded out of the nozzle it forms a flattened bead, assuming the edges of the track are unconstrained. This can be modelled as a rectangle with semicircular ends, due to the surface tension; Fig. 5.5.

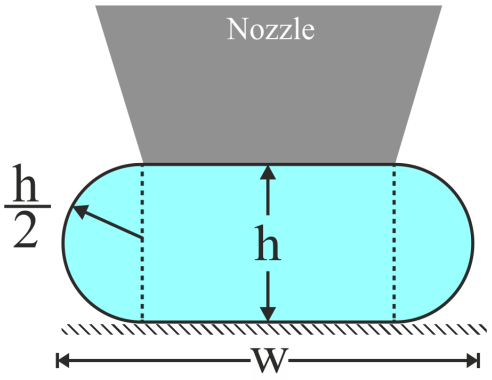

Figure 5.5: Cross sectional area of track of extruded plastic showing layer height, h and track width, W.

The cross sectional area of the plastic can be calculated as the area of a circle with diameter, h, and a rectangle of height h and width $W - h$, Eq. (5.6). The volume of plastic that must be extruded for a linear movement, V, is simply the cross sectional area

multiplied by the length of the motion, L, Eq. (5.7). In gcode, extrusion is controlled by giving a distance of raw filament to extrude. Therefore the volume, E, is divided by the cross sectional area of the filament to give the required length, Eq. (5.8). The filament diameter, D, in this case is 1.75mm.

$$A = \frac{\pi h}{4} + h(W - h) \tag{5.6}$$

$$V = A \times L \tag{5.7}$$

$$E = \frac{V}{\frac{\pi D^2}{4}} \tag{5.8}$$

5.2.1.2 Layer Generation

To extend this single track to a 3D layer, the set of coordinates is stepped and repeated along the y axis, the order of the points being reversed each time. This makes the nozzle go backwards and forwards along the arch, printing continuously. These layers are then stacked in the z axis to form the arch using simple Z offsetting. This string of coordinates and normal vectors are then parsed into gcode.

Stacking the layers in the z direction is not a method that generalises for use with all curved layer parts. It causes steep walls to be thinner than the more horizontal sections as the thickness is only increased in z. As this part is only a few layers thick the effect is not large, but can be seen in Fig. 5.7 (b). Offsetting the points along the normal vectors is a method that would work in this case, but also causes distortion in the shape, especially at corners [112].

A support structure was also created, to print the arch onto. This was produced by using equation driven curve in Solidworks, to match the arch, and then modelling a block which fits below this. The STL can then be positioned in the same place on the build plate as curved arch, and sliced using the conventional process. At first PVA filament was used for printing the support as this does not adhere strongly to the PLA part material and can be dissolved in water. Both materials were printed using the same nozzle; the process was paused and the materials swapped manually between the two sections. As this support structure was made up from planar layers the top surface was stepped. These impressions were embossed upon the underside of the curved arch, causing lines of stress concentration from which cracks would propagate, when strength testing. To remove these external influences, a smooth support structure was used. This was achieved by covering the printed structure with BuildTak, a adhesive backed

polymer sheet which is commercially available as a printing surface for FFF. It promotes adhesion to the print bed without requiring a heated build platform [223]. Results from the stepped support can be seen in Appendix D and the following experiment uses the smoothed surface, seen in Fig. 5.6.

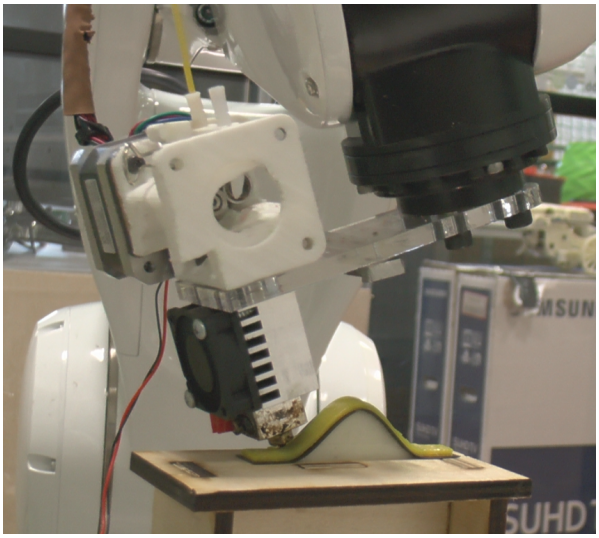

Figure 5.6: The surface of the support structure was coved in a thin black polymer sheet (BuilTak) to cover the steps caused by conventional AM's discrete layers. Arches were then printed using identical gcode to the previous samples.

Arches of the same dimensions were printed, both upright and sideways, using planar layers and automatically generated support, using Simplify3D as the slicing software. A simulation of the gcode paths is seen in Fig. 5.7 and the settings used in Table 5.2. The same major settings were used for the curved layers however there are many optimisations in commercial slicing software which were not implemented in the matlab code.

A new build platform was constructed which has a small area for printing upon and is raised up from the usual plate. As the extruder is offset from the wrist of the robot, when it is angled to print steep curves the robot arm could dip below $Z = 0$. Printing the arches upon this raised plinth removes the chances of a collision.

Table 5.1: Settings used to generate gcode for nonplanar layer arches using Matlab.

Setting	Value
Layer height	0.3mm
Print Speed	60mm/s
Temperature	200°C
Material	Polymaker PolyMax PLA
Support Material	PVA
Extrusion Multiplier	0.94
Cooling	Off
Cos Resolution	1000 points
Foot Resolution	10 points
Width	20 tracks
Layers	9
Extrusion Width	0.45mm
Scale	7.5

Table 5.2: Settings used to generate gcode for planar layer arches using Simplify 3D.

Setting	Value
Layer height	0.3mm
Print Speed	60mm/s
Temperature	200°C
Material	Polymaker PolyMax PLA
Support Material	Polymaker PolyMax PLA
Extrusion Multiplier	1
Cooling	Off
Perimeters	2
Infill Density	100%
Infill Pattern	Rectilinear ±45°
Width	9mm
Height	3mm
Extrusion Width	0.45mm

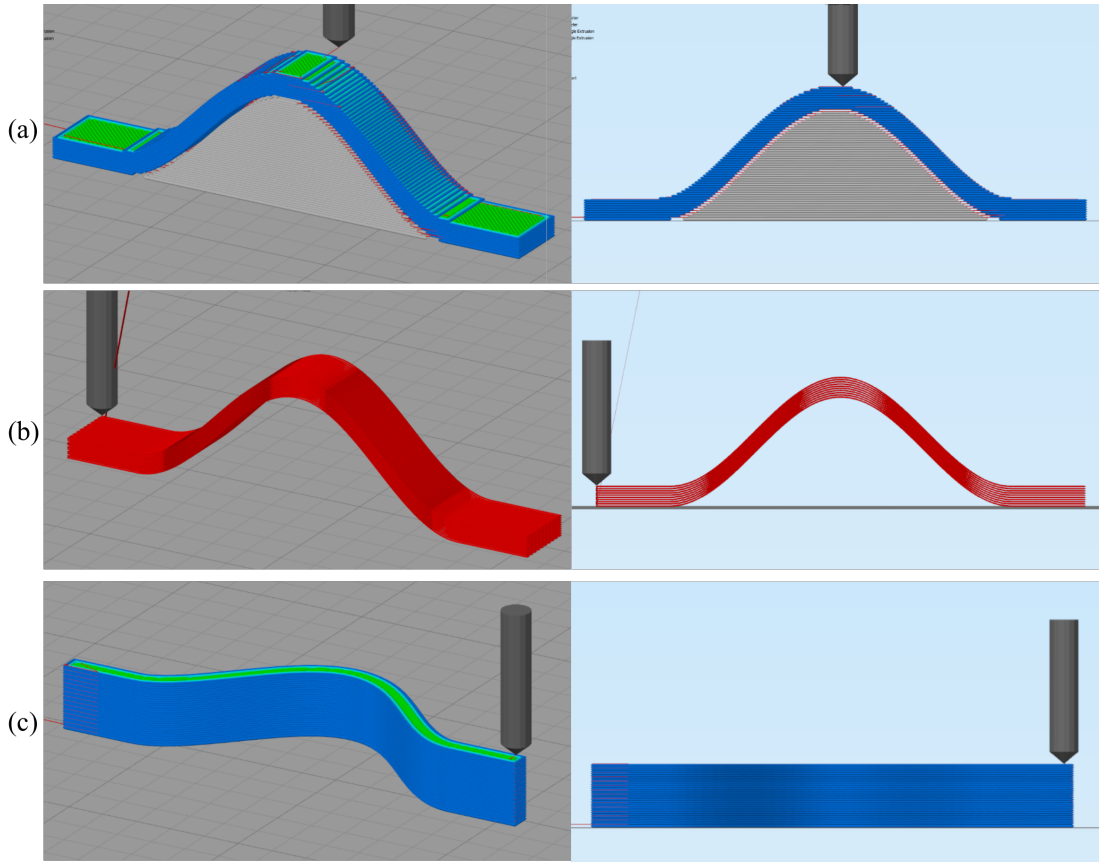

Figure 5.7: Isometric views (left) and front views (right) of the gcode used for (a) an upright arch printed with planar horizontal layers, (b) an arch printed with curved layers and (c) an arch printed upon its side using planar layers.

5.2.2 Mechanical Strength Tests

While curved layers have been shown to subjectively improve the surface of a shallowly curved surface [106], it is expect that they can have a much more significant impact upon the usability of FFF parts if they are used to improve the strength. Therefore in this experiment the samples will be subjected to tension as it allows force to be applied to the planar layer arch in a direction which is colinear to the layers. This orientation is the strongest, as seen in Section 3.8.2, so possible improvements to the maximum breaking force can be seen. To determine the difference between the two construction techniques, tensile tests were performed to find the maximum force the arches can sustain. The arches were gripped by the feet at each side of the arch by parallel grips and then pulled at a constant speed of 5mm/min using an Instron 3369

tensile testing system.

5.2.3 Motion Tracking

The positions that the robot will move to are defined by the user, but the robot's controller calculates the trajectory between these points. Linear interpolation is the chosen method for this, so the extruder should describe a straight line directly between positions. When the end effector is at a constant orientation this works well, the motion of the robot is predictable and straight lines can be defined by end points. Observation suggested that this was not the case when the orientation changes between two positions. Therefore a motion tracking system (NDI Optotrak Certus) was used to check the path before printing. Three of the active markers can be combined into a rigid body allowing both position and orientation to be recorded. One of these was placed on the base plate as a stationary reference, a second rigid body was secured to the end of the extruder robot with the origin at the tip of the extruder, using a 3D printed mount. To analyse the data, the beginning and end of the arch path were found visually using the first and last sharp change in direction, the initial and final movement of the robot can then be discarded. A 2D plane was then fitted to the data, as the input was a single pass along the arch shape which should result in motion just in the XZ plane. The data is then rotated to match this plane with the XZ plane of the reference marker. This was to remove steady state error introduced by the tracking system not being directly perpendicular to the markers. The tracked data was translated to begin at the origin. The tracked coordinates then line up with the input gcode so they can then be directly compared. As the tracking system works at 100Hz there are many more recorded points than the gcode command points, so a data set with the same number of points in is generated using the same equation which was used to produce the gcode. Consequently, for every X value, the corresponding Y and Z coordinates, and rotations around each axes, can be compared. The Mean Absolute Errors (MAE) in position are calculated using the Pythagorean theorem to get the length of the vector between the ideal coordinates and the measured coordinates in each of the three planes; XY, XZ and YZ.

5.3 Results: Printing of Nonplanar Layers

In this section the data from motion tracking is presented and analysed. The resulting samples from 3D printing arches using different build strategies are shown, along with the tensile test data for each type.

5.3.1 Motion Tracking Results and Discussion

The position results are displayed in Figs. 5.8 to 5.11, and the Mean Absolute Errors (MEA) in Table 5.3, for 10, 100 and 1000 points along the curve. The first figure includes images of a 3D model of the arch, with a red line to show the tracked path that the robot took and to provide context for the results graphs. The 10 point arch data clearly shows that the tip of the extruder deviates by approximately 3mm at the top of the curve. This is where the orientation change is greatest. The peaks where the tracked data touch the ideal path correspond with the points specified in the gcode. This shows that the robot has very low error at these points, but the inbuilt linear interpolation control does a poor job of keeping the extruder on a straight path when there is an orientation change. The errors are greatly reduced for the 100 and 1000 point paths. The XZ plane graphs show how the position matches the ideal position very closely. Increasing the number of points has reduced the changes in both position and orientation between the command points and so has kept the motion closer that the desired path. The error from the robot calculating a non-linear path can be reduced by forcing it to only calculate small steps. However, the reduction in errors is not proportional to the number of points used, as the points increase there are diminishing returns. But the robots, and the measuring system, have inherent errors so there is a lower limit to how far these errors can practically be reduced by increasing the quantity of points.

The number of points used does have a significant effect upon the speed of the end effector. By differentiating the position results, Figure 5.12 was obtained, which shows the speed with respect to time for 10, 100 and 1000 point arches. While all paths where set to use the same speed and accelerations, the decrease in step size between the points does not allow the robot as much time to accelerate between each point. This has the effect of slowing down the prints with more points, so that the 1000 point arch took around 14 seconds longer. The shape of the velocity graphs also reveals that the are sharp increases in speed as the robot traces the up and down slopes side of the

arch. This is likely due to the fact that little orientation change is required between the points. While the 1000 point arch was slower, the speed is much more consistent, which is important for print quality. This is due to the fact building up pressure in the nozzle to extrude molten plastic is not instantaneous, so variations in speed can be visible in the results.

The rotation results are shown in Figs. 5.13 to 5.15 for 10, 100 and 1000 points respectively. The rotations around X and Y are minimal for all three paths with mean absolute errors of less than half a degree. In the same manor as the positional data, the 10 point path shows that while the robot was at the correct orientation for many of the gcode points, the change in orientation is not consistent and there are variations of up to 0.3814rad (21.85°) around the Y axis. This would be too large if the path was being printed over an existing object as this could cause the nozzle to collide with the surface, or at the very least not smooth down the plastic that was being deposited. The overall errors also drop as the number of points increase, Table 5.3.

From these motion tracking tests it was decided to print the curved layers using 1000 gcode points. While the error is not greatly reduced when compared to the 100 points path, the speed has considerably less variation. These tests show that there is a minimum threshold to the number of points the should be used to describe a complex motion path. Large numbers of points may improve the theoretical accuracy, but they are likely to slow down both the motion of the robot and the preprocessing time sufficiently to be impractical. At extremely small step sizes it is unlikely that the robot would be able to physically make the motion. Further experiments would be required on a wider range of paths lengths and shapes to quantify this threshold however.

Table 5.3: Mean Absolute Errors (MEA) for the robot position and orientation when moving normal to an arch described by 10, 100, or 1000 points.

Data	10 Points	100 Points	1000 Points
Position MAE (mm)	1.0606	0.0945	0.0891
Orientation MAE (rad)	0.0482	0.0142	0.0112

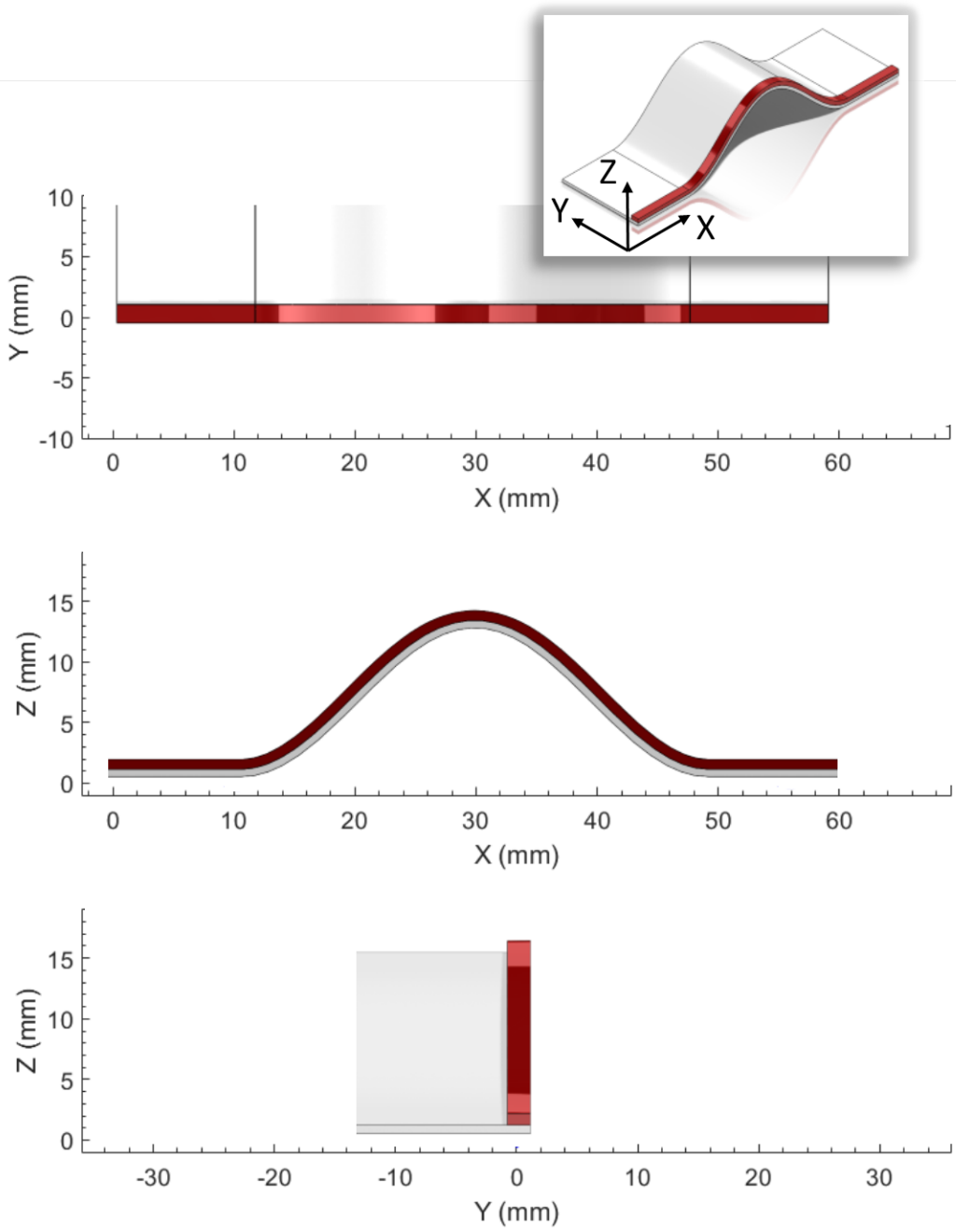

Figure 5.8: CAD model of an arch with a red line to show the tracked path that was recorded. Path is plotted from the top, side and front view. The inset shows the axes to help the reader understand how the 2D graphs correspond to the 3D path.

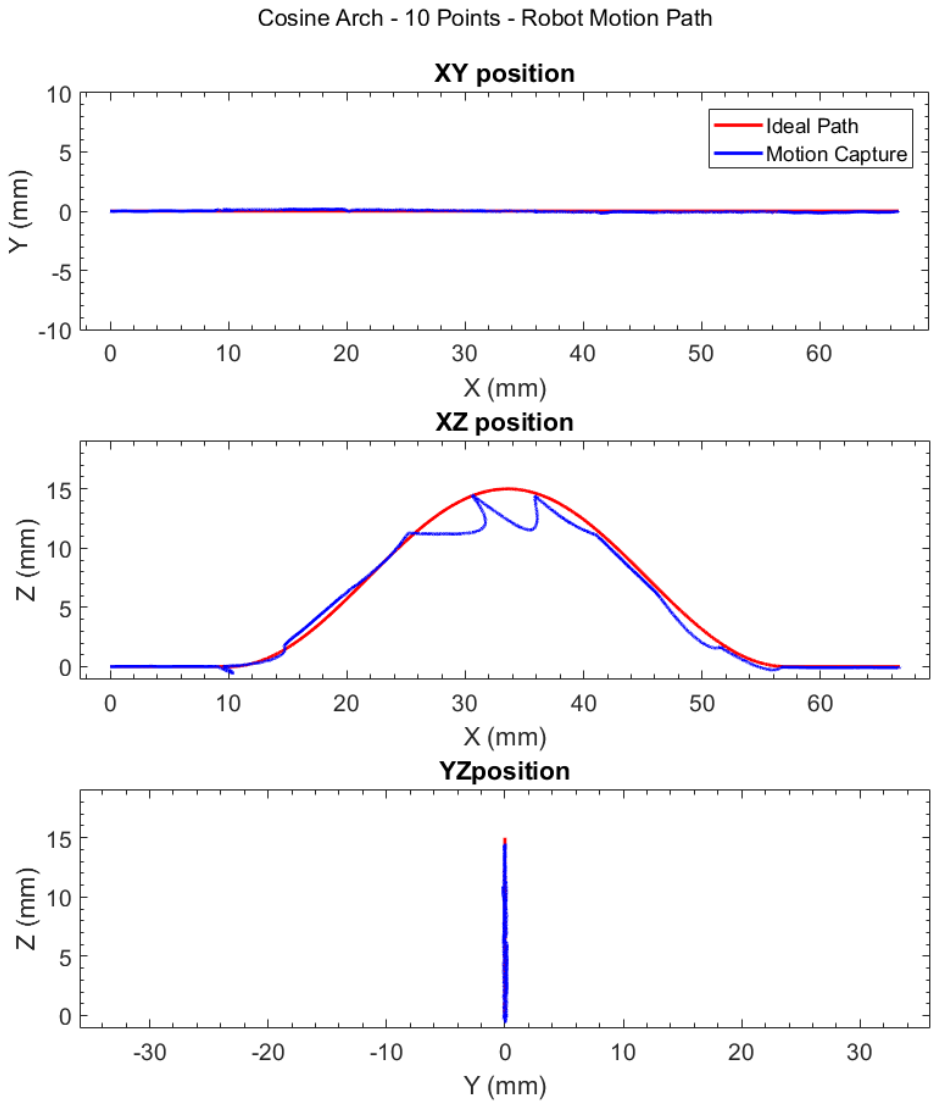

Figure 5.9: (Left) Position of robot arm when moving along a single curved track with varying orientation that was defined by ten gcode commands. Path is plotted from the top, side and front view.

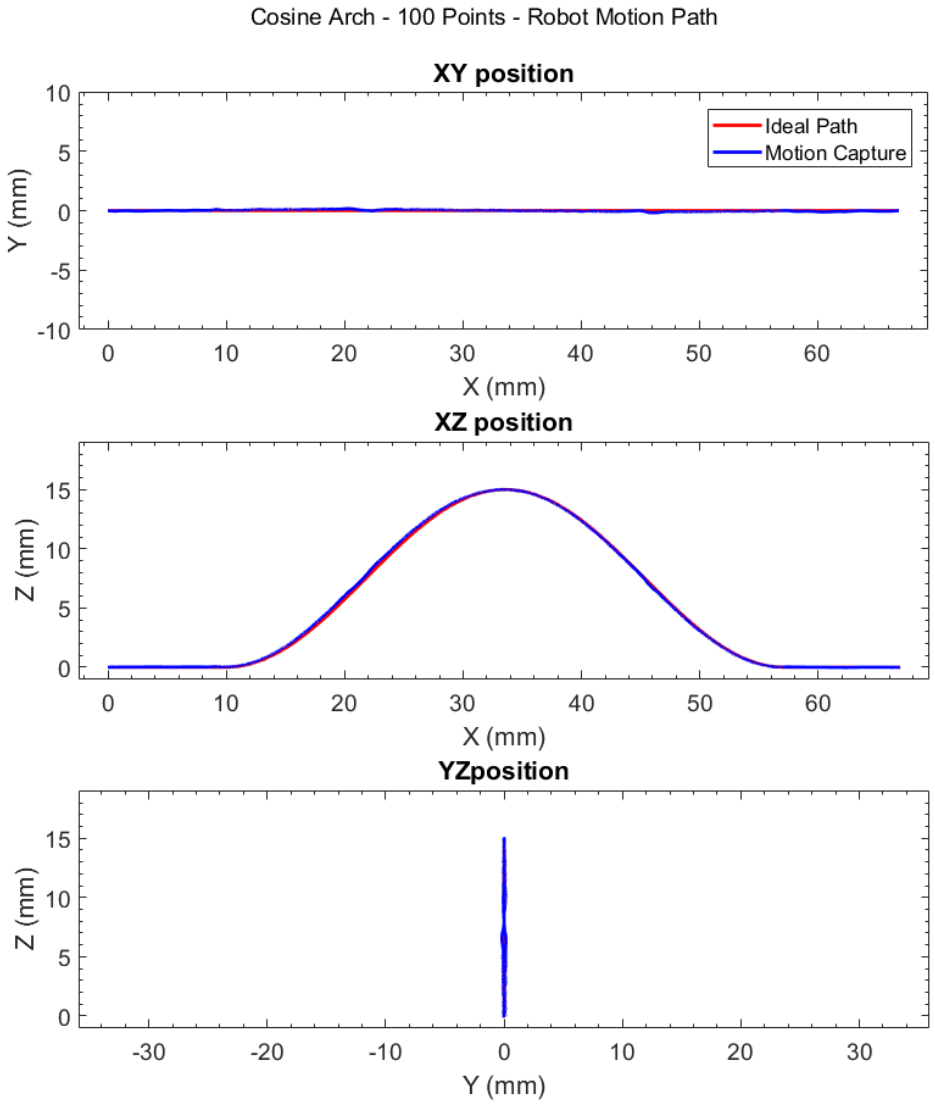

Figure 5.10: Position of robot arm when moving along a single curved track with varying orientation that was defined by one hundred gcode commands. There is little practical difference between these two paths, neither shows significant variation.

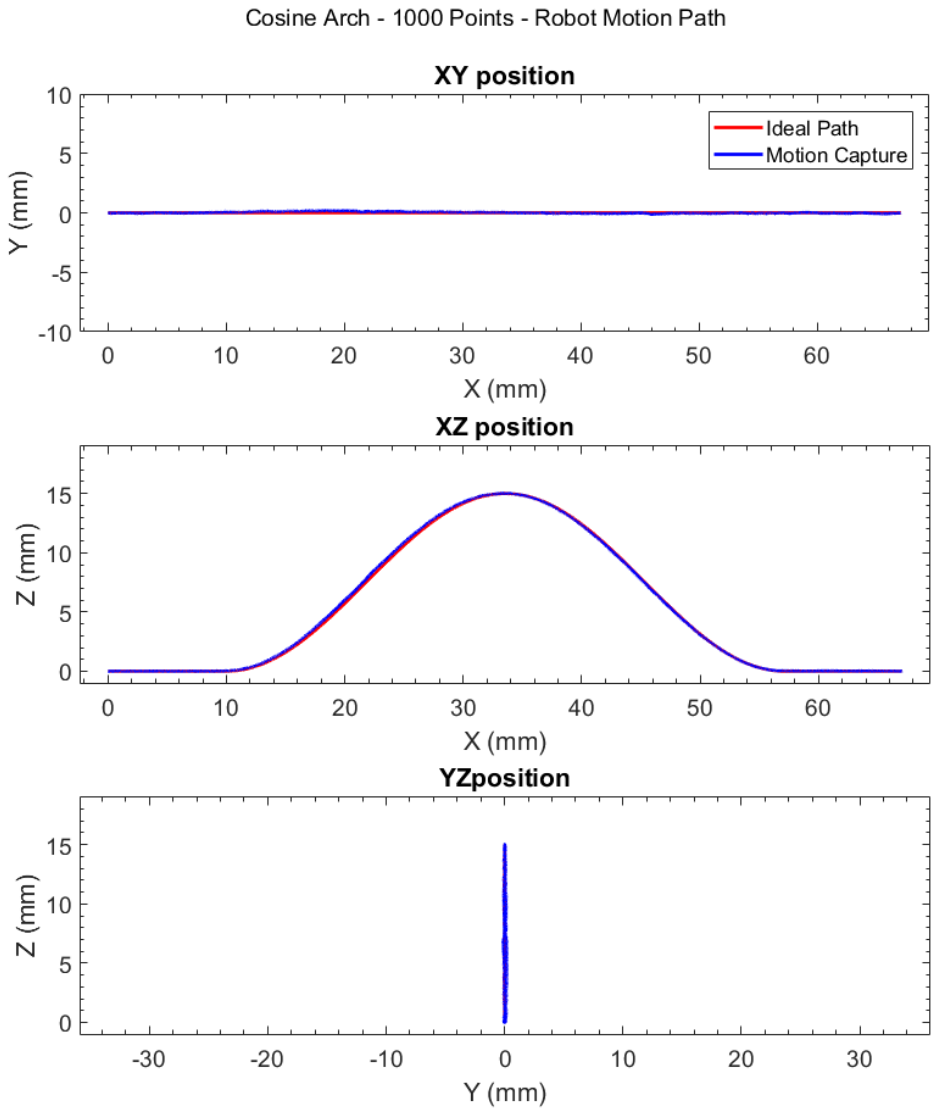

Figure 5.11: Position of robot arm when moving along a single curved track with varying orientation that was defined by one thousand gcode commands. There is little practical difference between the tracked and ideal paths.

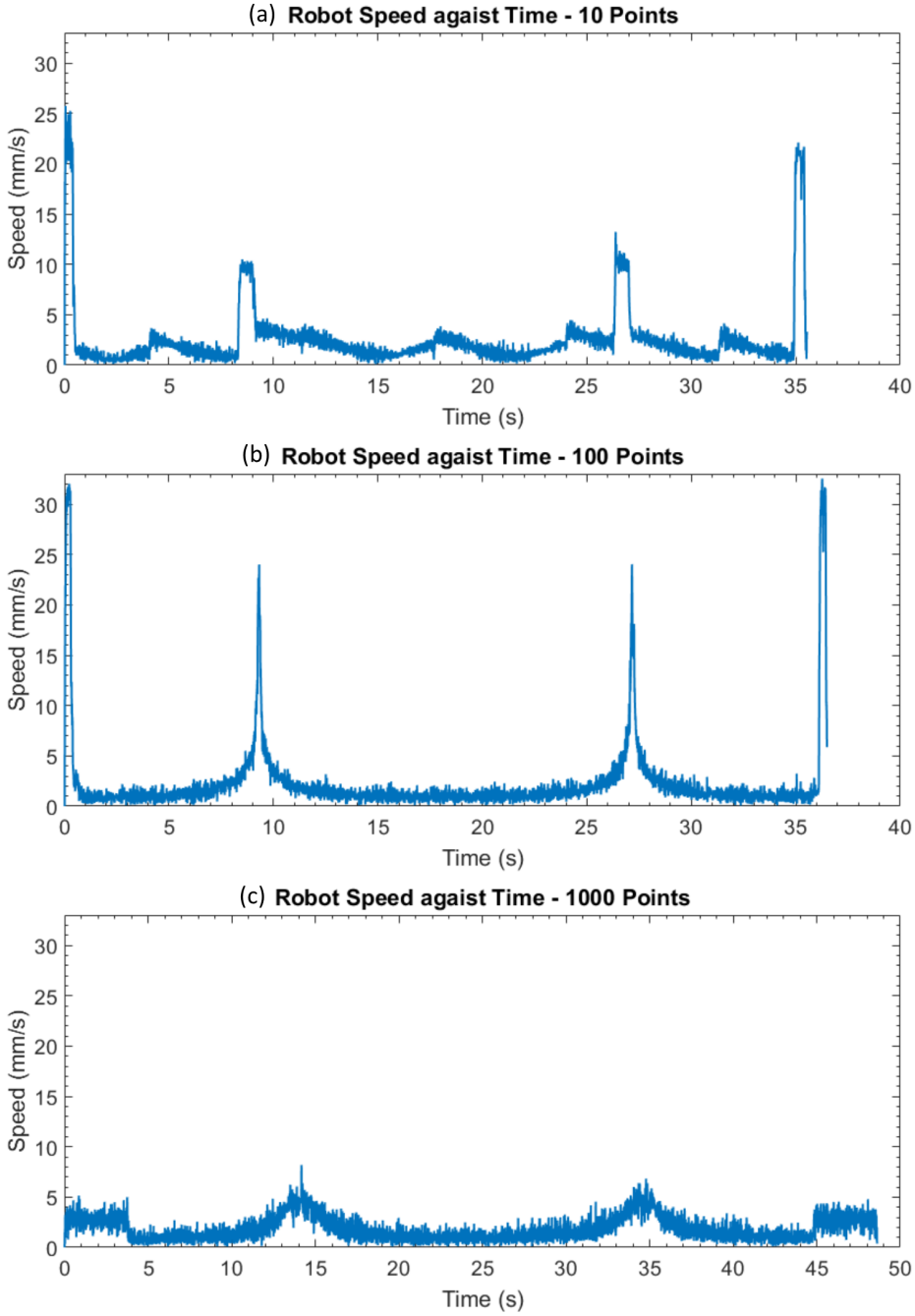

Figure 5.12: Speed of robot arm when moving along a single curved track with varying orientation that was defined by 10, 100 or 1000 gcode commands. (a) 10 point path has large variations and steep changes in speed. (b) 100 point path has a generally smoother motion, apart from the very large spikes, which correspond the the upwards and downwards slopes on the arch. (c) 1000 point path still has these variations, but they are of a much lower magnitude and the speed is more consistent. The higher speeds correspond with parts of the motion when the extruder robot is not having to do large changes in orientation.

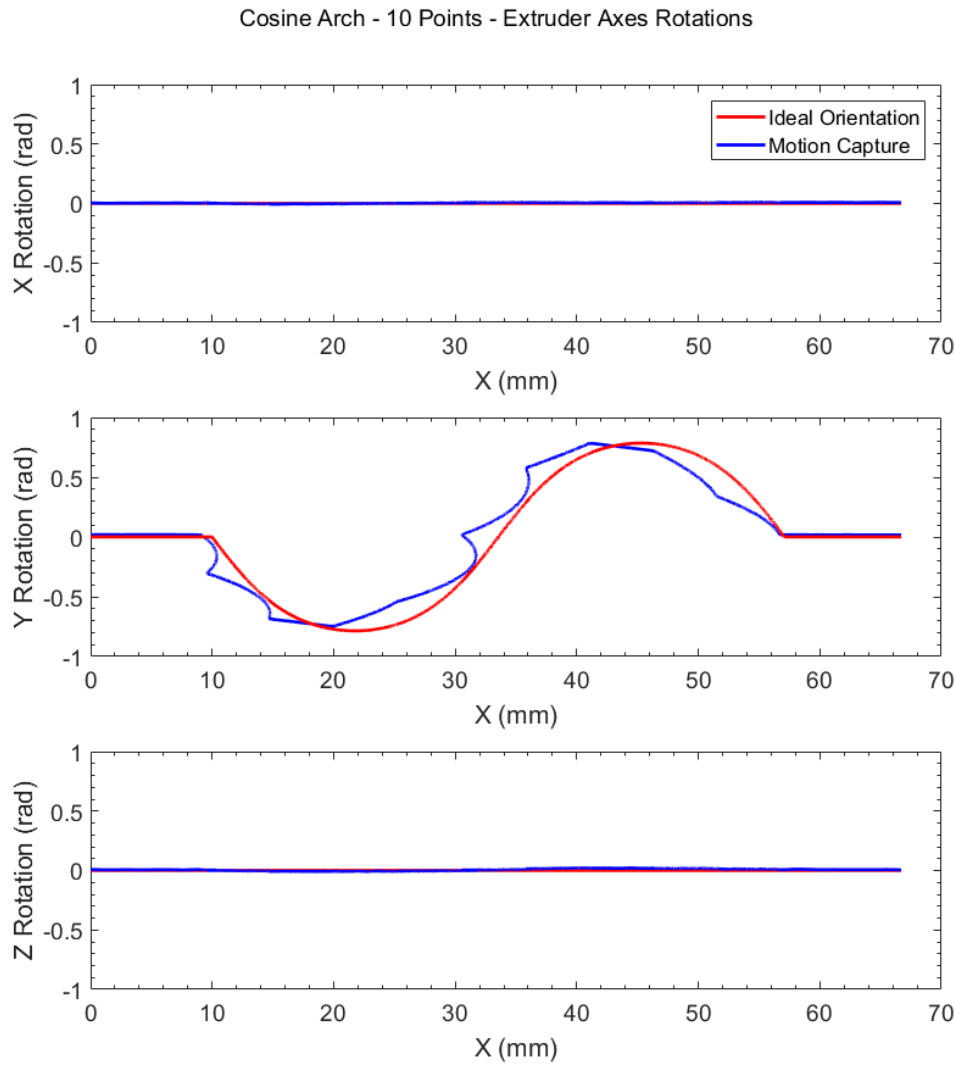

Figure 5.13: Orientation of robot arm when moving normal a single curved track that was defined by ten gcode commands. The robot constrains its rotations to be around the Y axis well, but there is considerable error between each programmed point.

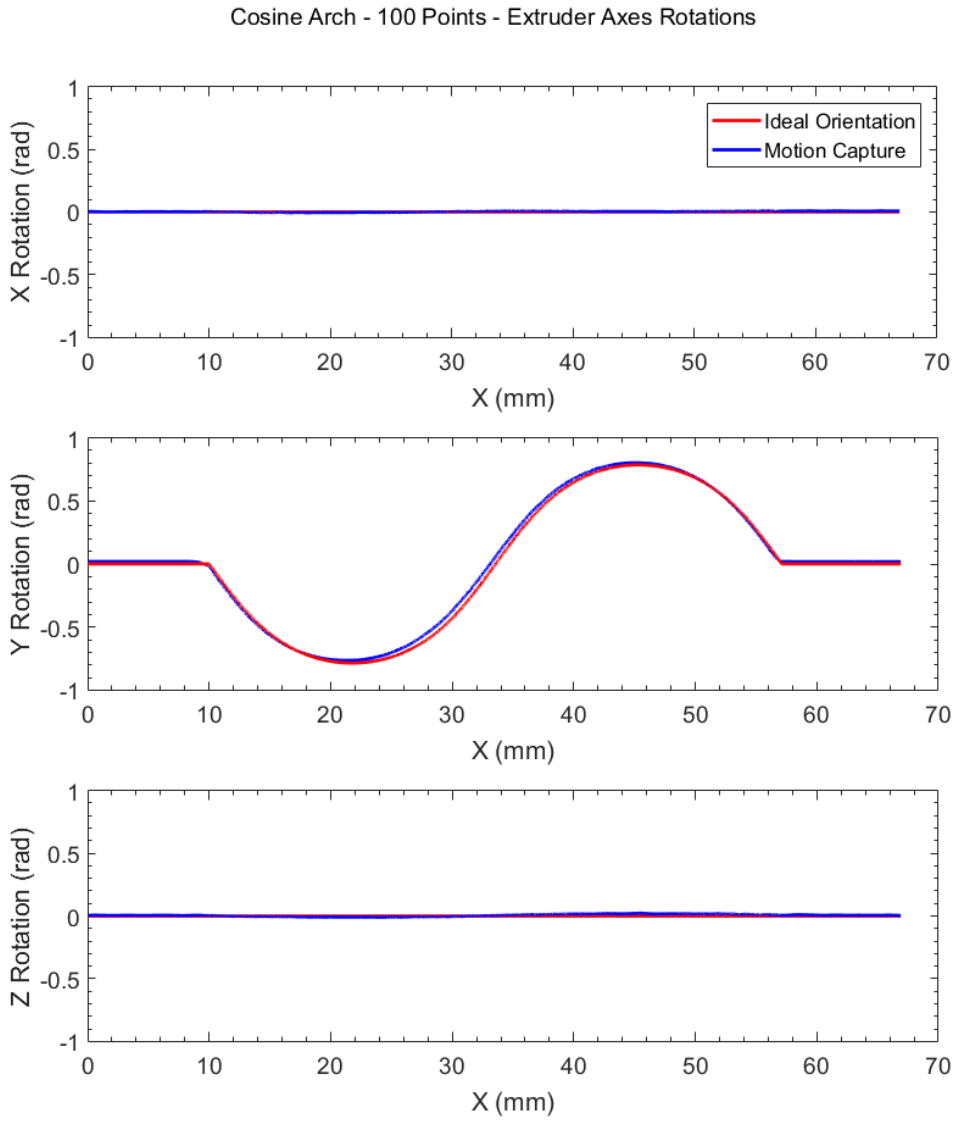

Figure 5.14: Orientation of robot arm when moving normal a single curved track that was defined by one hundred gcode commands. The rotations around the Y axis are much closer with no considerable deviation, although there is a very slight offset between the two traces.

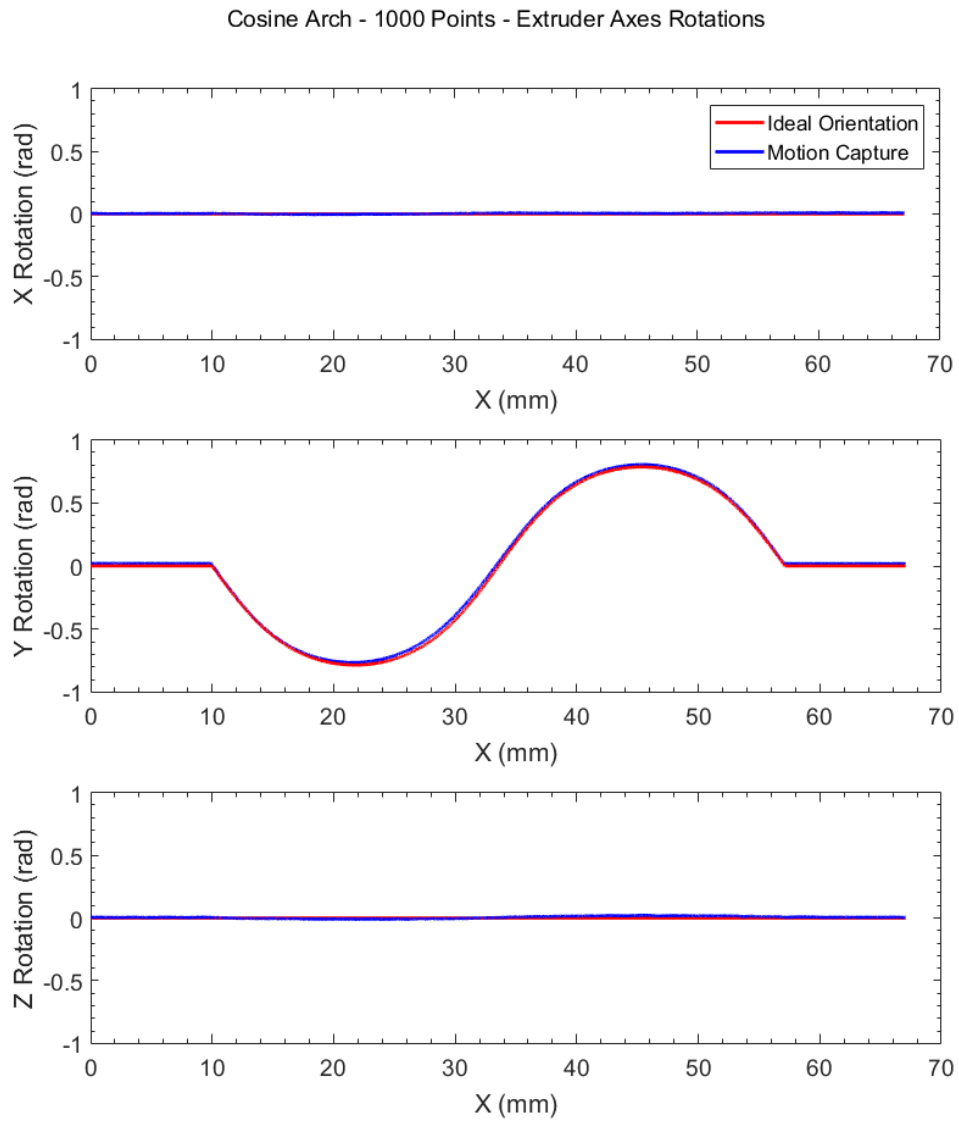

Figure 5.15: Orientation of robot arm when moving normal a single curved track that was defined by one thousand gcode commands. The tracked rotations closely match the programmed ones in all three axes.

5.3.2 Curved Layers

Printing curved layer arches is the first experiment where orientation continuously varies and as such it exposed an issue in the manufacturing of the extruder mount. The mounting holes were created with excessively large tolerances, causing the actual position of the extruder to no longer match the theoretical position in the model used for the kinematics calculations. When the nozzle is vertical this error is in the XY plane and as such only affected prints in previous chapters as a small steady state error. This caused no noticeable effect as the absolute position on the build plate is not important until one is printing upon an existing non-flat object. As the mount was now rotated, the error caused a slight offset in the nozzle path, so one side of the arch would print well but the nozzle would gouge into the support structure on the other. As the layers are only 0.3mm thick, a change of tens of microns can affect the results. The plate which attaches the extruder to the wrist was re-manufactured with tighter tolerances and the length of this was adjusted in the kinematic model.

Following this the arches were printed successfully, Fig. 5.16 shows the process and typical results. A visual inspection shows that the top surface is slightly ridged, as though the plastic is being forced around the sides of the nozzle. The extrusion multiplier was adjusted but there was no apparent difference to the surface so was not pursued further. The planar layer parts printed well, although the lack of cooling meant that the underside of the upright planar arch is rougher than usual. However a support structure was used to ensure that it printed successfully.

These arches were then strength tested as described previously in Section 5.2.2. The data is graphed in Fig. 5.17 and the maximum forces are summarised in Table 5.4. The arches printed on their sides using planar layers can clearly take more load before breaking (mean max. load: 727N). These samples straightened all the way until they were flat before breaking. This happened at either the junctions between the flat foot and curved arch, or just to the side of the centre. These are the points which have the largest bends and therefore are the most fatigued by straightening out. The arch printed in the upright position using planar layers is considerably weaker with a mean maximum load of 117N. All five samples broke in the same position, just to the side of the centre. The bumps in the upwards gradients on the graph (Fig. 5.17) show how the individual layers broke, causing a slight drop in the force applied, as the crack widening increased the length of the sample. The arches printed using curved layers started to

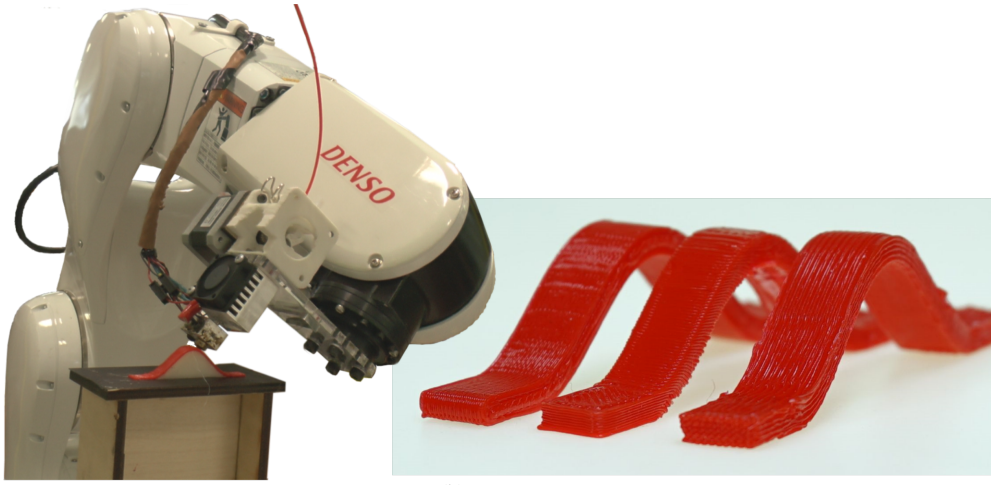

Figure 5.16: (a) Robot arm printing curved layers while keeping the nozzle normal to the surface. Typical samples printed (b) sideways with planar layers, (c) upright with planar layers and (d) upright with curved layers.

straighten in a very similar way to arches printed on their side, but three broke at the joint between the flat foot and the curved section, rather than in the centre. The mean maximum load is 184N, weaker than the arches printed in the sideways orientation, but 57% higher than the arch printed in the same orientation but with planar layers.

While there is clearly a strength improvement between the planar layers and curved layers upright arches, some of the differences in the way they failed can potentially be attributed to the differences in the infill pattern of the layers, rather than the shapes of the layers themselves. The upright planar layer arch was sliced using standard slicing so each layer is outlined twice and is infilled with a rectilinear raster path which alternates at $\pm 45°$ with each layer change. The alternating paths may have caused the arches to be more flexible than the curved layer samples, which is observed as the arches flatten. The curved layers on the other hand are comprised of a raster path which goes backwards and forwards along the whole length of the arch, lining up the tracks with the applied force and potentially imparting some advantage.

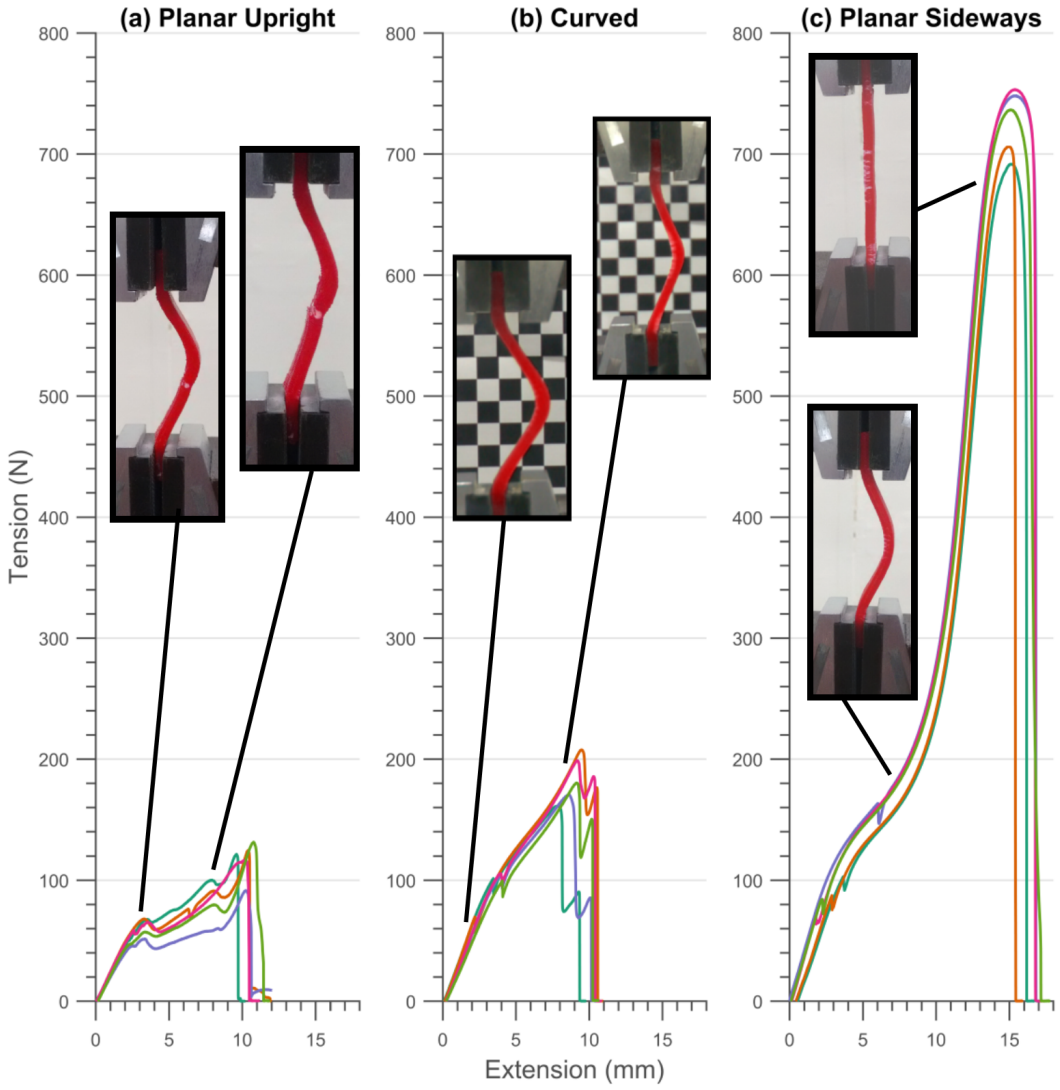

Figure 5.17: Tensile test results: (a) Arches printed upright using planar layers break at a significantly lower force as expected, these samples tend to break to the side of the centre and only partly straighten before a crack propagates from the inside, initially causing a decrease in the force until the additional slack is taken up and the part is in tension again. (b) Curved layers started to straighten out, cracks start at the junction of the foot or in the centre of the arch. (c) Arch printed on its side using planar layers, the arch straightens out fully before failing.

Table 5.4: Maximum loads for samples sets of each type of arch.

Sample No.	Planar Upright	Curved On Smooth Support	Planar Sideways
1	121.36	161.45	691.65
2	124.57	207.65	706.23
3	91.37	170.62	748.21
4	116.38	198.82	753.32
5	131.41	180.32	736.52
Mean	117.02	183.77	727.19
Std. Dev.	15.34	19.23	26.99

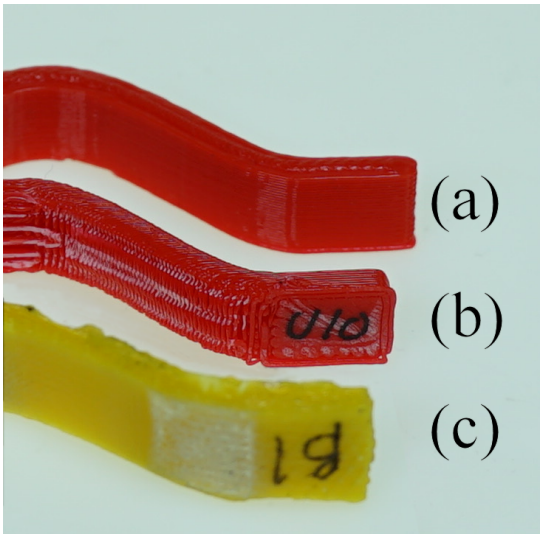

Figure 5.18: The underside of arch samples, (a) Samples printed on its side has a smooth consistent surface, (b) the arch printed upright with planar layers has a stepped surface with white marks where the support structure was removed, (c) The curved layer arch printed upon a smooth support structure has a smooth underside with some white marks where the support surface was peeled off.

5.4 Discussion and Conclusions

The ridged surface on the curved layer arches could be caused by excessive amount of plastic being extruded, such that it builds up enough to get pushed to the sides of the nozzle. The extrusion values are calculated via a theoretical cross section but the

use of Z offsetting causes the spacing between the layers to be inconsistent, the layers are closer together on the down-slopes of the arch - see Fig. 5.7 (b). It is likely that as this small decrease in layer height is not compensated for too much plastic is being extruded in these sections, which then gets dragged along the surface via the outside of the hot nozzle. The orientation changes also caused the nozzle to move slower than the set speed so it is feasible that a small amount of excess plastic was oozing out due to the back pressure.

The mean maximum load for the curved layer arches is 157% of the planar layered ones. This demonstrates that the curved layers can help parts to resist greater forces but there are caveats to their manufacturing, such as the need to introduce as few defects to the surface as possible. Solid curved structures with steep sides have not been reported previously in the literature and therefore this is an important result, it proves the concept of printing multiple curved layers while keeping the nozzle normal to the surface and suggests that significant improvements could be gained through their use. Previously curved arches printed with a 3 axis machine were shown to be 141% stronger under a 3 point compressive load [112], so while these results are not directly comparable, they in agreement.

While the curved arches are now much stronger than planar ones, they fall short of the loads required to break the arch printed upon its side. This arch was sliced using the conventional software so the tool paths are different from the curved arches so this will have some effect. The two most important factors that affect the mechanical properties of an FFF part are its build orientation and the infill paths [7]. The infill tracks are printed at $\pm 45°$ in alternate layers which could cause the arch to be more ductile, allowing it to straighten fully before breaking. These arches also printed quicker than the curved arches as the robot arm needed to move its linkages less to reposition the nozzle between each point. This could mean that the previous layers had not cooled completely before an new layer was printed over it, potentially improving the interlayer bonds. The curved arches printed on the smooth support stretch and flatten out partially, but still break before being fully flat. All of the five samples broke at the junction between one of the feet and the curve, rather than in the middle. At this point there is a visible defect which is caused by the robot arm moving at different speeds. While the speed of the robot is set at a constant value the cumulative speed of the end effector is not constant as seen by the motion tracking results. This change in

speed causes a defect in the print as the extrusion rate acceleration is not matched to that of the robot arm. This indicates that the curved layers could resist a higher force, potentially approaching that of the sideways samples, if this effect was removed. The shape of the graph also matches that of the sideways printed arch up until the curved one peaks. Using a sample that resembled the standard dogbone shape, but with a curve in the central section would help to ensure the break occurred in the curved layer section, if this test was to be repeated.

In the future a comprehensive study of the effects of curved layers on a range of mechanical characteristics should be undertaken. While there are applications where a part would be printed onto a support and then removed, as in this experiment, an interesting and useful application would be to reinforce FFF parts. An object could be printed using planar layers, both in the Z axis and with dynamic build orientations, and then conformal layers could be printed over this to minimise the isotopic effects of layers. Nonplanar layers also have the potential to improve the surface finish of parts. Steps are more prominent on shallow curves so it may be that this application is predominantly achieved using 3-axis machines, but there are likely to be applications where the layers should be oriented in one direction due to strength considerations but the surface texture should be at a different angle to this. The ability to print onto conformal surface also allows for the augmentation or repair of existing items which opens up a new application area for AM.

Chapter 6

MAAM Mechatronic Demonstrator

6.1 Introduction

Mobile robots have the potential to make a huge impact in many important areas of society. They can spare us from doing dull, dirty or dangerous work, increase productivity, and are an enabling technology for innovation in healthcare, construction and manufacturing [224]. Currently, however, the full adoption of robotic technology has not occurred in many sectors. The economics of mass manufacturing is one reason for this. To produce a robotic platform that is affordable it must be manufactured in large numbers and therefore in a general purpose design, in an attempt to capture a large sales market. These general purpose designs are not optimised for any specific task and are still expensive. This is partly due to the need to be general purpose, but also because the volumes are still relatively low. Bespoke, highly specialised robots that have been designed for an individual task would be much more effective. For example, the locomotion system would be specific to its environment, only the required sensors would be incorporated and the functionalities could be tailored as required.

Additive Manufacturing (AM) is well suited to producing bespoke robots as it produces parts directly from digital models, giving inherent flexibility to alter the design

from one print to the next. AM has a flat cost structure when compared to template based methods[1], so is economical for one off or small production runs [8, 9]. It can produce the complex shapes often required for robotic mechanisms and the additive method of building allows access to the internal geometry. Previously this has allowed components to be inserted during the build process and then be completely encase by continuing to deposit material on top. This is known as embedding. By removing the need for fastenings and other methods of assembly, it provides increased robustness and increased simplicity for manufacture. Novel robots and mechanisms have been created using this (for example [14, 46]), but the main embedding technique is limited and requires a sequence of manual actions.

Chapters 4 and 5 investigated how multiaxis additive manufacturing (MAAM) can increase the strength of parts and print overhangs without requiring supports. Another advantage of MAAM is the ability to deposit material onto and around complex existing structures or objects. Within this chapter, the use of MAAM to automatically embed objects within a printed structure is investigated. It is envisaged that this process could become an enabler in new integrated manufacturing and assembly methods.

6.2 Embedding

The assembly process for small, complex robots with many components can be a time consuming and skilled procedure, increasing manufacturing costs. When incorporating components inside a device using traditional manufacturing methods, the device enclosure must be split into two or more sections and the parts assembled and secured together. By reducing the number of sections, removing the need for many fastenings and automating the insertion of components, these costs and complexities could be eliminated.

Section 2.3.3 established that embedding components during AM is an effective way of incorporating functional components, materials and mechanisms. Embedding components during AM has been demonstrated in previous work but there are major limitations to the existing methods.

Figure 6.1 shows the procedure for embedding a component with vertical sides and a horizontal top. This is readily achievable with a standard 3 axis FFF machine and

[1] e.g. Injection moulding, casting or punching which all require the high initial cost of tooling to be offset against a large volume of products.

some manual intervention. A cavity, as deep as the component, is formed as the main part is being 3D printed. Once the extruder reaches the top of the cavity, the print process is paused and the component can be manually inserted. As long as the top of the component is flush with the top layer being printed, the printing process can be resumed and the next layer will be deposited over the component, embedding it. A practical example of this is to embed a nut. This provides strong, precise threads, which are difficult to 3D print using FFF.

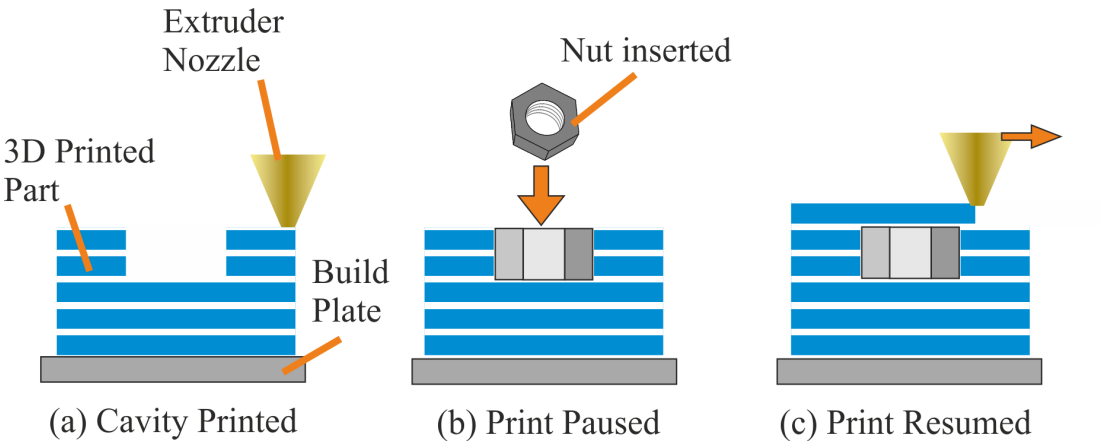

Figure 6.1: Procedure for embedding simple components (with vertical sides and a horizontal top) using a conventional 3D printer. (a) Print the part, leaving a cavity for the component to fit in. (b) Once the height of the cavity is the same as the height of the insert, pause the printer and manually insert the component. (c) Resume the print. The next layer will enclose the component in the cavity.

More complex components are incompatible with the simple embedding procedure and required modifications to either the tool path of the AM machine or modification to the shape of the item being embedded. To embed an item in an unmodified 3 axis AM machine, the component must not protrude above the current top layer or the nozzle with collide with it (Fig. 6.2 (a,i)). For components with a convex top surface, the cavity will be enclosed when the current layer being printed is level with the height of the component (Fig. 6.2 (a,ii)). Therefore all components must be modified to have vertical side walls, so they can be pushed down into a cavity, and a horizontal top so that the nozzle can print over it without obstruction. The geometry is modified by creating Shape Converters [4, 104]. These are additional parts which must be manufactured to tessellate with the component to be inserted, and simplify the outer

geometry. Figure 6.2 (a,iii) and (b) show single and multi-part examples of Shape Converters enabling embedding. A procedure for designing these has been developed [104], but the embedding procedure takes a number of manual steps and requires extra parts to be designed and manufactured.

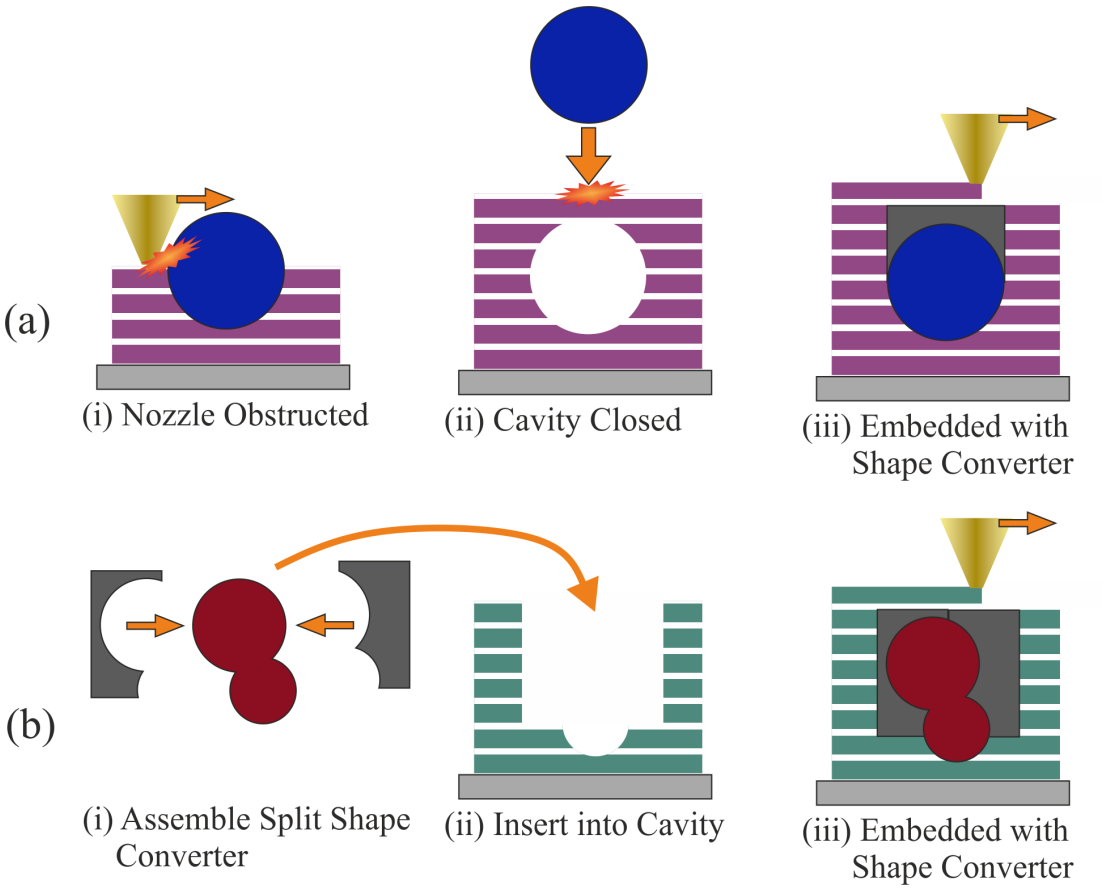

Figure 6.2: Cutaway side views of embedding during FFF. (a) A component with a convex top surface cannot be embedded without modification to the cavity, (i) as it will protrude from the top of the printed part if inserted when the cavity is wide enough. (ii) If the layers are built up enough to stop the collision, the cavity will have narrowed and closed, preventing insertion. (iii) To embed this shape, the cavity is created with vertical sides and a Shape Converter (grey) is used to fill in the void that is left. (b, i) More complex shapes with undercuts require multi-part Shape Converters so that they can be assembled around the component. (ii) These convert the outer shape to vertical sides so that it can be inserted downwards into the cavity and (iii) has a horizontal top so that printing can continue.

Rather than modifying the component, the tool path could be could be modified to

stop the nozzle colliding. This is a viable option for objects with shallow, convex top surfaces, as shown in Fig. 6.3 (a). The layers could be built up around the protruding object and the nozzle could be kept from moving across this space by modifying the gcode generation. However, this approach is very limited in terms of the components it could be used with. For more complex shapes, e.g. with undercuts or steep sides, the nozzle would not be able to reach many areas, so the item could not be fully encapsulated. Figure 6.3 (b) and (c) show two examples of the nozzle being physically unable to fill certain sections.

A multiaxis system, however, could embed components without the use of shape converters. It can change the orientation of the nozzle, allowing it to reach areas which are blocked when using 3 axis motion. Examples of potential tool paths are in Fig. 6.3 (d-f).

The conventional bottom up, planar layer approach to AM makes inserting and embedding with complex 3D shapes difficult. The existing methods are not only manual but require a cavity to be 3D printed, and the component is then inserted. Partial embedding, or printing onto a section of the component is not viable. With multiaxis deposition, existing items could not only be fully embedded, but also partially printed upon to augmented it with additively manufactured features. This could be used for mass customisation, a base part could be mass manufactured and then adjusted to suit an individual, using MAAM. This might be especially applicable to creating bespoke assistive devices for people with disabilities or for individualised items such as shoes. In a similar way, MAAM could be used for additive repair of many items. In the future, a mug with broken handle could have a new one directly printed onto it, in ceramic material. The refacing of a worn oil drill has been demonstrated with a metal multiaxis system [134].

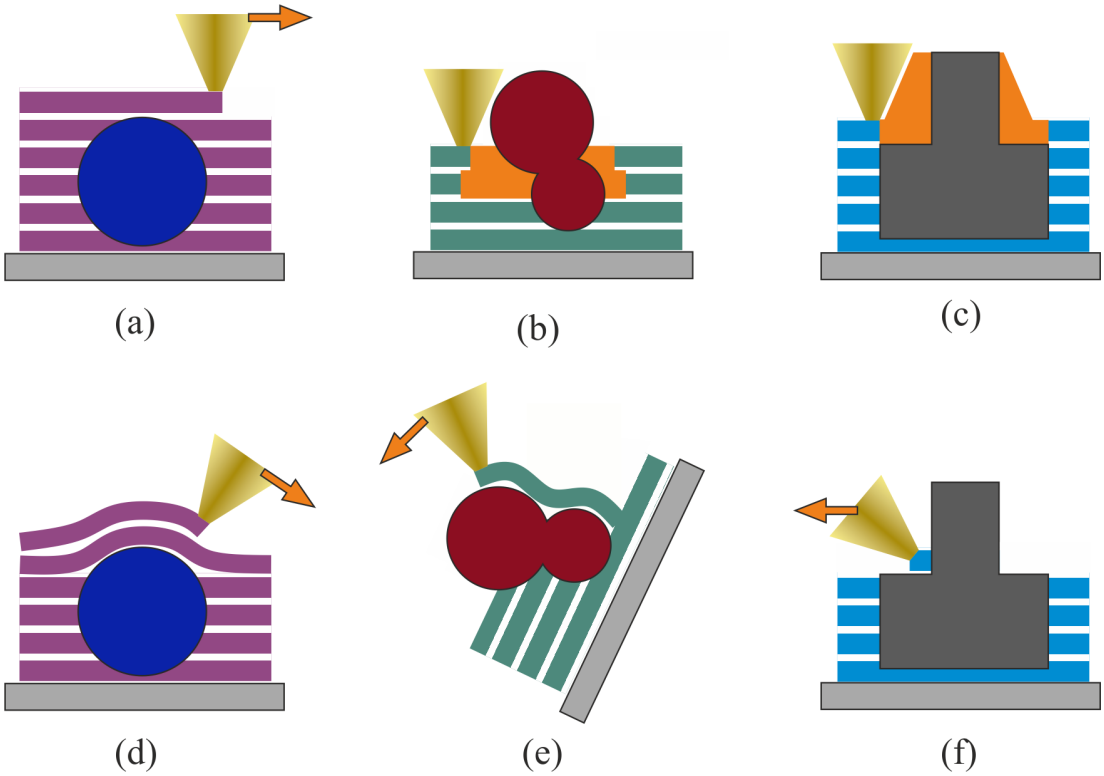

Figure 6.3: Cutaway side views of embedding during FFF, without Shape Converters. (a) Some simple shapes could be printed directly over, as long as the tool paths were modified so that the nozzle lifted up when travelling over the insert, or avoided that area. For more complex shapes with (b) undercuts or (c) steep sides and sharp corners, the tip of the nozzle cannot reach all of the areas required to securely embed the component (Areas the tip cannot reach are shaded orange). Multiaxis toolpaths could be used to (d) print conformally over curved surfaces. (e) The orientation of both the plate and nozzle can be changed using ARMS, so difficult areas can be accessed. (f) By angling the nozzle, plastic can be deposited into corners and against steep surfaces.

6.3 Extruder Requirements

To enable embedding and printing onto existing objects, the specification for the extruder was updated. Many sensors and actuators have regular shaped packages, such as boxes or cylinders. So for this initial work the requirements were set to enable these basic prisms to be embedded. In the future it may be a requirement of the system to print into acute angles and undercut shapes, and it is anticipated at minimal changes would be required, but the fundamental tests will not consider this scenario. In ad-

dition, embedding is likely to require the use of complex toolpaths with the nozzle in close proximity to other objects, therefore any complexity in path planning should be minimised by simplifying the extruder's shape. From these considerations it was decided that as a minimum, the ARMS extruder must;

- Be able to print against vertical walls,
- Be able to reach into $\leq 90°$ internal corners,
- Not be directional, i.e. is radially symmetrical around the nozzle's central axis.

The original extruder, introduced in Section 3.4.1, does not fulfil this specification. The nozzle could be angled to print against vertical walls, but it cannot print into 90° corners: Figure 6.4 shows the extruder printing nonplanar layers, as detailed in Chapter 5. The profile of this arch is close to the limit of the smallest angle that this extruder could print into. The angle formed by one side of the arch is obtuse (marked in green on Fig. 6.4 (a)). At its smallest, this angle is 135° and the transition from the horizontal section is smooth and gradual, as seen in Fig. 6.4 (b). The corner angle is limited because the extruder utilises heater cartridges, clamped in metal blocks just above the nozzle, to melt the plastic feedstock. These blocks would begin to contact the surfaces which formed the corner if the angle was smaller. These are marked in Fig. 6.4 (c).

Consideration must be given to the direction in which extruder is moving due to the following aspects of the design: The metal heater blocks are wider than they are deep, so the maximum tilt angle is dependant upon the axis the nozzle is rotated around. Also the feeder mechanism and motors can collide with the last link of the extruder robot arm because the whole extruder mechanism is offset sideways from the wrist of the robot. As an example of this Figure 6.5 shows that the top of the extruder gets very close to the side of the extruder robot arm when printing the curved layer arch.

To overcome the issues described and to fulfil the specification for embedding, a new extruder design was used. To remove the possibility of the extruder feed mechanism (know as the 'Cold End' of the extruder - see Section 3.4.1) colliding with the extruder robot, it was moved from on top of the Hot End and mounted on the second link of the extruder robot arm. The filament is now fed through a bowden tube which connects the feeder to the Hot End of the extruder. This is shown in Fig. 6.6 (a). The Cold End works in exactly the same way as the first extruder design. A lever arm

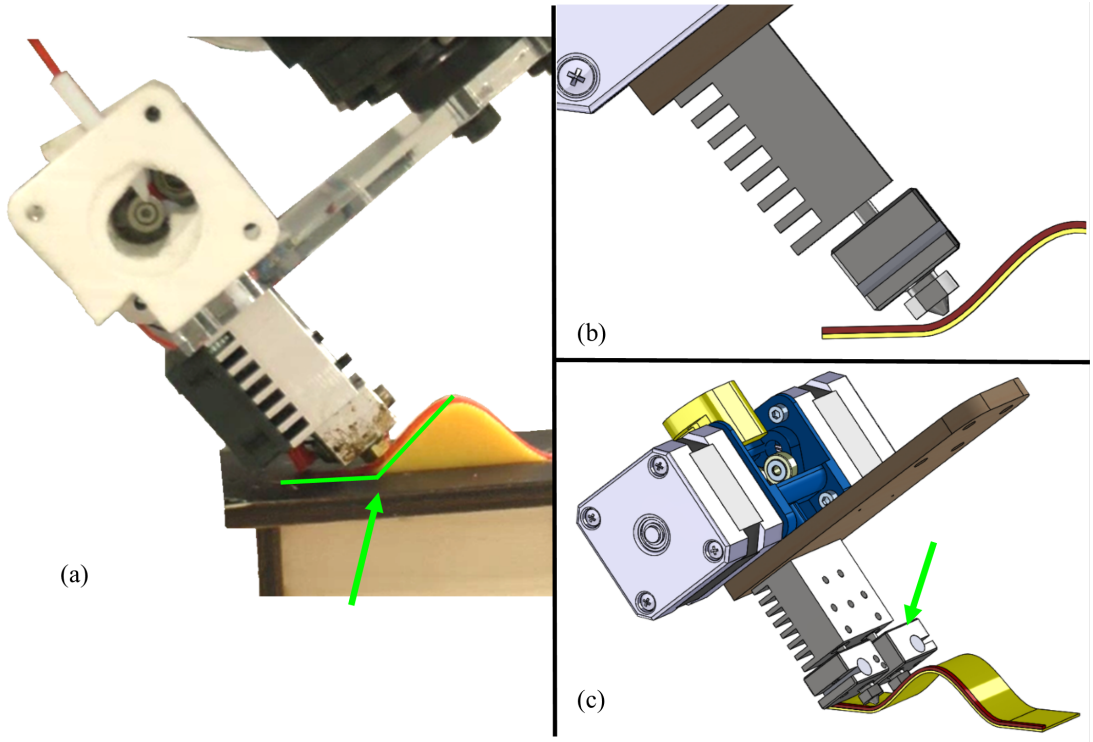

Figure 6.4: When printing nonplanar layers using the original extruder, only wide angled corners could be achieved without the heater block contacting the surfaces. (a) Minimum corner angle formed by the arch is marked in green. The heater wire is just touching the surface and the side of the nozzle and heater block would come into contact with the plastic if the angle was smaller. (b) Side view of the nozzle and arch so the tilt limits can be seen more clearly. The gradual change in angle allowed the arches to be printed successfully. (c) A Heater block is marked with the green arrow. It is wider than it is deep so the nozzle cannot be tilted the same amount in all directions. When two nozzles are being used on the extruder they also limit the directions in which the extruder can be tilted.

pinches the filament against a toothed gear which rotates to push the filament along the bowden tube and into the Hot End. A close up of this is in Fig. 6.6 (b). Separating the two sections also allowed the nozzle to be mounted co-axially to the robot's wrist, simplifying the kinematic model and also stopping the robot's wrist from going below the level of the build plate in normal operation (as was seen in Fig. 6.5).

The problem with the previous Hot End was that the heater and attachment block were large when compared to the diameter of the nozzle. In the new design a flexible heating element is wrapped around the nozzle, removing the need for these components,

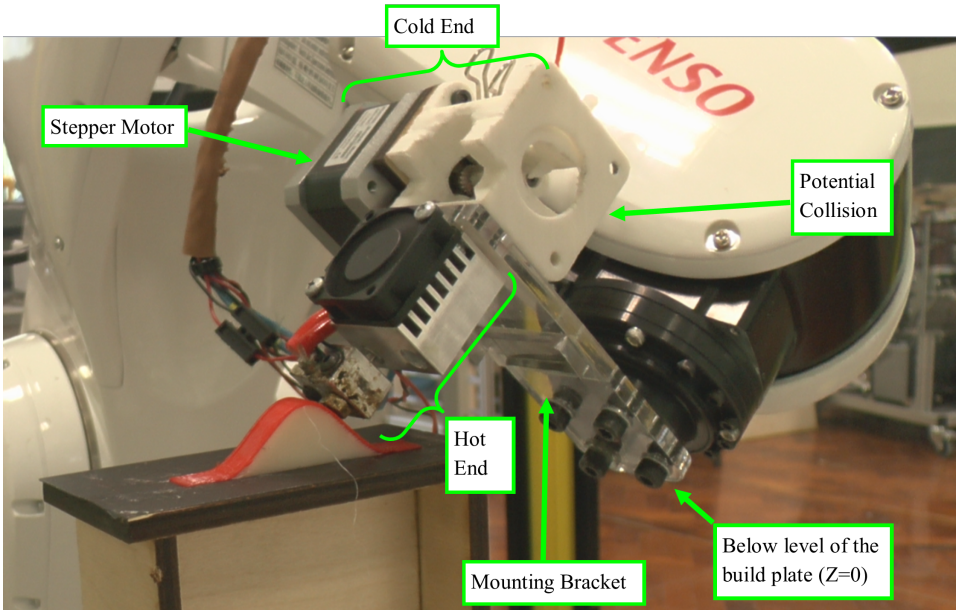

Figure 6.5: In some poses the stepper motor can collide with the robot arm, and the offset causes the wrist of the robot can go below the level of the extruder. The robot is close to such a position here, although no collision occurred as the base plate was angled carefully to avoid this. Both the feeder mechanism and hot end of the extruder are mounted on the wrist of the arm. The mechanism and stepper motor (known as the Cold End) are above the acrylic mounting plate and the metal hot end is below. The arches were printed on a small base plate, shown here, so that the wrist would not touch it when printing the curves.

and making the tip of the extruder narrow enough to easily reach into a right angled corner. Figure 6.6 details the components that make up the Hot End, and Fig. 6.7 shows a close up of this in a 90° corner. The components for this new extruder are from an inexpensive desktop 3D printer (CoLiDo D1315). For this prototype the original mounting bracket (marked in Fig. 6.7 (b)) was used to attach the Hot End to the wrist of the robot arm, using three metal standoffs and a laser cut acrylic bracket. The original bracket did not interfere with printing in the following experiments, but in the future the diameter of this could be reduced to allow experimenting with printing in more confined spaces.

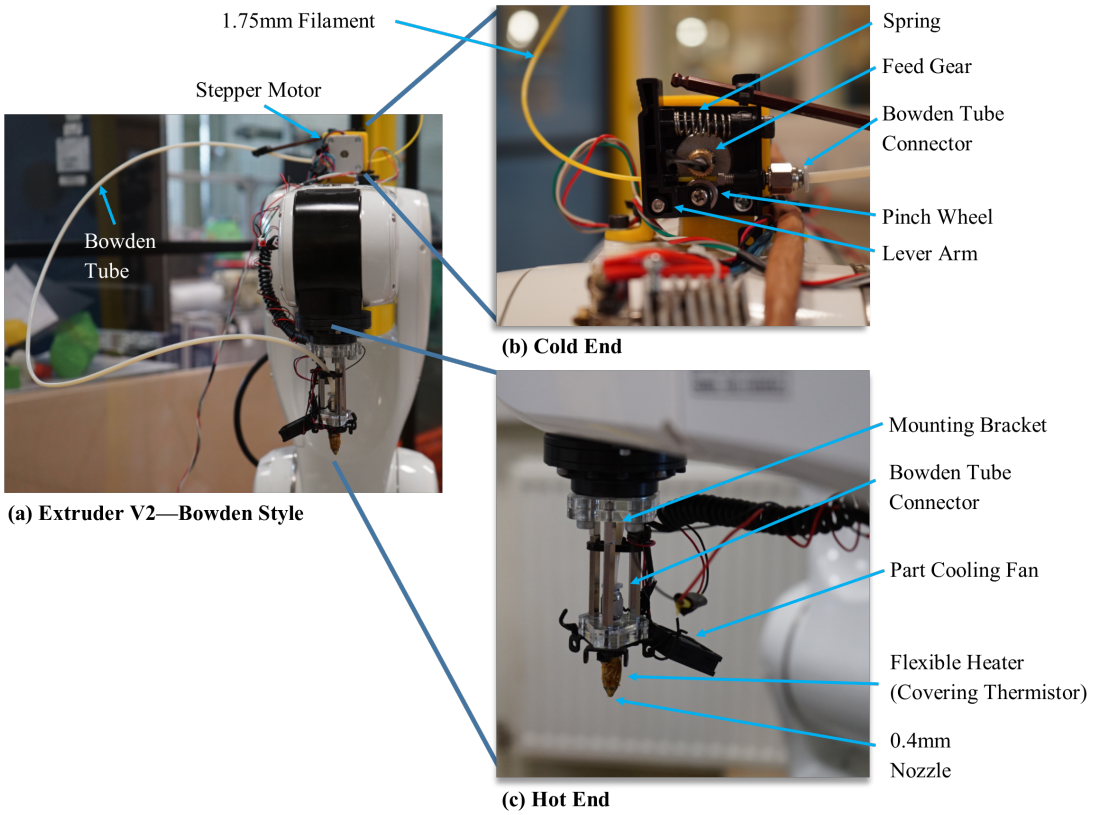

Figure 6.6: (a) The second extruder was chosen to minimise bulk around the nozzle allowing more freedom when printing onto or around objects. The drive mechanism (b) is separated and mounted on top of the robot, filament is pushed along a tube to the hot end (c) which is mounted coaxially to the robot's wrist and uses a flexible heating element wrapped around the nozzle, removing the need for a large heater block and cartridge.

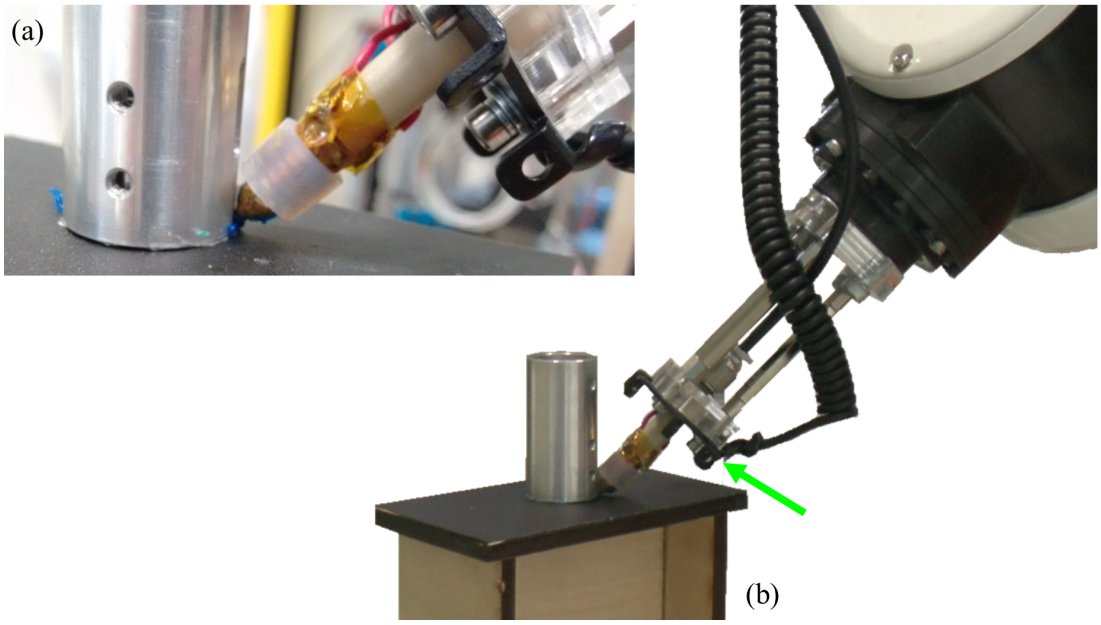

Figure 6.7: (a) Close up view of the narrow nozzle design reaching into an 90° corner. The flexible heater is wrapped around the nozzle, seen here covered in yellow Kapton tape and a silicone sleeve. (b) The nozzle and hot end assembly are both long enough to keep the bulky end of the robot away from the object being printed around. The original mounting bracket from the desktop printer is marked with the green arrow.

6.4 Method

In this chapter a demonstrator is printed to show how the Additive Robot Manufacturing System (ARMS) can combine MAAM methods to embed a functional component and print large overhangs with no support structures by dynamically changing the build axis. A model plane with an embedded DC motor was chosen for this. There are four main sections to this plane; the nose with embedded motor, the fuselage, the left wing, and the right wing. The methods used to prepare and print each part will be explained in turn below.

6.4.1 Embedding a cylindrical motor

A typical, low cost 3V DC motor was used for this application. It is a common component, and with a diameter of 24mm it was a suitable size both for printing around, and the size of the final plane. To print around the motor it was first attached to the end of the build plate robot. The propeller was secured to the motor shaft with a simple interference fit and then a jig was used to clamp this down in such a way as to be easy to remove once the plane had been printed. The propeller is clamped down by laser cut acrylic plates which can be seen in Fig. 6.8. Between the propeller and the motor, a split plate is used so that it can be removed from around the motor shaft without having to take off the propeller. To stop the motor freely rotating two bolts are screwed upwards through the top plates and into the motor housing. Holes in the bottom plate allow for easy access when assembling.

To embed the cylindrical motor, a thin wall of plastic must be deposited around it. Planar layers, stacked vertically, are used. Figure 6.9 shows this schematically. Even when using the narrow nozzle, the orientation of the nozzle must be dynamically altered as each ring is printed so that they are in contact with both the side of the motor and the previous layer. Figure 6.3 (c) and (f) shows the difference that tilting the nozzle away from vertical has on the areas that it can print into. Figure 6.7 shows this on the physical system; the angle stops the bracket, marked with the green arrow, from interfering with the cylinder or the base plate. 45° is used in this case as it keeps the extruder in the centre of the 90° corner, but this could be changed depending upon the geometry of the extruder or the component being printed around.

As the nozzle prints the circle of plastic in Fig. 6.9, it must simultaneously remain pointed towards the centre of the circle and be angled 45° from vertical. To do this

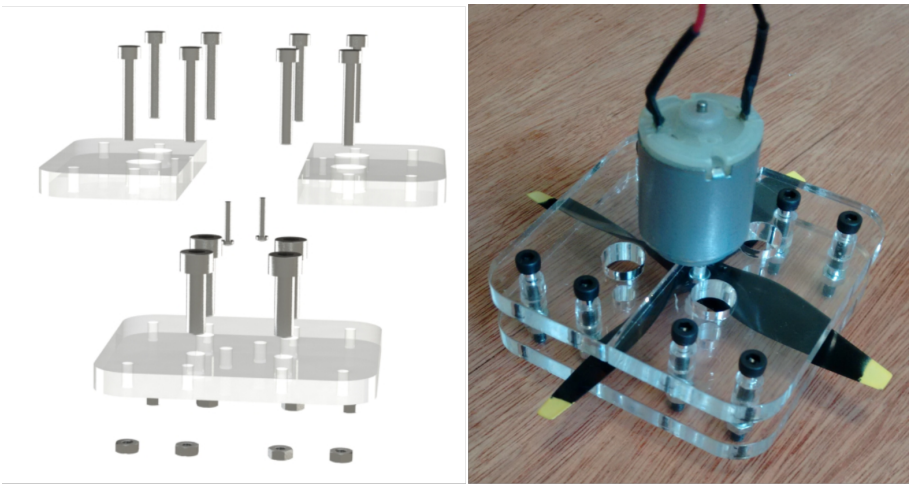

Figure 6.8: (a) Exploded view of CAD model of the jig to attach the motor and propeller to the robot arm. The bottom plate screws to the wrist of the robot, the top two plates go around the motor shaft and clamps down on the propeller. Two small screws go upwards through the top plates into the motor housing and prevent it from rotating. (b) A photograph of the assembled jig, this can then be attached to the robot's wrist with four bolts through the bottom plate.

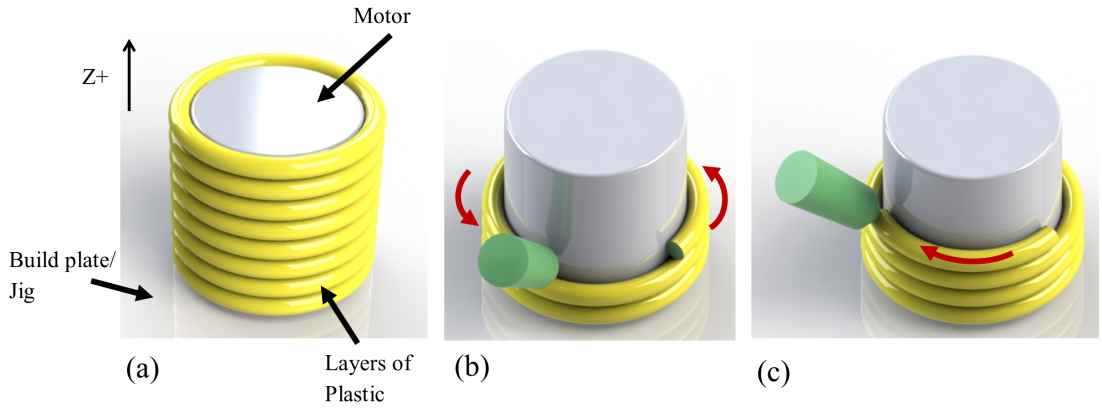

Figure 6.9: Schematic showing layers of plastic enclosing a cylindrical DC motor. (a) The layers are planar and are stacked in the vertical, Z+, direction. (b) The direction of each layer must be reversed as the robot cannot physically continuously rotate the extruder in one direction. The third layer is printed anticlockwise. When this layer is complete the nozzle moves up and (c) the fourth layer is printed clockwise.

requires the nozzle rotations around each axis to vary dynamically as shown in Fig. 6.10. The direction of the Z rotations has the be reversed for each layer. This is because the robot cannot continuously rotate its wrist joint, and also the wires and filament going into the extruder would tangle if the extruder continuously rotated around Z in one direction. Figure 6.9 shows a schematic of the extruder printing sequential layers in alternate directions. As conventional slicing software cannot generate this kind of complex motion in gcode, a custom script was developed (Matlab). The motor being embedded has steps in the housing (seen in Fig. 6.11 (a)) which mean that the cylinder can begin narrow and print under the edge of the motor, locking it in place within the plane. The diameter of the tool path widens so that the plastic fits tightly around the motor, then flares out further to match the front of the fuselage. The top is slightly elliptical to align closely with the end of the fuselage. A computer preview of the gocde path is in Fig. 6.11 (b).

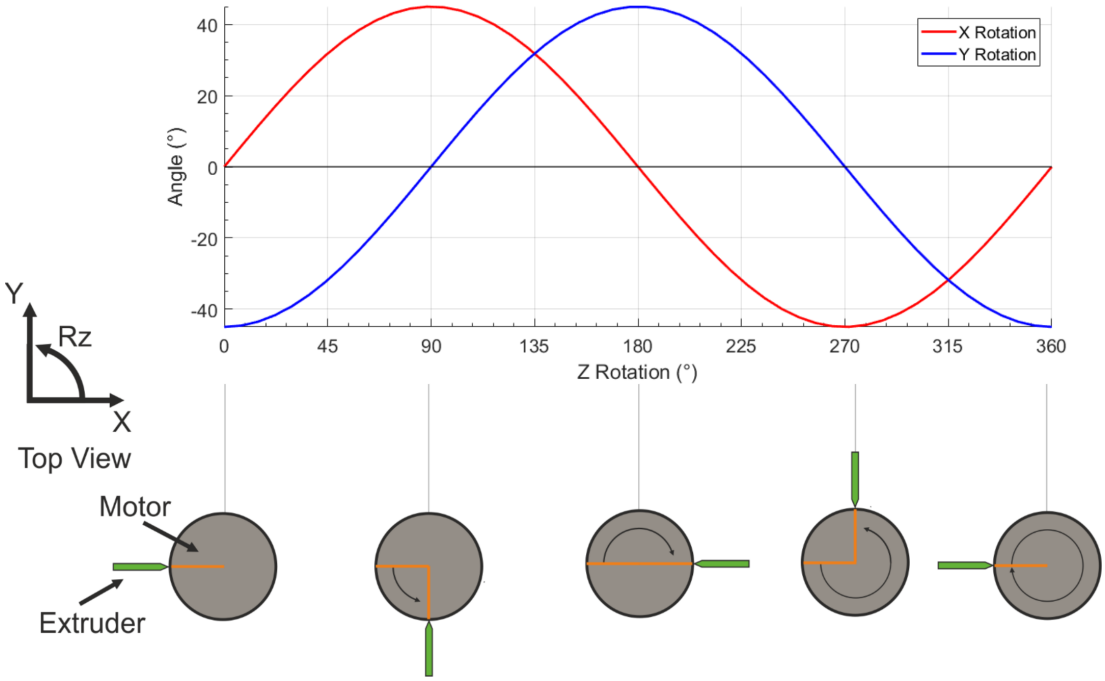

Figure 6.10: Graph of nozzle rotations around the X and Y axes, as the rotation around Z axis varies. As the circle of plastic is deposited around the motor, the Z rotation is varied to keep the nozzle pointing towards the centre of the motor. The rotations around the X and Y axes change in response to this to keep the nozzle at 45° from vertical. Below the graph is a top down representation of the motor and nozzle direction at different Z rotations.

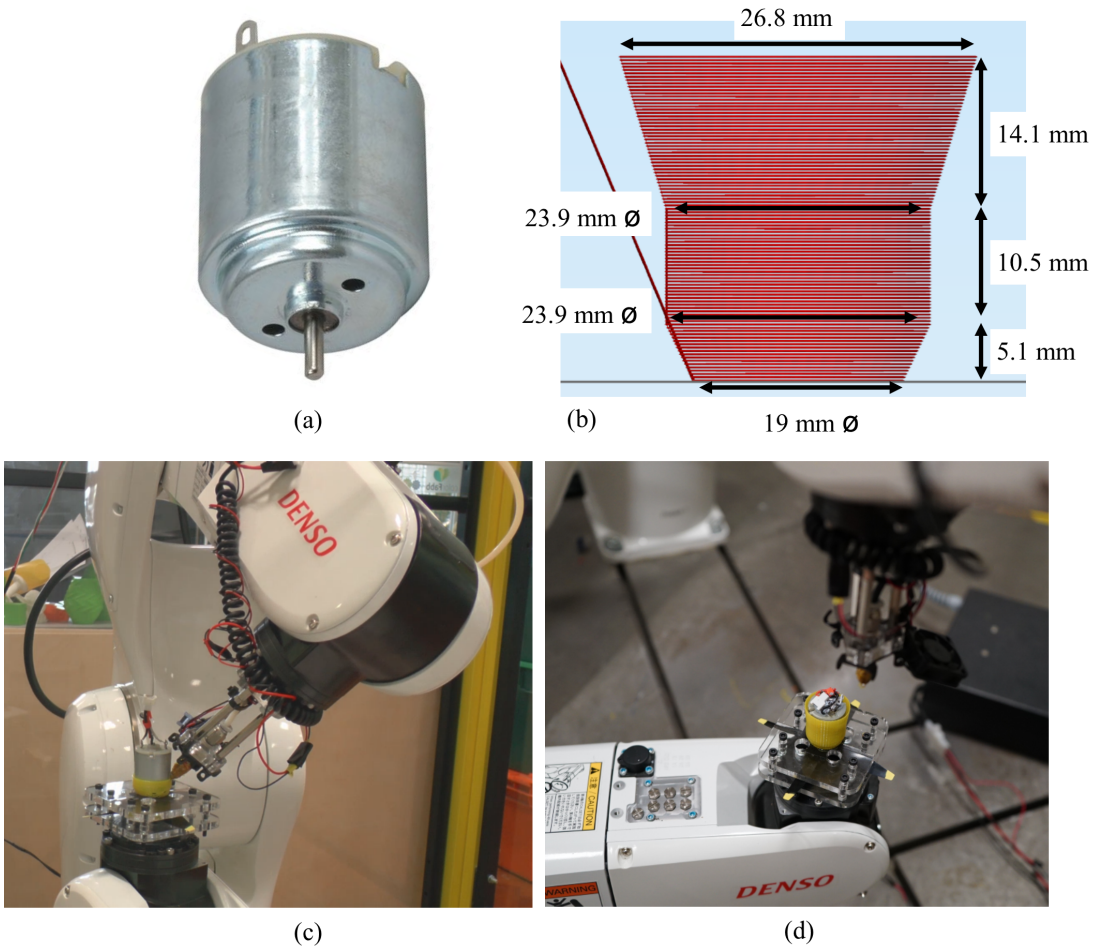

(a) (b) (c) (d)

Figure 6.11: (a) The DC motor that was embedded has steps in the housing (b) so the tool path can be narrower at the bottom stopping the motor coming out of the front of the plane. The middle section fits with the widest part of the motor and the top flares out to match with the start of the fuselage. (c) Robot printing closely around the motor housing, with the nozzle constantly kept at 45° from vertical and always pointing toward the centre of the motor. (d) Test print of the motor section finished, the top flares out from the motor ready for the next section. Motor wires are stuck down with putty to stop them tangling with the nozzle.

6.4.2 Printing the fuselage

Once the motor has been fully printed around, the nozzle is set to its usual upright orientation and the fuselage is printed on top of the plastic already deposited. To prepare the CAD file (from [225]) for slicing, the wings were separated from the body

using plane cuts and the fuselage was saved as an STL. The nozzle can be upright for this section, as there are no existing objects that it could collide with. Therefore, the fuselage was imported into a standard slicer (Simplify3D) and positioned 30mm above the build plate so that the section embedding the motor fits underneath. The fuselage was sliced to be hollow and have a single perimeter wall. Rather than stacking separate layers, the wall is printed as one continuous spiral which coils around to form the outside of the fuselage. This is commonly referred to as 'vase mode' in many slicers as it is an efficient way to print vase-like objects. This mode greatly speeds up the printing and also reduces the weight of the plane by removing the infill. The slicing settings that were used are summarised in Table 6.1 and a computer generated preview of the toolpath is in Fig. 6.12 (a).

To print around the motor, the build plate robot held it up relatively high and close to extruder robot. This is so that the extruder robot can reach all the way around the motor while keeping the nozzle tilted. However, when the build plate is so close to the extruder robot, the robot cannot reach very high or joint 5 will reach its limit. Therefore, after finishing embedding the motor, the custom M333 gcode command was used to change the build plate robot's joints, lowering the build plate so that there is space above it to print the fuselage. The end of the base plate robot is positioned as close to the floor to allow the tip of the plane's tail to be 415mm from the base.

Table 6.1: Slicer settings for fuselage and wings.

Setting	Value
Layer height	0.3mm
Print Speed	70mm/s
Temperature	200°C
Part Material	Polymaker PolyMax PLA
Cooling	On
Infill Density	0% (Vase Mode)
Infill Pattern	n/a (Vase Mode)
Perimeters	1 (Vase Mode)
Top and Bottom Layers	2
Software	Simplify3D

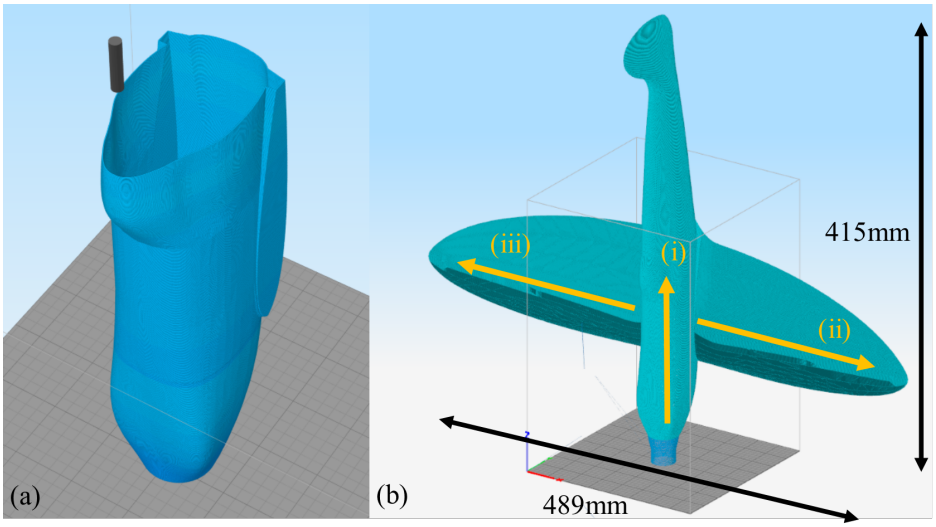

Figure 6.12: (a) Preview of the gcode for the start of the fuselage, showing the the effect of slicing with 'vase mode'. The middle is hollow and the wall is one perimeter wide. (b) Full preview of the whole plane with the motor embedding section shown in blue on the base plate. Yellow arrows indicate the direction of the build axis for the three sections. (i) Fuselage printed with layers stacked along the Z axis. Wings printed with extruder perpendicular to the fuselage. Layers build in the direction of the arrows. (ii) Printed first, fuselage rotated horizontal and extruder kept vertical. (iii) To print the second wing both the fuselage and the extruder are are rotated to keep them perpendicular to each other, and the wing within the combined workspace of the two arms.

6.4.3 Unsupported Overhanging Wings

The wings were sliced with the same settings as the fuselage, but so that they would not require supports, each was printed with a different build axis. These are shown in Fig. 6.12. Using the same method as in Section 4.3.2, the wings were saved with the same origin but different Z axis directions. These could then be imported into the slicing software, and the resulting gcode rotated using the LabVIEW program developed previously. For the robots to be able to print the wings, the orientation of the build plate must be changed between each section to ensure the printing remained inside the extruder robot's workspace. The different positions can be seen in Fig. 6.14 in the results section. There is currently no software tool to aid in choosing the position of the base such that the intended print is within the workspace of the extruder robot. This would be a useful future addition as, in this case, the position was chosen using trial

and error, with the printing positions being checked in simulation. Once positioned and sliced each section was preprocessed and concatenated to form a single file. This contains the instructions for each section and the base plate transitions between them. The complete gcode is shown in Fig. 6.12.

6.5 Results

Using the techniques described, a plane was successfully manufactured in one continuous print. No pauses or interventions were required, and total print time for the plane was 3h 43m. The process was filmed, and a sequence of stills from this are in Fig. 6.14 and a larger image in Fig. 6.13. The print quality was very high, the walls are smooth and there are no defects due to under or over extrusion of plastic. There is no discernible difference between the sections printed in different orientations and each section has adhered to the previous one. The front of the tail fin has some drooping strands as, when it was printed upright, these layers were overhanging at a too great an angle. In the future this could be overcome by printing this section with layers sliced at a different angle, as has been demonstrated in Chapter 4. A flight test was carried out but a larger wingspan and more powerful motor are required for this to be successful.

Figure 6.13: The final plane immediately after manufacturing. All sections were printed in one continuous process, starting around an existing component which was successfully embedded.

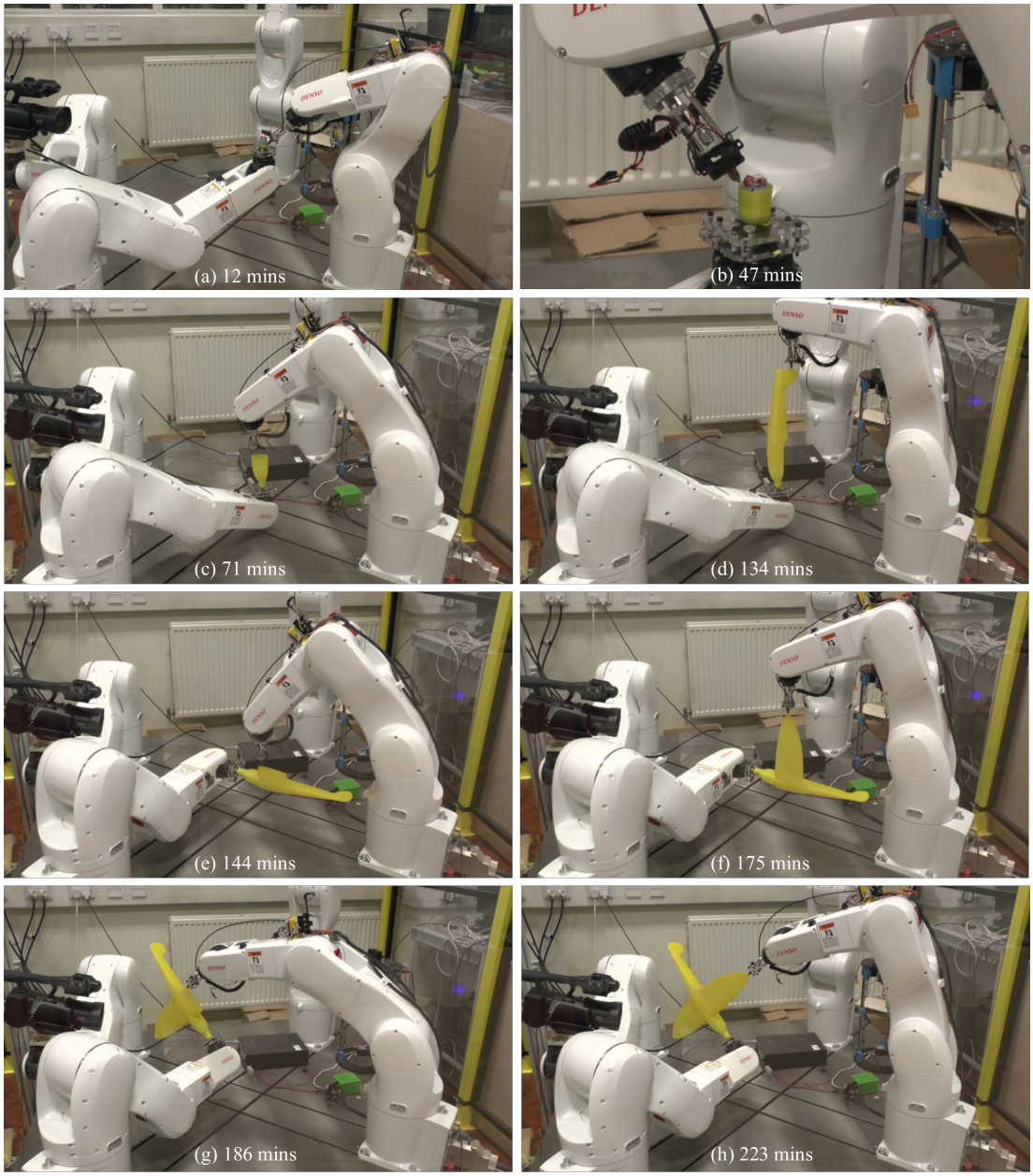

Figure 6.14: Model aircraft fabricated with an embedded actuator and no support structures. Propeller was attached beforehand and clamped in a jig, holding the motor in place to be built around. (a) The nozzle is continuously angled at 45° away from the motor so that it can print against the motor's vertical side. (b) Motor is fully embedded. (c) Nozzle vertical and build plate lowered to increase the build volume. (d) Fuselage printed hollow as one continuous wall. (e) Fuselage is rotated so that the wing can be built vertically removing any need for printing supports. (f) Nozzle kept vertical while printing the first wing. (g) Plane rotated backwards so that there is enough working room between the robots. The 2nd wing cannot be printed vertically as the 1st wing would touch the base plate, therefore the nozzle is angled to be perpendicular to the fuselage, again removing the need for supports. (h) Plane completed in one continuous print process with no stops or interventions.

6.6 Discussion and Conclusions

This demonstrator successfully shows some of the advantages of the multiaxis Additive Robot Manufacturing System (ARMS). When using conventional methods to print this shape as one piece, a large amount of support material would be required and may be difficult to remove from the thin-walled part. By using different build axes for different sections of the print no supports were needed. Individual features could be printed in an orientation which put the extruder perpendicular to the layers being deposited. This minimises the surface roughness.

The plane is also larger than the workspace of the extruder robot arm, with a length of 415mm and a wingspan of 489mm. However it could still be printed using ARMS as the system is capable of moving not only the extruder, but also the build plate. By moving the build plate, parts of the model that had already been printed could be moved out of the workspace and the new section kept within the this area, which is limited by achievable joint angles of the arms.

The motor was printed around successfully, and the molten plastic keyed into gaps on the motor housing, causing a tight fit so it remained securely in the front of the plane once the jig was removed. This is the first example of a functional component being incorporated into a device by being directly 3D printed around. The flexibility to embed components of any shape, seamlessly into a mechanical frame, could be highly valuable to future manufacturing of smart mechatronic devices. It could also be used to incorporate materials which cannot currently be 3D printed, or which require different and incompatible processes. For example, metal or rubber parts that have previously been cast, machined, or made using another AM process could be included into a robot, enabling selective tuning of a wide range of mechanical properties.

While this is not quite a robot that can "fly [1] or walk right out of the printer [2]", it shows the efficacy of ARMS, the techniques developed in this thesis, and its future potential as a manufacturing process for complex devices. It is clear that adding complimentary processes and combining previous research, into areas such as AM electronics, could yield integrated, bespoke and automatically fabricated robots in the near term. The printing process has also revealed some challenges which need to be addressed in the future. Not least of these is that the software tools for multiaxis path planning are limiting the complexity of the parts that can be printed. There is some prior work in the area of nonplanar layer slicing and sectioning for different orientations (Section 2.4.9),

which has not been explored here, so a future integration of this could improve the usability of the system for complex multiaxis prints. The author believes that a software tool kit, which is similar in many ways to existing subtractive CNC programs, could be a sensible first step in making a generalised multiaxis slicing program. For example, there are a number of methods for creating curved slices, but many have caveats and so only work in certain situations. By forcing the user to make some of the programming decisions, such as the technique to use for individual sections or features, a lot of the computational complexity that comes with having such a large number of ways to print could be avoided.

Chapter 7

Summary, Conclusions and Future Work

Multiaxis Additive Manufacturing (MAAM) has been shown to yield significant improvements to the properties of parts by overcoming fundamental issues with conventional 2.5D[1] deposition. In this thesis the development of a novel MAAM system has been presented along with experiments to verify and analyse the new methods for additive manufacturing that this enables. These include using: dynamic build orientations to fabricate unsupported overhangs; curved layers to improve strength; and multiaxis motions to embed existing components. This chapter will discuss these aspects in further detail, use the original objectives to draw conclusions and present suggestions for further work in this area.

7.1 Summary

The Additive Robot Manufacturing System (ARMS) is a novel system with improved performance and additional capabilities when compared to the state of the art in Mul-

[1]For flat layers, deposition tool paths are 2D but the layers do have some thickness. I.e. Deposition only happens in two dimensions, in the x-y plane. The Z axis is then incremented separately by one layer height.

tiaxis Additive Manufacturing (discussed in Chapter 2). The use of industrial robots allows for precise and repeatable motion, and the extrusion control was tuned so that the ARMS can print high quality objects, similar to the results from conventional FFF printers. The majority of systems using serial robot arms (e.g. [165, 166, 226]) do not come close to this surface quality or dimensional accuracy, and arguably nor do other multiaxis FFF systems (e.g. [103, 105, 143]). Parts which are comparable to existing FFF printers is important because it allows the efficacy of multiaxis techniques to be evaluated using direct comparisons. In addition to this, the ease of use and robustness of the system has allowed relatively large numbers of samples to be produced allowing for the measurement and quantification of results.

Previously there was only anecdotal evidence that FFF is successful when the extruder is not vertical. Most MAAM systems use limited motion or extrusion systems that did not allow direct comparisons to standard FFF, and some researchers avoid this question by using a stationary vertical extruder and moving the build plate using a multiaxis mechanism (e.g. [165]). This limits the potential to print onto existing large objects. In this work it was found that there was no observable effect to the surface roughness, even when printing upside down, freeing FFF to be usedwith complex multiaxis trajectories.

The progress made by this work will be summarised in context of the four inherent limitations that the conventional planar, horizontal method of AM imposes, especially when using FFF[1]. These are depicted in Fig. 7.1 along with the improvements that Multiaxis Additive Manufacturing (MAAM) can provide because of its ability to change the shape and orientation of the layers which build up a part.

1. *Overhanging features require support structures, Fig. 7.1 (a).*

   It was shown that the roughness of an overhanging surface is at a minimum when the layers are perpendicular to the surface being printed and the roughness increases, until the part becomes unprintable, when the angle of the layers tends towards the angle of the overhanging surface. Using this knowledge, ARMS was used to dynamically vary the layer orientation as overhangs were printed keeping the roughness at a minimum. This method also means that overlap between layers

[1] Other AM methods do not have all of these limitations, but all have at least one e.g. SLS does not require support structures but is unsuitable for embedding components, SLA can use very fine layers to reduce surface roughness due to stair stepping, but requires complex support structures.

can be kept within the range where no support structures are required. Fig. 7.1 (a,ii) depicts a schematic of this.

2. *Angled surfaces approximated by discrete steps. Fig. 7.1 (b).*

   Conformal curved layers can be used to smooth the surface of a part and this has received the most work previously of any of these four limitations, as it can be demonstrated using conventional 3-axis printers on shallow curvatures. ARMS is shown to be capable of printing curves of steeper surfaces than others, but this aesthetic aspect was not researched further in this thesis as it has little impact upon the goal of building more functional parts.

3. *Anisotropic mechanical properties. Fig. 7.1 (c)*

   In this thesis, steeply curved parts made with conformal layers are shown to break at 57% higher load when compared to the same part printed using planar layers. It is expected that this maximum load could be increased even further with finer control over the speed of the extruder. It is clear from this work that MAAM can significantly improve the mechanical strength of parts. Other properties, such as stiffness, could be tuned by changing the layer shapes and orientations but this investigation is left to future work.

4. *Embedding components is limited in manual insertion of simple shapes. Fig. 7.1 (d)*

   Dexterous manipulation of the extruder allows it to be moved over the surface of an object without colliding. While the final model plane cannot be called a robot, it clearly demonstrates that with some further development, ARMS could be used to rapidly fabricate robots with embedded components, without the need for manual intervention. The production of this demonstrator also showed how unique the ability to move the build plate is crucial, as a much larger object could be produced than would fit within the workspace of a fixed build plate. A new, narrow, extruder design was used for this work and is an important aspect for any MAAM system.

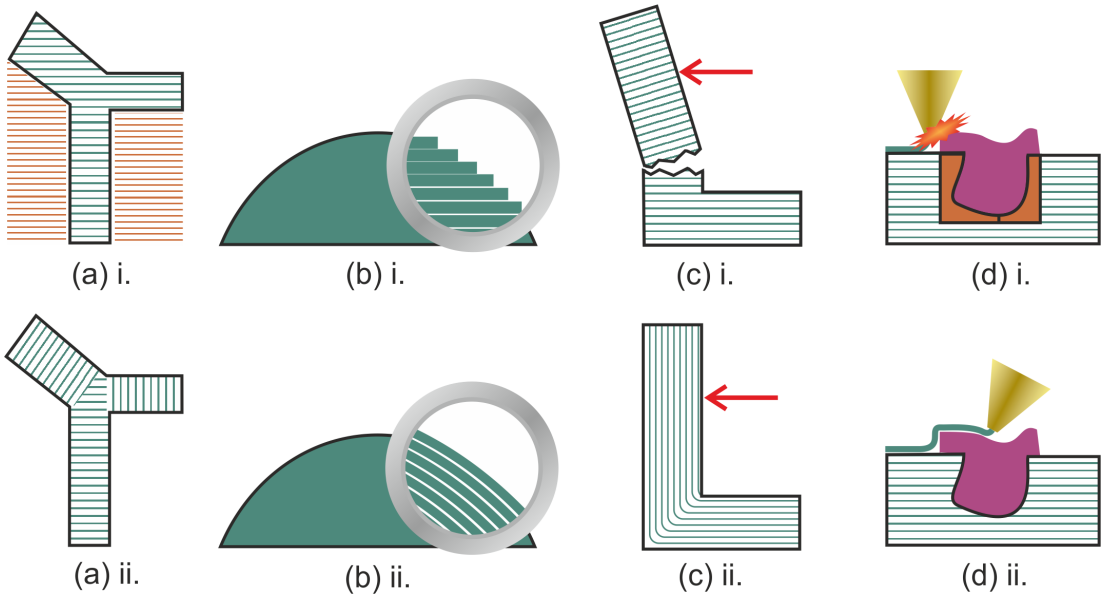

Figure 7.1: Conventional planar layers impose these disadvantages upon AM (a) i. Overhanging surfaces require support structures, (b) i. Curved surfaces approximated by discrete steps, (c) i. Anisotropic mechanical properties due to weaknesses between layers, and (d) i. Embedding components is limited to very specific geometries. Whereas Multiaxis Additive Manufacturing could deposit non-planar and non-horizontal layers, overcoming these limitations. (a) ii. Dynamic build orientations allow unsupported overhangs. (b) ii. Using either curved layers, or by changing the build axis orientation, surface roughness can be reduced. (c) ii. Layers can be optimised to improve strength, and (d) ii. Existing objects can be printed onto and around seamlessly.

7.2 Conclusions

The research described in this thesis covers the design, development and control of a novel multiaxis additive manufacturing system. A series of experiments verify it's efficacy and demonstrate the fundamental advantages of MAAM, adding significant insights to this new and expanding research field.

The aim of this work was to develop a multiaxis additive manufacturing (MAAM) system capable of printing curved and non-horizontal layers, and to evaluate the advantages of such a system for producing fully-integrated, assembly-free robots. The Additive Robot Manufacturing System (ARMS) that has been developed was shown to be capable of printing these features and the feasibility of printing an assembly-free robot is demonstrated through a case study. The original objectives were achieved as

follows:

- A review of current literature revealed how AM, in its various forms, is commonly used for the manufacturing of robotic devices. New materials, methods and technologies are being developed to enable the inclusion of complex mechanisms, multimaterials and electronics. From this it was clear that AM has some limitations and existing methods for embedding existing mechatronic components into robots are severely limited. Following this the small, but rapidly expanding field of multiaxis AM research was reviewed and used to inform key design choices.

- The novel 12 DOF Additive Robot Manufacturing System was designed to be a robust and extensible research platform, including development of the hardware, software and electronic subsystems. The complete system is used to show for the first time that serial robotic arms can be used to successfully 3D print small scale objects at a comparable, or better, standard than conventional FFF systems.

- Using the unique capabilities of a 12 DOF system, the effect of orientation with respect to gravity, on FFF, was assessed through the measurement of surface roughness of overhangs. It was shown that the orientation of the whole FFF system has no significant effect upon the surface of the parts. Therefore changing the extruder's orientation is a viable method of achieving multiaxis features such as curved layers.

- The relationship between the angle of an overhanging surface and the angle of the layers was shown to have a significant effect upon the roughness of the surface, as expected from previous research. Usually the layers are deposited along a fixed vector, but it was shown that the multiaxis system can vary this build axis dynamically throughout a single print. Therefore the layer angle can remain constant with respect to the overhang angle of a part. Using this ability, a 90° overhang was printed without support and with the same surface finish as the rest of the part.

- Nonplanar, curved, layers were successfully printed onto a pre-built support and have a greater curvature than previously demonstrated by others. The hypothesis that these layers could improve the mechanical strength of a part was confirmed,

with curved layer samples breaking at a 57% higher tensile force than the same samples printed using standard planar layers.

- A demonstrator was then produced as a case study to highlight the advantages of MAAM. Large unsupported overhangs were again shown. The whole object was larger than the build volume between the base plate and the extruder, as ARMS can move the effective workspace to only encompass the area currently being printed upon. Furthermore, a functional mechatronic actuator was incorporated into the device using complex extruder motions to directly print around it. This negated the need for further manual assembly, shape converters or post processing.

7.3 Future Work

ARMS has successfully demonstrated that MAAM is a viable approach to improving the mechanical properties of AM parts and can be an enabling technology for embedding components. However, due to the explorative nature of this work and the need to develop the experimental system, there are a number of areas which would benefit from further investigation. This section will briefly summarise these.

7.3.1 Nonplanar layers

Nonplanar layers were demonstrated, but not optimised, on ARMS. Research using 3-axis systems has shown that surfaces can be smoothed using layers conformal to curved geometry [106], but when printing curved layers using ARMS, the top surface was ridged due to excess plastic. Further process optimisation is required to improve the surface finish so that the system can be used to reduce the roughness of steeply curved surfaces.

The ability to improve the mechanical properties of 3D printed parts also requires further investigation. Experiments have shown improvements to the maximum compressive load [116, 166], pressure [138] and, in this work, tensile forces that parts can resist before breaking. Tam and Mueller [166] show how computational methods could optimise toolpaths to improve part strength based upon the position and magnitude of an applied force. Their work only focused on compressing thin shells with a predetermined curvature, so adding the ability to simulate other forces and shapes would be a

valuable tool for utilising MAAM to its best advantage.

In addition to printing parts wholly composed from curved or conformal layers, ARMS offers the opportunity to print objects using standard planar layers, then reinforce sections or features by adding conformal layers over the top. By adding this 'skin' of tracks in a different orientation to the layers it is likely that the anisotropic mechanical properties could be evened out. An initial proof of concept for this was recently published (Nov. 2017) with a single example which does show a 58% increase in yield strength for a dogbone tensile sample [227]. There are however some limitations to the paper which mean that further research is required to verify this effect. The surface is extremely poor so there is some question as to whether the improvement comes from merging standard layers by melting them together using the nozzle or through the addition on the skin (see Fig. 7.2). There is also no consideration of the possibility that the skinned sample is simply larger and contains more material irrespective of its method of deposition, so some increase would be expected. The limited number of samples (1) and surface quality are both attributed to difficulty of manufacture using their multiaxis system (presented in [226]), therefore ARMS is well suited to furthering the research in this area.

Taking this idea further, this method of augmenting existing items with conformal ribs and surfaces could be used with flexible materials to create tunable and guided flexing which may have future applications in soft robotics.

An additional area which is worthy of further investigation is the effect that curved layers can have upon the electrical resistance of a circuit printed using conductive polymers. Conductive filament, which contains a high ratio of an electrically conductive substance within the polymer, is commercially available and has been shown to allow 3D printing of simple circuits and connectors [83, 84]. Considering the eventual goal of building robots this could be a useful addition to the system. Previously researchers have published a theoretical paper which explains that the incomplete bonds between layers add resistance, so printing conductive tracks with continuous conformal strands of plastic could reduce the resistance when compared to building the same shape using many stacked layers [114, 115]. However, to the best of the authors knowledge, this has never been verified experimentally.

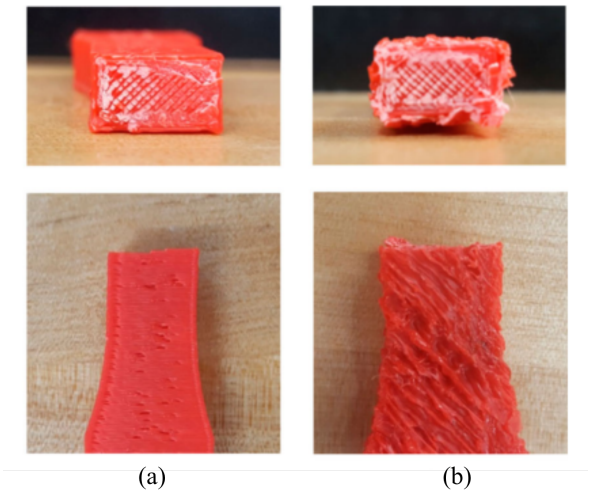

Figure 7.2: Broken tensile test samples (a) control specimen and (b) specimen skinned with 135° tracks around the outer surface. From [227]

7.3.2 Extruder and Nozzle

The final extruder for this system was capable of printing around an existing object, and does fulfil the requirements that were set, but there are some areas where it could be improved. Smaller incremental changes such as reducing the width of the mounting bracket would ensure the extruder is applicable to use in more confined spaces, but greater consideration is required to the part cooling system. Currently an un-ducted fan is simply directed at the tip of the nozzle. This could collide with parts as they are being printed over and does not provide uniform cooling to all sides of the part. Improvements could be gained by investigating the use of compressed air, supplied through low profile tubes or an actuation method that could lift the fan out of the way when required.

Other MAAM systems have just used a 5 Degree of Freedom (DOF) system, such as a Cartesian stage that would commonly be used for CNC machines. This allows many of the benefits of MAAM to be utilised, but ARMS gives the extruder a 6th DOF. Therefore the nozzle can be rotated, so a circular orifice is no longer required. Wide, rectangular nozzles could be used to quickly fill large sections when moved widthways, or used to print fine lines when the narrow edge is used. This potential should be investigated with consideration given to other applications and other shapes which

may be of use in specialist situations.

Another significant aspect of the nozzle is the surface of the tip around the orifice. This is usually flat to help smooth down deposited plastic, but when printing layers which are not flat themselves it is conceivable that this shape is not optimal. For example the corner formed by this flat surface on the tip of the nozzle may dig into the surface if the angle of deposition changes sharply. An experiment to find the effect of smoothing this corner, or using rounded tips would be informative.

7.3.3 Toolpath Planning

The lack of process planning software is one of the key difficulties when operating the ARMS. There are two main aspects which would benefit from software improvements: Workspace management for the robot arms; and multiaxis slicing.

Workspace management refers to the problem of keeping the calculated motions within the reach of both the base and extruder robot arms. While each robot has a large workspace as defined in Section 3.3, this is calculated by considering the points in space that the tip of the robot can reach irrespective of its orientation. When 3D printing, the extruder's orientation is defined and therefore the effective workspace is reduced. For long prints where the extruder's orientation is varied several times, such as the plane print in Chapter 6, it can be difficult to manually predict and then check if the robot can physically reach all of the required positions. An extension to the kinematic simulation, which checks that both robots can perform all of the actions required, and can also intelligently decide the best base plate position to enable this, would greatly increase the ease of printing more complex items.

The second piece of software that is needed to advance MAAM is a slicer that can calculate the complex toolpaths required for curved layers, changing the build axis or printing around objects without collisions. There has been some work in the area of multiaxis slicing, mainly for curved layers, but also for changing the build direction (see Section 2.4.9 for details). However, each method only focuses on one aspect, but to realise the full benefits of MAAM these strategies must be used together, illustrated by Chapter 6. Combining these poses a significant challenge. There are a large number of ways of building up an object when one considers that the build direction does not need to be fixed and the shape of the layers does not have to be planar and can change throughout the part. Consideration could also be given to how the shape of layers would

change the mechanical properties or the surface of the part. Such an unconstrained problem is very difficult to automate, especially as there is very little research in the practical use of these methods, and so there is no defined way to assess the best method for different use cases.

Therefore a fully automated, hands-off, program which is comparable to existing conventional slicers is not practical in the near term until the field of MAAM has advanced, but for it to do so quickly, new software tools are required. A viable intermediate would be to create a program which functioned in a similar way to 5 axis CNC programming software. This has a similar issue in that the problem of cutting a shape from a raw block of material has few constraints. To overcome this the software does not make high level decisions about the order or type of operation to perform, these decisions must be chosen by an experienced user. The program will then take care of calculating the tool paths to perform the chosen operations. Such a tool for additive processes would be very valuable to accelerating the progress of MAAM research.

7.3.4 Integrated manufacturing

The final aspect of suggested future work does not concern the development of MAAM, but rather of the whole ARMS. In order to fulfil the overall goal of rapidly fabricating bespoke robots, additional processes should be integrated into the system. One of the first functions that should be incorporated is pick-and-place so that existing components can be inserted during the build process. Then a method for including electrical connections will be required. There are a range of methods for this, as reviewed in Section 2.3.2, so this could include the use of a pneumatic deposition head for silver ink, or a tool which embeds wires or some other method. By adding a tool changing capability other processes such as soldering, laser engraving or subtractive machining could be incorporated by swapping out different end effectors. Multiaxis Additive Manufacturing is the novel enabling technology for this vision of a fully integrated local manufacturing system that can produce bespoke mechatronic devices and robots, but it should not be viewed in isolation. The addition of complimentary processes would enable more complex and capable systems to be manufactured.

Appendix A

System Development Supplementary Information

A.1 Extruder Control

The pseudo code below describes the program which runs on a microcontroller which serves as an interface between the computer and the extruder hardware.

```
Define Pin connections and Variables
Setup serial connection
Initialise PID Library with parameters p=10, i=0.5, d=5
//function to read from serial port
FOR length of buffer read serial port
Read a character
IF return character is read the message has ended
BREAK finish reading from port
ELSE
STORE character in Message variable
END IF
END FOR
```

```
//Check First Character
IF first character in Message is L then Message is a Heating command
//Heating Messages sent in format L1234R1234/r
SET left desired temperature to characters 2 to 5
SET right desired temperature to characters 7 to 10
ELSE IF first character is E then Message is extrusion control
//send in format ELF12345D1234/r E; extrusion control,
L or R; left or right extruder,F or R; direction, 1234 Frequency in Hz,
IF second character == L for left extruder
SET output pin to left motor pin
IF third character == F
SET left motor direction pin to HIGH for Forward
ELSE IF third character == R
SET left motor direction pin to LOW for Reverse
END IF
ELSE IF second character == R for right extruder
SET output pin to right motor pin
IF third character == F
SET right motor direction pin to HIGH for Forward
ELSE IF third character == R
SET right motor direction pin to LOW for Reverse
END IF
END IF
SET Frequency variable to characters 4-8
SET Duration variable to characters 10-13
OUTPUT pulses to output pin at 'Frequency' for 'Duration'
ELSE IF first character is F then Message is cooling fan control
//send in format F123 where 123 is PWM value in range 0-255
OUTPUT value of characters 2-4 to fan analogue pin
END IF

IF Temperature read interval has elapsed
INPUT left and right temperatures
```

```
Compute outputs using PID library and desired temperatures
OUTPUT voltage to left and right heater
END IF

IF Print output interval has elapsed
OUPUT temperature readings to serial for display on computer
END IF

REPEAT
```

A.2 Gcode Commands

The two following gcode commands are adapted to work with ARMS therefore their parameters and correct usage are documented here.

A.2.1 G0 & G1: Linear Move

These commands are both treated the same and are used to move the extruder in a straight line to a specific position and orientation on the build plate. The standard 3D printing version does not include the rotation parameters.

Parameters

Positions are in mm and rotations in radians.

`X` Position in X axis to move to.

`Y` Position in Y axis to move to.

`Z` Position in Z axis to move to.

`Rx` Angle around X axis to move to.

`Ry` Angle around Y axis to move to.

`Rz` Angle around Z axis to move to.

`E` Length of Filament to extrude, in mm.

`F` Speed of movement in mm/s.

Usage

```
G0 Xnnn Ynnn Znnn Rxnnn Rynnn Rznnn Ennn Fnnn
```

Not all parameters are needed but at least one is. This means that the output from a standard slicer, which only includes X, Y and Z, can be used without any modifications.

The previous values will be remembered, so the speed need only be set once for a number of movements for example.

A.2.2 M333: Move Build Plate Robot

This command is specific to this system and allows the user to reposition the build plate during printing. This can be useful to keep large items within the workspace of the extruder robot or to continue printing on the side of a part.

Parameters

Angles are in degrees. They refer to the joints of the Build Plate Robot.

`A` Joint 1 angle.

`B` Joint 2 angle.

`C` Joint 3 angle.

`D` Joint 4 angle.

`E` Joint 5 angle.

`F` Joint 6 angle.

Usage

```
M333 Annn Bnnn Cnnn Dnnn Ennn Fnnn
```

Not all parameters are needed but at least one is. The previous values will be remembered, so individual joints can be controlled.

A.3 Graphical User Interface

Included here are screen captures of each page in the GUI which allow the user to interact with the system.

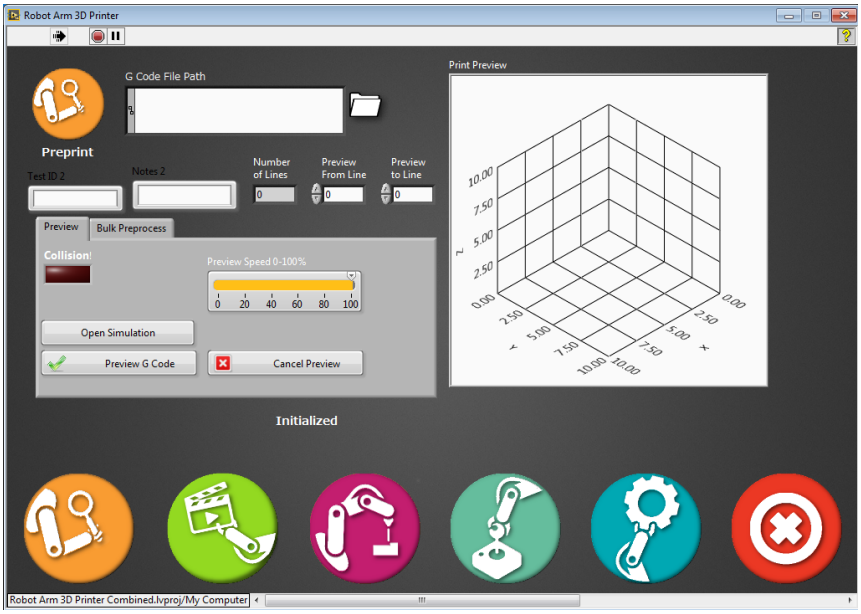

Figure A.1: Screen capture showing the Preprint screen where the user can preview or preprocess gcode.

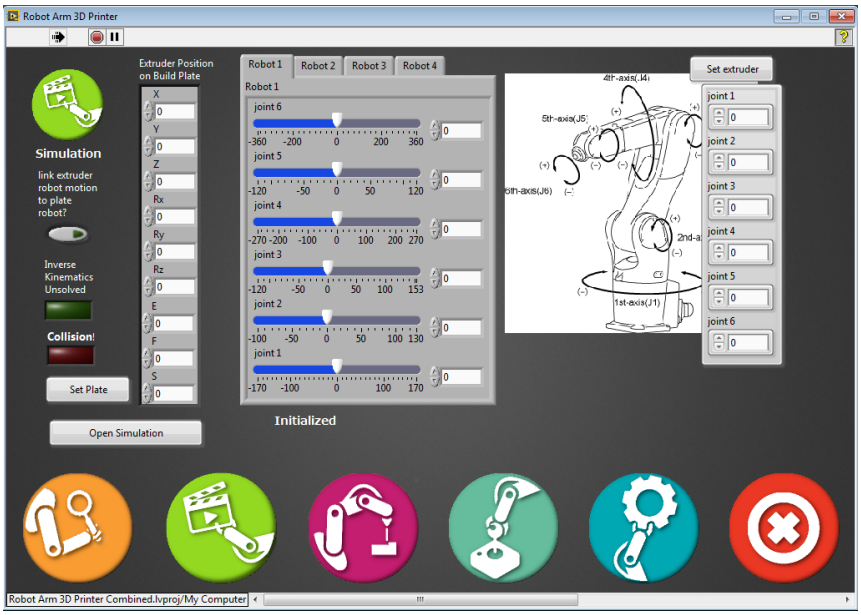

Figure A.2: Screen capture showing the Simulation screen where the user can open the simulation and control the four virtual robotic arms.

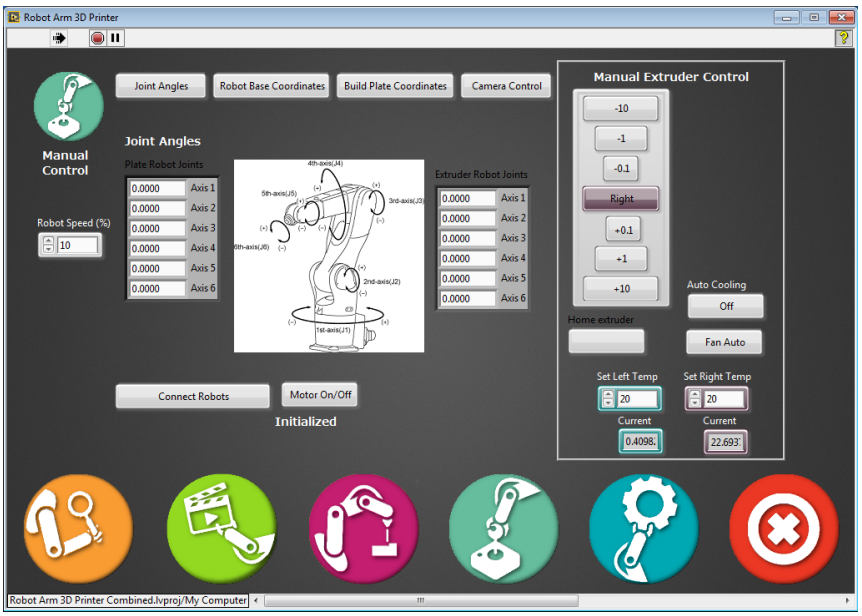

Figure A.3: Screen capture showing the Manual Control screen where the user can move the robot arms and the extruder.

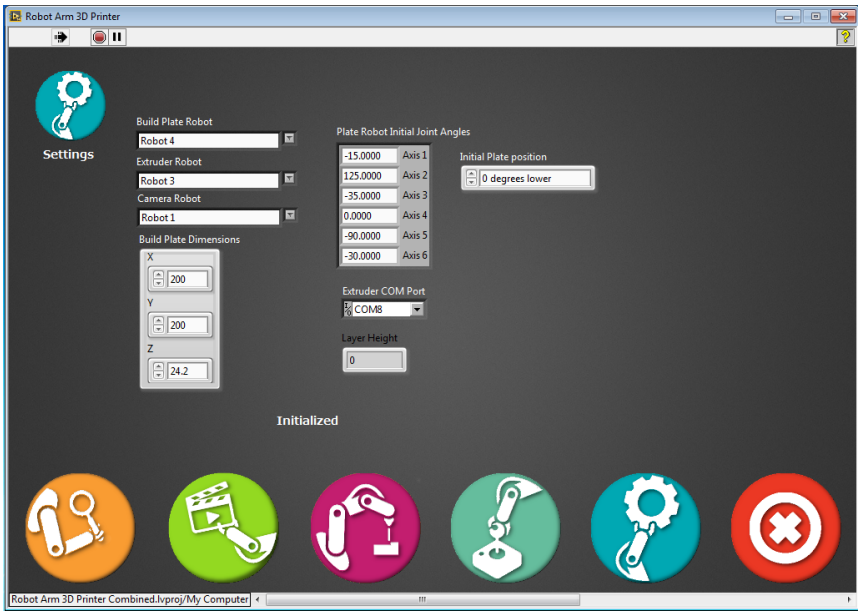

Figure A.4: Screen capture showing the settings screen where the user can view and edit important parameters.

Appendix B

Dynamic Build Orientation Supplementary Information

B.0.1 Experiment 1: FFF Printer Orientation Effects

Table B.1 lists the roughness and standard deviation for each overhang angle when printed in each printing orientation.

Table B.2 has the joint angles used for the extruder robot in these experiments, to orient the base plate as required while keeping it within the working area of the extruder robot.

Table B.3 is the ANOVA table generated by running the test in a statistical software package (SPSS).

Table B.4 shows the Tukey post hoc test results comparing each Print Orientation and Table B.5 compares the roughness between each overhang angles.

B. DYNAMIC BUILD ORIENTATION SUPPLEMENTARY INFORMATION

Table B.1: Descriptive Statistics for Print Orientation roughness results.

Overhang Angle (°)	Print Orientation (°)	Mean Ra (µm)	Std. Deviation	N
30.00	0.00	19.73	1.28	12
	45.00	20.12	1.54	12
	90.00	18.92	0.57	12
	135.00	19.70	1.32	12
	180.00	20.85	1.85	12
	Total	19.86	1.48	60
45.00	0.00	23.09	1.12	12
	45.00	22.66	1.30	12
	90.00	22.16	0.71	12
	135.00	22.32	0.69	12
	180.00	22.56	0.90	12
	Total	22.56	0.99	60
60.00	0.00	42.58	1.07	12
	45.00	41.86	1.22	12
	90.00	42.83	1.17	12
	135.00	42.96	0.89	12
	180.00	43.05	1.01	12
	Total	42.65	1.12	60
70.00	0.00	52.66	7.34	12
	45.00	51.65	8.31	12
	90.00	52.05	7.39	12
	135.00	53.25	9.35	12
	180.00	50.16	7.33	12
	Total	51.96	7.78	60
80.00	0.00	58.88	13.78	12
	45.00	63.32	16.91	12
	90.00	63.31	20.32	12
	135.00	62.91	23.55	12
	180.00	64.90	27.08	12
	Total	62.66	20.25	60

Table B.2: Build plate robot joint angles for printer orientation tests.

Print Orientation (°)	Joint angle (°)					
	J_1	J_2	J_3	J_4	J_5	J_6
0	-13	100	-30	0	-70	-75
45	-35	125	-35	-45	-90	0
90	-35	125	-35	-90	-90	0
135	-55	35	55	-135	-90	0
180	-40	10	80	0	90	180

Table B.3: ANOVA table for effects between Print Orientation and Overhang Angle on Ra (a R Squared = .749 (Adjusted R Squared = .728))

Source	Sum of Squares	Degrees of Freedom	Mean Square	F	P
Corrected Model	82739.29a	24	3447.47	34.26	0.00
Intercept	478543.97	1	478543.97	4756.19	0.00
Print Orientation	31.57	4	7.89	0.08	0.99
Overhang Angle	82390.01	4	20597.50	204.72	0.00
Print Orientation * Overhang Angle	317.71	16	19.86	0.20	1.00
Error	27669.12	275	100.62		
Total	588952.38	300			
Corrected Total	110408.41	299			

B. DYNAMIC BUILD ORIENTATION SUPPLEMENTARY INFORMATION

Table B.4: Tukey post hoc test results comparing each Print Orientation

Print Orientation (°), (I)	Print Orientation (°), (J)	Mean Difference (I-J)	Standard Error	P	95% Confidence Interval	
					Lower Bound	Upper Bound
0.00	45.00	-0.53	1.83	0.998	-5.56	4.50
	90.00	-0.46	1.83	0.999	-5.49	4.57
	135.00	-0.84	1.83	0.991	-5.87	4.19
	180.00	-0.91	1.83	0.987	-5.94	4.12
45.00	0.00	0.53	1.83	0.998	-4.50	5.56
	90.00	0.07	1.83	1.000	-4.96	5.10
	135.00	-0.31	1.83	1.000	-5.34	4.72
	180.00	-0.38	1.83	1.000	-5.41	4.65
90.00	0.00	0.46	1.83	0.999	-4.57	5.49
	45.00	-0.07	1.83	1.000	-5.10	4.96
	135.00	-0.38	1.83	1.000	-5.41	4.65
	180.00	-0.45	1.83	0.999	-5.49	4.58
135.00	0.00	0.84	1.83	0.991	-4.19	5.87
	45.00	0.31	1.83	1.000	-4.72	5.34
	90.00	0.38	1.83	1.000	-4.65	5.41
	180.00	-0.07	1.83	1.000	-5.10	4.95
180.00	0.00	0.91	1.83	0.987	-4.11	5.94
	45.00	0.38	1.83	1.000	-4.65	5.41
	90.00	0.45	1.83	0.999	-4.58	5.48
	135.00	0.07	1.83	1.000	-4.95	5.10

Table B.5: Tukey post hoc test results comparing each Overhang Angle. (* The mean difference is significant at the 0.05 level.)

Overhang Angle (°), (I)	Overhang Angle (°), (J)	Mean Difference (I-J)	Standard Error	P	95% Confidence Interval	
					Lower Bound	Upper Bound
30.00	45.00	-2.70	1.83	0.582	-7.72	2.33
	60.00	-22.79*	1.83	0.00	-27.82	-17.76
	70.00	-32.09*	1.83	0.00	-37.12	-27.06
	80.00	-42.80*	1.83	0.00	-47.83	-37.77
45.00	30.00	2.70	1.83	0.582	-2.33	7.72
	60.00	-20.09*	1.83	0.00	-25.12	-15.06
	70.00	-29.40*	1.83	0.00	-34.42	-24.37
	80.00	-40.10*	1.83	0.00	-45.13	-35.07
60.00	30.00	22.79*	1.83	0.00	17.76	27.82
	45.00	20.09*	1.83	0.00	15.06	25.12
	70.00	-9.30*	1.83	0.00	-14.33	-4.27
	80.00	-20.01*	1.83	0.00	-25.04	-14.98
70.00	30.00	32.09*	1.83	0.00	27.06	37.12
	45.00	29.40*	1.83	0.00	24.37	34.42
	60.00	9.30*	1.83	0.00	4.27	14.33
	80.00	-10.71*	1.83	0.00	-15.74	-5.68
80.00	30.00	42.80*	1.83	0.00	37.77	47.83
	45.00	40.10*	1.83	0.00	35.07	45.13
	60.00	20.01*	1.83	0.00	14.98	25.04
	70.00	10.71*	1.83	0.00	5.68	15.74

B.0.2 Experiment 2: Dynamic Build Orientation

Table B.1 shows the mean Ra and standard deviation for the surface roughness tests performed upon the overhanging arches printed with a dynamic build orientation.

Table B.7 is the ANOVA table results from testing whether there is a significant difference in the Ra for the overhang surfaces depending upon the surface angle.

Table B.8 lists the results for the Tukey post hoc test which compares every surface angle in a pairwise manor.

Table B.6: Descriptive Statistics for Dynamic Build Orientation roughness results.

Overhang Angle (°)	Mean Ra (µm)	Std. Deviation	N
30	26.15	1.87	9
45	28.73	2.51	9
60	27.15	0.99	9
70	28.63	2.12	9
80	27.47	2.06	9
Total	27.62	2.12	45

Table B.7: ANOVA table for effect of Overhang Angle on Ra (a R Squared = 0.211 (Adjusted R Squared = 0.133))

	Sum of Squares	Degrees of Freedom	Mean Square	F	P
Between Groups	41.931	4	10.483	2.681	0.045
Within Groups	156.416	40	3.910		
Total	198.347	44			

Table B.8: Tukey post hoc test results comparing each Overhang Angle

Overhang Angle (°), (I)	Overhang Angle (°), (J)	Mean Difference (I-J)	Standard Error	P	95% Confidence Interval	
					Lower Bound	Upper Bound
30	45	-2.58	0.93	0.061	-5.24	0.08
	60	-1.01	0.93	0.814	-3.67	1.65
	70	-2.48	0.93	0.078	-5.15	0.18
	80	-1.32	0.93	0.620	-3.98	1.34
45	30	2.58	0.93	0.061	-0.08	5.24
	60	1.57	0.93	0.453	-1.09	4.23
	70	0.10	0.93	1.000	-2.56	2.76
	80	1.26	0.93	0.661	-1.40	3.921
60	30	1.01	0.93	0.814	-1.65	3.67
	45	-1.57	0.93	0.453	-4.23	1.09
	70	-1.47	0.93	0.518	-4.14	1.19
	80	-0.31	0.93	0.997	-2.97	2.35
70	30	2.48	0.93	0.078	-0.18	5.15
	45	-0.10	0.93	1.000	-2.76	2.56
	60	1.47	0.93	0.518	-1.19	4.14
	80	1.16	0.93	0.724	-1.50	3.82
80	30	1.32	0.93	0.620	-1.34	3.98
	45	-1.26	0.93	0.661	-3.92	1.40
	60	0.31	0.93	0.997	-2.35	2.97
	70	-1.16	0.93	0.724	-3.82	1.50

B. DYNAMIC BUILD ORIENTATION SUPPLEMENTARY INFORMATION

Appendix C

3-Axis Curved Layers

C.1 Limitations on printing nonplanar layers due to 3-axis motion

Since its conception Additive Manufacturing has been based upon building up flat, horizontal layers to form an object. However this is not necessarily the optimum method for all geometries. Objects printed using the WirePrint method are constructed from 'zigzag' shaped layers, yielding a wireframe construction which reduces the print time while still defining the basic geometry [123]. It has also been proposed that layers that are not horizontal, or do not have a uniform thickness could be used to remove the stepped effect that most AM processes currently produce [105]. Combining these layer techniques with multidirectional deposition methods could give significant improvements.

An object has been produced using a 3 axis FFF 3D printer (Airwolf 5.5) using both flat and non-flat layers. This gives an example of the benefits of non-flat layers and helps assess the practicalities and limitations of this method when using an unmodified 3D printer. A plug-in for the slicing software Cura has previously been developed [119]. This is a piece of Python code which processes the generated gcode to add or edit the

commands. In this case the 'Wave' plug-in converts each flat layer into a sinusoidal profile. The amplitude of the wave increases as the layer height increases.

While the code is available to download there were a few bugs that needed to be fixed. Changing the starting layer parameter originally had no effect, causing issues with the first few layers as the raised sections of the layer did not stick well, while the lower sections cause the nozzle to be too close to the bed for reliable extrusion. The original tool path that was generated had large sections where no plastic was to be extruded. By adjusting the extrusion equation the preview of the tool path was greatly improved.

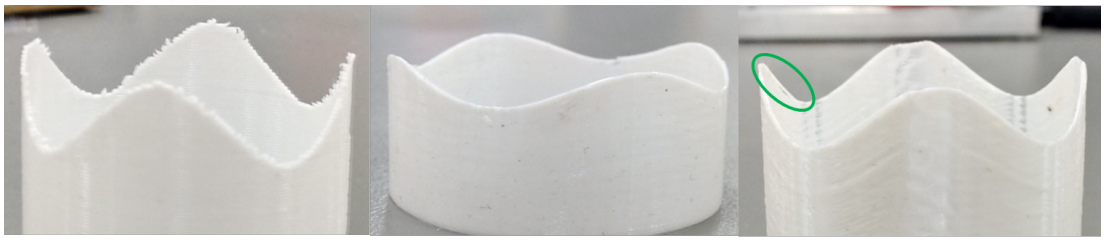

Figure C.1: Comparison of curved and planar layers printed using a 3 axis machine. (a) Curved top surface approximated using discrete layers showing stepped effect. (b) A smooth curved surface due to sinusoidal layers, however as the curves get steeper (c) the side of nozzle contacts the slope and a discrepancy in the speeds of the Z axis compared to the X & Y causes areas of under extrusion.

Figure C.1 shows three results from the experiment. (a) is a thin walled cylinder with a sinusoidal edge profile, with 4 peaks and amplitude of 5mm. The stepped effect caused by digitising a curve into flat layers is visible. The central image shows the surface finish that a curved layer gives. Instead of steps the top of the wave is totally smooth. This demonstrates how a layer which conforms to the surface geometry can improve the surface finish. The maximum amplitude of the wave is lower however so this cylinder is shorter, see Fig. C.3. The geometry of the nozzle limits the maximum angle a curved layer can be. The right hand image shows how these limitations appear as the amplitude increases. The top layer on the upward slope of the curve has not adhered to the previous one, and the layers below are not smooth. The heat radiating from the side of the nozzle deformed the sides as they thin and very close to the side of the nozzle, seen in Fig. C.2. When the angle of the slope exceeded the angle of

the sides of the heated nozzle they collided. At this point the nozzle started to melt and push the previous layer down, causing the gap that is highlighted in Fig. C.1 (c). These results clearly demonstrate that curved layers can improve the surface finish for some geometry. Conventional 3-axis 3D printers can produce these effects but have some limitations. Adding additional rotational axis would enable the nozzle to produce steeper layers without collisions.

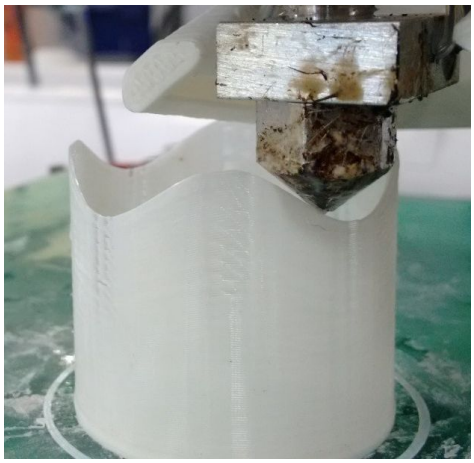

Figure C.2: The side of the nozzle is very close to part causing deformations due to high heat. As the amplitude of the curves increases with the height of the part this gap decreases until the nozzle collides with the part.

C.2 Plug-in Equations

The code that was used to generate the tool paths for the non-flat layer experiments was based upon an open source python script [119]. This works within Cura to postprocess the gcode. A flat topped, thin walled cylinder was imported and sliced using the standard settings. The plug-in then goes through the gcode line by line and changes the z value and the extrusion value. A circular sine wave is generated based upon the x and y coordinates of the nozzle and the desired number of waves, according to Eq. (C.1). This value is then used in Eq. (C.2) which takes into account the current height of the print and adjusts the z value accordingly. In this way the amplitude of the wave is low when the effect starts and gradually increases until it is the full amplitude set by the user on the final layer, seen in Fig. C.3. Table C.1 defines the symbols used and the values used.

$$d = 0.5 \sin\left(w \tan^{-1}\left(\frac{y - Y}{x - X}\right) + 1\right) \tag{C.1}$$

$$z' = zs + \frac{2adz}{m} - dl - l \tag{C.2}$$

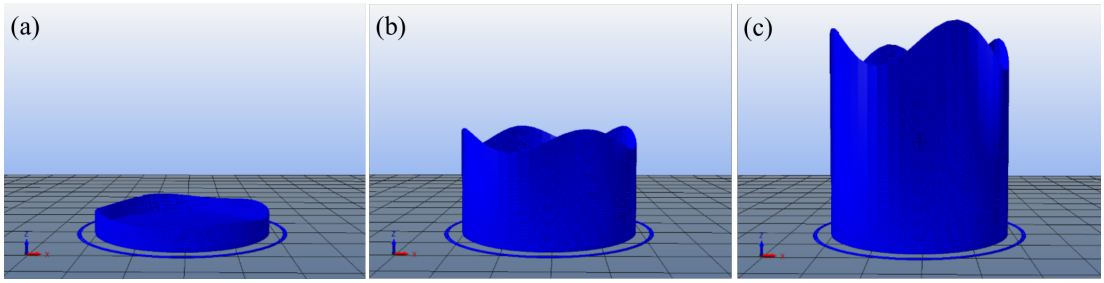

Figure C.3: Preview in slicing software of the curved layer gcode as the Z height increases from (a) to (c) the amplitude of the sine wave also increases.

Table C.1: Settings used to generate gcode for 3 axis nonplanar layers.

Symbol	Variable	Value Set for Experiment
d	factor generated for current nozzle X,Y position	N/A
w	Number of cycles	4
y	Nozzle Y coordinate	N/A
x	nozzle Y coordinate	N/A
z	nozzle Z coordinate	N/A
Y	Part centre Y coordinate	92.5mm
X	Part centre X coordinate	99mm
z'	New nozzle height	N/A
a	Wave Max. amplitude	5mm
m	Maximum Z height	N/A
l	Layer Height	0.2mm

Appendix D

Curved Layer Arches on Stepped Support

The initial results for curved layers were not as expected, Table D.1. Previously, curved layers have been reported to be stronger than flat ones [112] and it is well established that the bonds between layers are weaker than across layers. From observing the samples as they were extended it could be clearly seen, via a lightening in the plastic due to stretching, that the cracks propagated across the part from lines embossed into the underside by the support structure. The arch shape does cause a stress concentration on the middle of the underside when put in tension and the defects concentrate this enough to start a crack.

The curved layers have a very similar mean maximum load of 115N to the planar layer arch (117N) but the way they break is different, Fig. D.2. As these samples start to straighten fatigue marks can be seen starting from the underside of the arch and propagating to the top surface. One of these cracks will widen until there is a very thin connection between the two halves, this is when the maximum load is reached. The extension is then continued until the two halves are again in tension, then separated - this is the second peak in the data. These samples broke in the centre. Observations revealed that the points that these cracks were propagating from were ridges on the underside of the arch. These are impressions caused by printing onto support structures

made using conventional planar layers, the steps were embossed into the underside as the molten plastic was deposited, seen in Fig. D.1.

Following this a smooth printing surface was added to the top of the support structure and a new set of curved samples printed. The underside is much smoother, Fig. D.1, so there were no longer the same defects to cause stress concentrations.

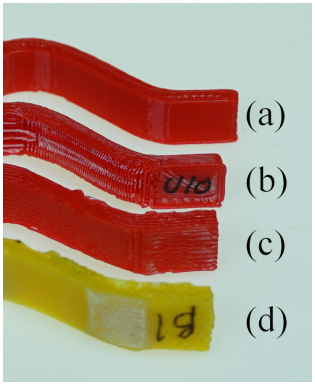

Figure D.1: The underside of arch samples, (a) Samples printed on its side has a smooth consistent surface, (b) the arch printed upright with planar layers has a stepped surface with white marks where the support structure was removed, (c) The curved layer arch as light impressions of layers from the support structure it was printed upon, (d) the curved layer arch printed upon a smooth support structure has a smooth underside with some white marks where the support surface was peeled off.

Table D.1: Maximum loads for samples upright arch samples.

Sample No.	Planar Upright	Curved On Layered Support
1	121.36	123.73
2	124.57	114.46
3	91.37	107.99
4	116.38	120.40
5	131.41	109.99
Mean	117.02	115.31
Std. Dev.	15.34	6.70

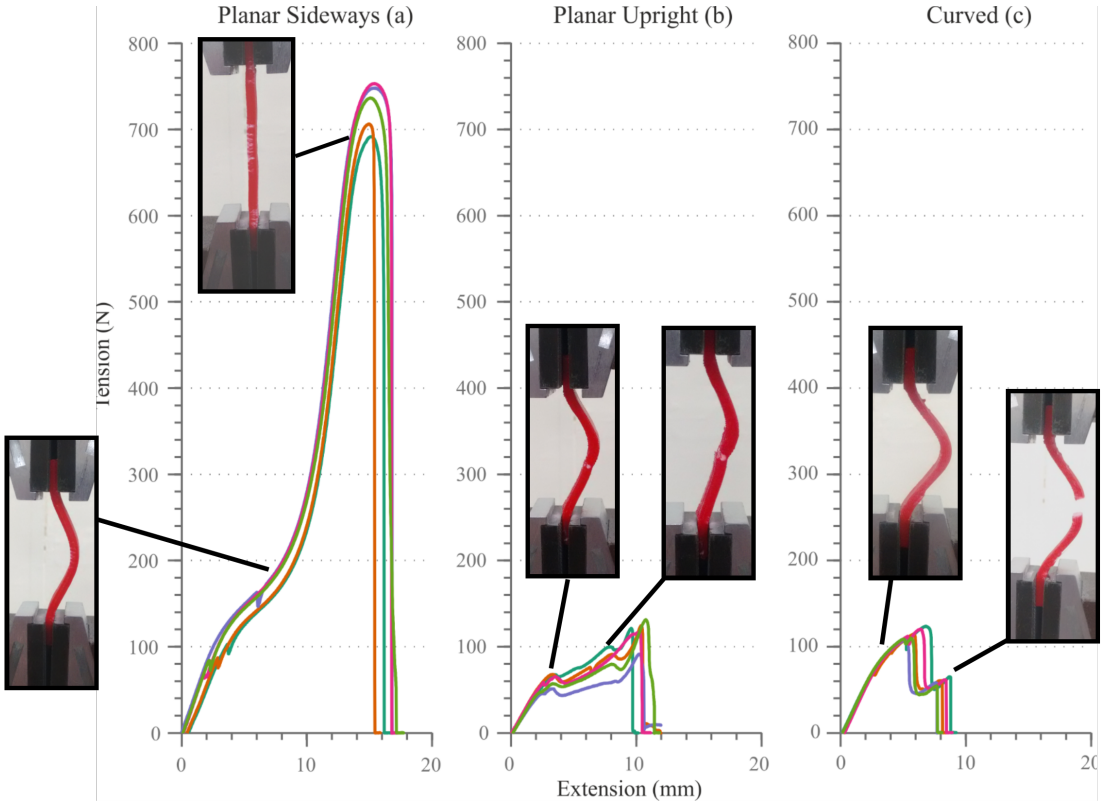

Figure D.2: Tensile test results: (a) Arch printed on its side using planar layers, the arch straightens out fully before failing. (b) Arches printed upright using planar layers breaks a a significantly lower force as expected, these samples tend to break the the side of the centre and only partly straighten before a crack propagates from the inside, initially causing a decrease in the force until the additional slack is taken up and the part is in tension again. (c) The curved layer samples have the same maximum force as the planar layer part printed at the same orientation, against expectations. These arches did not straighten much before crack propagated from the inside surface, the largest peak is caused by this crack opening up to the final layer along the top of the arch, the final smaller peak is when this final layer snaps.

References

[1] Neil Gershenfeld. How to make almost anything: The digital fabrication revolution. *Foreign Aff.*, 91:43, 2012.

[2] Hod Lipson. A grand challenge for additive manufacturing: Can we print a robot that will walk out of the printer? *3D Printing and Additive Manufacturing*, 2(2):41–41, 2015.

[3] Constantinos Mavroidis, Kathryn J. DeLaurentis, Jey Won, and Munshi Alam. Fabrication of non-assembly mechanisms and robotic systems using rapid prototyping. *Journal of Mechanical Design*, 123(4):516–524, 2000. 10.1115/1.1415034.

[4] Alok Kataria and David W. Rosen. Building around inserts: methods for fabricating complex devices in stereolithography. *Rapid Prototyping Journal*, 7(5):253–262, 2001.

[5] BS ISO. Iso/astm 52900: 2015 additive manufacturing - general principles - terminology. *Additive manufacturing general principles terminology. London: BSI Standards Limited*, 2015.

[6] Rhys Jones, Patrick Haufe, Edward Sells, Pejman Iravani, Vik Olliver, Chris Palmer, and Adrian Bowyer. Reprap - the replicating rapid prototyper. *Robotica*, 29(1):177–191, 2011.

[7] Anna Bellini and Selcuk Guceri. Mechanical characterization of parts fabricated using fused deposition modeling. *Rapid Prototyping Journal*, 9(4):252–264, 2003.

[8] Jim Cotteleer, Mark; Joyce. 3D opportunity: Additive manufacturing paths to performance, innovation, and growth, 2014.

[9] M Ruffo, C Tuck, and R Hague. Cost estimation for rapid manufacturing - laser sintering production for low to medium volumes. *Proceedings of the Institution of Mechanical Engineers, Part B: Journal of Engineering Manufacture*, 220(9):1417–1427, 2006.

[10] A. M. Mehta and D. Rus. An end-to-end system for designing mechanical structures for print-and-fold robots. In *2014 IEEE International Conference on Robotics and Automation (ICRA)*, pages 1460–1465, May 2014.

[11] G. S. Hornby, H. Lipson, and J. B. Pollack. Generative representations for the automated design of modular physical robots. *IEEE Transactions on Robotics and Automation*, 19(4):703–719, Aug 2003.

[12] Christopher Barnatt. *3D Printing: Second Edition*. CreateSpace Independent Publishing Platform; 2nd edition, 2014.

[13] Jorge G Cham, Sean A Bailey, Jonathan E Clark, Robert J Full, and Mark R Cutkosky. Fast and robust: Hexapedal robots via shape deposition manufacturing. *The International Journal of Robotics Research*, 21(10-11):869–882, 2002.

[14] Mark R Cutkosky and Sangbae Kim. Design and fabrication of multi-material structures for bioinspired robots. *Philosophical Transactions of the Royal Society A: Mathematical, Physical and Engineering Sciences*, 367(1894):1799–1813, 2009.

[15] Mohammad Vaezi, Srisit Chianrabutra, Brian Mellor, and Shoufeng Yang. Multiple material additive manufacturing - part 1: a review. *Virtual and Physical Prototyping*, 8(1):19–50, 2013.

[16] Rhys Owen Jones, Pejman Iravani, and Adrian Bowyer. Rapid manufacturing of functional engineering components, 2012.

[17] L. Mohon. Nasa marshall advances 3-d printed rocket engine nozzle technology. [Online]. Available from: www.nasa.gov, 2018. Accessed: 06/2018.

[18] Nannan Guo and Ming C. Leu. Additive manufacturing: technology, applications and research needs. *Frontiers of Mechanical Engineering*, 8(3):215–243, Sep 2013.

[19] R.J. Friel and R.A. Harris. Ultrasonic additive manufacturing â€“ a hybrid production process for novel functional products. *Procedia CIRP*, 6:35 – 40, 2013.

Proceedings of the Seventeenth CIRP Conference on Electro Physical and Chemical Machining (ISEM).

[20] C.Y. Kong and R.C. Soar. Fabrication of metalâ€“matrix composites and adaptive composites using ultrasonic consolidation process. *Materials Science and Engineering: A*, 412(1):12 – 18, 2005. International Conference on Recent Advances in Composite Materials.

[21] Ji Li, Tom Monaghan, Robert Kay, Ross James Friel, and Russell Harris. Enabling internal electronic circuitry within additively manufactured metal structures â€“ the effect and importance of inter-laminar topography. *Rapid Prototyping Journal*, 24(1):204–213, 2018.

[22] Xiaorong Xu, Wendy Cheng, Daniel Dudek, Motohide Hatanaka, Mark R Cutkosky, and Robert J Full. Material modeling for shape deposition manufacturing of biomimetic components. In *Proceedings of the ASME Design Engineering Technical Conference*, pages 10–14, 2000.

[23] Stratasys Ltd. Stratasys objet. [Online]. Available from: www.stratasys.com, 2017. Accessed: 09/2017.

[24] Nicholas A Meisel, Amelia M Elliott, and Christopher B Williams. A procedure for creating actuated joints via embedding shape memory alloys in PolyJet 3D printing. *Journal of Intelligent Material Systems and Structures*, 2014.

[25] Josef Prusa. Original prusa i3 mk2 multi material upgrade release dual/quad extrusion. [Online]. Available from: http://www.prusaprinters.org/original-prusa-i3-mk2-multi-material-upgrade-release/, 2016. Accessed: 09/2017.

[26] Evan Malone and Hod Lipson. Multi-material freeform fabrication of active systems. In *ASME 9th Biennial Conference on Engineering Systems Design and Analysis*, pages 345–353. American Society of Mechanical Engineers, 2008.

[27] David Espalin, Jorge Ramirez, Francisco Medina, and Ryan Wicker. Multi-material, multi-technology FDM system. In *23rd Annual International Solid Freeform Fabrication Symposium*, pages 828–835, 2012.

[28] Evan Malone and Hod Lipson. Fab@ home: the personal desktop fabricator kit. *Rapid Prototyping Journal*, 13(4):245–255, 2007.

[29] Pitchaya Sitthi-Amorn, Javier E Ramos, Yuwang Wangy, Joyce Kwan, Justin Lan, Wenshou Wang, and Wojciech Matusik. Multifab: a machine vision assisted platform for multi-material 3D printing. *ACM Transactions on Graphics (TOG)*, 34(4):129, 2015.

[30] Jae-Won Choi, Eric MacDonald, and Ryan Wicker. Multi-material microstereolithography. *The International Journal of Advanced Manufacturing Technology*, 49(5):543–551, 2010.

[31] Ryan B. Wicker and Eric W. MacDonald. Multi-material, multi-technology stereolithography. *Virtual and Physical Prototyping*, 7(3):181–194, 2012.

[32] Ryan B Wicker, Francisco Medina, and CJ Elkins. Multiple material microfabrication: extending stereolithography to tissue engineering and other novel applications. In *Proceedings of 15th Annual Solid Freeform Fabrication Symposium, Austin, TX*, pages 754–64. Wiley, 2004.

[33] Y. G. Im, S. I. Chung, J. H. Son, Y. D. Jung, J. G. Jo, and H. D. Jeong. Functional prototype development: inner visible multi-color prototype fabrication process using stereo lithography. *Journal of Materials Processing Technology*, 130â€“131(0):372–377, 2002.

[34] George A Popescu, Patrik Kunzler, and Neil Gershenfeld. Digital printing of digital materials. In *NIP & Digital Fabrication Conference*, pages 55–57. Society for Imaging Science and Technology, 2006.

[35] Jonathan Hiller and Hod Lipson. Design and analysis of digital materials for physical 3D voxel printing. *Rapid Prototyping Journal*, 15(2):137–149, 2009.

[36] George A Popescu, Tushar Mahale, and Neil Gershenfeld. Digital materials for digital printing. In *NIP & Digital Fabrication Conference*, pages 58–61. Society for Imaging Science and Technology, 2006.

[37] Kenneth C Cheung and Neil Gershenfeld. Reversibly assembled cellular composite materials. *science*, 341(6151):1219–1221, 2013.

[38] Benjamin Jenett, Sam Calisch, Daniel Cellucci, Nick Cramer, Neil Gershenfeld, Sean Swei, and Kenneth C Cheung. Digital morphing wing: active wing shaping

concept using composite lattice-based cellular structures. *Soft Robotics*, 4(1):33–48, 2017.

[39] Jonathan Hiller and Hod Lipson. Tunable digital material properties for 3D voxel printers. *Rapid Prototyping Journal*, 16(4):241–247, 2010.

[40] Will Langford, Amanda Ghassaei, and Neil Gershenfeld. Automated assembly of electronic digital materials. In *ASME 2016 11th International Manufacturing Science and Engineering Conference*. American Society of Mechanical Engineers, 2016.

[41] Robert MacCurdy, Anthony McNicoll, and Hod Lipson. Bitblox: Printable digital materials for electromechanical machines. *The International Journal of Robotics Research*, 33(10):1342–1360, 2014.

[42] Yonghua Chen and Chen Zhezheng. Joint analysis in rapid fabrication of nonassembly mechanisms. *Rapid Prototyping Journal*, 17(6):408–417, 2011.

[43] Sanjay Rajagopalan and Mark Cutkosky. Error analysis for the in-situ fabrication of mechanisms. *Journal of Mechanical Design*, 125(4):809–822, 2004.

[44] Hod Lipson, Francis C Moon, Jimmy Hai, and Carlo Paventi. 3-d printing the history of mechanisms. *Journal of Mechanical Design*, 127(5):1029–1033, 2005.

[45] Jacques Calì, Dan A Calian, Cristina Amati, Rebecca Kleinberger, Anthony Steed, Jan Kautz, and Tim Weyrich. 3d-printing of non-assembly, articulated models. *ACM Transactions on Graphics (TOG)*, 31(6):130, 2012.

[46] Kathryn J De Laurentis, Fung Felix Kong, and Constantinos Mavroidis. Procedure for rapid fabrication of non-assembly mechanisms with embedded components. In *ASME 2002 International Design Engineering Technical Conferences and Computers and Information in Engineering Conference*, pages 1239–1245. American Society of Mechanical Engineers, 2002.

[47] Kathryn J. De Laurentis and Constantinos Mavroidis. Rapid fabrication of a nonassembly robotic hand with embedded components. *Assembly Automation*, 24(4):394–405, 2004.

[48] Moritz Bächer, Bernd Bickel, Doug L James, and Hanspeter Pfister. Fabricating articulated characters from skinned meshes. *ACM Trans. Graph.*, 31(4):47–1, 2012.

[49] Yoshio Ishiguro and Ivan Poupyrev. 3D printed interactive speakers. In *Proceedings of the SIGCHI Conference on Human Factors in Computing Systems*, pages 1733–1742. ACM, 2014.

[50] Karl Willis, Eric Brockmeyer, Scott Hudson, and Ivan Poupyrev. Printed optics: 3D printing of embedded optical elements for interactive devices. In *Proceedings of the 25th annual ACM symposium on User interface software and technology*, pages 589–598. ACM, 2012.

[51] Yang Yang, Yonghua Chen, Ying Wei, and Yingtian Li. 3D printing of shape memory polymer for functional part fabrication. *The International Journal of Advanced Manufacturing Technology*, 84(9):2079–2095, 2016.

[52] Yang Yang, Yonghua Chen, Ying Wei, and Yingtian Li. Novel design and three-dimensional printing of variable stiffness robotic grippers. *Journal of Mechanisms and Robotics*, 8(6):061010, 2016.

[53] A. M. Dollar and R. D. Howe. A robust compliant grasper via shape deposition manufacturing. *Mechatronics, IEEE/ASME Transactions on*, 11(2):154–161, 2006.

[54] Robert Merz, FB Prinz, K Ramaswami, M Terk, and L Weiss. *Shape deposition manufacturing.* Engineering Design Research Center, Carnegie Mellon Univ., 1994.

[55] Erico Guizzo. irobot smashes its new robotic hand with baseball bat. [Online]. Available from: http://spectrum.ieee.org/, 2012. Accessed: 09/2017.

[56] E. MacDonald, R. Salas, D. Espalin, M. Perez, E. Aguilera, D. Muse, and R. B. Wicker. 3D printing for the rapid prototyping of structural electronics. *Access, IEEE*, 2:234–242, 2014.

[57] Matthew Paul Alonso, Evan Malone, Francis C Moon, and Hod Lipson. Reprinting the telegraph: Replicating the vail register using multi-materials 3D printing. *Cornell. edu. Web*, 30, 2012.

[58] Evan Malone, Kian Rasa, Daniel Cohen, Todd Isaacson, Hilary Lashley, and Hod Lipson. Freeform fabrication of zinc-air batteries and electromechanical assemblies. *Rapid Prototyping Journal*, 10(1):58–69, 2004.

[59] Evan Malone and Hod Lipson. Freeform fabrication of ionomeric polymer-metal composite actuators. *Rapid Prototyping Journal*, 12(5):244–253, 2006.

[60] Nano Dimension. Additive manufacturing of electronics. [Online]. Available from: www.nano-di.com, 2017. Accessed: 09/2017.

[61] Jason A Paulsen, Michael Renn, Kurt Christenson, and Richard Plourde. Printing conformal electronics on 3D structures with aerosol jet technology. In *Future of Instrumentation International Workshop (FIIW), 2012*, pages 1–4. IEEE, 2012.

[62] R Olivas, R Salas, D Muse, E MacDonald, and R Wicker. Structural electronics through additive manufacturing and micro-dispensing. In *IMAPS National Conference*, 2010.

[63] Voxel8. Voxel8 3D electronics printer. [Online]. Available from: www.voxel8.com, 2015. Accessed: 09/2017.

[64] Min-Saeng Kim, Won-Shik Chu, Yun-Mi Kim, Adrian Paulo Garcia Avila, and Sung-Hoon Ahn. Direct metal printing of 3D electrical circuit using rapid prototyping. *International Journal of Precision Engineering and Manufacturing*, 10(5):147–150, 2009.

[65] Rhys Jones. Printed circuitry: All covered up. [Online]. Available from: http://blog.reprap.org/2012/06/printed-circuitry-all-covered-up.html, 2012. Accessed: 09/2017.

[66] Evan Malone and Hod Lipson. Functional freeform fabrication for physical artificial life. In *Proceedings ALIFE*, volume 9, pages 100–105, 2004.

[67] Mike Toutonghi. Functionalize condcutive filament blog. [Online]. Available from: http://functionalize.com/blog/, 2015. Accessed: 05/2015.

[68] Daniel Periard, Evan Malone, and Hod Lipson. Printing embedded circuits. In *Proceedings of the 18th Solid Freeform Fabrication Symposium, Austin TX*, pages 503–12. Citeseer, 2007.

[69] Bryan Cox, Matt Saari, Bin Xia, Edmond Richer, Paul S. Krueger, and Adam L. Cohen. Fiber encapsulation additive manufacturing: Technology and applications update. *3D Printing and Additive Manufacturing*, 2017.

[70] C. Shemelya, F. Cedillos, E. Aguilera, D. Espalin, D. Muse, R. Wicker, and E. MacDonald. Encapsulated copper wire and copper mesh capacitive sensing for 3-D printing applications. *Sensors Journal, IEEE*, 15(2):1280–1286, 2015.

[71] Chiyen Kim, David Espalin, Alejandro Cuaron, Mireya A. Perez, Mincheol Lee, Eric MacDonald, and Ryan B. Wicker. Cooperative tool path planning for wire embedding on additively manufactured curved surfaces using robot kinematics. *Journal of Mechanisms and Robotics*, 7(2):021003–021003, 2015.

[72] David Espalin, Danny W Muse, Eric MacDonald, and Ryan B Wicker. 3D printing multifunctionality: structures with electronics. *The International Journal of Advanced Manufacturing Technology*, 72(5-8):963–978, 2014.

[73] Jacob Bayless, Mo Chen, and Bing Dai. Wire embedding 3D printer. *Engineering Physics Department, University of British Columbia*, 2010.

[74] Matt Saari, Bryan Cox, Edmond Richer, Paul S Krueger, and Adam L Cohen. Fiber encapsulation additive manufacturing: An enabling technology for 3D printing of electromechanical devices and robotic components. *3D Printing and Additive Manufacturing*, 2(1):32–39, 2015.

[75] R.B. Wicker, F. Medina, E. MacDonald, D.W. Muse, and D. Espalin. Methods and systems for connecting inter-layer conductors and components in 3D structures, structural components, and structural electronic, electromagnetic and electromechanical components/devices, 2014.

[76] Collin Clay. *Electrically conductive thermoplastic elastomers in application to additive manufacturing.* PhD thesis, Southern Methodist University, 2014.

[77] Bok Yeop Ahn, Steven B. Walker, Scott C. Slimmer, Analisa Russo, Ashley Gupta, Steve Kranz, Eric B. Duoss, Thomas F. Malkowski, and Jennifer A. Lewis. Planar and three-dimensional printing of conductive inks. *Journal of visualized experiments: JoVE*, 58:e3189, 2011.

[78] A. Brodeala, A. Bonea, C. Ionescu, M. Vladescu, and P. Svasta. Physical properties of silver inkjet printed circuits. In *Electronics Technology (ISSE), 2012 35th International Spring Seminar on*, pages 114–116, 2012.

[79] Yoshihiro Kawahara, Steve Hodges, Benjamin S. Cook, Cheng Zhang, and Gregory D. Abowd. Instant inkjet circuits: lab-based inkjet printing to support rapid prototyping of ubicomp devices, 2013.

[80] John Sarik, Alex Butler, Nicolas Villar, James Scott, and Steve Hodges. Combining 3D printing and printable electronics. In *Proceedings of TEI 2012 Works in Progress*. ACM, February 2012.

[81] S.B. Walker and J.A. Lewis. Reactive silver inks for patterning high-conductivity features at mild temperatures. *Journal of the American Chemical Society*, 134:1419–1421, 2012.

[82] Amit J. Lopes, In Hwan Lee, Eric MacDonald, Rolando Quintana, and Ryan Wicker. Laser curing of silver-based conductive inks for in situ 3D structural electronics fabrication in stereolithography. *Journal of Materials Processing Technology*, 214(9):1935–1945, 2014.

[83] Blackmagic3D. Conductive graphene PLA filament 100g. www.blackmagic3d.com/Conductive-p/grphn-pla.htm. Accessed: 09/2017.

[84] Simon J. Leigh, Robert J. Bradley, Christopher P. Purssell, Duncan R. Billson, and David A. Hutchins. A simple, low-cost conductive composite material for 3D printing of electronic sensors. *PLoS ONE*, 7(11):e49365, 2012.

[85] Min Liang, Corey Shemelya, Eric MacDonald, Ryan Wicker, and Hao Xin. 3-D printed microwave patch antenna via fused deposition method and ultrasonic wire mesh embedding technique. *IEEE Antennas and Wireless Propagation Letters*, 14:1346–1349, 2015.

[86] Efrain Aguilera, Jorge Ramos, David Espalin, Fernando Cedillos, Dan Muse, Ryan Wicker, and Eric MacDonald. 3D printing of electro mechanical systems. In *Proceedings of the Solid Freeform Fabrication Symposium*, pages 950–961, 2013.

[87] Jorge G Cham, Beth L Pruitt, Mark R Cutkosky, Mike Binnard, Lee E Weiss, and Gennady Neplotnik. Layered manufacturing with embedded components: process

planning considerations. In *ASME Design Engineering Technical Conferences, Sept*, pages 12–15, 1999.

[88] Robert RJ Maier, William N MacPherson, James S Barton, Mark Carne, Mark Swan, John N Sharma, Simon K Futter, David A Knox, Benjamin JS Jones, and Scott McCulloch. Embedded fiber optic sensors within additive layer manufactured components. *IEEE Sensors Journal*, 13(3):969–979, 2013.

[89] Johannes Glasschroeder, Emanuel Prager, and Michael F. Zaeh. Powder-bed-based 3D-printing of function integrated parts. *Rapid Prototyping Journal*, 21(2):207–215, 2015.

[90] J Li, T Wasley, TT Nguyen, VD Ta, JD Shephard, Jonathan Stringer, P Smith, E Esenturk, C Connaughton, and R Kay. Hybrid additive manufacturing of 3D electronic systems. *Journal of Micromechanics and Microengineering*, 26(10):105005, 2016.

[91] Aaron M Dollar and Robert D Howe. The SDM hand: a highly adaptive compliant grasper for unstructured environments. In *Experimental Robotics*, pages 3–11. Springer, 2009.

[92] Aaron M. Dollar and Robert D. Howe. The highly adaptive SDM hand: Design and performance evaluation. *The International Journal of Robotics Research*, 29(5):585–597, 2010.

[93] J. E. Clark, J. G. Cham, S. A. Bailey, E. M. Froehlich, P. K. Nahata, R. J. Full, and M. R. Cutkosky. Biomimetic design and fabrication of a hexapedal running robot. In *Robotics and Automation, 2001. Proceedings 2001 ICRA. IEEE International Conference on*, volume 4, pages 3643–3649 vol.4, 2001.

[94] Sean A Bailey, Jorge G Cham, Mark R Cutkosky, and Robert J Full. Comparing the locomotion dynamics of the cockroach and a shape deposition manufactured biomimetic hexapod. In *Experimental Robotics VII*, pages 239–248. Springer, 2001.

[95] Sean A Bailey, Jorge G Cham, Mark R Cutkosky, and Robert J Full. Biomimetic robotic mechanisms via shape deposition manufacturing. In *Robotics Research - International Symposium*, volume 9, pages 403–410, 2000.

[96] M Lanzetta and MR Cutkosky. Shape deposition manufacturing of biologically inspired hierarchical microstructures. *CIRP Annals-Manufacturing Technology*, 57(1):231–234, 2008.

[97] Kellar Autumn, Martin Buehler, Mark Cutkosky, Ronald Fearing, Robert J Full, Daniel Goldman, Richard Groff, William Provancher, Alfred A Rizzi, Uluc Saranli, et al. Robotics in scansorial environments. In *Unmanned ground vehicle technology VII*, volume 5804, pages 291–303. International Society for Optics and Photonics, 2005.

[98] Yih-Lin Cheng and Jia-Hung Lai. Fabrication of meso-scale underwater vehicle components by rapid prototyping process. *Journal of Materials Processing Technology*, 201(1-3):640–644, 2008.

[99] Sachin Chitta, Mustafa Karabas, Kevin C Galloway, and Vijay Kumar. Robotrikke: Design, modeling and experimentation with a robotic trikke. In *ASME 2006 International Design Engineering Technical Conferences and Computers and Information in Engineering Conference*, pages 741–748. American Society of Mechanical Engineers, 2006.

[100] Motohide Hatanaka and Mark R Cutkosky. Process planning for embedding flexible materials in multi-material prototypes. In *ASME 2003 International Design Engineering Technical Conferences and Computers and Information in Engineering Conference*, pages 325–333. American Society of Mechanical Engineers, 2003.

[101] M. R. Cutkosky, P. Dario, and C. Stefanini. A high force miniature gripper fabricated via shape deposition manufacturing. In *Robotics and Automation, 2003. Proceedings. ICRA '03. IEEE International Conference on*, volume 2, pages 1836–1841 vol.2, 2003.

[102] LE Weiss, FB Prinz, G Neplotnik, P Padmanabhan, L Schultz, and R Merz. Shape deposition manufacturing of wearable computers. In *Proceedings of the Solid Freeform Fabrication Symposium*, pages 10–12, 1996.

[103] Wei-chen Lee, Ching-chih Wei, and Shan-Chen Chung. Development of a hybrid rapid prototyping system using low-cost fused deposition modeling and five-axis machining. *Journal of Materials Processing Technology*, 214(11):2366–2374, 2014.

[104] Y. S. Liao, H. C. Li, and M. T. Chen. The study of rapid prototyping process with embedded functional inserts. *Journal of Materials Processing Technology*, 192â€“193(0):68–74, 2007.

[105] Xuan Song, Yayue Pan, and Yong Chen. Development of a low-cost parallel kinematic machine for multidirectional additive manufacturing. *Journal of Manufacturing Science and Engineering*, 137(2):021005, 2015.

[106] Robert JA Allen and Richard S Trask. An experimental demonstration of effective curved layer fused filament fabrication utilising a parallel deposition robot. *Additive Manufacturing*, 8:78–87, 2015.

[107] Yong Chen, Chi Zhou, and Jingyuan Lao. A layerless additive manufacturing process based on CNC accumulation. *Rapid Prototyping Journal*, 17(3):218–227, 2011.

[108] Xuejin Zhao, Yayue Pan, Chi Zhou, Yong Chen, and Charlie C. L. Wang. An integrated CNC accumulation system for automatic building-around-inserts. *Journal of Manufacturing Processes*, 15(4):432–443, 2013.

[109] Yayue Pan, Chi Zhou, Yong Chen, and Jouni Partanen. Multitool and multiaxis computer numerically controlled accumulation for fabricating conformal features on curved surfaces. *Journal of Manufacturing Science and Engineering*, 136(3):031007, 2014.

[110] Jianzhong Ruan, Todd E Sparks, Ajay Panackal, Frank W Liou, Kunnayut Eiamsa-ard, Kevin Slattery, Hsin-Nan Chou, and Mary Kinsella. Automated slicing for a multiaxis metal deposition system. *Journal of Manufacturing Science and Engineering*, 129(2):303–310, 2007.

[111] Bharath Vasudevarao, Dharma Prakash Natarajan, Mark Henderson, and Anshuman Razdan. Sensitivity of RP surface finish to process parameter variation. In *Solid Freeform Fabrication Proceedings*, pages 251–258, 2000.

[112] Sarat Singamneni, Asimava Roychoudhury, Olaf Diegel, and Bin Huang. Modeling and evaluation of curved layer fused deposition. *Journal of Materials Processing Technology*, 212(1):27–35, 2012.

[113] Sung-Hoon Ahn, Michael Montero, Dan Odell, Shad Roundy, and Paul K. Wright. Anisotropic material properties of fused deposition modelling ABS. *Rapid Prototyping Journal*, 8(4):248–257, 2002.

[114] Olaf Diegel, Sarat Singamneni, Ben Huang, and Ian Gibson. Curved layer fused deposition modeling in conductive polymer additive manufacturing. In *Advanced Materials Research*, volume 199, pages 1984–1987. Trans Tech Publ, 2011.

[115] Olaf Diegel, Sarat Singamneni, Ben Huang, and Ian Gibson. Getting rid of the wires: Curved layer fused deposition modeling in conductive polymer additive manufacturing. In *Key Engineering Materials*, volume 467, pages 662–667. Trans Tech Publ, 2011.

[116] B Huang and S Singamneni. Alternate slicing and deposition strategies for fused deposition modelling of light curved parts. *J. of Achievem in mat and manuf*, 55(2):511–517, 2012.

[117] Bin Huang and Sarat Singamneni. Curved layer adaptive slicing (CLAS) for fused deposition modelling. *Rapid Prototyping Journal*, 21(4):354–367, 2015.

[118] Bin Huang. *Alternate slicing and deposition strategies for Fused Deposition Modelling*. Thesis, School of Engineering, 2014.

[119] Joris van Tubergen. Printing in 3 dimensions, finally... [Online]. Available from: www.thingiverse.com/thing:75735, 2013. Accessed: 09/2017.

[120] Johann Rocholl. Kossel. [Online]. Available from: reprap.org/wiki/Kossel, 2012. Accessed: 02/2018.

[121] Thomas Llewellyn-Jones, Robert Allen, and Richard Trask. Curved layer fused filament fabrication using automated toolpath generation. *3D Printing and Additive Manufacturing*, 3(4):236–243, 2016.

[122] Pavlos Bakagiannis, Akrarn Ahmed, Christiana Vlanti, and Theodor Grousopoulos. *Plastic Architectures (Pet Flakes)*. Thesis, Insitute for Advanced Architecture of Catalonia, 2012.

[123] Stefanie Mueller, Sangha Im, Serafima Gurevich, Alexander Teibrich, Lisa Pfisterer, François Guimbretière, and Patrick Baudisch. WirePrint: 3D printed previews for fast prototyping, 2014.

[124] Yasusi Kanada. Method of designing, partitioning, and printing 3D objects with specified printing direction. In *2014 International Symposium on Flexible Automation (ISFA 2014)*, 2014.

[125] WobbleWorks Inc. 3Doodler the world's first 3D printing pen. [Online]. Available from: www.the3doodler.com, 2015. Accessed: 02/2018.

[126] Eddie Karassenstein. Man creates flying hexacopter drone with 3Doodler 3D printing pen. [Online]. Available from: www.3dprint.com/12158/3doodler-3d-printed-drone/, 2014. Accessed: 02/2018.

[127] Prabhjot Singh and Debasish Dutta. Multi-direction slicing for layered manufacturing. *Journal of Computing and Information Science in Engineering*, 1(2):129–142, 2001.

[128] Jun Zhang and Frank W Liou. Adaptive slicing for a five-axis laser aided manufacturing process. In *Proceedings of the ASME Design Engineering Technical Conference*. American Society of Mechanical Engineers (ASME), 2001.

[129] Prabhjot Singh, Y Moon, Debasish Dutta, and Sridhar Kota. Design of a customized multi-directional layered deposition system based on part geometry. In *Annual Solid Freeform Fabrication Symposium, Austin, TX, Aug*, pages 4–6, 2003.

[130] Kunnayut Eiamsa-ard, Jun Zhang, and Frank W Liou. Skeleton-based geometric reasoning for adaptive slicing in a five-axis laser aided manufacturing process system. In *Solid Freeform Fabrication Conference, University of Texas-Austin*, 2001.

[131] R Dwivedi and R Kovacevic. Process planning for multi-directional laser-based direct metal deposition. *Proceedings of the Institution of Mechanical Engineers, Part C: Journal of Mechanical Engineering Science*, 219(7):695–707, 2005.

[132] Divya Kanakanala, Swathi Routhu, Jianzhong Ruan, Xiaoqing Frank Liu, and Frank Liou. A multi-axis slicing method for direct laser deposition process. In

ASME 2010 International Design Engineering Technical Conferences and Computers and Information in Engineering Conference, pages 425–432. American Society of Mechanical Engineers, 2010.

[133] Lan Ren, Todd Sparks, Jianzhong Ruan, and Frank Liou. Integrated process planning for a multiaxis hybrid manufacturing system. *Journal of Manufacturing Science and Engineering*, 132(2):021006, 2010.

[134] Michael Kerschbaumer, Georg Ernst, and Paul O'Leary. Tool path generation for 3D laser cladding using adaptive slicing technology. *Proc. 24th ICALEO, Miami, USA*, 2005.

[135] Jianzhong Ruan, Kunnayut Eiamsa-ard, and F. W. Liou. Automatic process planning and toolpath generation of a multiaxis hybrid manufacturing system. *Journal of Manufacturing Processes*, 7(1):57–68, 2005.

[136] Rajeev Dwivedi, Srdja Zekovic, and Radovan Kovacevic. A novel approach to fabricate uni-directional and branching slender structures using laser-based direct metal deposition. *International Journal of Machine Tools and Manufacture*, 47(7-8):1246–1256, 2007.

[137] Hsuan-kuan Huang and Grier C. I. Lin. Rapid and flexible prototyping through a dual-robot workcell. *Robotics and Computer-Integrated Manufacturing*, 19(3):263–272, 2003.

[138] William S Yerazunis, John C Barnwell III, and Daniel N Nikovski. Strengthening abs, nylon, and polyester 3D printed parts by stress tensor aligned deposition paths and five-axis printing. In *International Solid Freeform Fabrication Symposium*, 2016.

[139] N. Seward and I. A. Bonev. A new 6-dof parallel robot with simple kinematic model. In *Robotics and Automation (ICRA), 2014 IEEE International Conference on*, pages 4061–4066, 2014.

[140] Huaishu Peng, Rundong Wu, Steve Marschner, and François Guimbretière. On-the-fly print: Incremental printing while modelling. In *Proceedings of the 2016 CHI Conference on Human Factors in Computing Systems*, pages 887–896. ACM, 2016.

[141] Rhino. Rhinoceros, design, modelm present, analyze, realize. [Online]. Available from: rhino3d.com, 2017. Accessed: 09/2017.

[142] Frederik Wulle, Daniel Coupek, Florian Schäffner, Alexander Verl, Felix Oberhofer, and Thomas Maier. Workpiece and machine design in additive manufacturing for multi-axis fused deposition modeling. *Procedia CIRP*, 60:229–234, 2017.

[143] Øyvind Kallevik Grutle. 5-axis 3D printer. Master's thesis, University of Olso, Department of Informatics, 2015.

[144] Nils Bausch, David P. Dawkins, Regina Frei, and Susanne Klein. 3D printing onto unknown uneven surfaces. *IFAC-PapersOnLine*, 49(21):583–590, 2016.

[145] Alexander Teibrich, Stefanie Mueller, François Guimbretière, Robert Kovacs, Stefan Neubert, and Patrick Baudisch. Patching physical objects. In *Proceedings of the 28th Annual ACM Symposium on User Interface Software & Technology*, pages 83–91. ACM, 2015.

[146] VSHAPER. Vshaper 5-axis machine. [Online]. Available from: vshaper.com/en/3d-printers/5-axis-machine/, 2017. Accessed: 02/2018.

[147] Ethereal Machines Pvt Ltd. The ethereal halo. [Online]. Available from: etherealmachines.com/products/halo, 2017. Accessed: 02/2018.

[148] Dirk vander Kooij. The endless chair. www.dirkvanderkooij.com, 2010. [Online]. Available from: Accessed: 09/2017.

[149] Jasper Menger. 3D robot printing. [Online]. Available from: www.3d-robotprinting.com, 2014. Accessed: 09/2017.

[150] Zhiyuan Wang, Renwei Liu, Todd Sparks, and Frank Liou. Large-scale deposition system by an industrial robot (i): Design of fused pellet modeling system and extrusion process analysis. *3D Printing and Additive Manufacturing*, 3(1):39–47, 2016.

[151] Anna Kulik, Petr Naovikov, and Inder Parakash Singh. Stone spray. Thesis, IAAC, Digital Tectonics 'FABBOTS 3.0' Research & Development Studio, 2012.

[152] Sasha Jokic, Starsk Lara, and Nasim Fashami. Fab clay. Thesis, IAAC, Digital Tectonics 'FABBOTS 3.0' Research & Development Studio, 2012.

[153] Viridis 3D. Robotic 3D printing platform. [Online]. Available from: www.viridis3d.com. Accessed: 09/2017.

[154] George Q. Zhang, Xiongzi Li, Remus Boca, Jeremy Newkirk, Biao Zhang, Thomas A. Fuhlbrigge, Helen K. Feng, and Nick J. Hunt. Use of industrial robots in additive manufacturing - a survey and feasibility study. In *ISR/Robotik 2014; 41st International Symposium on Robotics; Proceedings of*, pages 1–6, 2014.

[155] Neri Oxman, Markus Kayser, Jared Laucks, and Michal Firstenberg. Robotically controlled fiber-based manufacturing as case study for biomimetic digital fabrication. *Green Design, Materials and Manufacturing Processes, CRC Press (London)*, pages 473–8, 2013.

[156] Andrew John Wit, Simon Kim, Mariana Ibañez, and Daniel Eisinger. Craft driven robotic composites. *3D Printing and Additive Manufacturing*, 3(1):2–9, 2016.

[157] Neri Oxman, Jared Laucks, Markus Kayser, Elizabeth Tsai, and Michal Firstenberg. Freeform 3D printing: Towards a sustainable approach to additive manufacturing. *Green Design, Materials and Manufacturing Processes*, page 479, 2013.

[158] Steven Keating and Neri Oxman. Compound fabrication: A multi-functional robotic platform for digital design and fabrication. *Robotics and Computer-Integrated Manufacturing*, 29(6):439–448, 2013.

[159] Neri Oxman, Jorge Duro-Royo, Steven Keating, Ben Peters, and Elizabeth Tsai. Towards robotic swarm printing. *Architectural Design*, 84(3):108–115, 2014.

[160] Ji Shi, Xun Liu, Ruihua Luo, Yuqi Cui, Lei Yu, and Philip Yuan. Robotic extrusion (6-axis KUKA+ABS 3D printing). [Online]. Available from: www.behance.net/gallery/22536831/ROBOTIC-EXTRUSION(6-Axis-KUKAABS-3D-Printing), 2014. Accessed: 09/2017.

[161] Volker Helm, Jan Willmann, Andreas Thoma, Luka Piškorec, Norman Hack, Fabio Gramazio, and Matthias Kohler. Iridescence print: Robotically printed

lightweight mesh structures. *3D Printing and Additive Manufacturing*, 2(3):117–122, 2015.

[162] Brian Harms, Haejun Jung, Vince Huang, and Yaying Chen. Suspended depositions. [Online]. Available from: www.nstrmnt.com, 2012. Accessed: 09/2017.

[163] Sasa Jokic, Petr Novikov, Joris Laarman, van der Velden Gijs, Riegman Stefanie, Markopoulou Areti, Fraguada Luis, Scheurer Fabian, Ramsgard Thomsen Mette, and Geurtjens Tim. Mataerial. [Online]. Available from: www.mataerial.com, 2012. Accessed: 09/2017.

[164] Joris Laarman. MX3D metal printing. [Online]. Available from: www.jorislaarman.com, 2014. Accessed: 09/2017.

[165] Byron James Brooks, Khalid Mahmood Arif, Steven Dirven, and Johan Potgieter. Robot-assisted 3D printing of biopolymer thin shells. *The International Journal of Advanced Manufacturing Technology*, pages 1–12, 2016.

[166] Kam-Ming Mark Tam and Caitlin T. Mueller. Additive manufacturing along principal stress lines. *3D Printing and Additive Manufacturing*, 4(2):63–81, 2017.

[167] Ismayuzri Ishak, Joseph Fisher, and Pierre Larochelle. Robot arm platform for additive manufacturing: Multi-plane printing. In *Proceedings of the 2016 Florida Conference on Recent Advances in Robotics (FCRAR 2016)*, 2016.

[168] S. J. Grunewald. Arevo labs takes 3d printing 3d with new 6-axis composite part additive manufacture platform. [Online]. Available from: www.3dprint.com/105787/arevo-labs-6-axis-ram-platform3doodler-3d-printed-drone/, 2015. Accessed: 02/2018.

[169] C. Wu, C. Dai, G. Fang, Y. J. Liu, and C. C. L. Wang. RoboFDM: A robotic system for support-free fabrication using FDM. In *2017 IEEE International Conference on Robotics and Automation (ICRA)*, pages 1175–1180, 2017.

[170] Adam G. Stevens, C. Ryan Oliver, Matthieu Kirchmeyer, Jieyuan Wu, Lillian Chin, Erik S. Polsen, Chad Archer, Casey Boyle, Jenna Garber, and A. John Hart. Conformal robotic stereolithography. *3D Printing and Additive Manufacturing*, 3(4):226–235, 2016.

[171] Eric MacDonald and Ryan Wicker. Multiprocess 3D printing for increasing component functionality. *Science*, 353(6307), 2016.

[172] Zmorph. The multitool 3D printer. [Online]. Available from: www.zmorph3d.com. Accessed: 09/2017.

[173] Zicheng Zhu, Vimal Dhokia, and Stephen T. Newman. The development of a novel process planning algorithm for an unconstrained hybrid manufacturing process. *Journal of Manufacturing Processes*, 15(4):404–413, 2013.

[174] Frank Medina, AJ Lopes, AV Inamdar, Robert Hennessey, JA Palmer, BD Chavez, Don Davis, Phil Gallegos, and RB Wicker. Hybrid manufacturing: Integrating direct-write and stereolithography. *Proceedings of the 2005 Solid Freeform Fabrication*, 2005.

[175] Amit Joe Lopes, Eric MacDonald, and Ryan B Wicker. Integrating stereolithography and direct print technologies for 3D structural electronics fabrication. *Rapid Prototyping Journal*, 18(2):129–143, 2012.

[176] Steven Ambriz, Jose Coronel, Bob Zinniel, Ron Schloesser, Chiyen Kim, Mireya Perez, David Espalin, and Ryan B. Wicker. Material handling and registration for an additive manufacturing-based hybrid system. *Journal of Manufacturing Systems*, 45:17–27, 2017.

[177] Seth Allen and Deba Dutta. On the computation of part orientation using support structures in layered manufacturing. In *Proceedings of Solid Freeform Fabrication Symposium, University of Texas at Austin, Austin, TX, June*, pages 259–269. DTIC Document, 1994.

[178] K. Thrimurthulu, Pulak M. Pandey, and N. Venkata Reddy. Optimum part deposition orientation in fused deposition modeling. *International Journal of Machine Tools and Manufacture*, 44(6):585–594, 2004.

[179] Yicha Zhang and Alain Bernard. Using am feature and multi-attribute decision making to orientate part in additive manufacturing. In *High value manufacturing: Advanced research in virtual and rapid prototyping. Proceedings of the 6th International Conference on Advanced Research in Virtual and Rapid Prototyping*, pages 411–416, 2013.

[180] Mst Faujiya Afrose, S. H. Masood, Pio Iovenitti, Mostafa Nikzad, and Igor Sbarski. Effects of part build orientations on fatigue behaviour of FDM-processed PLA material. *Progress in Additive Manufacturing*, 1(1):21–28, 2016.

[181] Jae-Won Choi, Francisco Medina, Chiyen Kim, David Espalin, David Rodriguez, Brent Stucker, and Ryan Wicker. Development of a mobile fused deposition modeling system with enhanced manufacturing flexibility. *Journal of Materials Processing Technology*, 211(3):424–432, 2011.

[182] Y. Yang, H. T. Loh, J. Y. H. Fuh, and Y. S. Wong. Feature extraction and volume decomposition for orthogonal layered manufacturing. *Computer-Aided Design*, 35(12):1119–1128, 2003.

[183] Yashpal Patel, Aashish Kshattriya, Sarat B Singamneni, and A Roy Choudhury. Application of curved layer manufacturing for preservation of randomly located minute critical surface features in rapid prototyping. *Rapid Prototyping Journal*, 21(6):725–734, 2015.

[184] Debapriya Chakraborty, B. Aneesh Reddy, and A. Roy Choudhury. Extruder path generation for curved layer fused deposition modeling. *Computer-Aided Design*, 40(2):235–243, 2008.

[185] Bin Huang and Sarat Singamneni. A mixed-layer approach combining both flat and curved layer slicing for fused deposition modelling. *Proceedings of the Institution of Mechanical Engineers, Part B: Journal of Engineering Manufacture*, 229(12):2238–2249, 2015.

[186] 3D HUBS. FDM quality guidelines. [Online]. Available from: www.3dhubs.com, 2017. Accessed: 02/2018.

[187] Ultimaker. Ultimaker 2+ specifications. [Online]. Available from: ultimaker.com, 2017. Accessed: 02/2018.

[188] Alberto Boschetto and Luana Bottini. Surface improvement of fused deposition modeling parts by barrel finishing. *Rapid Prototyping Journal*, 21(6):686–696, 2015.

[189] 'Gyrobot'. E3d cyclops/chimera micro extruder. [Online]. Available from: www.thingiverse.com/thing:852748, 2015. Accessed: 02/2018.

[190] Thomas R Kramer, Frederick M Proctor, and Elena R Messina. The NIST RS274NGC interpreter-version 3. Technical report, NIST, 2000.

[191] Christer Ericson. *Real-time collision detection*. CRC Press, 2004.

[192] Casey Muratori. Implementing GJK. [Online]. Available from: mollyrocket.com/849, 2006. Accessed: 01/2018.

[193] Peter Corke. *Robotics, vision and control: fundamental algorithms in MATLAB*, volume 73. Springer, 2011.

[194] J Denavit and RS Hartenberg. Kinematic modelling for robot calibration. *Trans. ASME Journal of Applyed Mechanics*, 22:215–221, 1955.

[195] MakerBot. Cute octopus says hello CAD model. [Online]. Available from: www.thingiverse.com/thing:27053, 2012. Accessed: 01/2018.

[196] ASTM. Astm d638-14, standard test method for tensile properties of plastics. *ASTM International, West Conshohocken, PA*, 2014.

[197] Céline Bellehumeur, Longmei Li, Qian Sun, and Peihua Gu. Modeling of bond formation between polymer filaments in the fused deposition modeling process. *Journal of Manufacturing Processes*, 6(2):170–178, 2004.

[198] B. M. Tymrak, M. Kreiger, and J. M. Pearce. Mechanical properties of components fabricated with open-source 3-d printers under realistic environmental conditions. *Materials and Design*, 58:242–246, 2014.

[199] 'nervoussystem'. Cellular lamp CAD model. [Online]. Available from: www.thingiverse.com/thing:19104, 2012. Accessed: 01/2018.

[200] 'BenitoSanduchi'. Zigzag vases. [Online]. Available from: www.thingiverse.com/thing:36912, 2012. Accessed: 01/2018.

[201] 'NickRBrewer'. Yoda with chin support. [Online]. Available from: www.thingiverse.com/thing:48060, 2013. Accessed: 01/2018.

[202] 'CreativeTools'. #3dbenchy - the jolly 3D printing torture-test by creativetools.se. [Online]. Available from: www.thingiverse.com/thing:763622, 2015. Accessed: 01/2018.

[203] 'openbionics'. Miniature robotic hand for ninjaflex by open bionics. [Online]. Available from: www.thingiverse.com/thing:739806, 2015. Accessed: 01/2018.

[204] Bharath Vasudevarao, Dharma Prakash Natarajan, Mark Henderson, and Anshuman Razdan. Sensitivity of rp surface finish to process parameter variation. In *Solid Freeform Fabrication Proceedings*, pages 251–258. The University of Texas Austin, 2000.

[205] Stratasys Ltd. 3D printing at infinite lengths & 8-axis freedom for strong composites. [Online]. Available from: www.stratasys.com/demonstrators, 2016. Accessed: 11/2017.

[206] Daniel Günther, Bastian Heymel, Johannes Franz Günther, and Ingo Ederer. Continuous 3d-printing for additive manufacturing. *Rapid Prototyping Journal*, 20(4):320, 2014.

[207] Blackbelt. Blackbelt continous 3D printer. [Online]. Available from: www.blackbelt-3d.com, 2017. Accessed: 11/2017.

[208] NN Kumbhar and AV Mulay. Finishing of fused deposition modelling (FDM) printed parts by CO2 laser, December 2016 2016.

[209] Mumtaz Kamran and Hopkinson Neil. Top surface and side roughness of inconel 625 parts processed using selective laser melting. *Rapid Prototyping Journal*, 15(2):96–103, 2009.

[210] PB Bacchewar, SK Singhal, and PM Pandey. Statistical modelling and optimization of surface roughness in the selective laser sintering process. *Proceedings of the Institution of Mechanical Engineers, Part B: Journal of Engineering Manufacture*, 221(1):35–52, 2007.

[211] R. I. Campbell, M. Martorelli, and H. S. Lee. Surface roughness visualisation for rapid prototyping models. *Computer-Aided Design*, 34(10):717–725, 2002.

[212] Daekeon Ahn, Jin-Hwe Kweon, Soonman Kwon, Jungil Song, and Seokhee Lee. Representation of surface roughness in fused deposition modeling. *Journal of Materials Processing Technology*, 209(15):5593–5600, 2009.

[213] Make Magazine. Make: 2015 3D printer shoot out test models. [Online]. Available from:www.thingiverse.com/thing:533472, 2014. Accessed: 10/2017.

[214] Pulak M Pandey, N Venkata Reddy, and Sanjay G Dhande. Improvement of surface finish by staircase machining in fused deposition modeling. *Journal of materials processing technology*, 132(1):323–331, 2003.

[215] EN ISO. 4288-geometrical product specifications (gps)-surface texture: profile method–rules and procedures for the assessment of surface texture. *International Organization for Standardization, Genève*, 1996.

[216] EN ISO. ISO 16610-22 (2006), geometrical product specifications (GPS â€“ filtration - linear profile filters: Spline filters. *International Organization for Standardization, Genève*, 2015.

[217] PM Pandey. *Enhancement of surface finish in fused deposition modeling*. PhD thesis, IIT Kanpur, 2003.

[218] A. Boschetto, V. Giordano, and F. Veniali. Modelling micro geometrical profiles in fused deposition process. *The International Journal of Advanced Manufacturing Technology*, 61(9):945–956, 2012.

[219] Rudolf N Cardinal and Michael RF Aitken. *ANOVA for the behavioral sciences researcher*. Psychology Press, 2006.

[220] 'Nop Head'. Why slicers get their dimensions wrong. [Online]. Available from: hydraraptor.blogspot.co.uk, 2014. Accessed: 12/2017.

[221] 'James'. Calculating the flow rate value. [Online]. Available from: adventuresin3-dprinting.blogspot.co.uk, 2011. Accessed: 12/2017.

[222] Gary Hodgson, Alessandro Ranellucci, and Jeff Moe. Flow math. [Online]. Available from: manual.slic3r.org, 2017. Accessed: 12/2017.

[223] BuildTak. Blackbelt 3D printing surface. [Online]. Available from: www.buildtak.eu, 2017. Accessed: 12/2017.

[224] SPARC. Robotics 2020 Multi-Annual Roadmap For Robotics In Europ Horizon 2020 Call ICT-2017. Technical report, SPARC The Partnership For Robotics In Europe, 2016.

[225] Nahid Mubin. Supermarine spitfire. [Online]. Available from: grabcad.com/library/supermarine-spitfire-2, 2017. Accessed: 01/2018.

[226] Joseph R Kubalak, Craig D Mansfield, Taylor H Pesek, Zachary K Snow, Edward B Cottiss, Oliver D Ebeling-Koning, Matthew G Price, Mark H Traverso, L David Tichnell, and Christopher B Williams. Design and realization of a 6 degree of freedom robotic extrusion platform. In *Solid Freeform Fabrication*, 2016.

[227] Joseph R. Kubalak, Alfred L. Wicks, and Christopher B. Williams. Using multi-axis material extrusion to improve mechanical properties through surface reinforcement. *Virtual and Physical Prototyping*, pages 1–7, 2017.